

# **HYBRID COMPOSITE MATERIALS AND MANUFACTURING**

by

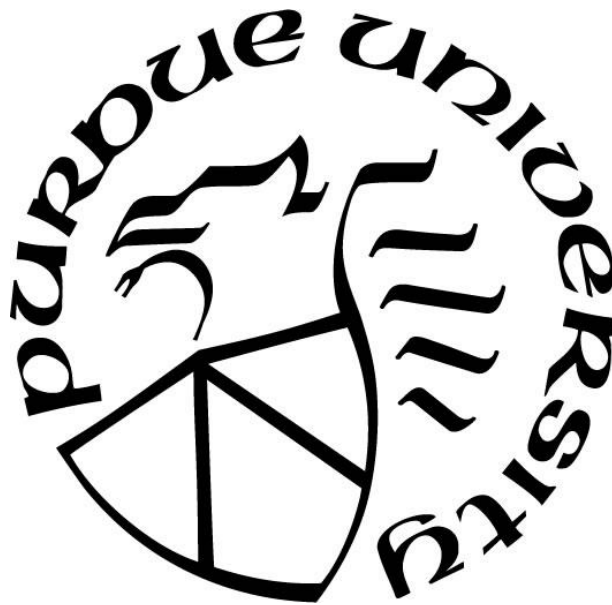
**Diana Gabrielle Heflin**

**A Dissertation**

*Submitted to the Faculty of Purdue University*

*In Partial Fulfillment of the Requirements for the degree of*

**Doctor of Philosophy**



School of Materials Engineering

West Lafayette, Indiana

May 2022

**THE PURDUE UNIVERSITY GRADUATE SCHOOL**  
**STATEMENT OF COMMITTEE APPROVAL**

**Dr. Jan-Anders Mansson, Chair**

School of Materials Engineering

**Dr. Byron Pipes**

School of Aeronautics and Astronautics

**Dr. Jeffrey Youngblood**

School of Materials Engineering

**Dr. Johnathan Goodsell**

School of Aeronautics and Astronautics

**Approved by:**

Dr. David F. Bahr

*Dedicated to Martin and Teresa Heflin*

## **ACKNOWLEDGMENTS**

I would like to thank Hexpol TPE AB for providing the TPE and ELG composites for providing the recycled carbon fiber nonwoven mat. Thank you to my committee, Dr. Jeff Youngblood, Dr. Johnathan Goodsell, and Dr. Byron Pipes, for your advice and support throughout the PhD process. Thank you to Dr. Jan-Anders Mansson for providing a research direction grounded in real-world applications. Your guidance and enthusiasm kept me excited about my research. Finally, I would like to thank the MDLab research group for their help performing lab work, discussing research challenges, and catching my mistakes. I couldn't have done it without you all.

# TABLE OF CONTENTS

|  |    |
|--|----|
| LIST OF TABLES .....   | 8  |
| LIST OF FIGURES .....  | 9  |
| LIST OF ABBREVIATIONS .....  | 14 |
| ABSTRACT.....  | 16 |
| 1. INTRODUCTION .....  | 18 |
| 1.1 Introduction to Composite Properties and Manufacturing Methods .....         | 18 |
| 1.2 State of the Composites Industry.....  | 20 |
| 1.3 Advanced Manufacturing .....   | 22 |
| 1.3.1 High-Rate Resin Transfer Molding .....                                     | 22 |
| 1.3.2 Hybrid Injection Molding.....  | 24 |
| 1.3.3 Advanced Preform Production .....  | 27 |
| 1.4 Thesis Overview .....  | 30 |
| 1.5 References .....   | 34 |
| 2. BACKGROUND .....  | 40 |
| 2.1 Background: Epoxy/Polyamide Combinations .....                               | 40 |
| 2.1.1 Cure Kinetics .....  | 43 |
| 2.1.2 Solution-Dissolved Blends .....  | 46 |
| 2.1.3 Fine PA Particles in EP Matrix .....                                       | 48 |
| 2.1.4 EP-Matrix Composites containing Fibers and PA .....                        | 53 |
| 2.1.5 Fiber-Reinforced EP Composites with PA Interleaves .....                   | 57 |
| 2.1.6 Fiber-Reinforced EP Composites with Discrete PA Particle Interlayers ..... | 61 |
| 2.1.7 Other Applications of PA-EP Interactions .....                             | 63 |
| 2.1.8 Section Summary .....  | 64 |
| 2.2 Background: Polyamide/TPE Combinations.....                                  | 65 |
| 2.2.1 PA/Elastomer Blends .....  | 66 |
| 2.2.2 TPE onto PA Overmolding .....  | 69 |
| 2.2.3 Other Thermoplastic/TPE Overmolding .....                                  | 70 |
| 2.2.4 Section Summary .....  | 71 |
| 2.3 Background: Aluminum/Thermoplastic Combinations .....                        | 71 |

|       |   |     |
|-------|---|-----|
| 2.3.1 | Surface Treatment of Aluminum to Promote Adhesion.....                          | 72  |
| 2.3.2 | Spontaneous Adhesion between Aluminum and Thermoplastics .....                  | 74  |
| 2.3.3 | Section Summary .....   | 75  |
| 2.4   | Chapter Conclusions.....  | 76  |
| 2.5   | References .....  | 77  |
| 3.    | PROCESSING OF DISSIMILAR MATERIALS .....  | 92  |
| 3.1   | Processing of Dissimilar Materials: Epoxy/Polyamide.....                        | 93  |
| 3.1.1 | Experimental Methods .....  | 94  |
| 3.1.2 | Results .....   | 99  |
| 3.1.3 | Discussion .....  | 101 |
| 3.1.4 | Section Summary .....   | 104 |
| 3.2   | Processing of Dissimilar Materials: Polyamide/TPE .....                         | 105 |
| 3.2.1 | Experimental Methods .....  | 105 |
| 3.2.2 | Results .....   | 107 |
| 3.2.3 | Discussion .....  | 108 |
| 3.2.4 | Section Summary .....   | 111 |
| 3.3   | Chapter Conclusions.....  | 111 |
| 3.4   | References .....  | 112 |
| 4.    | CRASH PERFORMANCE OF DISSIMILAR MATERIALS.....                                  | 115 |
| 4.1   | Crash Performance of Dissimilar Materials: Epoxy/Polyamide .....                | 116 |
| 4.1.1 | Experimental Methods .....  | 117 |
| 4.1.2 | Results and Discussion.....   | 121 |
| 4.1.3 | Section Summary .....   | 128 |
| 4.2   | Crash Performance of Dissimilar Materials: Aluminum/Recycled Thermoplastic..... | 129 |
| 4.2.1 | Experimental Methods .....  | 130 |
| 4.2.2 | Results .....   | 132 |
| 4.2.3 | Discussion .....  | 137 |
| 4.2.4 | Section Summary .....   | 140 |
| 4.3   | Chapter Conclusions.....  | 140 |
| 4.4   | Chapter Acknowledgements.....   | 141 |
| 4.5   | References .....  | 141 |

|  |     |
|--|-----|
| 5. MANUFACTURING AND PERFORMANCE ANALYSIS OF AN INJECTION OVERMOLDED POLYAMIDE/TPE HYBRID COMPOSITE..... | 146 |
| 5.1 Introduction .....   | 147 |
| 5.1 Experimental Methods.....  | 149 |
| 5.1.1 Materials.....   | 149 |
| 5.1.2 Sample Preparation .....   | 149 |
| 5.1.3 Mechanical Performance: Pull-Out Testing.....  | 151 |
| 5.1.4 Mechanical Performance: 3-Point Bending .....  | 153 |
| 5.1.5 TPE Characterization .....   | 154 |
| 5.1.6 Characterization Summary .....   | 159 |
| 5.2 Results .....  | 159 |
| 5.2.1 Tow Pull-Out Testing.....  | 159 |
| 5.2.2 3-Point Bending.....   | 162 |
| 5.3 Predictive Technical Cost Model .....  | 165 |
| 5.4 Chapter Conclusions.....   | 168 |
| 5.5 Chapter Acknowledgements.....  | 170 |
| 5.6 References .....   | 170 |
| 6. THESIS CONCLUSIONS.....   | 175 |
| APPENDIX A: CHAPTER 4 – DAMAGE AREA CT IMAGES.....   | 177 |

## LIST OF TABLES

|   |     |
|---|-----|
| Table 2.1. EP pre-polymer, PA6, PA6,6, and PA12 chemical formulas. ....   | 43  |
| Table 3.1. Sample nomenclature and processing conditions. ....  | 95  |
| Table 3.2. G <sub>IC</sub> values obtained from Wedge and DCB Testing, given with standard error. ....                            | 99  |
| Table 4.1. Sample orientation, processing temperatures, and nomenclature.....   | 118 |
| Table 4.2. Representative projected damage area determined via CT scanning of impacted samples.<br>.....                          | 127 |
| Table 4.3. Summary of aluminum and PA6/CF hybrid samples used in quasi-static indentation and<br>drop-weight impact testing. .... | 131 |
| Table 4.4. Peak load and absorbed energy measured during the QSI load cycle for the thin<br>aluminum group of samples.....        | 136 |
| Table 4.5. Peak load and absorbed energy during the QSI load cycle for the thick aluminum group<br>of samples. ....               | 137 |
| Table 5.1. Summary of samples.....  | 151 |
| Table 5.2. Summary of injection molding parameters.....   | 151 |
| Table 5.3. Selected cost modeling parameters.....   | 166 |



## LIST OF FIGURES

|  |    |
|--|----|
| Figure 1.1. Specific stiffness and strength ranges for common engineering materials [1].....   | 18 |
| Figure 1.2. Composite tensile strength ranges by processing method [2]. .....  | 19 |
| Figure 1.3. Predicted carbon fiber market growth by industry through 2030 [4].....   | 20 |
| Figure 1.4. New United States regulations (solid black line) for CO <sub>2</sub> emissions in passenger cars produced through 2027 [6].....  | 21 |
| Figure 1.5. RTM manufacturing process schematic. From [10].....  | 23 |
| Figure 1.6. Schematic of multi-material injection molding process. From [23].....  | 25 |
| Figure 1.7. Schematic of the insert overmolding process. From [23].....  | 26 |
| Figure 1.8. Example of a 3D filament-found truss structure, from [36]. .....   | 28 |
| Figure 1.9. Overview of high-rate fiber forming process. ....  | 28 |
| Figure 1.10. Complex structural preforms made from 3D printing with continuous fibers [43].  | 29 |
| Figure 1.11. Custom fabric created via additive manufacture of continuous fiber-reinforced polymer. From Dickson et al [44].....   | 30 |
| Figure 1.12. Scale-up of knowledge from traditional materials science through advanced manufacturing. ....   | 32 |
| Figure 1.13. Dissertation logic flow, from foundation to manufacturing-informed case study. ..   | 33 |
| Figure 2.1. Primary EP-PA reaction, attack on oxirane ring by PA nitrogen atom. Adapted from Zhong et al [76].....   | 43 |
| Figure 2.2. Secondary EP-PA reaction. Adapted from Zhong et al[76]. ....   | 44 |
| Figure 2.3. Interlaminar and interfacial shear strength as a function of PA content in EP-carbon fiber composites. From Kim et al[82].....   | 45 |
| Figure 2.4. Shear strength of PA-EP adhesive as a function of exposure time in water and humidity. From Delollis et al[86].....  | 47 |
| Figure 2.5. Shear failure modes of a lightly crosslinked EP (a), highly crosslinked EP at room temperature (b), and highly crosslinked EP at 160°C (c). From Lu et al[89]. ....                      | 49 |
| Figure 2.6. PA12 fiber bridging in EP (a) and PA12 deformation in EP (b). From Cardwell et al[90]. ....  | 50 |
| Figure 2.7. PA6 particle in EP at mixing temperatures of 30°C, 210°C, 220°C, and 230°C (a). Crystalline PA6 lamellae deflecting crack fingers at a growing crack front (b). From Kim et al[91]. .... | 51 |

|   |     |
|---|-----|
| Figure 2.8. Fracture energy absorbed as function of PA composition (left) and of PA particle size (right). From Kim et al[92].  | 51  |
| Figure 2.9. Critical stress intensity factor as a function of PA6 concentration. From Girodet et al[93].  | 52  |
| Figure 2.10. PA yarns melted between plies of carbon fiber. From Beier et al[100].  | 54  |
| Figure 2.11. An idealized schematic of the comingled PA and structural fibers in a thermoset matrix. From Hogg et al[101].  | 54  |
| Figure 2.12. Relative size of PA and structural fibers in EP matrix. From Thanomsilp et al[102].  | 55  |
| Figure 2.13. Increasing impact energy and decreasing interlaminar shear strength as functions of number of PA interlayers. From Favre[107].   | 58  |
| Figure 2.14. Two cohesive failure mechanisms observed in PA interleaves. From Favre[107].   | 58  |
| Figure 2.15. Electrospinning schematic (a) and SEM image of electrospun fibers (b). From Akangah et al [110].   | 59  |
| Figure 2.16. Interfacial fracture toughness of EP-carbon fiber composites that are selectively toughened with PA interleaves. From Daelemans et al[116].                            | 61  |
| Figure 2.17. PA-toughened interlayer in CF/EP prepreg. From Caprino et al[118].   | 62  |
| Figure 2.18. Mechanical interlocking between PA6 interlayer and carbon fiber composite. From Beiss et al[120].  | 63  |
| Figure 2.19. Schematic representation of (a) hydrogen bonding and (b) covalent bonding between SBS-g-MA and PA12. From Naeim abadi et al [122].                                     | 67  |
| Figure 2.20. Reaction between PA imide group and maleic anhydride, followed by hydrolysis of amide group. From Van Duin et al [123].  | 68  |
| Figure 2.21. Schematic of micropore formation on the surface of aluminum due to an electrochemical anodization process, from Yin et al [145].                                       | 74  |
| Figure 2.22. Friction Lap Welding process for joining polymer to metal. From Liu et al[149].  | 75  |
| Figure 3.1. Asymmetric Wedge Test geometry.   | 96  |
| Figure 3.2. Double cantilever beam geometry.  | 97  |
| Figure 3.3. DCB geometry with features of interest labeled, adapted from[18].   | 98  |
| Figure 3.4. Cube root of corrected compliance, $C/N$ , vs. crack length, $a$ , used to determine MBT correction factor $\Delta$ for interfacial fracture toughness calculation[18]. | 98  |
| Figure 3.5. SEM images of PA6/GF fracture surfaces from EP/PA177 (a) and EP/PA197 (b) samples at 1000x magnification.   | 100 |
| Figure 3.6. SEM images of EP/CF fracture surfaces from EP/PA177 (a) and EP/PA197 (b) samples at 1000x magnification.  | 101 |

|   |     |
|---|-----|
| Figure 3.7. $G_{IC}$ values obtained from Wedge Testing for EP/PA samples, plotted with standard error and $G_{IC}$ for EP/EP197.[15].....  | 102 |
| Figure 3.8. Average $G_{IC}$ (prop.) values for the EP/PA DCB samples, shown with standard error and $G_{IC}$ (prop.) for EP/EP197. ....  | 103 |
| Figure 3.9. Floating roller peel fixture, ASTM D3167.[36] .....   | 106 |
| Figure 3.10. Representative force-displacement curve for the TPE and PA peel test. ....   | 107 |
| Figure 3.11. Mean peel strengths of PA/TPE plates processed at two different sets of processing conditions, plotted with the 95% confidence interval of the mean. ....                                | 108 |
| Figure 3.12. Fracture surfaces of peeled PA/TPE samples after testing. Samples processed at (a) 177°C and (b) 197°C. ....   | 110 |
| Figure 4.1. Laminate stacking sequence. Wavy lines represent PA/CF plies, while circles and horizontal lines indicate 0° and 90° epoxy/CF plies, respectively. ....                                   | 118 |
| Figure 4.2. Sample holding fixture for QSI and Drop-Weight Impact Testing. ....   | 119 |
| Figure 4.3. Representative defect ROI from the crack segmentation tool shown. The defect ROI represented a region with high probability for damage. ....  | 121 |
| Figure 4.4. Representative force-displacement curves for EP-up samples (left) and PA-up samples (right). ....   | 122 |
| Figure 4.5. Peak load experienced during QSI testing.....   | 123 |
| Figure 4.6. Energy absorbed by samples during QSI testing.....  | 124 |
| Figure 4.7. Dent depth measured immediately after impact for the case where the epoxy surface was impacted (left) and the case where the PA surface was impacted (right).....                         | 125 |
| Figure 4.8. Percent of impact energy absorbed during drop-weight impact testing for the case where the epoxy surface was impacted (left) and the case where the PA surface was impacted (right). .... | 126 |
| Figure 4.9. Projected damage area in samples damaged via drop-weight impact for EP-up samples (left) and PA-up samples (right). Damage area is plotted here with energy absorbed during impact. ....  | 127 |
| Figure 4.10. Material combinations used in this study. Samples consisted of an aluminum plate, a composite laminate, or a combination of both.....  | 130 |
| Figure 4.11. Dent depth results for low-velocity impact of thin Al/composite hybrid samples. ....   | 133 |
| Figure 4.12. Dent depth results for low-velocity impact of thick Al/composite hybrid samples. ....  | 134 |
| Figure 4.13. Representative force vs. displacement curves from QSI tests for PA6/CF composite, 0.4mm Al, and 0.4mm Al/composite hybrid laminates. ....  | 135 |

|  |     |
|--|-----|
| Figure 4.14. Representative force vs. displacement curves from QSI tests for PA6/CF composite, 2mm thick Al, and 2mm Al/composite hybrid laminates. ....   | 136 |
| Figure 4.15. Force divided by sample thickness vs. displacement for QSI of thin aluminum and PA6/CF hybrid composites. ....  | 138 |
| Figure 4.16. Force divided by sample thickness vs. displacement for QSI of thick aluminum and PA6/CF hybrid composites. ....   | 139 |
| Figure 5.1. Schematic of hybrid overmolding process. ....  | 150 |
| Figure 5.2. Tow (left) and overmolded part (right) geometry used in this study. ....   | 150 |
| Figure 5.3. Pull-out testing sample (a) and fixture (b). ....  | 152 |
| Figure 5.4. 3-point bend fixture with single L-bracket arm. ....   | 153 |
| Figure 5.5. DSC heating curve for a TPE sample heated at a constant rate, with the melt onset and peak temperatures indicated. ....  | 155 |
| Figure 5.6. TGA curves for two different TPE formulations, TPE A (dashed green line, used in overmolding trials) and TPE B (solid green line). ....  | 156 |
| Figure 5.7. Dynamic and complex viscosity of a TPE measured at a constant frequency of 1Hz and a strain of 1% under a temperature ramp from 50 °C to 260 °C at a ramp rate of 5 °C /min. ....  | 157 |
| Figure 5.8. Dynamic and complex viscosity of a TPE measured at a range of angular frequencies. Each test was conducted isothermally at 10°C increments, with temperatures ranging from 120°C (top line) to 210°C (bottom line). .... | 158 |
| Figure 5.9. Dynamic and complex viscosity of a TPE measured at a range of angular frequencies. Each test was conducted isothermally at 10°C increments, with temperatures ranging from 220°C (top line) to 260°C (bottom line). .... | 159 |
| Figure 5.10. Representative force-displacement curve obtained during tow pull-out testing. ...   | 160 |
| Figure 5.11. Interfacial shear strength of PA/CF tows overmolded with TPE. Tows heated to either 22°C, 80°C, or 180°C before overmolding. ....   | 160 |
| Figure 5.12. Force vs. displacement curves for beams tested in 3-point bending. ....   | 163 |
| Figure 5.13. Peak force during bending testing for 1-tape and 3-tape preforms at 22°C, 80°C, and 180°C before overmolding. Shown with standard deviation. ....   | 164 |
| Figure 5.14. Energy absorbed during bending testing for 1-tape and 3-tape preforms at 22°C, 80°C, and 180°C before overmolding. Shown with standard deviation. ....  | 165 |
| Figure 5.15. Schematic of processing line used to develop cost model. ....   | 166 |
| Figure 5.16. Effect of annual production volume on part cost for 3-tape and 1-tape tows. Jumps in cost indicate required capital investment to reach target volumes. ....  | 167 |
| Figure 5.17. Cost breakdown per part for 1-tape and 3-tape tow parts, 120,000 parts/year production volume. ....   | 168 |

Figure 5.18. Load-displacement curves for 3-tape tow overmolded with PA6, 3-tape tow overmolded with TPE, and TPE with no tow reinforcement..... 169

## LIST OF ABBREVIATIONS

|                        |                                      |              |                                   |
|------------------------|--------------------------------------|--------------|-----------------------------------|
| <b>ABS</b>             | Acrylonitrile Butadiene Styrene      | <b>MA</b>    | Maleic Anhydride                  |
| <b>CF</b>              | Carbon Fiber                         | <b>MBT</b>   | Modified Beam Theory              |
| <b>CFRP</b>            | Carbon Fiber Reinforced Polymer      | <b>MDI</b>   | 4,4'-diphenylmethane diisocyanate |
| <b>C-RTM</b>           | Compression Resin Transfer Molding   | <b>NBR</b>   | Acrylonitrile Butadiene Rubber    |
| <b>CT</b>              | Computerized Tomography              | <b>PA</b>    | Polyamide                         |
| <b>DCB</b>             | Double Cantilever Beam               | <b>PA12</b>  | Polyamide 12                      |
| <b>DGEBA</b>           | Bisphenol A Diglycidyl Ether         | <b>PA6</b>   | Polyamide 6                       |
| <b>DSC</b>             | Differential Scanning Calorimetry    | <b>PA6,6</b> | Polyamide 6,6                     |
| <b>EP</b>              | Epoxy                                | <b>PBT</b>   | Polybutylene Terephthalate        |
| <b>GF</b>              | Glass Fiber                          | <b>PC</b>    | Polycarbonate                     |
| <b>G<sub>I</sub></b>   | Mode-I fracture toughness            | <b>PET</b>   | Polyethylene Terephthalate        |
| <b>G<sub>IC</sub></b>  | Mode-I critical fracture toughness   | <b>PI</b>    | Polyimide                         |
| <b>G<sub>IIc</sub></b> | Mode-II critical fracture toughness  | <b>PMMA</b>  | Polymethylmethacrylate            |
| <b>GMA</b>             | Glycidyl Methacrylate                | <b>PP</b>    | Polypropylene                     |
| <b>HP-RTM</b>          | High Pressure Resin Transfer Molding | <b>PS</b>    | Polystyrene                       |
| <b>IFSS</b>            | Interfacial Shear Stress             | <b>QC</b>    | Quality Control                   |
| <b>IR</b>              | Infrared                             | <b>QSI</b>   | Quasi-Static Indentation          |

|             |                                   |              |                                      |
|-------------|-----------------------------------|--------------|--------------------------------------|
| <b>ROI</b>  | Region of Interest                | <b>RTM</b>   | Resin Transfer Molding               |
| <b>SBS</b>  | Styrene Butadiene Styrene         | <b>T-RTM</b> | Thermoplastic Resin Transfer Molding |
| <b>SEBS</b> | Styrene Ethylene Butylene Styrene | <b>TGA</b>   | Thermogravimetric Analysis           |
| <b>SEM</b>  | Scanning Electron Microscopy      | <b>TPE</b>   | Thermoplastic Elastomer              |
| <b>TPO</b>  | Thermoplastic Polyolefin          | <b>TPU</b>   | Thermoplastic Polyurethane           |
| <b>TPS</b>  | Styrenic block copolymer          | <b>TPV</b>   | Thermoplastic Vulcanate              |

## ABSTRACT

Composite materials have become widely used for high-performance applications, particularly in the aerospace industry where annual production volumes are low and a higher part cost can be supported. During the last decades composite materials are beginning to see use in a broader range of applications, including the automotive and sports equipment industries. Simultaneously, there is increasing demand from consumers and regulatory bodies to make cars more fuel efficient and in the case of EV's longer drive range, which can be accomplished by reducing vehicle weight. Composite materials have high specific stiffnesses and strengths, resulting in weight savings when they are used to replace traditionally metal components. However, in order for widespread adoption of composite parts to be viable for the automotive industry, high-rate manufacturing must be realized to reach the required production volumes and part costs.

Toward this goal, advanced composite manufacturing techniques have been developed. These techniques typically combine high automation with careful material selection, which can include fast-curing resins and thermoplastics with adapted melt viscosities and thermomechanical properties. They also allow for complex part geometries to be produced in a single step, reducing the need for additional assembly time. Further, they can be used to easily create multi-material components, which can result in parts that benefit from the desirable mechanical properties of the constituent materials without sacrificing performance.

This thesis develops a framework for the design and high-rate manufacture of multi-material components. First, a critical literature review is conducted to develop a clear understanding of existing research into combinations of dissimilar materials, including epoxy/polyamide, thermoplastic elastomer/polyamide, and aluminum/thermoplastic. It is shown that, for all material combinations studied, interfacial delamination and subsequent deformation are the primary energy absorption mechanisms and that manufacturing conditions may affect interfacial bond strength. Based on this foundation, adhesion testing is performed on devoted sample configurations fabricated under controlled molding conditions. For these material combinations, interfacial adhesion can be significantly improved with carefully selected processing temperatures, even to the extent that adhesive bond between dissimilar materials can be stronger than the cohesive bond in the constituent materials. Next, impact and quasi-static



indentation testing were performed to determine the effects of interfacial adhesion and part design on crash performance. The materials tested all benefit from the placement of a more ductile material on the impacted side of the sample (top surface), indicating a more favorable dissipation of the contact stresses from the impactor, and a higher strength material on the bottom surface where it can withstand tensile stresses imposed by impact-induced bending.

Finally, a complex part consisting of a unidirectional polyamide/carbon fiber preform and a thermoplastic overmold is manufactured via a hybrid overmolding process. Interfacial temperature during overmolding is varied to confirm if the same improvements in interfacial bond strength seen in the compression molding test samples are attainable under realistic high-rate manufacture conditions. Additionally, the preform volume is varied to examine the effect of the preform reinforcement on a part's bending performance. For this system, varying the preform temperature had no effect on interfacial bond strength. A predictive technical cost model is also used to determine the effect of manufacturing changes on part costs. Increasing the tow volume three-fold increased the absorbed energy by more than 30% and requires an increased cost of only 3.8%.

This thesis proves that a tough, multi-material part can be rapidly produced via hybrid overmolding. It was demonstrated that a complex shaped part could be produced at a complete line cycle time of approximately 90 seconds making it a viable method to produce high-performance, low-cost components.

# 1. INTRODUCTION

## 1.1 Introduction to Composite Properties and Manufacturing Methods

Composite materials are combinations of two or more materials with different properties to create a new material with synergetic performance. Most commonly, the term refers to fiber reinforcement, typically carbon or glass fibers, surrounded by a polymer matrix. Composite materials often have higher specific strength than common engineering metals with comparable specific stiffness. This means that a composite can achieve comparable strength to metal with a much lower part weight.

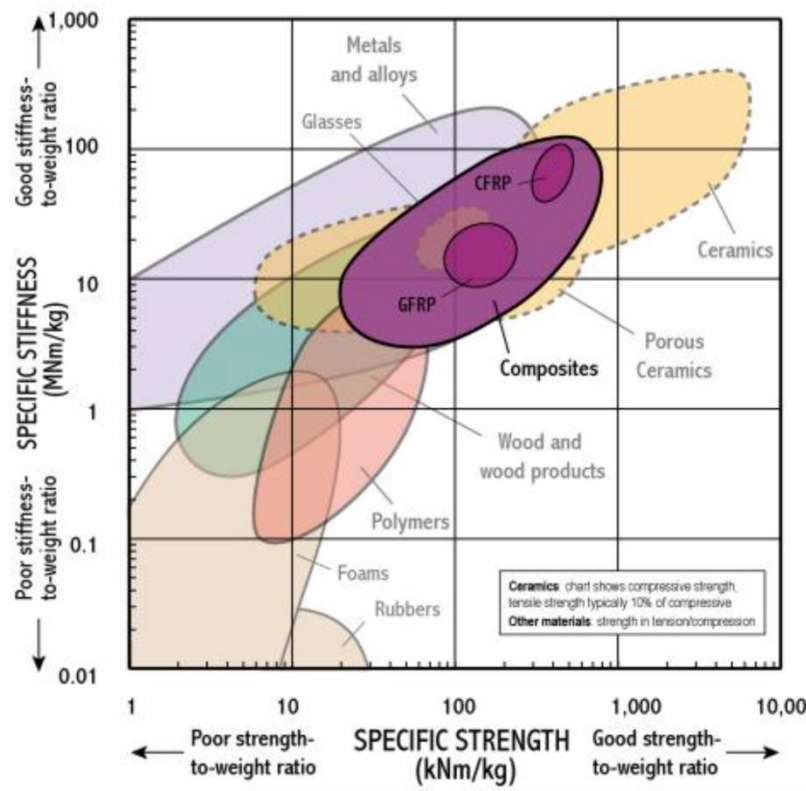


Figure 1.1. Specific stiffness and strength ranges for common engineering materials [1].

Fiber-reinforced composites are inherently anisotropic, strongest along the fiber direction and comparatively weak in the other directions. Fiber length also affects mechanical properties, as longer “continuous” fibers make a composite material relatively stiffer and stronger along the fiber

direction. These factors make composite material properties highly sensitive to manufacturing processes, as illustrated in Figure 1.2.

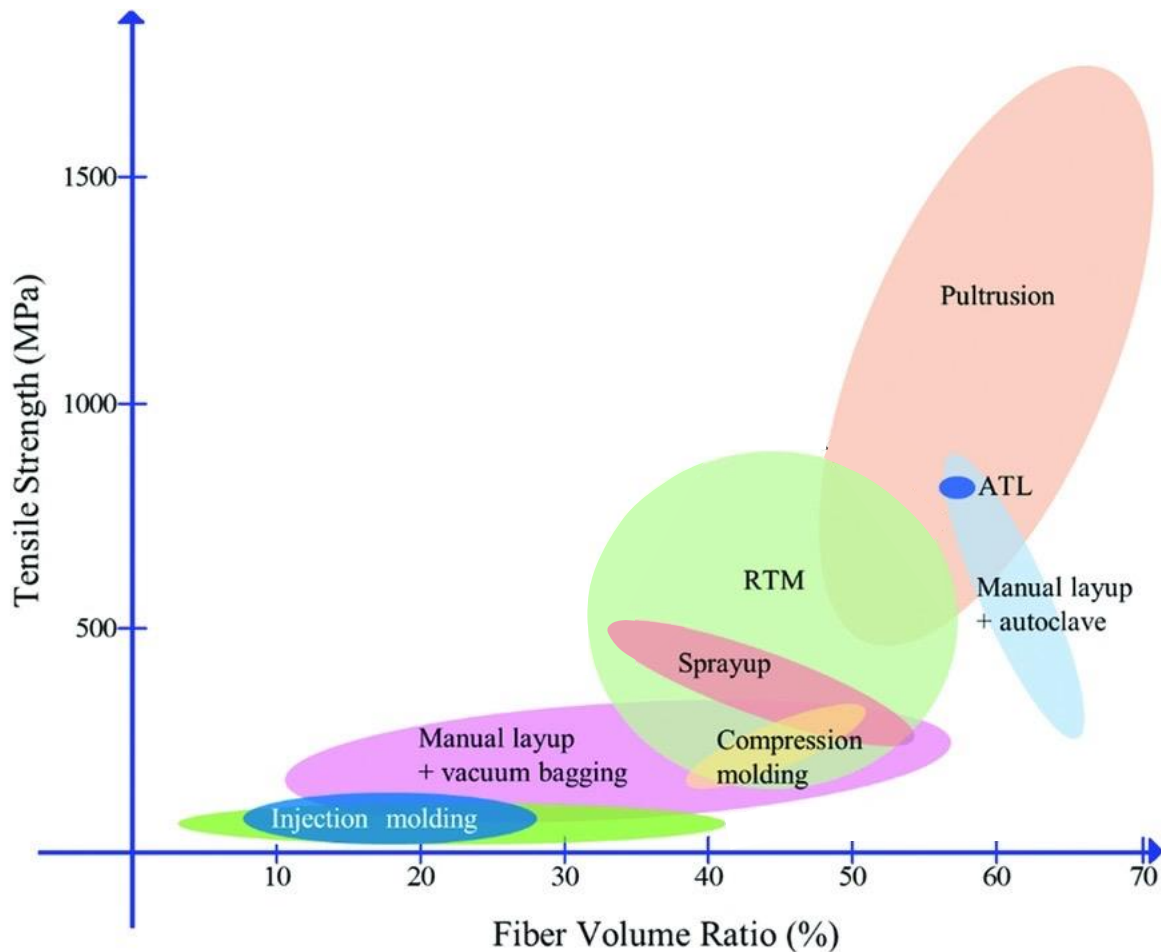


Figure 1.2. Composite tensile strength ranges by processing method [2].

Processes that can achieve high fiber alignment, high fiber content, and low void content, such as pultrusion, can result in composites with superior mechanical properties along the fiber direction. However, these processes typically require long cycle times, extensive energy use, or both, to achieve the high compaction pressures necessary to efficiently consolidate the composites. At the other end of the scale, mechanical properties are sacrificed in favor of other advantages such as rapid processing, as with injection molding, or flexible manufacture, as with additive manufacture. These manufacturing techniques necessarily involve short reinforcement fibers, which offer relatively poor mechanical properties.

Therefore, there is great opportunity in combining the low cycle times of high-rate methods with the high stiffness and strength of unidirectional composites.

## 1.2 State of the Composites Industry

The global composites industry accounted for \$71.1 billion in 2020 and is forecast to almost double to \$128.8 billion by 2028 [3]. Though composite use has traditionally been dominated by the aerospace industry, aerospace growth has slowed while significant growth is predicted in other industries. These areas of growth include traditionally high-volume, cost-driven areas such as the automotive and commodity sporting goods industries, a trend illustrated for carbon fibers in Figure 1.3.

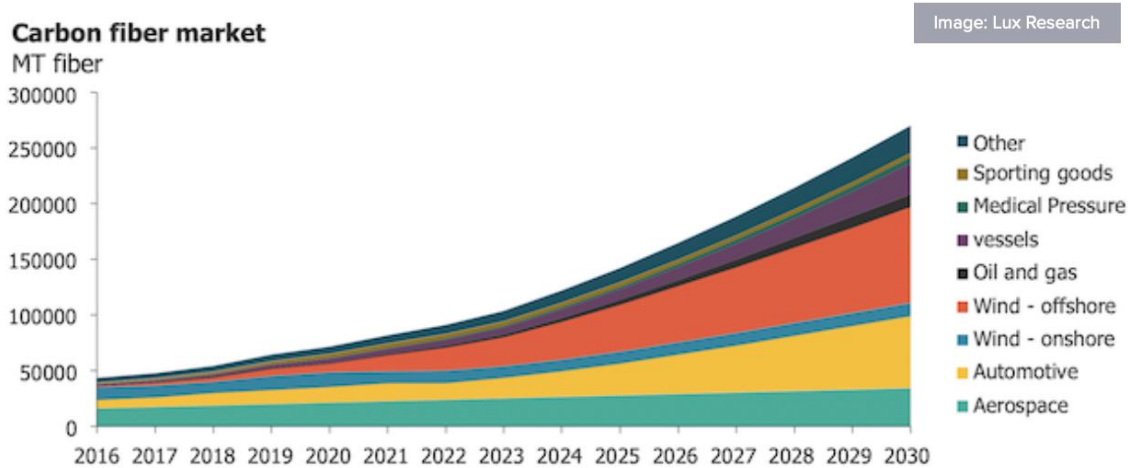


Figure 1.3. Predicted carbon fiber market growth by industry through 2030 [4].

In the United States, new regulations continue to reduce the allowable emissions for newly manufactured vehicles, as illustrated in Figure 1.4. Emissions may be reduced via vehicle weight reduction, as a lighter vehicle requires less energy to operate. Composite materials allow for significant weight reduction without losses in mechanical properties such as stiffness and strength. For the EV market the weight reduction is essential for an increase in driving range and thereby the consumer attractiveness. On average, glass fiber reinforced composites can reduce vehicle weight by 25-35%, while carbon fiber reinforced composites can reduce weight by 50-70% [5].

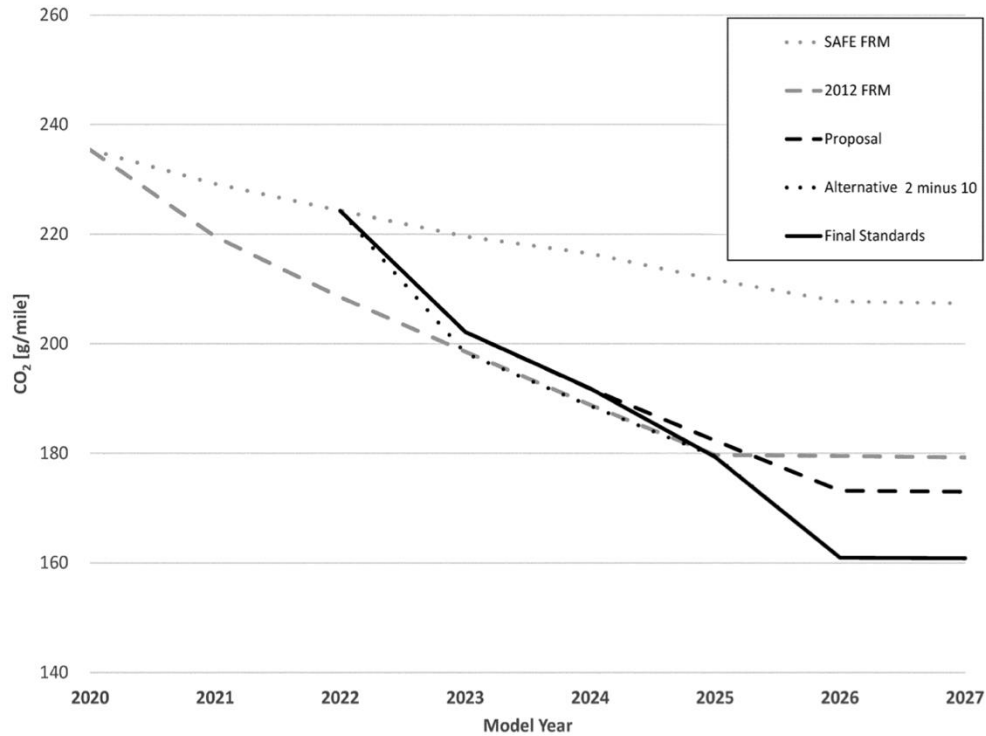


Figure 1.4. New United States regulations (solid black line) for CO<sub>2</sub> emissions in passenger cars produced through 2027 [6].

Although carbon fibers can be “environmentally costly” to produce, the benefits of lightweighting typically outweigh the costs, especially when a lifetime of vehicle emissions are considered [7]. Glass fiber reinforced composites also offer a compromise—although the weight savings are less than they are with carbon fibers, they have a lower carbon footprint to produce.

Recycling carbon fibers offers an avenue to reduce emissions, as the recycling process uses significantly less energy than virgin carbon fiber production [8]. Recycling offers a solution for residual material from composite production processes, as well as end of service life parts.. Further, some regulation agencies require that some minimum amount of material in new vehicles be recycled, and recycled carbon fibers offer a way to meet these goals while improving fuel efficiency via lightweighting.

In order to be effectively used in automotive applications, composite materials must be able to be produced rapidly and inexpensively. Traditional composite manufacturing methods involve a large degree of manual labor and typically have long cycle times, and therefore do not

scale to high-volume processes. New material systems and manufacturing methods must be developed to make composite production viable.

### **1.3 Advanced Manufacturing**

As demand for composites increases, accompanied by their adoption into increasingly diverse industries, advanced manufacturing techniques are required to meet more challenging target production volumes and cost limits. These manufacturing methods often involve advanced materials and may incorporate two or more material forms in order to exploit the beneficial properties of the constituent components. Advanced manufacturing processes allow for formation of complex parts in a single processing step, eliminating the need for additional joining processes and the associated weak spots.

Examples of these advanced manufacturing processes include high-rate resin transfer molding (RTM) and hybrid injection molding. RTM involves the infiltration of low viscosity resin, typically a thermoset such as epoxy, into a fiber bed to create complex part geometries. This fiber bed may be modified to include a thermoplastic phase, such as polyamide, which can improve the part toughness without increasing cycle time. Hybrid injection molding describes the process of injection molding structural rigidity onto a continuous fiber reinforcement. A thermoplastic-reinforced preform with a thermoplastic elastomer (TPE) overmolded structure can result in parts that benefit from the high strength of the preform and the energy absorption of the TPE.

#### **1.3.1 High-Rate Resin Transfer Molding**

Resin transfer molding (RTM) describes the process in which a resin is driven through reinforcement fiber-beds to create a composite part. It is typically performed with thermosetting resins, as the relatively low viscosity enables a favorable infiltration of the fiber-bed. The resin must then cure in-situ, either under ambient conditions or at elevated temperatures and pressures. Traditional thermosetting resins require long cycle times, on the order of 10 to 15 minutes (not including fiber-bed preparation), to ensure full resin impregnation and cure.

High-pressure RTM (HP-RTM) utilizes elevated pressure in the range of 100-150bar to drive the resin into the fiber bed, allowing total impregnation in a matter of seconds. Fast-curing resins can bring cycle times down further, allowing in extreme cases for completed parts in 1.5-5

minutes (not including fiber-bed preparation) [9]. The process can also be fully automated, which also assists in high-rate manufacturing.

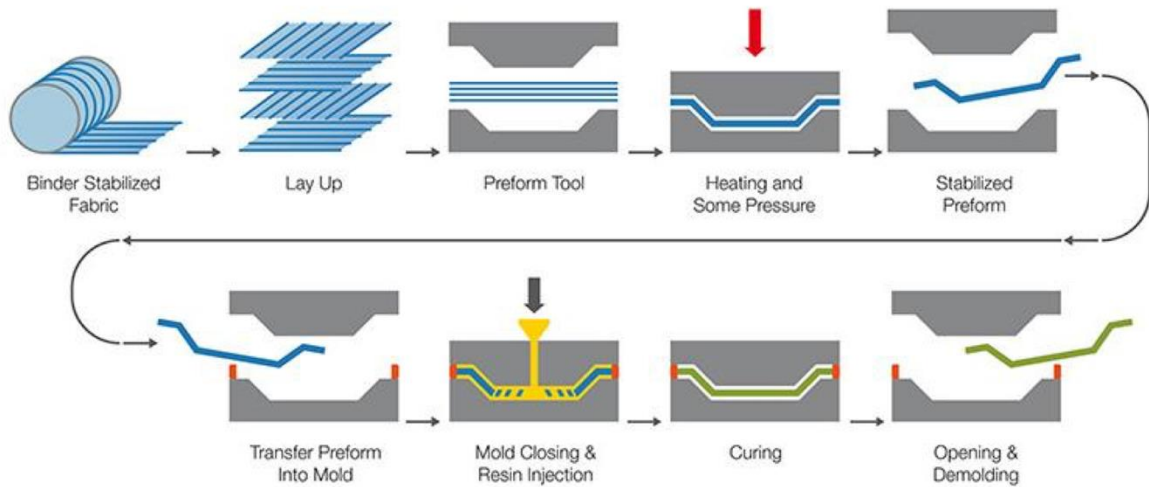


Figure 1.5. RTM manufacturing process schematic. From [10].

HP-RTM is already used for several automotive applications, which tend to have higher production volumes than aerospace applications [11]–[13]. BMW has used HP-RTM in production of roof and side panels, finding that the ability to rapidly manufacture complex parts with limited variability reduced their production costs by 50%. Volkswagen used a thermoplastic RTM process to create b-pillar reinforcements, utilizing a resin with a 2-3 minute polymerization reaction time to rapidly manufacture these high-strength parts [13].

Compression RTM (CRTM) relies on compression force to mechanically drive the resin into the fiber bed. Typically, the mold is partially closed and resin is flowed in at low pressure, where it sits on the surface of the preform. When the mold is fully closed, the closing clamp force pushes the resin through the thickness of the preform. CRTM can also reach high production rates as the infiltration time is greatly reduced—the resin only has to flow through the thickness, typically on the order of millimeters, rather than transversely through the fiber bed.

Comparisons between traditional RTM, HP-RTM, and CRTM conclude that the HP-RTM results in higher carbon footprint, due to the high pressures needed for processing and the production of the heavy-duty aluminum molds required to withstand the high injection pressures [14]. For a given resin system and mold, researchers found that the fill time for RTM was three times longer than the fill time for HP-RTM, which in turn was five times longer than the fill time

for CRTM [15]. Because the resin system and part geometry were identical, differences in cycle time were dominated by these differences in fill time. The CRTM process resulted in the lowest cost per part, as fewer machines were required to reach target production volumes due to the low cycle time.

Thermoplastic RTM (T-RTM) is another developing application of RTM technology [16], [17]. Thermoplastic matrices offer enhanced toughness, processability, and recyclability compared to thermosets, but traditional thermoplastic resins are too viscous to effectively infiltrate fiber beds during an RTM cycle. T-RTM utilizes low-viscosity monomers to flow through the fibers, followed by in-situ polymerization. Polyamide (PA) is a promising candidate for T-RTM, as it polymerizes at moderate temperatures (130-180°C) and converts relatively quickly, in the range of 2-5 minutes [18]–[20]. Further development is required, as T-RPM processes currently suffer from difficulties in homogeneous and controlled polymerization as well as issues related to residual water and low-molecular weight species interfering with the polymerization process.

Thermoplastics can also be used to toughen composites based on thermoset-matrices. Thermoplastic phases have been introduced in a variety of ways, including as fine particles bonded to the interlayers of the carbon fiber preform [21] and as a dip coating over the surface of the fiber preform [22]. In cases where the thermoplastic reinforcement is added as a second phase, it is important to ensure adequate bonding to the preform fibers to eliminate movement or washout of the thermoplastic as the thermoset advances. The mold is typically heated during RTM processes to facilitate resin cure, but a heated mold has the added benefit of increasing polymer chain mobility in the thermoplastic, which may enhance bonding between the thermoset and the thermoplastic phases.

Advances in RTM processes, including HP-RTM, C-RTM, and T-RTM, allow for increased processing versatility with decreased cycle times that make RTM a viable method to create complex parts with high production volumes. Increased customization is possible with the introduction of other materials, such as thermoplastics, into the fiber preform.

### **1.3.2 Hybrid Injection Molding**

Injection molding is another polymer manufacturing process that can create complex parts with low cycle times. Unlike RTM, however, injection molding is traditionally performed with thermoplastics. Polymer pellets are melted in a heated barrel with a rotating screw to facilitate



uniform melting. During molding, the screw rams forward to push molten polymer into a mold cavity, where the polymer cools sufficiently to be de-molded without causing damage or deformation. Cycle times are very low, typically on the order of one minute or less. Additionally, short glass or carbon reinforcement fibers can be added to the polymer pellets to improve the stiffness and strength of the material.

Injection overmolding describes the process of injection molding one material onto another. It can be divided into two main categories—multi-material injection molding and insert injection molding. Multi-material injection molding, illustrated schematically in Figure 1.6, involves the injection of a first material, followed immediately by the injection of a second material onto the first material, which is often still molten. Though this process requires both materials to be injection moldable, it allows for rapid part manufacture in a single step, reducing the cost and part variability that come from two distinct processes. Further, the back-to-back processing steps mean that the first material injected may still be molten during the injection of the second material, which may improve adhesion between the two phases.

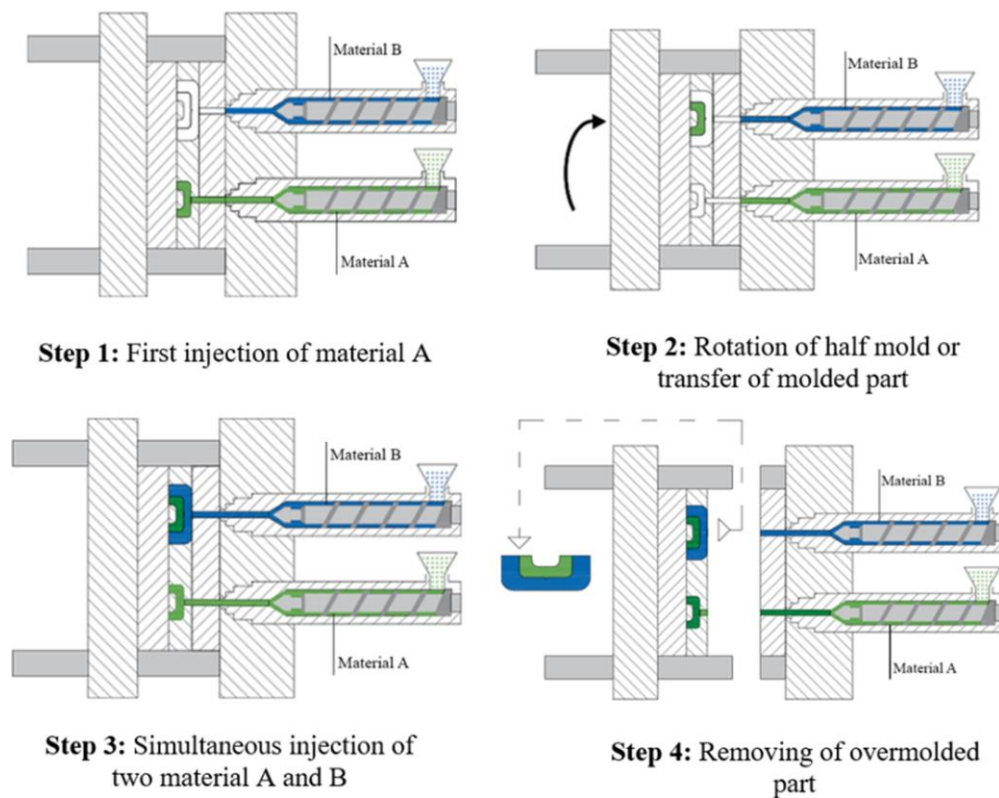


Figure 1.6. Schematic of multi-material injection molding process. From [23].

Insert injection molding, illustrated in Figure 1.7, involves placing a previously manufactured part into the mold cavity to be injection molded onto. This process allows for a greater variety of substrate materials, as the substrate does not need to be injection moldable and can therefore include stronger and more complex reinforcements such as metals and continuous fiber-reinforced composites and fabrics. This process also allows for surface treatments to be introduced to improve compatibility between the substrate and the overmold. However, insert injection molding requires two distinct processing steps to produce the two phases, which may prove economically infeasible.

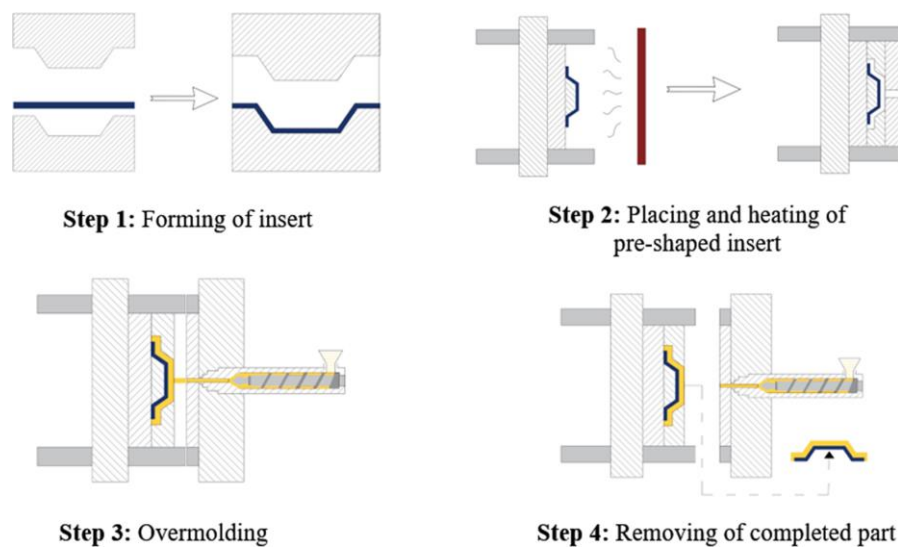


Figure 1.7. Schematic of the insert overmolding process. From [23].

A schematic of the insert overmolding process is shown in Figure 1.7. Step 1, the forming of the insert, can occur in multiple ways including compression molding, traditional composite layup, or smart preform production, which will be discussed in section 1.3.3. This forming can happen in then injection mold immediately before overmolding or in a separate process. Step 2, preheating the insert, will tend to improve the adhesion between the overmolding material and the insert, but is optional.

For injection overmolding processes, material compatibility is crucial and can be improved via a variety of different methods. The simplest is to select miscible materials, [24]–[27]. However, if this is impractical for a given application, materials can be selected for their ability to develop covalent bonds across the interface, or one of the materials may be grafted with a compatibilizer

that can covalently bond across the interface[28], [29]. Beyond material selection, processing conditions can be adjusted to improve interfacial bonding. Several researchers have determined the interfacial temperature during overmolding to be the most important factor controlling bonding between thermoplastic components in an overmolding process [30]–[33]. An elevated temperature may allow local melting of the substrate, allowing improved molecular motion and interdiffusion over the interface. Adhesion may be further improved if the processing conditions are exploited to allow cross-interface crystallization [34], [35].

Injection overmolding is an effective way to produce hybrid parts from thermoplastic materials with low cycle times. The insert overmolding process allows for overmolding onto a wider variety of materials, including metals, composite fabrics, and unidirectional composites, which can provide improved mechanical properties beyond those possible with short fiber reinforced injection molding thermoplastics. This molding technique is often referred to as hybrid injection molding when continuous fiber substrates are used.

### **1.3.3 Advanced Preform Production**

The use of continuous fiber preforms allows for selective reinforcement only where it will be most beneficial to a structure. This limits costs and waste associated with the more expensive continuous fibers. New manufacturing technologies enable rapid production of complex skeletal geometries that can be subsequently used to create completed parts via processes such as RTM or hybrid injection molding.

Filament winding involves wrapping a continuous fiber prepreg tow around a mold or jig, often in a fully automated process using a robot to precisely place the prepreg tow. Structures are typically made from thermoplastic tows, as they may be melted to facilitate forming and surface melting during secondary processing may improve adhesion between the tow and the surrounding material. However, tows with thermoset matrices may also be used [36].

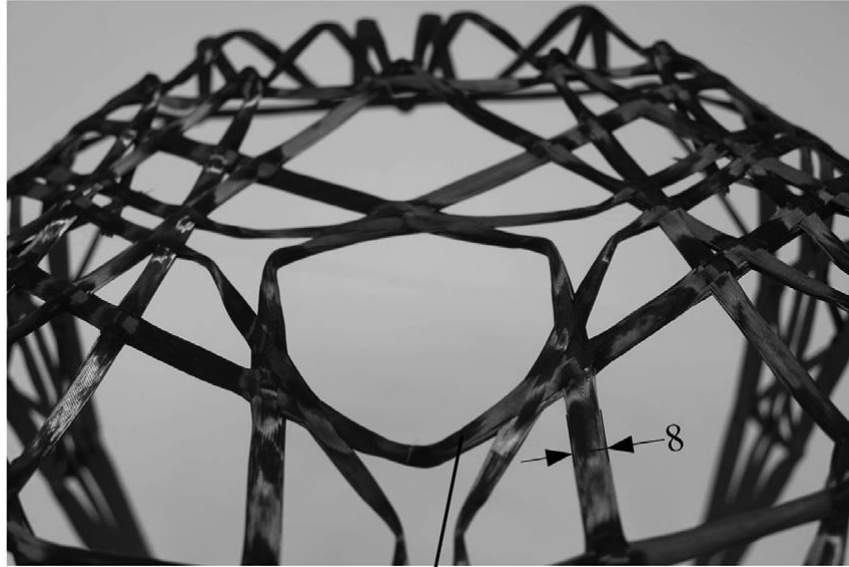


Figure 1.8. Example of a 3D filament-found truss structure, from [36].

Advanced preforms can also be made using the process illustrated in Figure 1.9, where a pre-impregnated (prepreg) thermoplastic composite tape is preheated in an oven and then fed through a heated robotic head. The prepreg is wrapped around a custom jig on a motorized table to create a continuous fiber-reinforced preform.

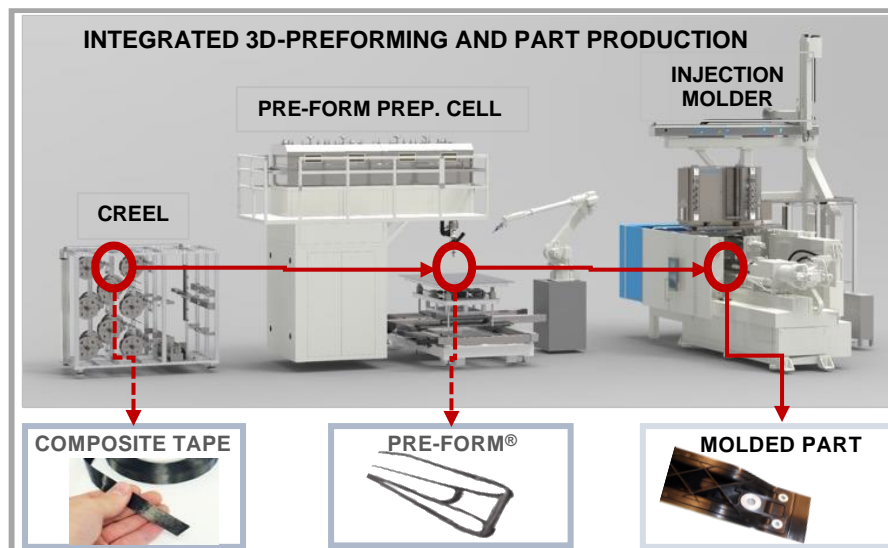


Figure 1.9. Overview of high-rate fiber forming process.

Early research has found that a continuous fiber preform can result in huge improvements to failure load[37]–[39]. Additionally, the overmolding material is crucial for energy transfer, as it prevents premature part failure due to brittle matrix failure in the tow [38]. Increasing the thickness of the preform is another method to make the system more robust, as it introduces redundancy that comes with a higher number of reinforcement fibers [40].

3D printing technology can also be modified to incorporate continuous fiber reinforcement [2], [41]–[45]. This may be accomplished with either a dual nozzle method in which the polymer filament and continuous fiber are fed through two different nozzles, or a coaxial extrusion method in which the fiber reinforcement is combined with melted filament before extrusion [45]. In both methods, there may be fiber- and resin-rich regions and inconsistent extrusion diameters, indicating that further research is needed into process refinement.



Figure 1.10. Complex structural preforms made from 3D printing with continuous fibers [43].

Early research on 3D printing with continuous fiber reinforcement has shown the benefit of the fibers on tensile and flexural strength along the fiber direction [45]. These features can be exploited in the manufacture of complex preforms, such as those shown in Figure 1.10.

Additive manufacture of continuous fiber materials can also be used to create custom fabrics, as shown in Figure 1.11 [44]. Such fabrics benefit from a higher degree of inter-layer properties than traditional 3D printed materials. They also allow for more customizability than commercial composite fabrics, as they can be printed to the desired part shape and with features

such as holes for subsequent attachment to other parts. This improves part mechanical properties and reduces scrap waste.

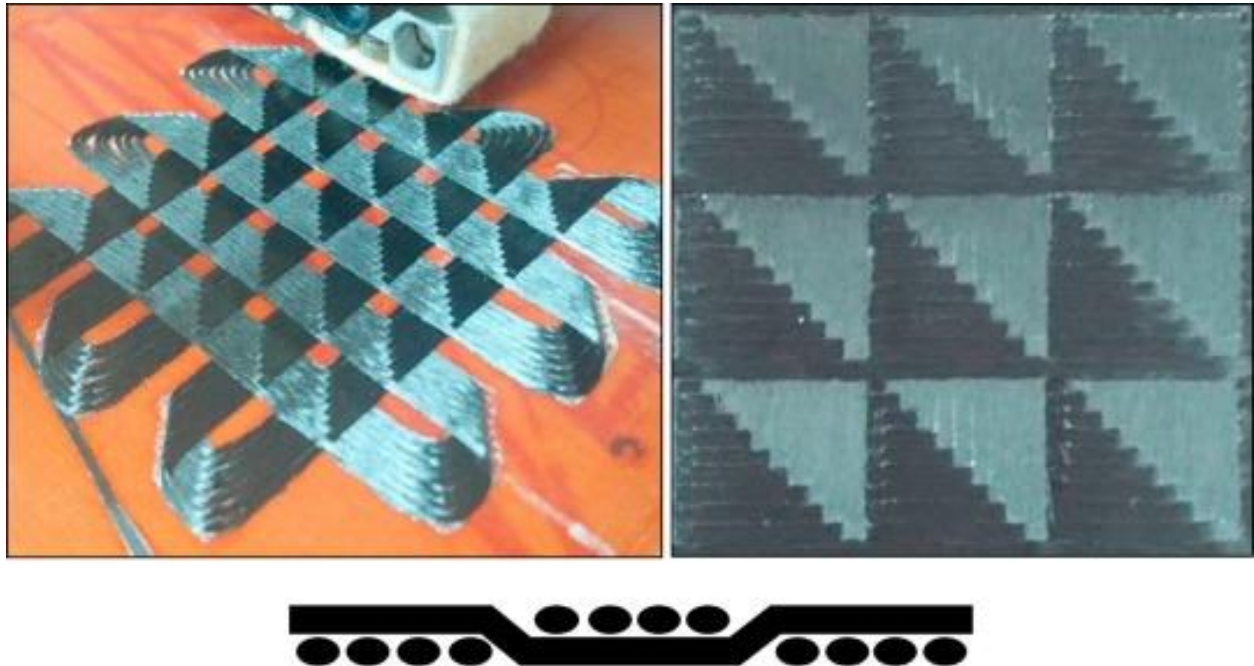


Figure 1.11. Custom fabric created via additive manufacture of continuous fiber-reinforced polymer. From Dickson et al [44].

Additive manufacturing of continuous fiber preforms offers a high degree of manufacturing flexibility. Since molds are not required, new and complex preform geometries can easily be created. Since fibers are only placed where they are needed, cycle times can remain low and material waste is limited. This makes smart preforms a viable way to improve the mechanical properties of a complex, rapidly-manufactured part.

## 1.4 Thesis Overview

Traditional materials science involves developing an understanding of the process-structure-property relationship of a given material system. This is typically done for basic, lab-scale processes and part geometries to limit the influence of competing factors on part properties. In order for new material systems and processes to be used in manufacturing systems, lab-scale knowledge must be expanded/scaled to consider the relationship between manufacturing, design,



and performance. In this broader view, manufacturing includes not only material considerations such as level and time dependent rates of temperature and pressures, but it also includes considerations such as machine limitations and cycle time. Design considers the part geometry but also its manufacturability. Part performance includes economic factors such as material and manufacturing cost, as well as traditional material properties. In summary, development of a manufacturing-design-performance relationship requires an understanding of the process-structure-property relationship, as well as the end use of a material system.

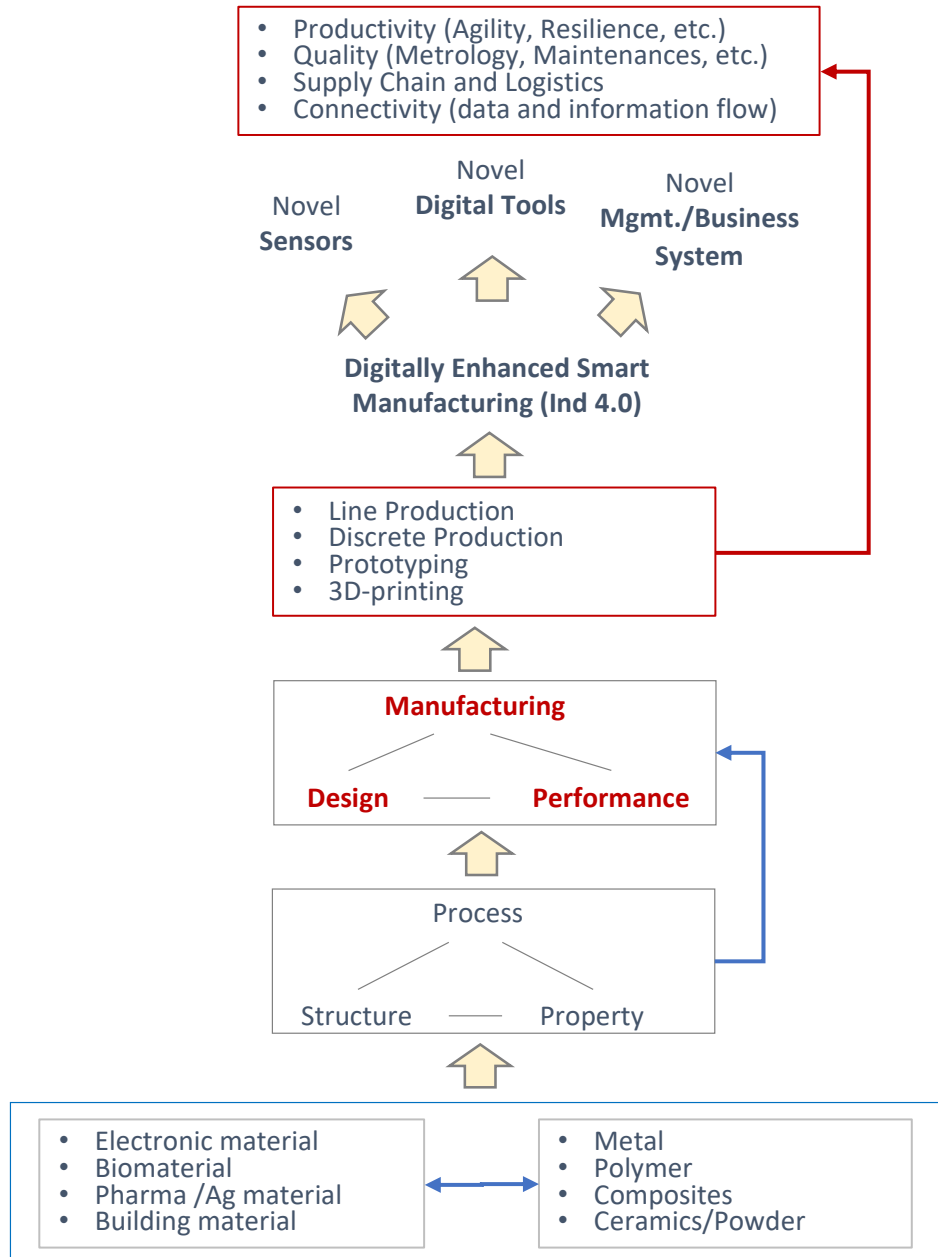


Figure 1.12. Scale-up of knowledge from traditional materials science through advanced manufacturing.



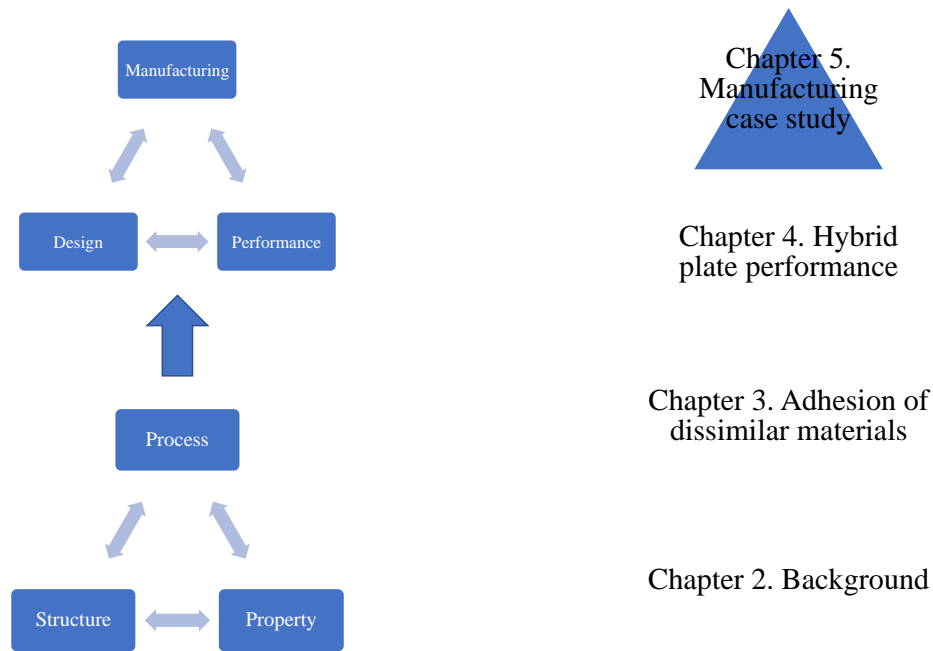


Figure 1.13. Dissertation logic flow, from foundation to manufacturing-informed case study.

This dissertation examines the effect of manufacturing and design on performance for hybrid composite structures, focusing on scale-up of lab-scale composites knowledge to develop industrial recommendations that consider the practicalities of real manufacturing. In service of this, Chapter 2 provides a critical literature review of hybrid material systems including epoxy/polyamide, polyamide/thermoplastic elastomer, and polymer/aluminum. This existing data from lab-scale research provides a foundation grounded in materials science fundamentals. The selection of these three diverse material systems provides a broad lens through which to explore the topic, from which some common threads can be extracted.

Chapter 3 builds on the principles explored in Chapter 2 to develop macro-scale toughening of a composite part. Chapter 2 demonstrates the importance of interfacial adhesion between dissimilar materials on energy transfer in a hybrid composite part, so this section characterizes the factors that affect that adhesion. A simplified flat plate geometry and compression molding process are used to determine how realistic and actionable changes to a manufacturing process affect interfacial adhesion between dissimilar materials.

Chapter 4 uses the same simplified manufacturing and geometry used in Chapter 3 to examine the effect of manufacturing-controlled changes to interfacial adhesion on mechanical

performance. Crash performance was selected as the mechanical behavior of interest, because all of the material combinations used here combine one more ductile material for energy absorption and one stronger one to provide structural support. Although this section still uses a simplified part geometry, design considerations begin to play a role as relative material placement becomes important for performance.

Finally, Chapter 5 synthesizes the work of the previous chapters to explore how the simplified systems compare to real-world manufacturing, and if lab-scale experimentation can be used to adequately characterize more complex manufacturing and part geometries. This chapter also includes a technical cost model to assess the viability of the process., as well as to understand the financial cost of changes to the manufacturing process.

## 1.5 References

- [1] “Specific stiffness - Specific strength.” [http://www-materials.eng.cam.ac.uk/mpsite/interactive\\_charts/spec-spec/basic.html](http://www-materials.eng.cam.ac.uk/mpsite/interactive_charts/spec-spec/basic.html) (accessed Mar. 21, 2022).
- [2] G. D. Goh, Y. L. Yap, S. Agarwala, and W. Y. Yeong, “Recent Progress in Additive Manufacturing of Fiber Reinforced Polymer Composite,” *Advanced Materials Technologies*, vol. 4, no. 1, p. 1800271, Jan. 2019, doi: 10.1002/ADMT.201800271.
- [3] “2021 Statistics: U.S. and Global Composite Materials Market.” <https://www.globenewswire.com/news-release/2021/12/13/2350524/0/en/2021-Statistics-U-S-and-Global-Composite-Materials-Market-Will-Surpass-128-82-Billion-at-7-52-CAGR-Growth-Vantage-Market-Research-VMR.html> (accessed Mar. 20, 2022).
- [4] “CFRP Market at \$64 Billion by 2030.” <https://www.plasticstoday.com/composites/cfrp-market-64-billion-2030> (accessed Mar. 20, 2022).
- [5] “Lightweight Materials for Cars and Trucks | Department of Energy.” <https://www.energy.gov/eere/vehicles/lightweight-materials-cars-and-trucks> (accessed Mar. 19, 2022).
- [6] “ENVIRONMENTAL PROTECTION AGENCY 40 CFR Parts 86 and 600 Revised 2023 and Later Model Year Light-Duty Vehicle Greenhouse Gas Emissions Standards”, Accessed: Mar. 19, 2022. [Online]. Available: <http://www.regulations.gov>

- [7] J. C. Kelly, J. L. Sullivan, A. Burnham, and A. Elgowainy, "Impacts of Vehicle Weight Reduction via Material Substitution on Life-Cycle Greenhouse Gas Emissions," *Environmental Science and Technology*, vol. 49, no. 20, pp. 12535–12542, Oct. 2015, doi: 10.1021/ACS.EST.5B03192.
- [8] R. A. Witik, R. Teuscher, V. Michaud, C. Ludwig, and J. A. E. Månson, "Carbon fibre reinforced composite waste: An environmental assessment of recycling, energy recovery and landfilling," *Composites Part A: Applied Science and Manufacturing*, vol. 49, pp. 89–99, Jun. 2013, doi: 10.1016/J.COMPOSITESA.2013.02.009.
- [9] P. K. Mallick, "Thermoset matrix composites for lightweight automotive structures," *Materials, Design and Manufacturing for Lightweight Vehicles*, pp. 229–263, Jan. 2021, doi: 10.1016/B978-0-12-818712-8.00006-9.
- [10] A. Ahmadova, "Numerical Modelling of porosity generation, movement, and compaction during the RTM process," 2018. Accessed: Mar. 15, 2022. [Online]. Available: <https://www.researchgate.net/publication/331330329>
- [11] "HP-RTM on the rise | CompositesWorld." <https://www.compositesworld.com/articles/hp-rtm-on-the-rise> (accessed Mar. 15, 2022).
- [12] C. Fais, "Lightweight automotive design with HP-RTM," *Reinforced Plastics*, vol. 55, no. 5, pp. 29–31, Sep. 2011, doi: 10.1016/S0034-3617(11)70142-4.
- [13] M. Bitterlich, "Tailored to Reactive Polyamide 6," *Kunststoffe International*, pp. 47–51, 2014.
- [14] A. Vita, V. Castorani, M. Germani, and M. Marconi, "Comparative life cycle assessment of low-pressure RTM, compression RTM and high-pressure RTM manufacturing processes to produce CFRP car hoods," *Procedia CIRP*, vol. 80, pp. 352–357, 2019, doi: 10.1016/J.PROCIR.2019.01.109.
- [15] M. Baskaran *et al.*, "MANUFACTURING COST COMPARISON OF RTM, HP-RTM AND CRTM FOR AN AUTOMOTIVE ROOF," pp. 22–26, 2014.
- [16] T. Ageyeva, I. Sibikin, and J. G. Kovács, "A Review of Thermoplastic Resin Transfer Molding: Process Modeling and Simulation," *Polymers 2019, Vol. 11, Page 1555*, vol. 11, no. 10, p. 1555, Sep. 2019, doi: 10.3390/POLYM11101555.

- [17] C. Gomez, D. Salvatori, B. Caglar, R. Trigueira, G. Orange, and V. Michaud, “Resin Transfer molding of High-Fluidity Polyamide-6 with modified Glass-Fabric preforms,” *Composites Part A: Applied Science and Manufacturing*, vol. 147, p. 106448, Aug. 2021, doi: 10.1016/J.COMPOSITESA.2021.106448.
- [18] R. W. Hillermeier and J. C. Seferis, “Interlayer toughening of resin transfer molding composites,” *Composites Part A: Applied Science and Manufacturing*, vol. 32, no. 5, pp. 721–729, May 2001, doi: 10.1016/S1359-835X(00)00088-9.
- [19] Z. Wu, X. S. Yi, and A. Wilkinson, “Interlaminar fracture toughness of carbon fibre/RTM6-2 composites toughened with thermoplastic-coated fabric reinforcement,” *Composites Part B: Engineering*, vol. 130, pp. 192–199, Dec. 2017, doi: 10.1016/J.COMPOSITESB.2017.08.003.
- [20] N. Aliyeva, H. S. Sas, and B. Saner Okan, “Recent developments on the overmolding process for the fabrication of thermoset and thermoplastic composites by the integration of nano/micron-scale reinforcements,” *Composites Part A: Applied Science and Manufacturing*, vol. 149, p. 106525, Oct. 2021, doi: 10.1016/J.COMPOSITESA.2021.106525.
- [21] L. M. Arzondo *et al.*, “Sequential injection overmolding of an elastomeric ethylene-octene copolymer on a polypropylene homopolymer core,” *Polymer Engineering and Science*, 2004, doi: 10.1002/pen.20216.
- [22] M. v. Candal, A. Gordillo, O. O. Santana, and J. J. Sánchez, “Study of the adhesion strength on overmoulded plastic materials using the essential work of interfacial fracture (EWIF) concept,” *Journal of Materials Science*, vol. 43, no. 15, pp. 5052–5060, Aug. 2008, doi: 10.1007/S10853-008-2667-1/FIGURES/10.
- [23] J. Qiu, A. Tsuboi, K. Izumi, H. Wu, S. Guo, and Y. Huang, “Effects of interfacial morphology on the welding strength of injection-molded polyamide,” *Polymer Engineering and Science*, vol. 47, no. 12, pp. 2164–2171, Dec. 2007, doi: 10.1002/PEN.20950.
- [24] A. M. Harte and J. F. Mc Namara, “Overinjection of thermoplastic composites: I. Processing and testing of components,” *Journal of Materials Processing Technology*, vol. 182, no. 1–3, pp. 12–20, Feb. 2007, doi: 10.1016/J.JMATPROTEC.2006.06.016.

- [25] G. Jiang, W. U. Hong, Y. A. N. Bowen, G. U. O. Shaoyun, and J. Huang, “Reinforcement of solid-melt interfaces for semicrystalline polymers in a sequential two-staged injection molding process,” *Journal of Polymer Science, Part B: Polymer Physics*, vol. 47, no. 11, pp. 1112–1124, Jun. 2009, doi: 10.1002/POLB.21719.
- [26] J. E. Bidaux, G. D. Smith, N. Bernet, J. A. E. Månson, and J. Hilborn, “Fusion bonding of maleic anhydride grafted polypropylene to polyamide 6 via in situ block copolymer formation at the interface,” *Polymer*, vol. 37, no. 7, pp. 1129–1136, 1996, doi: 10.1016/0032-3861(96)80839-1.
- [27] C. J. G. Plummer, P. E. Bourban, J. E. Zanetto, G. D. Smith, and J. A. E. Månson, “Nonisothermal fusion bonding in semicrystalline thermoplastics,” *Journal of Applied Polymer Science*, vol. 87, no. 8, 2002, doi: 10.1002/app.11528.
- [28] G. D. Smith, C. J. G. Plummer, P.-E. Bourban, and J.-A. E. Månson, “Non-isothermal fusion bonding of polypropylene,” *Polymer*, vol. 42, pp. 6247–6257, 2001, [Online]. Available: [www.elsevier.nl/locate/polymer](http://www.elsevier.nl/locate/polymer)
- [29] R. Giusti and G. Lucchetta, “Modeling the adhesion bonding mechanism in overmolding hybrid structural parts for lightweight applications,” in *Key Engineering Materials*, 2014, vol. 611–612, pp. 915–921. doi: 10.4028/www.scientific.net/KEM.611-612.915.
- [30] R. Akkerman, M. Bouwman, and S. Wijskamp, “Analysis of the Thermoplastic Composite Overmolding Process: Interface Strength,” *Frontiers in Materials*, vol. 7, p. 27, Feb. 2020, doi: 10.3389/FMATS.2020.00027/BIBTEX.
- [31] R. Chandran, C. J. G. Plummer, P. E. Bourban, and J. A. E. Månson, “Morphology and interfacial strength of nonisothermally fusion bonded hard and soft thermoplastics,” *Polymer Engineering & Science*, vol. 58, no. S1, pp. E82–E92, May 2018, doi: 10.1002/PEN.24662.
- [32] S. Yamaguchi, Y. W. Leong, T. Tsujii, M. Mizoguchi, U. S. Ishiaku, and H. Hamada, “Effect of crystallization and interface formation mechanism on mechanical properties of film-insert injection-molded poly(propylene) (PP) film/PP substrate,” *Journal of Applied Polymer Science*, vol. 98, no. 1, pp. 294–301, Oct. 2005, doi: 10.1002/APP.21590.

- [33] P. Bauer, Y. N. Becker, N. Motsch-Eichmann, K. Mehl, I. Müller, and J. Hausmann, “Hybrid thermoset-thermoplastic structures: An experimental investigation on the interface strength of continuous fiber-reinforced epoxy and short-fiber reinforced polyamide 6,” *Composites Part C: Open Access*, vol. 3, p. 100060, Nov. 2020, doi: 10.1016/J.JCOMC.2020.100060.
- [34] B. Beck, H. Tawfik, J. Haas, Y.-B. Park, and F. Henning, “Automated 3D Skeleton Winding Process for Continuous-Fiber-Reinforcements in Structural Thermoplastic Components,” *Advances in Polymer Processing 2020*, pp. 150–161, 2020, doi: 10.1007/978-3-662-60809-8\_13.
- [35] V. Heinzle, T. Huber, F. Henning, and P. Elsner, “Process development of injection molded parts with wound fiber structures for local reinforcement,” *AIP Conference Proceedings*, vol. 1593, pp. 736–740, 2014, doi: 10.1063/1.4873882.
- [36] T. Botzkowski, S. Galkin, S. Wagner, S. P. Sikora, and L. Kärger, “Experimental and numerical analysis of bolt-loaded open-hole laminates reinforced by winded carbon rovings,” *Composite Structures*, vol. 141, pp. 194–202, May 2016, doi: 10.1016/J.COMPSTRUCT.2016.01.057.
- [37] J. Haas, O. N. Hassan, B. Beck, L. Kärger, and F. Henning, “Systematic approach for finite element analysis of thermoplastic impregnated 3D filament winding structures – General concept and first validation results,” *Composite Structures*, vol. 268, p. 113964, Jul. 2021, doi: 10.1016/J.COMPSTRUCT.2021.113964.
- [38] R. Matsuzaki *et al.*, “Three-dimensional printing of continuous-fiber composites by in-nozzle impregnation,” *Scientific Reports 2016 6:1*, vol. 6, no. 1, pp. 1–7, Mar. 2016, doi: 10.1038/srep23058.
- [39] C. Oztan *et al.*, “Microstructure and mechanical properties of three dimensional-printed continuous fiber composites:,” <https://doi.org/10.1177/0021998318781938>, vol. 53, no. 2, pp. 271–280, Jul. 2018, doi: 10.1177/0021998318781938.
- [40] Z. Hou, X. Tian, J. Zhang, and D. Li, “3D printed continuous fibre reinforced composite corrugated structure,” *Composite Structures*, vol. 184, pp. 1005–1010, Jan. 2018, doi: 10.1016/J.COMPSTRUCT.2017.10.080.

- [41] A. N. Dickson, K. A. Ross, and D. P. Dowling, “Additive manufacturing of woven carbon fibre polymer composites,” *Composite Structures*, vol. 206, pp. 637–643, Dec. 2018, doi: 10.1016/J.COMPSTRUCT.2018.08.091.
- [42] S. M. F. Kabir, K. Mathur, and A. F. M. Seyam, “A critical review on 3D printed continuous fiber-reinforced composites: History, mechanism, materials and properties,” *Composite Structures*, vol. 232, p. 111476, Jan. 2020, doi: 10.1016/J.COMPSTRUCT.2019.111476.

## **2. BACKGROUND**

Extensive research has been conducted on various combinations of materials. This chapter provides an in-depth review of this prior work, which serves as a foundation for this thesis. Three main categories of material combinations are explored: epoxy (EP) with Polyamide (PA), PA with Thermoplastic Elastomers (TPE), and aluminum with thermoplastics. Although this chapter is divided into these three sections, there are consistent through-lines that apply to all three types of material combination, including:

- Materials can be combined to form hybrid structures that take advantage of the desirable qualities of both materials.
- Adhesion plays an important role in energy transfer between dissimilar materials
- The addition of a ductile material to a more brittle one can be an effective toughening method, improving energy absorption primarily via debonding and deformation

The literature review primarily served as base when exploring novel approaches for cost-effective hybrid molded composites.

### **2.1 Background: Epoxy/Polyamide Combinations**

Epoxyes are high-strength polymers that have diverse applications in adhesives, coatings, and composites. They are formed from pre-polymers with epoxide end groups (table 1). These groups are highly unstable due to their high ring strain and the polarity of the oxygen molecule[1]. The polymers formed from the crosslinking of these pre-polymers are quite brittle, which can prove detrimental to properties such as damping, fracture toughness, and impact resistance. Therefore, there is great interest in toughening epoxyes through the addition of a second component that can be combined homogeneously with the EP or incorporated as a second phase.

Though PA has properties that make it desirable for toughening epoxyes, there has not been much research on such blends. However, there has been extensive research on toughening epoxyes using other materials, and these blends can still offer insights into the behavior of PA-toughened materials. One of the most common EP-toughening materials is rubber, which is often incorporated into uncured EP in particle form. The rubber particles serve as ductile phases that can absorb



impact energy and inhibit crack growth[2]–[5]. Garg and Mai[6] propose some of the toughening mechanisms in rubber-toughened epoxies based on research done on such systems. They suggest that the particles cavitate while simultaneously promoting shear band growth in the EP. The shear bands grow in response to tensile loads and are arrested by other rubber particles. Garg and Mai also present rubber particle crack bridging as a potential secondary energy absorption mechanism. Though these observations are based on rubber-toughened epoxies, the same toughening mechanisms may also apply to lightly crosslinked EP systems that are toughened with other kinds of particles. However, the primary toughening mechanisms Garg and Mai suggest are incompatible with highly-crosslinked systems, where the matrices are unable to deform or shear.

Bagheri et al[7] find that there is a critical rubber concentration above which the maximum matrix shear deformation does not increase and may even decrease. Particle size is hypothesized to have a minimal effect on matrix toughness—though larger particles are able to bridge across cracks, particle bridging is only a secondary toughening mechanism, so larger particle size does not have a significant impact. One caveat is that the particles must be sufficiently large to interact with the crack tip.

Thermoplastics have also been used to toughen EP resins due to their potential for compatibility with epoxies[8]–[14]. Crystalline thermoplastic regions can absorb energy through deformation of crystalline regions as well as through plastic deformation of the amorphous regions. Hodgkin et al[8] summarize factors that can make specific thermoplastics ideally suited for use as EP toughening agents. They find that generally, an ideal thermoplastic toughening agent will have reactive end groups, a thermally stable backbone that is partially miscible in EP, high molecular weight, and a co-continuous or phase-inverted morphology with EP. Further, in contrast with rubber-toughened systems, epoxies with higher crosslink densities benefit more from thermoplastic toughening than lightly crosslinked systems do.

Frigione et al[11] suggest that lightly-crosslinked thermosets can be effectively toughened by the inclusion of soft or rubbery particles, while highly-crosslinked thermoset resins require a strong bond to the toughening agent to benefit from toughening. In highly-crosslinked systems, glassy inclusions with similar moduli to the resin will generally provide the most effective toughening, as stress concentrations at the interface will be small, limiting debonding.

When incorporating thermoplastics into highly crosslinked epoxies, strong adhesion between the two phases is critical. Extensive work has been conducted to determine the primary

theories of adhesion[15]–[24]. It is generally agreed that the factors that contribute to adhesion include:

- Mechanical interlocking, where an adhesive may fill in rough regions of a solid substrate
- Chemical bonding, where reactive groups may form covalent, ionic, or hydrogen bonds across the interface
- Diffusion theory, which describes intermingling of polymer chains due to diffusion across the interface
- Physical adsorption, which describes van der Waals interactions between dipoles on either side of the interface
- Electrostatic theory, wherein charge differences may create an electrostatic double layer at the interface
- Weak boundary layer theory, where contaminants on the surface can form a cohesively weak boundary layer.

These factors can all contribute to adhesion to varying degrees, depending on the material system. Adhesion can be improved by selecting material systems that have the potential to take advantage of these principles. Some thermoplastics that are commonly used to toughen epoxies include polysulfones[25]–[47], polyetherimide[48]–[57], poly(phthalazone ether ketone)[58]–[60], polyphenylene oxide[61]–[64], polyimide[65]–[69], and poly(ether ether ketone)-based polymers with modified end groups[54], [70]–[72].

PA is of particular interest as a thermoplastic toughening agent due to its potential to form covalent chemical bonds with EP. Further, both PA and EP are polar molecules. This compatibility enhances their miscibility, promoting interdiffusion to allow for mechanical as well as chemical crosslinking[1]. Polyamides are polymers in which monomers are linked with amide bonds. Different types of PA are characterized by the number of carbon atoms in the monomers. Some common PAs and their structures are shown in Table 2.1. The fewer carbon atoms there are between amide groups, the closer the reactive amide groups are to each other, and the more polar and reactive the polymer is overall.

Table 2.1. EP pre-polymer, PA6, PA6,6, and PA12 chemical formulas.

|                         |  |
|-------------------------|--|
| DGEBA<br>EP Pre-Polymer |  |
| PA6                     |  |
| PA6,6                   |  |
| PA12                    |  |

### 2.1.1 Cure Kinetics

The PA-EP cure reaction is well documented due to the popularity of PA as a curing agent to create EP-PA networks for use in adhesives and coatings[73]–[75]. The reaction proceeds primarily through attack on the EP ring by the PA nitrogen atoms, as depicted below[76].

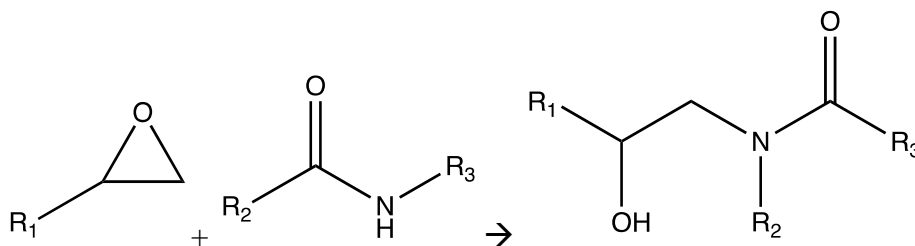


Figure 2.1. Primary EP-PA reaction, attack on oxirane ring by PA nitrogen atom. Adapted from Zhong et al [76].

Wang and Chen[77] studied PA-EP blends and determined that there are three distinct phases of such blends: a semicrystalline pure PA phase, an amorphous PA-EP phase, and an amorphous pure EP phase. The blends exhibited maximum tensile strength at 5% EP content, due to the effect of stress-induced crystallization in the PA-rich phase. The maximum shear stress occurs at 30% EP content, where increased crosslinking with increased EP content has a reinforcing effect on shear strength.

Zhong and Guo[76] studied the cure kinetics of a PA-EP blended system over a wide range of compositions, finding that the primary reaction proceeds as illustrated in Figure 2.1. However, there is a second reaction mechanism, pictured below, that has a much higher activation energy.

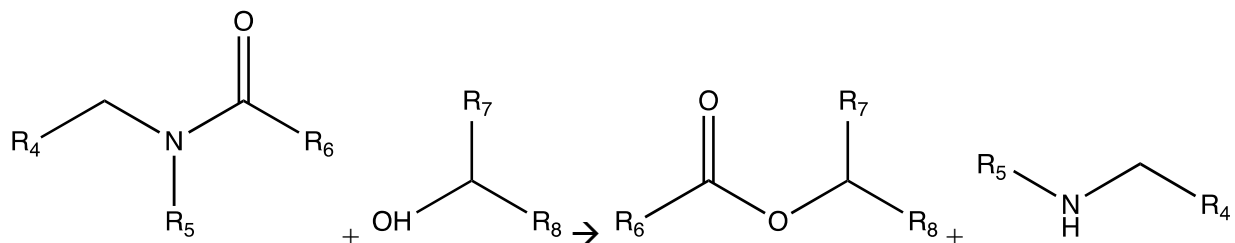


Figure 2.2. Secondary EP-PA reaction. Adapted from Zhong et al[76].

This reaction becomes dominant when the EP is in stoichiometric excess, above 63wt% for this system. The secondary reaction uses the product of the first reaction as a reactant and can therefore only occur after the first. This, combined with the fact that the reaction only occurs at high EP concentrations, suggests that it becomes the dominant mechanism only when there are few primary reactive sites remaining. Prime and Sacher[78] also observed a secondary reaction that only occurred at elevated temperatures, confirming the presence of a secondary reaction with a higher activation energy than the primary reaction.

All compositions Zhong tested resulted in a single amorphous phase after cure, although both 80:20 and 90:10 PA to EP ratios were crystallizable after curing. This conflicts with Wang's findings of three distinct phases in cured PA-EP blends. Both groups used alcohol-soluble PA, which was mixed with EP resin and dried fully before testing. A key difference between the two projects is that Zhong[76] did not add an EP curing agent to the system, meaning EP pre-polymer could only react with PA chains. The choice of EP curing agent can affect the cured morphology

of thermoplastic-toughened epoxies[79], which may offer a partial explanation for the difference in morphology between Zhong's and Wang's studies.

Zhong[76] and Wang[77] do agree in finding that a polyamide phase can still crystallize after bonding to EP, provided the EP concentration is sufficiently low. Zhong suggests that the crystallization threshold is 20wt% EP, while Wang finds that this threshold is 5wt% EP.

De Schoenmaker[80] et al studied the effect of PA nanofibers on EP cure behavior. They found that PA fibers had a catalytic effect on the cure reaction between EP pre-polymers and the amine curing agent, although they hypothesized that this effect could come from the release of absorbed water from the PA fibers. In a follow-up work by van der Heijden et al[81], the effect of water content is investigated further. They find that dry PA fibers have a slight catalyzing effect on the EP resin, an effect that is enhanced by the presence of water in the system. The EP pre-polymers preferentially adsorb to the PA surface, which plasticizes the EP. The reaction quickly becomes diffusion-limited due to covalent crosslinking at the surface of the PA fibers. It is important to understand the effect of absorbed water on the reaction of PA with EP since PA that has not been thoroughly dried will contain water. In most manufacturing contexts, it is reasonable to assume that PA used will contain absorbed water.

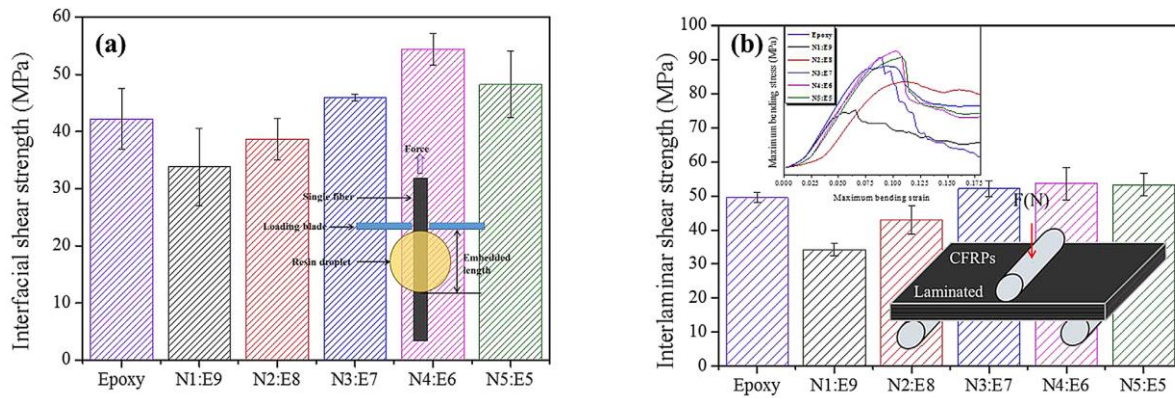


Figure 2.3. Interlaminar and interfacial shear strength as a function of PA content in EP-carbon fiber composites. From Kim et al[82].

Kim et al[82] studied the reaction kinetics of a homogeneous PA6-EP matrix surrounding a carbon fiber fabric. They found that a 40:60 PA:EP ratio yielded the most favorable composite, with a maximum in interfacial and interlaminar shear strength. These results support Zhong's[76] theory that for EP content above approximately 63%, a secondary reaction mechanism is dominant,

and it appears that this reaction is unfavorable for mechanical properties based on the decline in performance above this EP content. Composites made with 10wt% and 20wt% PA performed worse than neat EP, so in these composites the PA had a detrimental effect.

The cure kinetics of the EP-PA cure reaction give important insight into the macroscopic EP-PA interaction. The system can form covalent crosslinks, which will enhance the interaction between the two materials. This improved interaction will in turn prevent the two components from debonding, which will improve the mechanical properties.

### **2.1.2 Solution-Dissolved Blends**

Dissolving PA in solution is a popular way to create homogeneous PA-EP blends. Vyas and Iroh[83] studied the crystallization behavior of homogenized PA6-EP blends. The PA was able to crystallize in the presence of EP pre-polymer due to the formation of hydrogen bonds between portions of the PA chain, while the amorphous region of the PA formed covalent bonds with the EP pre-polymer to form a crosslinked network. This work agrees with Wang's[77] supposition that homogenized EP-PA blends form a multiphase structure upon cure.

Gorton[84] found that incorporating a small amount (15wt%) of EP into a PA resin doubles the PA joint strength by suppressing the yield and non-linear stress/strain behavior of the polymer and forcing an apparent linear-elastic to brittle fracture behavior. An amide curing agent profoundly increases the amount of crosslinking between the PA and the EP, especially at lower EP content—suggesting that the curing agent actually can improve the mechanical properties of the system rather than competing with the PA reactive sites. The curing agent likely enables the EP to intertwine with the PA chains, increasing mechanical interlocking. This indicates that for this system, mechanical interlocking is the primary toughening mechanism afforded by the PA.

Bakar et al[85] dissolved varying amounts of PA6 into an EP resin and observed an increase in impact strength, flexural strength, and resistance to crack propagation over neat EP. A combination of EP with 5wt% PA6 provided the greatest improvement in impact strength and critical stress intensity factor and fracture energy over neat EP. At higher PA concentrations, the improvement in mechanical properties was reduced, eventually falling below the neat EP values. This supports the idea that there is a critical thermoplastic concentration that will allow for optimal EP toughening. However, the PA should have better impact behavior than EP, so this decrease in impact properties with increasing PA content shows the emergence of a competing mechanism

with the toughening benefit of added PA. Perhaps the increase in interfacial EP/PA areas is detrimental to the impact properties of this system.

Because of PA's hydrophilic nature, water absorption is a concern for blends containing PA. Delollis and Montoya[86] studied the effect of prolonged exposure to liquid and vapor water on the shear strength of a PA-EP adhesive. While the shear strength of the samples reached an approximately steady value after two months of exposure to high humidity, the strength of the specimens exposed to water never reached a steady value (Figure 2.4).

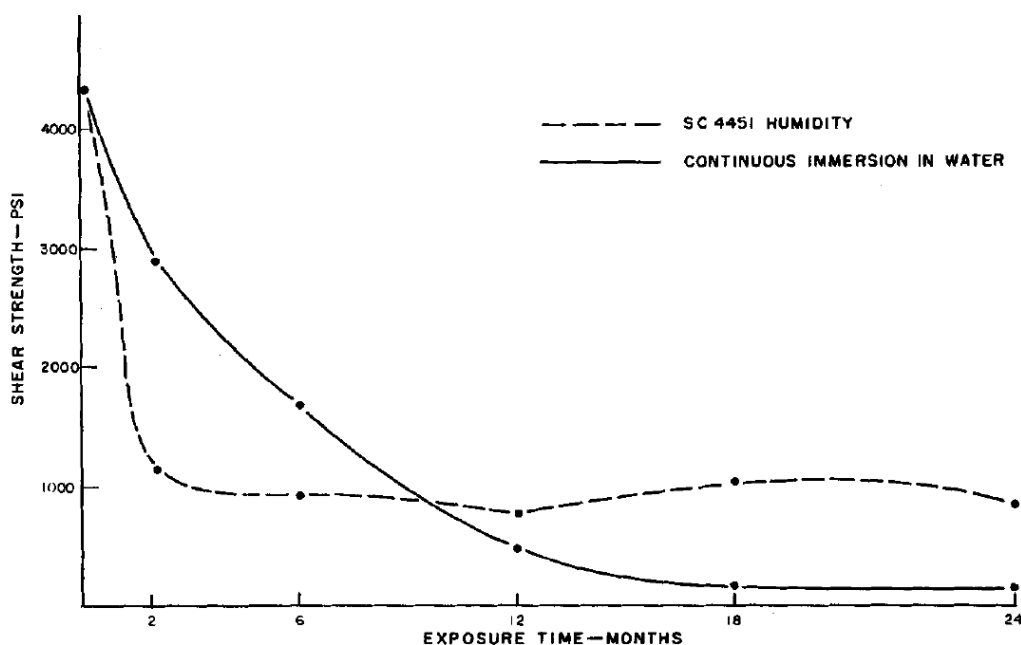


Figure 2.4. Shear strength of PA-EP adhesive as a function of exposure time in water and humidity. From Delollis et al[86].

This suggests that the PA-EP adhesive could be used in a humid environment as long as the decrease in strength was anticipated and designed for, but it would be unsuitable in a liquid water environment. The strength is reduced by the PA preferentially absorbing the water, which weakens the interaction between the adhesive and the adherend. In a design where the PA can covalently bond to EP and is not required to adhere to anything else, it is possible that the effect of moisture on the system would be less appreciable. The polar water molecules would still interact with the polar PA chains, but the covalent bonds between polymer chains will remain intact.

Butt and Cotter[87] studied the effect of humidity on the strength and failure of an EP-PA adhesive. Exposure to humidity negatively affected many of the properties of the test specimens. However, both thermal and dynamic mechanical properties were by drying, while moisture-induced losses in adhesive strength were irreversible due to the degradation of adhesive bonds by the water.

Ishisaka and Kawagoe[88] found that the equilibrium water concentration in both EP and PA6 was heavily dependent on relative humidity of the environment. However, while the PA6 diffusion coefficient also exhibited a strong dependence on relative humidity, the EP diffusion coefficient was relatively invariant with environment. Therefore, EP will reach its equilibrium water content after an approximately constant exposure time while the required exposure time to reach equilibrium water content in PA will vary with environment. Further, the equilibrium water content in PA6 was approximately two times greater than that of EP in all environments. This behavior is important to consider when determining whether a material's properties have reached a steady state or will continue to change with prolonged exposure to a humid environment.

Even though forming a homogeneous solution of EP and PA is only one way to combine the two materials, the results still provide valuable insights that are applicable to other methods of joining the two. The partial miscibility of PA in EP is encouraging, as it suggests that the two materials can be combined successfully to form covalent crosslinks and improve the mechanical properties over neat EP. Water absorption is a concern in all PA systems, as the polar water molecules are drawn to the polar amide groups, which leads to degradation of mechanical properties.

### **2.1.3 Fine PA Particles in EP Matrix**

An alternative to creating a homogeneous PA-EP solution is introducing the two phases separately. A common way to do this is to add fine PA particles to uncured EP, eliminating the need for solvents or extreme temperatures and making the process more economical and environmentally friendly. During the EP cure cycle, the temperature is elevated so that PA chain mobility increases to the point where interaction between the EP pre-polymers and the PA chains is possible.

Lu et al[89] studied the toughening mechanisms in particle-modified EP systems. Highly crosslinked resins failed through the debonding of the modifier particles from the matrix, yielding



a decrease in the fracture toughness. Lightly crosslinked resins were able to deform in shear, improving fracture toughness (Figure 2.5). This confirms that energy absorption mechanisms in PA particle-toughened EP resins are the same as those found for other particle-toughened EP systems[6]–[8].

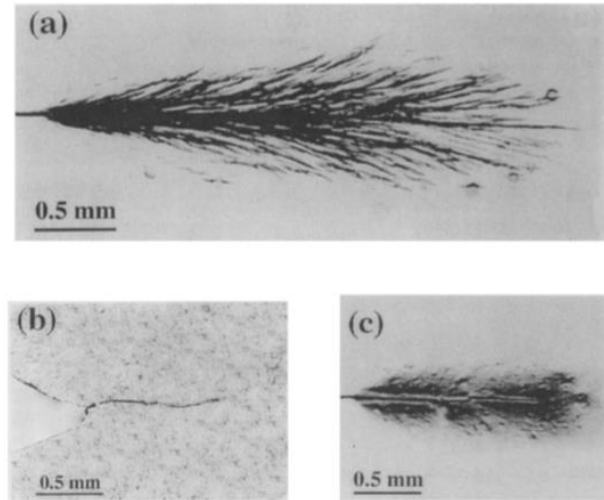


Figure 2.5. Shear failure modes of a lightly crosslinked EP (a), highly crosslinked EP at room temperature (b), and highly crosslinked EP at 160°C (c). From Lu et al[89].

Cardwell and Yee[90] attempted to toughen a highly crosslinked EP resin with PA12 particles. They successfully toughened the system at low strain rates, proving that the PA12-EP bond is sufficiently strong that PA 12 can be used to toughen highly-crosslinked epoxies. This is achieved as the PA bridges across the crack, increasing the material's fracture toughness (Figure 2.6a), and plastically deforms without causing damage to the surrounding matrix (Figure 2.6b).

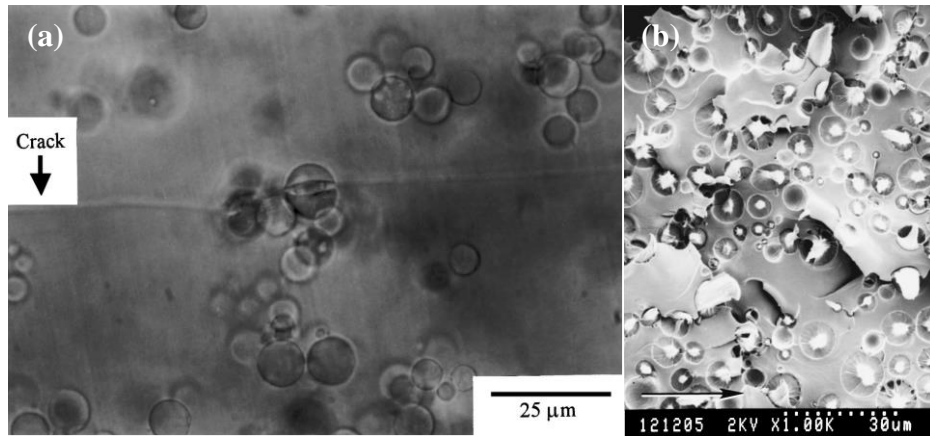


Figure 2.6. PA12 fiber bridging in EP (a) and PA12 deformation in EP (b). From Cardwell et al[90].

Cardwell identifies several characteristics of successful thermoplastic matrix toughening agents, including good matrix-toughener adhesion and high work to fracture in the thermoplastic. These two properties must be carefully balanced, as strong matrix-thermoplastic adhesion can inhibit plastic deformation of the thermoplastic before failure.

Kim et al[91] studied the effect of mixing temperature on the structure and fracture energy of EP toughened with 5wt% PA6 particles. The maximum fracture energy was in samples mixed just below the PA melting temperature, at which point the PA began to dissolve (Figure 2.7a). There was no difference in modulus or yield stress as a result of mixing temperature. The PA reacted with the EP to form covalent bonds, but also formed crystalline lamellae in the interphase. Further crystallization was not possible due to the high viscosity of the blends resulting from the chemical crosslinking. The crystalline lamellae in the interphase are on the same length scale as the crack fingers that extend from the crack front, which enables the lamellae to deflect the crack fingers, toughening the material (Figure 2.7b). This study points to the importance of elevating the processing temperature to just under the PA melting temperature for full development of fracture toughness.

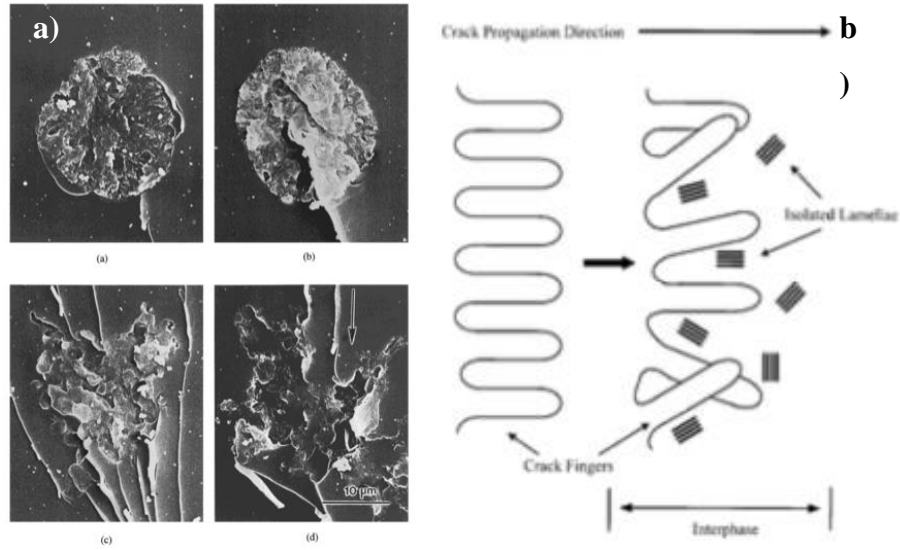


Figure 2.7. PA6 particle in EP at mixing temperatures of 30°C, 210°C, 220°C, and 230°C (a). Crystalline PA6 lamellae deflecting crack fingers at a growing crack front (b). From Kim et al[91].

Kim and Robertson[92] used crystalline PA6 particles to toughen an EP matrix, up to 20wt% PA. The resulting matrix experienced an approximately linear increase in fracture toughness with increasing PA concentration, with a further improvement from decreasing particle size, as evident in Figure 2.8. The elastic modulus, glass transition temperature and yield strength all remained unchanged with the addition of PA particles.

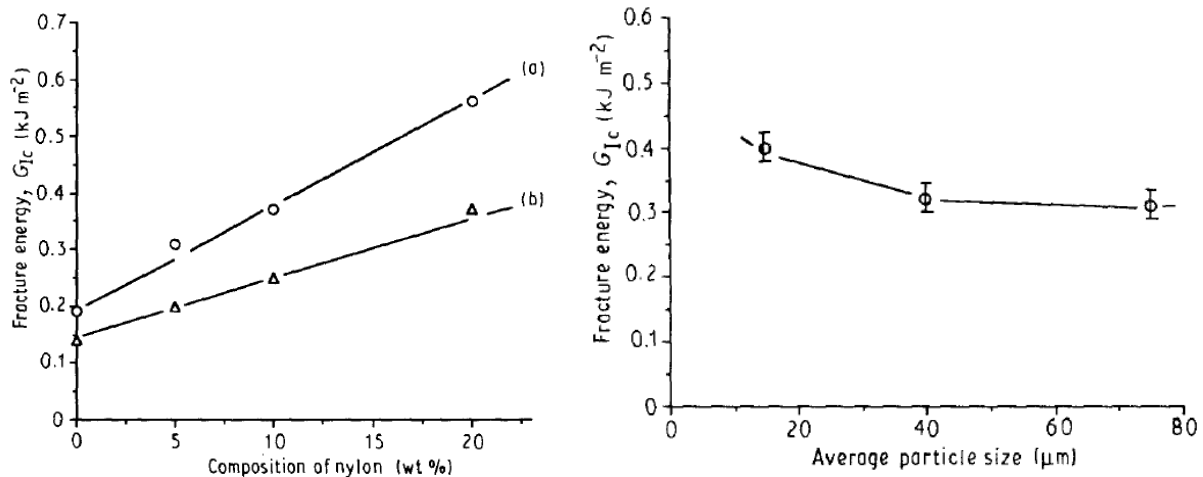


Figure 2.8. Fracture energy absorbed as function of PA composition (left) and of PA particle size (right). From Kim et al[92].

Girodet et al[93] used PA6 and PA12 particles below their melting points, which enabled them to maintain their original shape when mixed with EP. Neither PA type had any effect on the EP elastic properties, but PA6-toughened epoxies experienced a linear increase in critical stress intensity factor with increasing PA concentration (Figure 2.9) while PA12 had no effect on critical stress intensity factor. These differences are likely caused by the stronger bond between PA6 and EP than between PA12 and EP due to the more reactive nature of PA6. The strong PA6-EP bond enables failure to occur through a bridging mechanism as Cardwell describes[90].

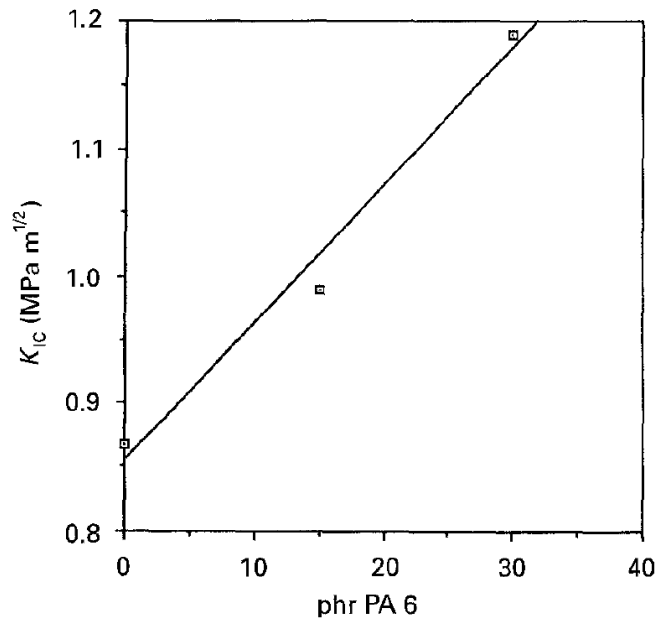


Figure 2.9. Critical stress intensity factor as a function of PA6 concentration. From Girodet et al[93].

These studies show that it is possible for EP to interact with PA below the PA melting point without an additional solvent. At the EP cure temperature, the PA chain mobility is sufficient to allow the PA chains to intermingle with the EP pre-polymer. Further, the PA particles are able to provide different toughening mechanisms when they comprise continuous regions than when they are mixed to form continuous blends with EP, as PA particles are able to reroute and absorb energy applied to the matrix. This different energy absorption mechanism means that the PA-EP adhesion must also be considered and optimized to obtain the desired properties.

#### **2.1.4 EP-Matrix Composites containing Fibers and PA**

Composites have recently grown in use due to their high specific strength, allowing them to replace heavier metals that have traditionally been used in automotive or aerospace applications. However, commonly used EP-fiber composites are brittle and must be modified in order to perform well in applications where impact resistance or damping is needed[94]–[97]. The addition of PA to these systems allows for toughening without sacrificing mechanical performance. PAs are typically incorporated as discrete separate phases since creating a homogeneous matrix increases resin viscosity, making fiber impregnation difficult.

Jang et al[98] used several thermoplastic and reinforcement fiber weaves overmolded with EP resin to study impact behavior. They found that the ability of the thermoplastic to deform in response to impact is essential for energy absorption, and the EP-PA system studied limited the PA deformation-to-failure from 20% in neat PA to 4% in the hybrid system. Therefore, for an application where high impact energy absorption is important, this system could benefit from reduced PA-EP adhesion, allowing for increased PA deformation.

Beier et al[99], [100] used PA yarns with low melting temperatures to stitch together non-crimp carbon fiber fabrics. The PA yarns are able to melt into the EP matrix during processing, as in Figure 2.10.

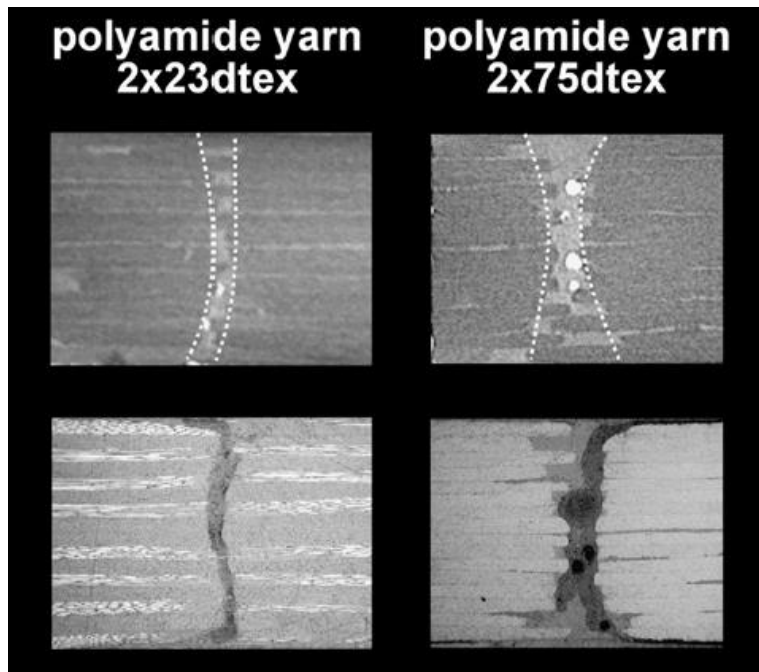


Figure 2.10. PA yarns melted between plies of carbon fiber. From Beier et al[100].

The yarns allow for improvements in  $G_{IC}$  and tensile strength relative to composites without PA stitching yarns. However, the yarns proved detrimental to compression after impact strength. Beier et al believe that some of the decreases in mechanical properties could be due to the inability of the low melting temperature fibers to support the applied loads. Perhaps stitching the composites with a different grade of PA yarn might prevent this reduction in properties.

Hogg[101] examined the toughening effect of comingling thermoplastic fibers, including PA, into plain weave carbon fiber fabrics that were overmolded with EP resin through resin transfer molding. A schematic of the comingled fiber system is shown in Figure 2.11.

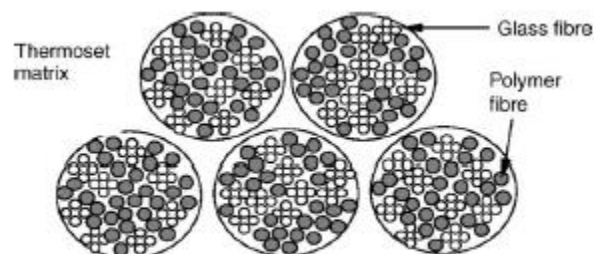


Figure 2.11. An idealized schematic of the comingled PA and structural fibers in a thermoset matrix. From Hogg et al[101].

The PA fibers improved the impact resistance and Mode-I and Mode-II fracture toughness of the EP-carbon fiber system, primarily by inhibiting delamination growth in the composite. However, the large diameter of the PA threads relative to the carbon fibers led to a very low carbon fiber volume fraction, around 25% (Figure 2.12).

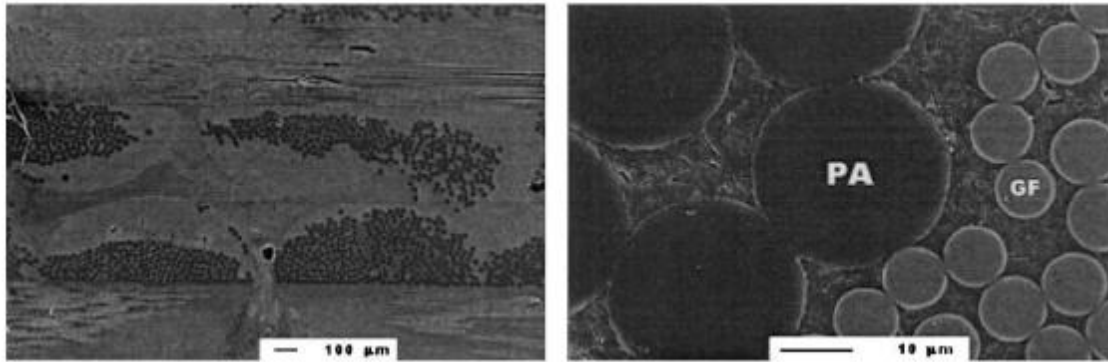


Figure 2.12. Relative size of PA and structural fibers in EP matrix. From Thanomsilp et al[102].

This low carbon fiber content led to a significant decrease in strength from traditional carbon fiber-EP composites, which typically have fiber volume fractions of approximately 60%. Therefore, this study does not provide a valuable basis for comparison with high performance composite materials, and such a material could not be a viable substitute in a high-strength application.

Thanomsilp and Hogg[102] also studied impact resistance of composites made from comingled woven thermoplastic and glass fibers impregnated with EP resin. They found that systems in which the thermoplastic fibers melted into the EP during cure did not perform any better than glass fiber-EP systems with no thermoplastic added, indicating a toughened matrix has no effect on impact toughness in this geometry. However, when the thermoplastic fibers remained intact during cure, the composite experienced increased energy absorption due to the delamination and subsequent deformation of the thermoplastics, similar to the toughening mechanisms found in particle-toughened epoxies. This effect was less pronounced in systems where the EP-thermoplastic adhesion was stronger, as deformation in the thermoplastic phase was inhibited by interaction with the brittle EP matrix. Again, it is clear that there is a delicate balance between strong thermoplastic-EP adhesion for enhanced structural integrity of a finished part and weak interaction to allow the thermoplastic phase to deform. Although Thanomsilp found no improvement in impact toughness due to matrix toughening, thermoplastic-toughened matrices do

offer other improvements to mechanical performance which should be considered when designing a composite system.

Other work by Thanomsilp and Hogg[103] supports the claim that incorporating PA fibers into a woven reinforcement fabric can improve  $G_{IC}$ . However, they found that the inclusion of PA fibers had a detrimental effect on  $G_{IIC}$  of glass fiber-based composites, in contrast to the improvement in  $G_{IIC}$  seen when PA fibers were incorporated into carbon fiber-based composites[101]. While one study uses carbon fibers and the other uses glass fibers, the composite geometries are otherwise similar and there is no explanation offered for the discrepancy in the effect on  $G_{IIC}$ .

Another method of incorporating thermoplastic into a fibrous composite is to coat individual fibers or woven fabrics in the thermoplastic before impregnating the system with EP. Varelidis et al[104] compared two methods of coating carbon fibers with PA6,6 before impregnation with EP. They concluded that the solution dip coating method, which yielded composites with high-molecular weight PA6,6, provided improved adhesion between the fibers and the matrix over uncoated fibers. However, fibers coated through an interfacial coating method had low-molecular weight PA chains and experienced a decrease in adhesion to the EP matrix from those in composites without polymer coatings.

Varelidis et al[105] also used the solution dip coating and interfacial polymerization methods to coat Kevlar fabrics with PA6,6 before impregnating them with EP resin. They observed that the PA decreased interlaminar shear stress and interfacial fracture toughness, although the solution coating method generally had less of a detrimental effect on these properties than the interfacial method. This provides further evidence that highly-crosslinked PA is preferable to lightly-crosslinked PA in enhancing composite mechanical properties, although both can negatively affect certain properties. The PA coating was found to increase the water uptake of the composite because of the highly hydrophilic nature of the PA, confirming that the findings of Delollis[86] and Butt[87] for water absorption in homogenized PA-EP systems are applicable to composite systems.

Skourlis et al[106] coated individual carbon fibers with a thin layer of PA using an in-situ polyamidization coating method. These coated fibers were used to manufacture unidirectional composites in an EP matrix. A thin PA coating enhanced the tensile and impact properties, but had



a detrimental effect on the flexural properties. The reason for this is unclear due to the complicated stress field involved in three-point bend tests.

Incorporating PA in EP-fiber composites can greatly toughen the system. In systems where continuous PA fibers are comingled with reinforcing glass or carbon fibers, the composites benefitted from the ability of the PA fibers to deform under applied load and inhibit crack growth through EP-PA crosslinking. The studies on PA-coated fibers point to the importance of PA molecular weight in a combined system, as low molecular weight provided insufficient interlocking to toughen the systems. It has already been shown that mechanical interlocking between the EP and the PA is crucial in enhancing mechanical properties, and the studies on the effect of various fiber coatings explain the role of molecular weight in this mechanical interlocking.

#### **2.1.5 Fiber-Reinforced EP Composites with PA Interleaves**

Another popular method to improve the fracture properties of an EP-matrix composite is to include a ductile interleaf between some or all composite layers. These interlayers bond composite plies together and absorb energy, reducing any dissimilarity in fiber properties between plies. The idea was introduced by Favre[107], who studied the effect of various delamination promoters as interlayers, including PA6, on the Charpy fracture behavior of EP-carbon fiber composites. He found that increasing the number of thin (50 nm thickness) PA films increased the Charpy impact energy while decreasing the interlaminar shear strength of the composite laminate (Figure 2.13).

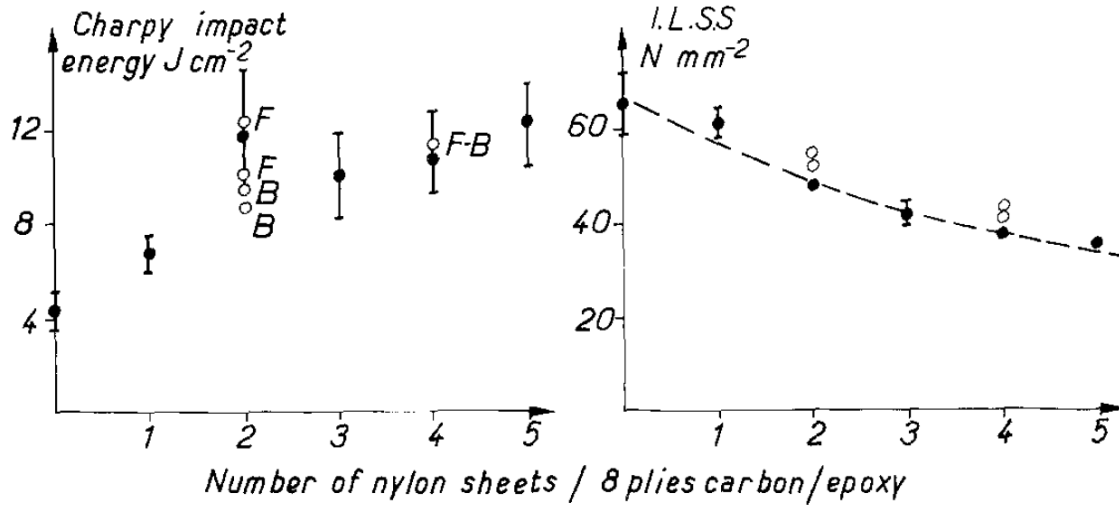


Figure 2.13. Increasing impact energy and decreasing interlaminar shear strength as functions of number of PA interlayers. From Favre[107].

He observed that the composites with PA interleaves failed cohesively (Figure 2.14) and that the adhesive bond between the PA and EP remained intact, though it is unclear if this adhesion is mechanical or chemical in nature. Since these reinforced composites are limited by the relative weakness of the pure PA region, work must be done to reduce the volume of the neat PA phases.

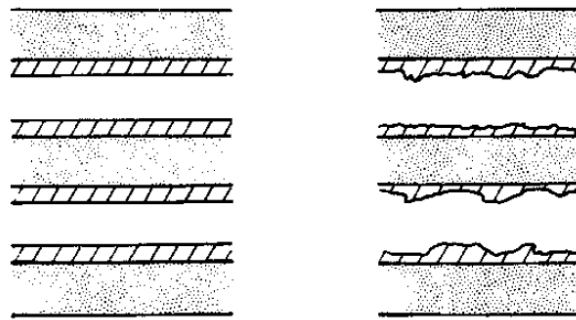


Figure 2.14. Two cohesive failure mechanisms observed in PA interleaves. From Favre[107].

Masters[108] interleaved composites to improve impact and delamination resistance, two areas that are crucial in mechanical behavior of structural composites. He confirms that interleaves assist in arresting crack propagation, reducing impact damage and increasing the amount of impact energy absorbed by the composites.

One approach to reduce the volume of the thermoplastic interleaves, introduced by Dzenis and Reneker[109], is to use electrospun thermoplastics as interleaves. Electrospinning is a process

by which a polymer solution is discharged from an extruder and an electric field is used to split the extruded solution into nanofibers (Figure 2.15a). This results in a mat comprised of nanoscale fibers (Figure 2.15b).

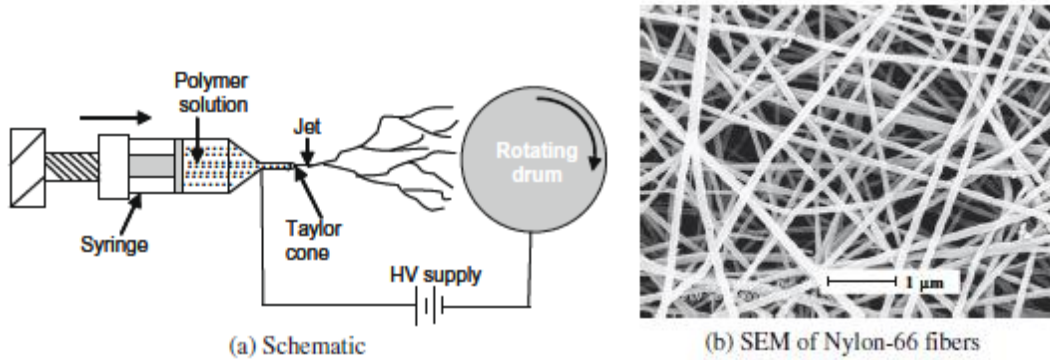


Figure 2.15. Electrospinning schematic (a) and SEM image of electrospun fibers (b). From Akangah et al [110].

The electrospun sheets have a significantly higher surface area to volume ratio, allowing for greatly improved adhesion over traditional interleaves. Further, their fibrous structure and high void content allows them to behave almost like Velcro® and mechanically interlock with EP, improving the adhesion.

Daelemans et al[111] studied the optimal characteristics of electrospun interleaves. Randomly oriented fibers afford better improvements in mechanical properties than aligned fibers. They can toughen the composites through nanofiber bridging both at the interface and through the toughened interlayer.

Daelamans et al[112] offered explanations for interleaved composite toughening mechanisms across three length scales. They propose that toughening occurs at the matrix, interlaminar region, and laminate resin levels, with different mechanisms at each length scale contributing to overall toughening. At the smallest scale, the matrix level, electrospun nanofibers can deform and bridge across a growing crack front. At the intermediate level, the interlaminar region, the crack path travels through the toughened interlayer, which dissipates energy. At the largest scale, toughening effects found on the smaller scales have an additive effect to toughen the composite laminate. They find that adhesion between EP and PA is poor, leading to poor composite energy absorption. This is likely because of the use of an EP resin that cures below the PA glass transition temperature. Therefore, the PA chain mobility during processing was low, preventing

the chains from rearranging to bond to the EP. Further, Prime and Sacher[78] find that the secondary EP-PA reactions occur above the processing temperature, so this system could not take advantage of the additional crosslinking reactions and strength therefrom.

Mechanical properties of composites developed with this method have been well-documented for electrospun PA 6,6 interleaves. Akangah et al[110] incorporated electrospun PA6,6 interlayers between plies of a unidirectional carbon fiber-EP composite and found that the interlayer increased the threshold impact force by ~60% and decreased the impact damage rate. Akangah did not measure the composite stiffness or strength, so it is unclear if the interleaves had any detrimental effect on these properties.

Palazzetti et al[113] find that electrospun PA nanofibers provide carbon fiber-EP composites with toughening after impact. Although the laminates containing nanofibers show an 11% decrease in stiffness from unmodified composites, they show a 160% improvement in damping over unmodified composites. Further, the nanofibers can bridge across a fractured EP matrix, which leads to higher stiffness in toughened composites with fractured matrices than with intact matrices.

Tstotsis[114] shows that including thin PA veils at the interlayers of carbon fiber/EP composites produced with resin transfer molding (RTM) can decrease the area of damage because of impact and improve the compression after impact response. Open-hole compression and shear strength are not reduced with interlayer inclusion and can, in some cases, be improved. They find that PA interlayers with higher melting temperatures perform better than those with lower temperatures, although the highest interleaf melting temperature tested was only 160°C. Other PA grades, including PA 6, have higher melting temperatures that may be better suited for interleaving based on this research.

Palazzetti et al[115] also examined the effect of placing an electrospun PA6,6 interlayer at the midplane of a carbon fiber/EP composite on the Mode-I and Mode-II fracture toughness and found the interlayer increased the amount of energy the laminates could absorb. It is unclear what the effect of including interleaves between other layers would be, although it could be predicted that increasing the number of interlayers would increase the flexural modulus of the composite.

Daelemans et al[116] found that PA interleaves could reduce the Mode-I fracture toughness from un-toughened composites by preventing the carbon fibers from bridging across the crack and toughening the material. However, if an un-toughened region was left at the edge of the crack,

allowing carbon fibers to bridge across the crack, the PA interlayer was able to slow crack propagation. This effect is visible in the development of interfacial fracture toughness along the length of a selectively interleaved sample, as shown in Figure 2.16. Because cracks can form anywhere in a material, perhaps this knowledge could be exploited by including porous interlayers or by selectively toughening composites at their interlayers to allow for the carbon fibers to bridge across cracks and for the PA to inhibit crack propagation.

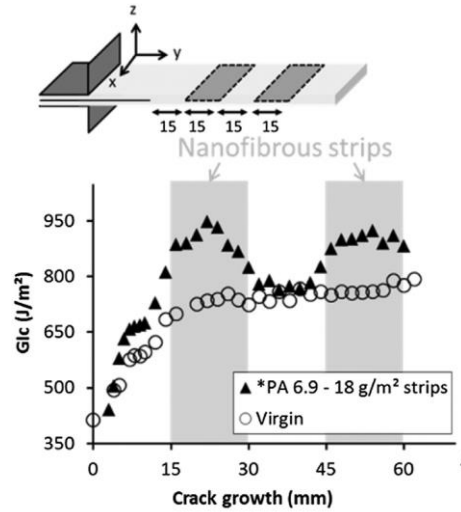


Figure 2.16. Interfacial fracture toughness of EP-carbon fiber composites that are selectively toughened with PA interleaves. From Daelemans et al[116].

Though composites with electrospun interlayers benefit from a lower PA volume fraction than traditional interlayered sheets, PA interlayers of any kind can improve the impact toughness of an EP-based composite. With both electrospun and non-electrospun interleaves, the bonding between the PA and the EP is sufficient to prevent adhesive failure. As with other PA-EP blends, the volume of PA phases must be carefully chosen to limit any detrimental effect on the composite strength.

### 2.1.6 Fiber-Reinforced EP Composites with Discrete PA Particle Interlayers

Groleau et al[117] interleaved highly- and lightly-crosslinked EP-matrix composites with PA 12 particles to examine the particles' effect on energy absorption. This method of incorporating fine particles at composite interlayers combines principles of particle-toughened EP and interleaved composites. Their findings agree with what might be predicted based on studies of

particle-toughened epoxies without composite fibers. In the lightly-crosslinked composites, the EP matrices themselves were able to deform to dissipate the applied load and the presence of PA particles had no appreciable effect. In contrast, the highly-crosslinked systems benefitted from the PA particle deformation and bridging. The full benefit of the particle toughening is not realized because the composites fail at the ply-matrix interface. This suggests that there is strong adhesion between the particles and the matrix, which could be particularly high in this system because the composites are processed above the PA melting temperature, which allows the particles to melt into the matrix.

Caprino et al[118] studied the shear properties of a unidirectional EP-CF prepreg toughened with a thin (0.015mm) layer of PA particles suspended in EP resin (Figure 2.17).

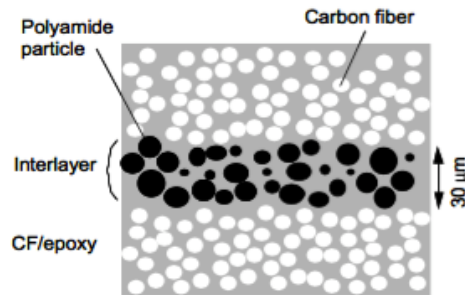


Figure 2.17. PA-toughened interlayer in CF/EP prepreg. From Caprino et al[118].

They found that the shear modulus of the composite was lower in the through-thickness than in the plane of the material due to the effect of the PA in the interlayers. However, the observed through-thickness shear modulus was lower than expected. Further research is required to determine the factors that cause this reduction in modulus.

Hojo et al[119] studied the Mode-I delamination fatigue properties on the same particle-interleaved prepreg used by Caprino[118]. The Mode-I crack first traveled through the toughened interlayer, where the crack growth resistance was 3x higher than that of an untoughened EP-CF prepreg. When the crack travels out of the toughened interlayer to the interface with the untoughened lamina, the toughened prepreg experiences crack growth resistance of 1.6x that of the reference material. In the toughened region, the crack is deflected by methods previously discussed in heterogeneous PA-EP mixtures. The second phase of crack growth observed in this study suggests that a composite can be toughened by thermoplastic particle interlayers even if the particles are not in the path of the crack.

PA particle toughened composite combines the toughening mechanisms of fine particles suspended in EP and ductile interlayers placed between plies of an EP-CF composite. The success of this type of material suggests that other mechanical and chemical interactions explored in this paper can be used in combination to produce hybrid materials with tailored properties.

### 2.1.7 Other Applications of PA-EP Interactions

Several other studies have been undertaken that take advantage of the interaction of PA and EP.

Beiss et al[120] used short glass fiber-reinforced PA 6 to adhere EP/woven glass fiber composites together. By using friction to adhere the PA composite to the EP, they observed an improvement of about 100% in the tensile shear strength over samples created by overmolding thermosets with PA. This is because the short glass fibers in the PA are abrasive, so during the welding process the fibers wear down the EP, exposing the woven glass fibers and creating resin-free pockets in the EP/glass fiber weave. The friction-melted PA can fill these pockets (Figure 2.18) and increase mechanical interlocking, and thereby bond strength, between the EP and the PA. This study quantifies the effect of surface roughness on bonding, suggesting that pretreating a surface would improve its adhesion and mechanical properties. Adhesion could perhaps be further enhanced if the materials are combined before the EP is fully cured, allowing for chemical bonding in addition to mechanical interlocking.

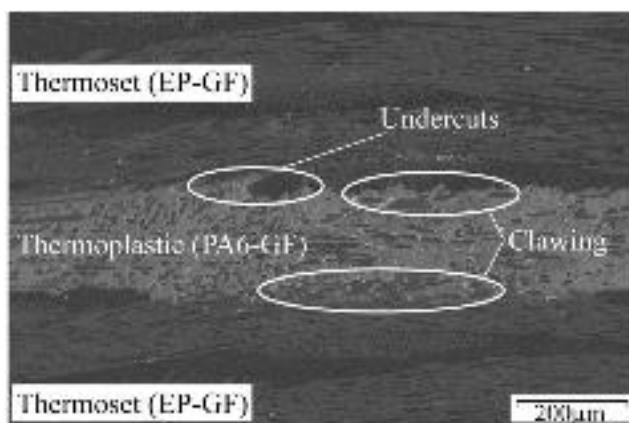


Figure 2.18. Mechanical interlocking between PA6 interlayer and carbon fiber composite. From Beiss et al[120].

Hou[121] also exploits the PA-EP bond for use in friction welding. He co-cures PA films and EP/carbon fiber preregs to form a network of intermingled polymer chains before friction welding components together by melting the PA regions together. Unlike Beiss[120], the PA and EP are combined before the EP cures, allowing the potential for PA-EP covalent bonding in addition to the mechanical interlocking. Room temperature single lap shear strength was 75% greater in Hou's composite than in Beiss's, illustrating the importance of chemical as well as mechanical interlocking for adhesion.

### **2.1.8 Section Summary**

A thorough review of current work in combining PA and EP has been presented. The primary EP-PA reaction allows for chemical crosslinking between chains of the two materials, while a secondary reaction can improve this crosslinking at higher temperatures and EP contents. Whether PA is dissolved in solution before being combined with EP or incorporated as a discrete second phase, the PA can toughen the EP, albeit through different mechanisms. PA can also toughen EP-based composites, using similar mechanisms to those found in particle-toughened epoxies. In essence, these toughened composites simply contain larger or differently shaped PA phases than the fine particle-toughened epoxies. No matter the design of the system, there must be a careful balance between the ductility-promoting PA and the strength of the system. These properties can be adjusted to allow for desired properties in a finished product.

Many findings presented in this work can be extended to other combinations of dissimilar polymers. Reaction kinetics can be studied to select polymers with compatible reactive groups to promote formation of covalent crosslinks, which greatly improves adhesion. Even if the polymers are partially immiscible, as PA and EP are, the polymers can be successfully combined under a broad range of conditions. Further, this paper contains suggestions on methods to exploit blend compositions, geometries, and processing conditions to obtain a product that improves the properties of interest without sacrificing others. For example:

- Material strength will be highest if the weaker phases are small. This allows for more effective stress transfer to the stronger phase, limiting premature cohesive failure in the weak phase



- Hydrophilic molecules will absorb moisture, which can have a plasticizing effect on material properties. This effect must be considered in part design, and it is often desirable to dry such polymers before manufacture.
- Fine particles of a ductile phase suspended in a brittle matrix are able to deflect growing cracks and plastically deform, improving energy absorption.
- If there is a thermoplastic phase in the material combination of interest, elevating the processing temperature to just below the thermoplastic melting temperature promotes chain entanglement and improves adhesion.
- Longer polymer chains can improve mechanical entanglement between polymers.
- Interleaving brittle-matrix composites with ductile polymers improves composite energy absorption whether the interlayers are electrospun or not.

## **2.2 Background: Polyamide/TPE Combinations**

There are some applications for which the combination of EP and PA, though often tougher than neat EP, may not be well-suited. For applications that require significant deformation before failure, or a soft-touch surface for improved feel and control, a combination of softer materials may be needed. For some cases, the combination of a thermoplastic with an elastomer may be beneficial.

Elastomers are materials that can sustain significant deformation before failure relative to traditional engineering polymers. They typically consist of macromolecules that allow for high failure strain, interspersed with a chemically or physically crosslinked structure that resists permanent deformation upon the removal of an applied force. Thermoplastic elastomers (TPE) are a subset of elastomers that can be melted, allowing for ease of processability and the potential for recycling. TPEs usually have a phase-separated microstructure with alternate glassy and rubbery regions, where the glassy regions provide structure and support to the extensible rubbery regions. When heat is applied, the glassy regions melt, reducing the overall TPE viscosity to be flowable.

TPEs are divided into classes based on the types of structures that form their glassy and rubbery phases. Styrenic block copolymers (TPE-S or TPS) consist of thermoplastic regions of styrene alternating with rubbery repeat units. Common rubbery repeat units for TPS include butadiene (SBS) and ethylene and butylene (SEBS). Thermoplastic polyurethanes (TPE-U or TPU) are formed from linear copolymers with alternating short and long regions with diisocyanate

end groups. The short regions have decreased distance between these end groups, resulting in high-polarity regions in which the end groups are drawn together to create hard crystalline regions. Thermoplastic polyolefins (TPE-O or TPO) consist of mechanically blended thermoplastics and elastomers, often with fillers added to modify the blend properties.

Many TPEs are non-polar and non-reactive, making them immiscible with polar molecules such as PA. However, there are a number of ways to improve TPE compatibility with such molecules, often by the addition of a compatibilizing or co-reactive agent. Typically, this involves grafting reactive molecules onto TPE chains, allowing for improved miscibility and introducing the potential for covalent crosslinking between the TPE and the PA. The reaction mechanisms of PA with compatibilized TPE have been well-studied, as have the mechanical properties of these blends.

An area that has not been so thoroughly studied is the macroscale combination of PA with TPE. However, high-rate processes such as hybrid injection molding are well characterized for combinations of other thermoplastics with TPEs. This, combined with a thorough understanding of the interactions between PA and compatibilized TPE, illustrate a clear path forward toward hybrid molding TPE onto PA substrates.

### **2.2.1 PA/Elastomer Blends**

Naeim abadi et al [122] found that SBS grafted with maleic anhydride (SBS-*g*-MA) was able to form strong interfacial bonds with PA12 in a polymer blend, despite the immiscibility of unmodified SBS with PA. They find that the materials interact via both hydrogen bonding and a covalent bond between the maleic anhydride and the nitrogen molecule of the PA12 amide group. PA12 has greater polymer chain distance between polar amide groups than PA6 or PA6,6 and is therefore less polar and more compatible with nonpolar molecules such as SBS, which may allow for slightly improved chain entanglement. However, it appears that these two bonding methods will be available to all PA grades in combination with maleated TPE.

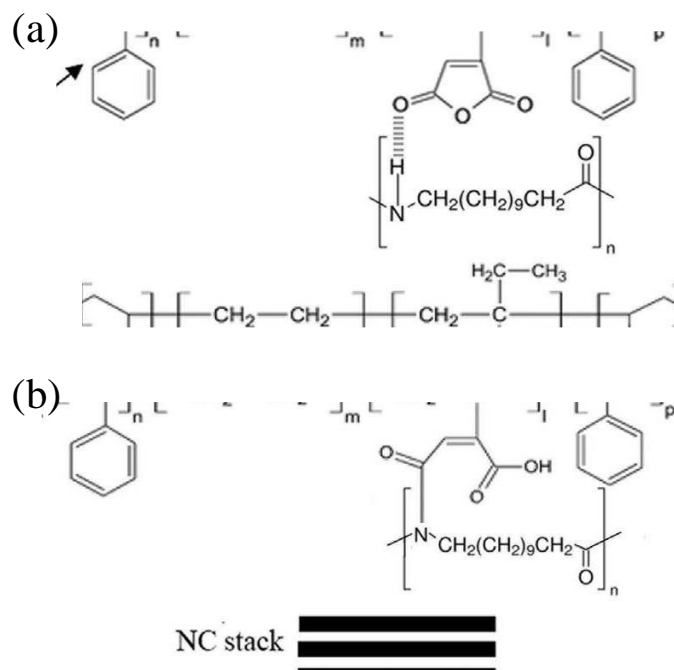


Figure 2.19. Schematic representation of (a) hydrogen bonding and (b) covalent bonding between SBS-g-MA and PA12. From Naeim abadi et al [122].

The PA reaction with MA is further elucidated by Van Duin et al [123], as shown in Figure 2.20. They find that the primary reaction occurs between the imide group at the end of a PA chain and the central oxygen molecule of the MA. The water molecule produced by this reaction may then go on to hydrate an amide group further along the PA chain, dividing the chain and providing another imide group that may react with the MA. This process creates a highly crosslinked interface between the two polymer phases and may, given time, begin to degrade the PA.

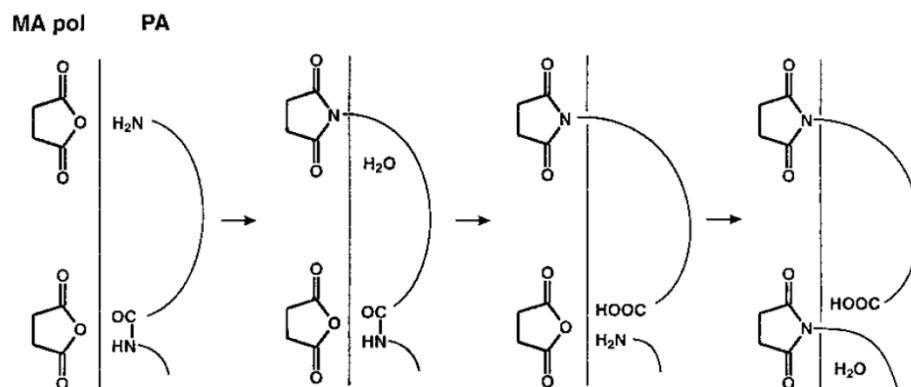


Figure 2.20. Reaction between PA imide group and maleic anhydride, followed by hydrolysis of amide group. From Van Duin et al [123].

Tomova and Radusch [124] created blends of PA6, PA6,6, and maleated rubber (EO-g-MA), finding that the monofunctionality of the PA6 led to decreased interfacial tension between the PA and the rubber, which in turn resulted in smaller rubber particles than in the PA6,6 blends, where the interfacial tension was higher.

Ebrahimi Jahromi et al [125] created ternary blends of PA6, nanoclay, and acrylonitrile butadiene rubber (NBR), either with or without glycidyl methacrylate (GMA) as a compatibilizer. They found that, while the nanoclay had a slight influence on mechanical properties, the GMA compatibilizer had a much larger effect, increasing both the tensile strength and the impact strength of the blends. This improvement in properties is attributed to the improved bond strength between the PA6 and the NBR-g-GMA relative to the bond strength between PA6 and NBR.

Kim et al [126] studied the effect of maleic anhydride concentration on PA6/rubber blends. They found that as the MA content increased, the rubber particles formed *in-situ* became smaller as the improved compatibility between phases reduced the energy required to form PA/rubber interfaces. They also found that as adhesion between the PA6 and the modified rubber increased, so too did the impact strength of samples made from the blend.

Huang et al [127] found that increased SEBS-g-MA content in PA/SEBS-g-MA binary blends greatly reduced the yield strength, but adding even a small amount of SEBS-g-MA, approximately 10wt%, created super-toughened blends. Above 10wt% SEBS-g-MA, they saw no further improvement in Izod impact performance with increased TPE content. They also found

that smaller SEBS-g-MA particle size increased the elongation to break but had no discernable influence on the yield strength or impact performance for the particle size range tested.

Tjong et al conducted a series of studies on the performance of short glass fiber-reinforced PA6,6 toughened with particles of SEBS-g-MA [128]–[130]. They found that the presence of the maleated SEBS can significantly improve impact performance, especially when the glass fiber content is low. When no glass fibers are present in the blends, energy is primarily absorbed through cavitation of the rubber particles and matrix shear yielding [128]. When glass fibers are present, fiber delamination and pull out dominate.

### **2.2.2 TPE onto PA Overmolding**

Braüer et al [131] examined the effect of an adhesion promotor, in this case 4,4'-diphenylmethane diisocyanate (MDI) on the adhesion between PA6 and overmolded TPU. The adhesion promotor improved the bond strength by up to 50% due to covalent bonding between the MDI and the amide groups of the PA6 chains.

Pompe et al [132] examined the effect of processing condition on the adhesion between PA6 and overmolded TPU modified with an adhesion promoter. They use a multi-material injection molding process, finding that best adhesion between the two components is achieved when the first component is allowed to cool so that there is a temperature gradient between the first and second material. However, the first material must remain sufficiently warm so that the overmolding material is able to locally heat the bi-material interface, allowing the interface to anneal.

Persson et al [133] studied the effect of processing condition on multi-material injection molded parts made from PA12 with varying amounts of glass fiber overmolded with a TPE modified for adhesion to PA. They saw similar effects as Pompe [132], where both increased TPE overmolding temperature and increased substrate temperature improved adhesion by increasing the interfacial temperature. They also found that increased glass fiber content in the PA12 substrate had a negative effect on bond strength.

Overmolding has been shown to work well for combinations of TPE and PA, but further research is needed into the processing and mechanical properties of such blends.

### 2.2.3 Other Thermoplastic/TPE Overmolding

Finally, insights gained from overmolding TPE onto other thermoplastics can inform the design and manufacture of parts made from TPE overmolded onto PA. Overmolding of a TPE onto a thermoplastic substrate consists of three phases, as proposed by Weng et al [134]:

- Wetting the substrate with the TPE melt
- Interaction between the TPE and thermoplastic polymer chains, which may consist of interdiffusion or bonding
- Solidification, which may include specific crystallization conditions

These steps follow the theories of favorable adhesion conditions discussed in section 2.1. As with all dissimilar material combinations, interfacial bond strength can be improved through the selection of materials that can exploit one or more of the theories of adhesion. For example, a TPE with a lower surface energy will wet well onto a higher energy substrate, and a TPE that is miscible or able to covalently bond with the substrate will improve specific interactions.

Arzondo et al [135] overmolded solid polypropylene (PP) with a molten TPE, finding that strong interfacial bonding can occur even when the interface temperature is well below the PP melting point. They attribute this adhesion primarily to molecular motion in the TPE overmold, as they observe little variation when the interfacial temperature is above the PP melt temperature.

Candal et al [136] found that for PP overmolded with elastomeric thermoplastic vulcanate (TPV), the temperature of the molten TPE had a significant effect on bond strength while mold temperature and hold pressure had less of an influence in the ranges tested.

Similarly, Rossa-Sierra et al [137] found that increasing the TPU overmold temperature yielded a notable improvement in bond strength, although the best way to improve the bond strength between a thermoplastic substrate and TPU overmold was to increase the surface roughness of the solid substrate. They also find little effect of flow rate on bond strength. This suggests that any improved wetting of the substrate that comes from reduced TPU melt viscosity is insufficient to have a noticeable effect on bond strength.

Conversely, Chandran et al [138] found that, for TPE overmolded onto isotactic polypropylene (iPP), mold temperature had the greatest influence on bond strength, although they did not vary the overmolding temperature. They also observed adhesion when the interfacial

temperature was below the iPP melting temperature, which they attribute in part to a local reduction in melt temperature at the surface due to migration of plasticizer from the TPE melt into the iPP.

#### **2.2.4 Section Summary**

Improved adhesion between the TPE particles and the PA matrix resulted in improved impact performance. Though PA is generally incompatible with TPEs, reactive molecules including maleic anhydride and glycidyl methacrylate may be grafted onto TPE chains to act as compatibilizers. Extensive research has been conducted on the behavior of PA and TPE blends, including the effect of compatibilizers, reaction mechanisms, and failure modes. TPEs have been used to successfully toughen these blends of PA, primarily via TPE particle cavitation and PA shear yielding.

For overmolding applications, interfacial temperature between the substrate and the TPE overmold appears to be the most important factor for improving adhesion. When the temperature is too low, neither the overmold nor the substrate will have sufficient chain mobility to interact across the interface. Interfacial temperature can be increased by increasing the temperature of the overmolding melt, the substrate in the mold, or both, and a larger thermal gradient across the interface can further improve the bond strength, provided a melting and re-solidification of the interface.

### **2.3 Background: Aluminum/Thermoplastic Combinations**

Aluminum is widely used in a variety of applications due to its low cost, light weight, and weldability, making it suitable for high-rate manufacturing. Thermoplastics can offer the ability to create complex part geometries in a single processing step through high-rate manufacturing such as injection molding, eliminating the need for additional joining steps that would be required with traditional metal forming. Further, polymers typically offer thermal and electrical resistance, and can therefore be used to insulate aluminum.

Composite materials made with polymeric matrices and glass or carbon reinforcing fibers can also be combined with aluminum. Short-fiber reinforced polymers can be processed using the

same high-rate techniques as neat polymers, allowing for the same complex part formation with the advantage of improved stiffness and strength properties.

One application where this combination of materials may be beneficial is in automotive body panels. For weight reduction aluminum has been a suitable alternative. However, aluminum is very ductile, making it prone to surface dents from minor impacts from hail or pebbles on the road. Those these dents may not harm the structure of the vehicle, they are undesirable. Polymer-reinforced composites, on the other hand, have superior resistance to surface dents, and damage is often undetectable with the naked eye. For these cases, a composite surface sheet can protect the surface quality of aluminum body panels, while a lower layer of aluminum can reduce costs and provide convenient welding points. This allows these hybrid body panels to be incorporated into existing production lines and processes.

In most practical applications, the polymer will not be in direct contact with the bulk aluminum—rather, it will be in contact with an aluminum oxide, or alumina, layer on the surface of the aluminum. The oxide layer forms extremely quickly on aluminum surfaces exposed to oxygen, so any hybrid materials produced outside of an environmental chamber will involve the interaction of a polymer with an aluminum oxide.

### **2.3.1 Surface Treatment of Aluminum to Promote Adhesion**

For many material combinations and applications, adhesion between metals and thermoplastics needs to be enhanced. This is typically accomplished via some pretreatment of the metal surface, which can be divided into two categories—dry adhesion and wet adhesion. Dry adhesion involves mechanical surface abrasion and can include laser machining and abrasive blasting. Wet processing relies on chemical processes such as chemical etching and anodization. Both dry and wet processing techniques work by increasing the metal surface area available for bonding.

#### ***Dry Processing***

Dry processing typically does not involve chemical etchants and is therefore often relatively environmentally friendly. However, it can require capital investment in expensive equipment, particularly if regular, predictable structures are desired.



Ramani et al [139]–[141] conducted a series of experiments to determine the effect of various processing parameters on the bond strength between sand-blasted metals and injection overmolded polymers. They found that the metal substrate temperature was the most important factor controlling adhesion. If the metal was not heated no bond was formed, as the polymer cooled too quickly to form intimate contact with the metal.

Enami et al [142] examine the effect of laser-formed surface toughness on the bond strength of aluminum overmolded with polybutylene terephthalate (PBT). They found that adhesion was best when there were more, smaller dimples in the aluminum and that surface roughness inside the dimples improved adhesion. Under the right processing conditions, they were able to attain adhesive shear strengths stronger than the bulk polymer shear strength. This suggests having many smaller interaction points between the aluminum and the polymer, evenly distributed across the interface is important for strong interface formation. Thus, a controlled and designed surface configuration is a prerequisite for a strong and durable polymer/aluminum material combination.

Taki et al [143] used laser ablation to create a microgrid on an aluminum surface before injection overmolding with acrylonitrile butadiene styrene (ABS), polystyrene (PS) and glass-filled PBT. Laser ablation was able to create deeper surface features than particle ablation, which tended to improve the bond strength between the aluminum and the polymer overmold. However, this improvement was limited by the ability of the polymer to infiltrate the microgrid, especially at lower substrate temperatures. When the substrate temperature was sufficiently high to allow polymer infiltration before cooling, strong interfacial bonds were achieved.

### ***Wet Processing***

Wet processing can typically be done with minor equipment investments. However, the chemicals involved in etching can require special disposal processes and can be harmful to humans and the environment.

Fabrin et al [144] pretreated aluminum bars with an acid-alkaline pretreatment to create a porous surface, then overmolded onto the bars with TPE. They did not preheat the aluminum bars before overmolding, but they found that thicker aluminum (>0.5mm) acted as a heat sink and resulted in weaker interfaces, as the overmolded TPE cooled too quickly upon contact with the cool aluminum to fully penetrate the porous metal surface.

Yin et al [145] used an electrochemical anodization process to pretreat their aluminum sheets that resulted in a surface layer of alumina studded with nanopores. These nanopores allowed for mechanical interlocking between the aluminum sheet and the PBT overmolded material. Aluminum sheets that were treated at higher voltages had larger nanopores, which resulted in stronger bonding. As the nanopore size decreases from 14.3nm to 7.8nm, the polymer melt is less able to fill the nanopores.

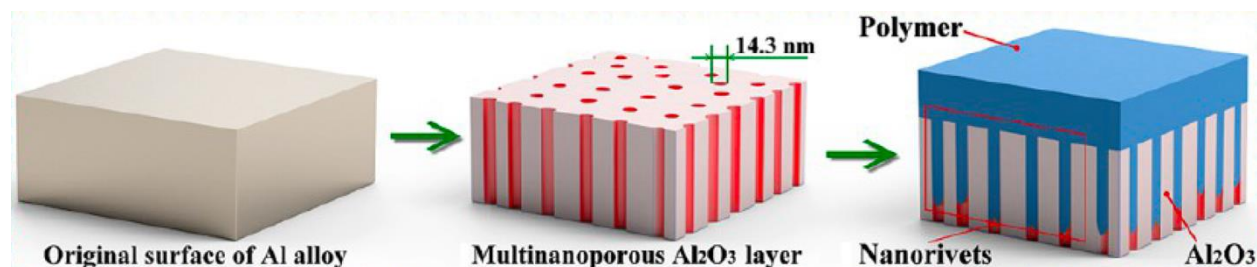


Figure 2.21. Schematic of micropore formation on the surface of aluminum due to an electrochemical anodization process, from Yin et al [145].

A previous study from the same group [146] involved only a chemical treatment of the aluminum before overmolding with PBT. Though they were able to attain a larger pore size than with their electrochemical treatments, they observed an incomplete coating of the aluminum surface with alumina, which they believe resulted in weaker bond than they found with the electrochemical process as the micropores are only formed in the alumina.

Yusof et al [147] also found that aluminum anodization improved bond strength to PET above what was possible without anodization. Further, they found that bond strength also increased with increased interfacial temperature, which thereby facilitates interpenetration of the PET into the surface undulations of the aluminum.

### 2.3.2 Spontaneous Adhesion between Aluminum and Thermoplastics

Though surface treatment processes can improve the adhesion between thermoplastics and metals, the enhanced interfacial bond may not be necessary for some applications, and in some cases thermoplastics may be able to covalently bond to metal surfaces without requiring a surface treatment step.

Liu et al [148] find that polymers with a carbonyl group, including PA, polyethylene terephthalate (PET), polycarbonate (PC), and polymethylmethacrylate (PMMA) may be able to covalently bond with metal atoms in the oxide layer on the surface of a metal. Their work confirms the spontaneous formation of an Al-O-C bond between the carbonyl group in PA6,6 and alumina.

Subsequent studies have successfully combined PA6 with metal sheets via friction lap welding [149]. Friction lap welding is a process that uses a rotating, moving tool with downward pressure to create heat via friction. This heat softens the materials and allows them to interact across the interface, forming a bond. Liu et al[149] found that when the tool rotation speed was high and its transverse speed was low—i.e., when the temperature was highest due to friction—the bond between the aluminum and the PA6 was improved. However, they observed a phenomenon that is common to many high-temperature metal-polymer joining processes—the formation of bubbles in the thermoplastic due to degradation caused by local extreme temperatures[147], [150]–[152]. A strong bond can still form even with these bubbles, and the bond strength may even be improved by their presence[151], but the part life is likely reduced due to polymer degradation. Therefore, the processing conditions should be carefully monitored to limit degradation.

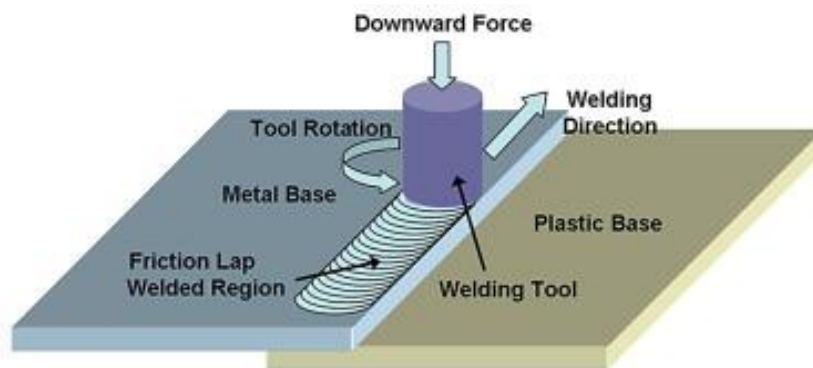


Figure 2.22. Friction Lap Welding process for joining polymer to metal. From Liu et al[149].

### 2.3.3 Section Summary

There are numerous ways to improve polymer adhesion to alumina via aluminum surface preparations, including both dry and wet processing techniques. Though both have advantages and disadvantages—dry processing can create more locally controlled surfaces but can be costly, while wet processing does not require large capital investment but can involve chemicals that are harmful

to people and the environment—the bond improvement techniques are the same regardless of surface preparation technique. Both methods rely on increasing the aluminum area available for bonding by creating small-scale surface roughness.

The surface roughness should be evenly distributed across the aluminum surface for better bonding. Processing conditions must be carefully chosen so that the polymer remains melted long enough to create intimate contact with the aluminum. If the imposed aluminum surface roughness consists of pores that are too small, polymers will not be able to effectively infiltrate the pores, even under carefully selected processing conditions.

Some polymers, notably those that contain carbonyl groups, can spontaneously bond to the aluminum molecules in the alumina surface layer. This creates a strong interface without the additional processing and costs associated with extensive aluminum surface preparation. Although the interface strength can be improved with these surface preparation steps, it may not be necessary. The decision to use a surface treatment or not should be made for a given application and will depend on the polymer to be combined with aluminum.

## **2.4 Chapter Conclusions**

A thorough critical review of the mechanisms involved in combining several types of dissimilar materials has been presented. Though materials can be combined in a variety of geometries, at length scales ranging from microns to meters, the underlying principles do not change. A wide variety of material systems may be combined to exploit the beneficial properties of both. In many cases, a more ductile material is added to a stiffer and stronger material to improve toughness without sacrificing part strength. There may be additional benefits as well, such as thermal and electrical shielding in the case of thermoplastic addition to aluminum.

For all material combinations, the bi-material interface is critical for energy transfer. The theories of adhesion outlined in this section are universal and apply to all material combinations. Adhesion can be achieved via a variety of methods including chemical bonding, polymer interdiffusion, and mechanical interlocking, and all three of the material combinations studied here can take advantage of these three methods. PA amide groups can covalently bond to EP epoxide rings, TPE compatibilizer groups can covalently bond to PA amide groups, and various thermoplastics, including PA, can covalently bond to the alumina layer on an aluminum surface. Polymer interdiffusion can occur in EP/PA and TPE/PA blends, and increased processing

temperature can increase polymer chain mobility and thereby considerably contribute to the overall performance. Finally, mechanical interlocking can be achieved by incorporating surface roughness onto a solid substrate. The liquid polymer—which may be uncured EP, melted TPE, or melted PA—can flow into the substrate surface and solidify, improving adhesion. Mechanical interlocking will also be improved in these cases if the processing temperature is increased, as this will reduce the liquid viscosity and improve surface roughness impregnation.

A major energy absorption mechanism in these multi-material systems is the debonding and subsequent deformation of the more ductile material. Therefore, particularly in geometries where the ductile material is encased in a more brittle material (e.g. particle-toughened resins, thermoplastic interleaves) the interfacial bond strength must be weak enough to allow the interface to fail and the ductile material to deform. However, once the interface has failed, there is limited energy transfer to the ductile phase.

The rest of this thesis focuses on macro-scale material toughening, in which a large ductile sample size is combined with a more brittle one to create bi-layered systems. Because the ductile phases used here are large and not encased in a brittle material, debonding may not be required to allow for deformation, meaning that efficient energy transfer across the interface can occur even after ductile phase deformation. This may in turn enable greater energy overall energy absorption. The following chapters also examine the effect of processing condition on interfacial adhesion, and in turn on part performance.

## 2.5 References

- [1] J. E. McMurry, *Organic Chemistry: Chem 10172 & Chem 20273*, 8th ed. Cengage Learning, 2012.
- [2] A. C. Garg and Y.-W. Mai, “Failure Mechanisms in Toughened Epoxy Resins-A Review,” *Compos. Sci. Technol.*, vol. 31, pp. 179–223, 1988.
- [3] F. J. McGarry, “Building Design with Fibre Reinforced Materials,” *P. R. Soc. A*, vol. 319, p. 59, 1970.
- [4] W. D. Bascom, R. L. Cottingham, R. L. Jones, and P. Peyser, “The Fracture of Epoxy- and Elastomer-Modified Epoxy Polymers in Bulk and as Adhesives,” *J. Appl. Polym. Sci.*, vol. 19, pp. 2545–2562, 1975.

- [5] J. N. Sultan and F. J. McGarry, "Effect of Rubber Particle Size on Deformation Mechanisms in Glassy Epoxy," *Polym. Eng. Sci.*, vol. 13, no. 1, pp. 29–34, 1973.
- [6] A. C. Garg and Y.-W. Mai, "Failure Mechanisms in Toughened Epoxy Resins—A Review," *Compos. Sci. Technol.*, vol. 31, pp. 179–223, 1988.
- [7] R. Bagheri, B. T. Marouf, and R. A. Pearson, "Rubber-Toughened Epoxies: A Critical Review," *J. Macromol. Sci C.*, vol. 49, pp. 201–225, 2009.
- [8] J. H. Hodgkin, G. P. Simon, and R. J. Varley, "Thermoplastic Toughening of Epoxy Resins: a Critical Review," *Polym. Advan. Technol*, vol. 9, pp. 3–10, 1998.
- [9] R. Mülhaupt, "Flexibility or Toughness?—The Design of Thermoset Toughening Agents," *Chimia*, vol. 44, pp. 43–52, 1990.
- [10] P. Vijayan, P. ; Puglia, D. ; Al-Maadeed, M. A. S. A. ; Kenny, J. M. ; Thomas, and S., "Elastomer/Thermoplastic Modified Epoxy Nanocomposites: The Hybrid Effect of 'Micro' and 'Nano' Scale," *Mat Sci. Eng R*, vol. 116, pp. 1–29, 2017.
- [11] M. E. Frigione, L. Mascia, and D. Acierno, "Oligomeric and Polymeric Modifiers for Toughening of Epoxy Resins," *Eur. Polym. J*, vol. 31, no. 11, pp. 1021–1029, 1995.
- [12] R. Mezzenga, L. Boogh, and J.-A. E. Månson, "A Review of Dendritic Hyperbranched Polymer as Modifiers in Epoxy Composites," *Compos. Sci. Technol.*, vol. 61, pp. 787–795, 2001.
- [13] Y. Huang, D. L. Hunston, A. J. Kinloch, and C. K. Riew, "Mechanisms of Toughening Thermoset Resins," *Toughened Plastics I*, pp. 1–35, 1993.
- [14] D. Ratna, "Modification of Epoxy Resins for Improvement of Adhesion: A Critical Review," *J. Adhes. Sci. Technol*, vol. 17, no. 12, pp. 1655–1668, 2003.
- [15] K. W. Allen, "Some Reflections on Contemporary Views of Theories of Adhesion," *Int. J. Adhes. Adhes.*, vol. 13, no. 2, pp. 67–72, 1993.
- [16] K. W. A. Allen, "Review of Contemporary Views of Theories of Adhesion," *J. Adhesion*, vol. 21, pp. 216–277, 1987.
- [17] M. Kryszewski, A. Galeski, and E. Martuscelli, "Polymer Blends: Processing Morphology, and Properties," *Springer Science+Business Media: New York*, vol. 2, 1984.
- [18] J. Comyn, *Adhesion Science*. RSC Publishing, 1997.

- [19] W. C. Wake, "Theories of Adhesion and Uses of Adhesives: A Review," *Polymer*, vol. 19, pp. 291–308, 1978.
- [20] A. J. Kinloch, *Adhesion and Adhesives: Science and Technology*. London: Chapman & Hall, 1987.
- [21] G. Fourche, "An Overview of the Basic Aspects of Polymer Adhesion Part I: Fundamentals," *Polym. Eng. Sci.*, vol. 35, no. 12, pp. 957–967, 1995.
- [22] H. W. Kammer and J. Piglowshi, "Adhesion between Polymers," *Polymer Blends*, pp. 19–34, 1984.
- [23] G. Fourche, "An Overview of the Basic Aspects of Polymer Adhesion. Part II: Application to Surface Treatments," *Polym. Eng. Sci.*, vol. 35, no. 12, pp. 968–975, 1995.
- [24] R. Awaja, M. Gilbert, G. Kelly, B. Fox, and P. J. Pigram, "Adhesion of Polymers," *Progress of Polymer Science*, vol. 34, pp. 948–968, 2009.
- [25] J. L. Hedrick, I. Yilgor, M. Jurek, J. C. Hedrick, G. L. Wilkes, and J. E. McGrath, "Chemical Modification of Matrix Resin Networks with Engineering Thermoplastics: 1 Synthesis, Morphology, Physical Behaviour and Toughening Mechanisms of Poly(arylene ether sulphone) Modified Epoxy Networks," *Polymer*, vol. 32, no. 11, pp. 2020–2032, 1991.
- [26] C. B. Bucknall and I. K. Partridge, "Phase Separation in Epoxy Resins Containing Polyethersulphone," *Polymer*, vol. 24, pp. 639–644, 1983.
- [27] R. S. Raghava, "Role of Matrix-Particle Interface Adhesion on Fracture Toughness of Dual Phase Epoxy-Polyethersulfone Blend," *J. Polym. Sci. Pol. Phys*, vol. 25, pp. 1017–1031, 1987.
- [28] R. S. Raghava, "Development and Characterization of Thermosetting-Thermoplastic Polymer Blends for Applications in Damage-Tolerant Composites," *J. Polym. Sci. Pol. Phys*, vol. 26, pp. 65–81, 1988.
- [29] J. L. Hedrick, M. J. Jurek, I. Yilgor, and J. E. McGrath, "Chemical Modification of Matrix Resin Networks with Engineering Thermoplastics. III. Synthesis and Properties of Epoxy Networks Modified with Amine Terminated Poly(Aryl Ether Sulfone) Oligomers," *Polym. Prepr*, vol. 26, pp. 293–295, 1985.
- [30] Y. Fu Z. & Sun, "Epoxy Toughened by Thermoplastics," *Polym. Prepr.*, vol. 29, pp. 177–178, 1988.

- [31] A. J. MacKinnon, S. D. Jenkins, P. T. McGrail, and R. A. Pethrick, "A Dielectric and Mechanical, Rheological and Electron Microscopy Study of Cure and Properties of a Thermoplastic-Modified Epoxy Resin," *Macromolecules*, vol. 25, pp. 3492–3499, 1992.
- [32] A. J. MacKinnon, S. D. Jenkins, P. T. McGrail, and R. A. Pethrick, "Cure and Physical Properties of Thermoplastic Modified Epoxy Resins Based on Polyethersulfone," *J. Appl. Polym. Sci*, vol. 58, pp. 2345–2355, 1995.
- [33] B.-G. Min, J. H. Hodgkin, and Z. H. Stachurski, "Reaction Mechanisms, Microstructure, and Fracture Properties of Thermoplastic Polysulfone-Modified Epoxy Resin," *J. Appl. Polym. Sci*, vol. 50, pp. 1065–1073, 1993.
- [34] T. H. Yoon, S. C. Liptak, D. B. Priddy Jr., and J. E. McGrath, "Adhesive and Mechanical Properties of Reactive Polysulfone Modified Epoxy Resins," *J. Adhesion*, vol. 45, no. 1–4, pp. 191–203, 1994.
- [35] R. J. Varley and J. H. Hodgkin, "Effect of Reinforcing Fibres on the Morphology of a Toughened Epoxy/Amine System," *Polymer*, vol. 38, no. 5, pp. 1005–1009, 1997.
- [36] I. Martinez, M. D. Martin, A. Eceiza, P. Oyanguren, and I. Mondragon, "Phase Separation in Polysulfone-Modified Epoxy Mixtures. Relationships between Curing Conditions, Morphology and Ultimate Behavior," *Polymer*, vol. 41, pp. 1027–1035, 2000.
- [37] B.-G. Min, Z. H. Stachurski, and J. H. Hodgkin, "Microstructural Effects and the Toughening of Thermoplastic Modified Epoxy Resins," *J. Polym. Sci*, vol. 50, pp. 1511–1518, 1993.
- [38] P. Huang, S. Zheng, J. Huang, and Q. Guo, "Miscibility and Mechanical Properties of Epoxy Resin/Polysulfone Blends," *Polymer*, vol. 38, no. 22, pp. 5565–5571, 1997.
- [39] J. L. Hedrick, I. Yilgor, G. L. Wilkes, and J. E. McGrath, "Chemical Modification of Matrix Resin Networks with Engineering Thermoplastics 1. Phenolic Hydroxyl Terminated Poly(Aryl Ether Sulfone)-Epoxy Systems," *Polym. Bulletin*, vol. 13, pp. 201–208, 1985.
- [40] I. Blanco, G. Cicala, L. Faro, C. ; Recca, and A., "Improvement of Thermomechanical Properties of a DGEBS/DDS System Blended with a Novel Thermoplastic Copolymer by Realization of a Semi-IPN Network," *J. Appl. Polym. Sci*, vol. 88, pp. 3021–3025, 2003.



- [41] G. di Pasquale, O. Motta, A. Recca, J. T. Carter, P. T. McGrail, and D. Acierno, “New High-Performance Thermoplastic Toughened Epoxy Thermosets,” *Polymer*, vol. 38, no. 17, pp. 4345–4348, 1997.
- [42] D. Dumont, D. Seveno, J. de Coninck, C. Bailly, J. Devaux, and D. Daoust, “Interdiffusion of Thermoplastics and Epoxy Resin Precursors: Investigations Using Experimental and Molecular Dynamics Methods,” *Polym. Int*, vol. 61, pp. 1263–1271, 2012.
- [43] A. J. Kinloch, M. L. Yuen, and S. D. Jenkins, “Thermoplastic-Toughened Epoxy Polymers,” *J. Mater. Sci*, vol. 29, pp. 3781–3790, 1994.
- [44] R. S. Brooker, A. J. Kinloch, and A. C. Taylor, “The Morphology and Fracture Properties of Thermoplastic-Toughened Epoxy Polymers,” *J. Adhesion*, vol. 86, no. 7, pp. 726–741, 2010.
- [45] C. B. Bucknall and I. K. Partridge, “Phase Separation in Crosslinked Resins Containing Polymeric Modifiers,” *Polym. Eng. Sci.*, vol. 26, no. 1, pp. 54–62, 1986.
- [46] Y. Yu, M. Wang, W. Gan, Q. Tao, and S. Li, “Polymerization-Induced Viscoelastic Phase Separation in Polyethersulfone-Modified Epoxy Systems,” *J. Phys. Chem. B*, vol. 108, pp. 6208–6215, 2004.
- [47] E. van Overbeke, J. Devaux, R. Legras, J. T. Carter, P. T. McGrail, and V. Carlier, “Phase Separation in Epoxy-Copolyethersulfone Blends: Morphologies and Local Characterisation by Micro-Raman Spectroscopy,” *Polymer*, vol. 44, pp. 4899–4908, 2003.
- [48] M. Naffakh, M. Dumon, and J. F. Gérard, “Study of a Reactive Epoxy-Amine Resin Enabling in situ Dissolution of Thermoplastic Films during Resin Transfer Moulding for Toughening Composites,” *Compos. Sci. Technol.*, vol. 66, pp. 1376–1384, 2006.
- [49] C. B. Bucknall and A. H. Gilbert, “Toughening Tetrafunctional Epoxy Resins Using Polyetherimide,” *Polymer*, vol. 30, pp. 213–217, 1989.
- [50] D. J. Hourston, J. M. Lane, and N. A. MacBeath, “Toughening of Epoxy Resins with Thermoplastics. II. Tetrafunctional Epoxy Resin-Polyetherimide Blends,” *Polym. Int*, vol. 26, pp. 17–21, 1991.

- [51] D. J. Hourston and J. M. Lane, "The Toughening of Epoxy Resins with Thermoplastics: 1. Trifunctional Epoxy Resin-Polyetherimide Blends," *Polymer*, vol. 33, no. 7, pp. 1379–1383, 1992.
- [52] J. B. Cho, J. W. Hwang, K. Cho, J. H. An, and C. E. Park, "Effects of Morphology on Toughening of Tetrafunctional Epoxy Resins with Poly(ether imide)," *Polymer*, vol. 34, no. 23, pp. 4832–4836, 1993.
- [53] M. C. Chen, D. J. Hourston, F.-U. Shafer, and T. N. Huckerby, "Miscibility and Fracture Behaviour of Epoxy Resin-Nitrated Polyetherimide Blends," *Polymer*, vol. 36, no. 17, pp. 3287–3293, 1995.
- [54] L. Bonnaud, A. Bonnet, J. P. Pascault, H. Sautereau, and C. C. Riccardi, "Different Parameters Controlling the Initial Solubility of Two Thermoplastics in Epoxy Reactive Solvents," *J. Appl. Polym. Sci*, vol. 83, pp. 1385–1396, 2002.
- [55] H. Li, W. Gan, L. Zhao, and S. Li, "Studies on the Phase Separation of a Polyetherimide Modified Epoxy Resin VI. Effect of Surface Energy on Reaction-Induced Phase Separation of Epoxy Resin Modified with Polyetherimide," *J. Macromol. Sci. A*, vol. 40, no. 8, pp. 833–846, 2003.
- [56] M. T. Heitzmann, M. Hou, M. Veidt, L.-J. Vandi, and R. Paton, "Morphology of an Interface between Polyetherimide and Epoxy Prepreg," *Adv. Mat. Res*, pp. 184–188, 295–393, 2012.
- [57] D. J. Hourston, J. M. Lane, and H. X. Zhang, "Toughening of Epoxy Resins with Thermoplastics: 3. An Investigation into the Effects of Composition on the Properties of Composition on the Properties of Epoxy Resin Blends," *Polym. Int*, vol. 42, pp. 349–355, 1997.
- [58] Y. Zu, S. Zhou, and J. Xigao, "Fracture Toughening of Epoxy Resins by Addition of a Novel Thermoplastic PPAEs," *Appl. Mech. Mater*, vol. 161, pp. 153–156, 2012.
- [59] Y. Xu, S. Zhou, G. Liao, and X. Jian, "Curing Kinetics of DGEBA Epoxy Resin Modified by Poly(phthalazinone ether ketone) (PPEK)," *Polym. Plast. Technol*, vol. 51, no. 2, pp. 128–133, 2012.
- [60] R. Liu, J. Wang, Q. He, L. Zong, and X. Jian, "Interaction and Properties of Epoxy-Amine System Modified with Poly (phthalazinonone ether nitrile ketone)," *J. Appl. Polym. Sci*, vol. 133, p. 42938, 2016.

- [61] R. A. Pearson and A. F. Yee, "Toughening Mechanisms in Thermoplastic-Modified Epoxies: 1. Modification using Poly(Phenylene Oxide)," *Polymer*, vol. 34, no. 17, pp. 3658–3670, 1993.
- [62] S. J. Wu, T. K. Lin, and S. S. Shyu, "Cure Behavior, Morphology, and Mechanical Properties of the Melt Blends of Epoxy with Polyphenylene Oxide," *Int. J. Appl. Polym. Sci*, vol. 75, pp. 26–34, 2000.
- [63] S. J. Wu, N. P. Tung, T. K. Lin, and S. S. Shyu, "Thermal and Mechanical Properties of PPO Filled Epoxy Resins Compatibilized by Triallylisocyanurate," *Polym. Int*, vol. 49, no. 1, pp. 1452–1457, 2000.
- [64] R. A. Pearson and A. F. Yee, "The Preparation and Morphology of PPO-Epoxy Blends," *J. Appl. Polym. Sci*, vol. 48, pp. 1051–1060, 1993.
- [65] J. N. Hay, B. Woodfine, and M. Davies, "Toughening of Epoxy Resins by Polyimides Synthesized from Bisanilines," *High Perform. Polym*, vol. 8, pp. 35–56, 1996.
- [66] N. Biette, T. Pascal, and B. Sillion, "Polyimide-Modified Epoxy System: Time-Temperature-Transformation Diagrams, Mechanical and Thermal Properties," *Polymer*, vol. 35, no. 3, pp. 558–564, 1994.
- [67] K. Gaw, M. Kikei, M. Kakimoto, and Y. Imai, "Preparation of Polyamide-Epoxy Composites," *React. Func. Polym*, vol. 30, pp. 85–91, 1996.
- [68] K. O. Gaw and M. Kakimoto, "Polyimide-Epoxy Composites," *Adv. Polym. Sci*, vol. 140, pp. 107–136, 1999.
- [69] T. Agag and T. Takeichi, "Synthesis and Characterization of Epoxy Film Cured with Reactive Polyimide," *Polymer*, vol. 40, pp. 6557–6563, 1999.
- [70] B. Francis, S. Thomas, J. Jose, R. Ramaswamy, L. Rao, and V., "Hydroxyl Terminated Poly(ether ether ketone) with Pendent Methyl Group Toughened Epoxy Resin: Miscibility, Morphology and Mechanical Properties," *Polymer*, vol. 46, pp. 12372–12385, 2005.
- [71] A. Asif, L. Rao, V. ; Saseendran, V. ; Ninan, and K. N., "Thermoplastic Toughened Layered Silicate Epoxy Ternary Nanocomposites—Preparation, Morphology, and Thermomechanical Properties," *Polym. Eng. Sci.*, vol. 49, no. 4, pp. 756–767, 2009.

- [72] B. Francis *et al.*, “Diglycidyl Ether of Bisphenol-A Epoxy Resin Modified Using Poly(ether ether ketone) with Pendent tert-Butyl Groups,” *J. Polym. Sci. Pol. Phys.*, vol. 45, pp. 2481–2496, 2007.
- [73] D. E. Floyd, D. E. Peerman, and H. Wittcoff, “Characteristics of the Polyamide-Epoxy Resin System,” *J. Appl. Chem.*, vol. 7, pp. 250–260, 1957.
- [74] M. M. Renfrew, H. Wittcoff, D. E. Floyd, and D. W. Glaser, “Coatings of Polyamide and Epoxy Resin Blends,” *Ind. Eng. Chem.*, vol. 46, no. 10, pp. 2226–2232, 1954.
- [75] M. J. Doyle, A. F. Lewis, and H.-M. Li, “Time-Temperature Cure Behavior of Epoxy Based Structural Adhesives,” *Polym. Eng. Sci.*, vol. 19, no. 10, pp. 687–691, 1979.
- [76] Z. Zhong and Q. Guo, “Miscibility and Cure Kinetics of Nylon/Epoxy Reactive Blends,” *Polymer*, vol. 39, no. 15, pp. 3451–3458, 1998.
- [77] Y.-Y. Wang and S. A. Chen, “Polymer Compatibility: Nylon-Epoxy Resin Blends,” *Polym. Eng. Sci.*, vol. 20, no. 12, pp. 823–829, 1980.
- [78] R. B. Prime and E. Sacher, “Kinetics of epoxy cure: 2. The System Bisphenol-A Diglycidyl Ether/Polyamide,” *Polymer*, vol. 13, pp. 455–458, 1972.
- [79] I. Blanco, G. Cicala, O. Motta, and A. Recca, “Influence of a Selected Hardener on the Phase Separation in Epoxy/Thermoplastic Polymer Blends,” *J. Appl. Polym. Sci.*, vol. 94, pp. 361–371, 2004.
- [80] B. de Schoenmaker, S. van der Heijden, S. Moorkens, H. Rahier, G. van Assche, and K. de Clerck, “Effect of Nanofibers on the Curing Characteristics of an Epoxy Matrix,” *Compos. Sci. Technol.*, vol. 79, pp. 35–41, 2013.
- [81] S. van der Heijden, B. de Schoenmaker, H. Rahier, G. van Assche, and K. de Clerck, “The Effect of the Moisture Content on the Curing Characteristics of an Epoxy Matrix in the Presence of Nanofibrous Structures,” *Polym. Test.*, vol. 40, pp. 265–272, 2014.
- [82] K.-W. Kim *et al.*, “Cure Behaviors and Mechanical Properties of Carbon Fiber-Reinforced Nylon 6/Epoxy Blended Matrix Composites,” *Compos. Part B*, vol. 112, pp. 15–21, 2017.
- [83] A. Vyas and J. O. Iroh, “In Situ Growth of Multilayered Crystals in Amorphous Matrix: Thermal, Dynamic Mechanical, and Morphological Analysis of Nylon-6/Epoxy Composites,” *J. Appl. Polym. Sci.*, pp. 3319–3327, 2013.

- [84] B. S. Gorton, "Interaction of Nylon Polymers with Epoxy Resins in Adhesive Blends," *J. Appl. Polym. Sci*, vol. 8, pp. 1287–1295, 1964.
- [85] M. Bakar, I. Wojtania, I. Legocka, and J. Gospodarczyk, "Property Enhancement of Epoxy Resins by Using a Combination of Polyamide and Montmorillonite," *Adv. Polym. Tech*, vol. 26, no. 4, pp. 223–231, 2008.
- [86] N. J. Delollis and O. Montoya, "Mode of Failure in Structural Adhesive Bonds," *J. Appl. Polym. Sci*, vol. 11, pp. 983–989, 1967.
- [87] R. I. Butt and J. L. Cotter, "The Effect of High Humidity on the Dynamic Mechanical Properties and Thermal Transitions of an Epoxy-Polyamide Adhesive," *J. Adhesion*, vol. 8, pp. 11–19, 1976.
- [88] A. Ishisaka and M. Kawagoe, "Examination of the Time-Water Content Superposition on the Dynamic Viscoelasticity of Moistened Polyamide 6 and Epoxy," *Int. J. Appl. Polym. Sci*, vol. 93, pp. 560–567, 2004.
- [89] F. Lu, C. J. G. Plummer, W. J. Cantwell, and H.-H. Kausch, "Toughening Mechanisms in Modified Epoxy Resins with Different Crosslink Densities," *Polym. Bulletin*, vol. 37, pp. 399–406, 1996.
- [90] B. J. Cardwell and A. F. Yee, "Toughening of Epoxies through Thermoplastic Crack Bridging," *J. Mater. Sci*, vol. 33, pp. 5473–5484, 1998.
- [91] S. C. Kim, J. Y. Kim, S. H. Lim, W. H. Jo, and C. R. Choe, "Effects of Mixing Temperatures on the Morphology and Toughness of Epoxy/Polyamide Blends," *J. Appl. Polym. Sci*, vol. 72, pp. 1055–1063, 1999.
- [92] J. K. Kim and R. E. Robertson, "Toughening of Thermoset Polymers by Rigid Crystalline Particles," *J. Mater. Sci*, vol. 27, pp. 161–174, 1992.
- [93] C. Girodet, E. Espuche, H. Sautereau, B. Chabert, R. Ganga, and E. Valot, "Influence of the Addition of Thermoplastic Preformed Particles on the Properties of an Epoxy/Anhydride Network," *J. Mater. Sci*, vol. 31, pp. 2997–3002, 1996.
- [94] J.-K. Kim and Y.-W. H. S. Mai, "High Fracture Toughness Fibre Composites with Interface Control—A Review," *Compos. Sci. Technol*, vol. 41, pp. 333–378, 1991.
- [95] S. Deng, L. Djukic, R. Paton, and L. Ye, "Thermoplastic-Epoxy Interactions and their Potential Applications in Joining Composite Structures—A Review," *Compos. Part A*, vol. 68, pp. 121–132, 2015.

- [96] N. Sela and O. Ishai, "Interlaminar Fracture Toughness and Toughening of Laminated Composite Materials: A Review," *Composites*, vol. 20, no. 5, pp. 423–435, 1989.
- [97] R. Palazzetti and A. Zucchelli, "Electrospun Nanofibers as Reinforcement for Composite Laminates Materials—A Review," *Compos. Struct.*, vol. 182, pp. 711–727, 2017.
- [98] B. Z. Jang, L. C. Chen, C. Z. Wang, H. T. Lin, and R. H. Zee, "Impact Resistance and Energy Absorption Mechanisms in Hybrid Composites," *Compos. Sci. Technol.*, vol. 34, pp. 305–335, 1989.
- [99] U. Beier, J. K. W. Sandler, V. Altstädt, H. Spanner, and C. Weimer, "Mechanical Performance of Carbon Fibre-Reinforced Composites Based on Stitched and Bindere Preforms," *Compos. Part A*, vol. 40, pp. 1756–1763, 2009.
- [100] U. Beier *et al.*, "Mechanical Performance of Carbon Fibre-Reinforced Composites Based on Preforms Stitched with Innovative Low-Melting Temperature and Matrix Soluble Thermoplastic Yarns," *Compos. Part A*, vol. 39, pp. 1572–1581, 2008.
- [101] P. J. Hogg, "Toughening of Thermosetting Composites with Thermoplastic Fibers," *Mat. Sci. Eng. A*, vol. 412, pp. 97–103, 2005.
- [102] C. Thanomsilp and P. J. Hogg, "Penetration Impact Resistance of Hybrid Composites Based on Commingled Yarn Fabrics," *Compos. Sci. Technol.*, vol. 63, pp. 467–482, 2003.
- [103] C. Thanomsilp and P. J. Hogg, "Interlaminar Fracture Toughness of Hybrid Composites Based on Commingled Yarn Fabrics," *Compos. Sci. Technol.*, vol. 65, pp. 1547–1563, 2005.
- [104] P. C. Varelidis, R. L. McCullough, and C. D. Papaspyrides, "The Effect on the Mechanical Properties of Carbon/Epoxy Composites of Polyamide Coatings on the Fibers," *Compos. Sci. Technol.*, vol. 59, pp. 1813–1823, 1999.
- [105] P. C. Varelidis, D. G. Papakostopoulos, C. I. Pandazis, and C. D. Papaspyrides, "Polyamide Coated Kevlar Fabric in Epoxy Resin: Mechanical Properties and Moisture Absorption Studies," *Compos. Part A*, vol. 31, pp. 549–558, 2000.
- [106] T. Skourlis, T. Duvis, and C. D. Papaspyrides, "The Role of a Polyamide Interphase on Carbon Fibres Reinforcing an Epoxy Matrix," *Compos. Sci. Technol.*, vol. 48, pp. 119–125, 1993.
- [107] J.-P. Favre, "Improving the Fracture Energy of Carbon Fibre-Reinforced Plastics by Delamination Promoters," *J. Mater. Sci.*, vol. 12, pp. 43–50, 1977.

- [108] J. E. Masters, "Improved Impact and Delamination Resistance through Interleafing," *Key Eng. Mater.*, vol. 37, pp. 317–348, 1989.
- [109] Y. A. Dzenis and D. H. Reneker, "Delamination Resistant Composites Prepared by Small Diameter Fiber Reinforcement at Ply Interfaces," *U.S. Patent*, vol. 1, p. 2, Jun. 1998.
- [110] P. Akangah, S. Lingaiah, and K. Shivakumar, "Effect of Nylon-66 Nano-Fiber Interleaving on Impact Damage Resistance of Epoxy/Carbon Fiber Composite Laminates," *Compos. Struct*, vol. 92, pp. 1432–1439, 2010.
- [111] L. Daelemans, S. van der Heijden, I. de Baere, H. Rahier, W. van Paepegem, and K. de Clerck, "Using Aligned Nanofibres for Identifying the Toughening Micromechanisms in Nanofibre Interleaved Laminates," *Compos. Sci. Technol*, vol. 124, pp. 17–26, 2016.
- [112] L. Daelemans, S. van der Heijden, I. de Baere, H. Rahier, W. van Paepegem, and K. de Clerck, "Damage-Resistance Composites Using Electrospun Nanofibers: A Multiscale Analysis of the Toughening Mechanisms," *ACS Appl. Mater. Inter*, vol. 8, pp. 11806–11818, 2016.
- [113] R. Palazzetti, A. Zucchelli, and I. Trendafilova, "The Self-Reinforcing Effect of Nylon 6,6 Nano-Fibres on CFRP Laminates Subjected to Low Velocity Impact," *Compos. Struct*, vol. 106, pp. 661–671, 2013.
- [114] T. K. Tsotsis, "Interlayer Toughening of Composite Materials," *Polym. Composite*, pp. 70–86, 2009.
- [115] R. Palazzetti *et al.*, "Influence of Electrospun Nylon 6,6 Nanofibrous Mats on the Interlaminar Properties of Gr-Epoxy Composite Laminates," *Compos. Struct*, vol. 94, pp. 571–579, 2012.
- [116] L. . Daelemans, S. van der Heijden, I. de Baere, H. Rahier, W. van Paerpegem, and K. de Clerck, "Nanofibre Bridging as a Toughening Mechanism in Carbon/Epoxy Composite Laminates Interleaved with Electrospun Polyamide Nanofibrous Veils," *Compos. Sci. Technol*, vol. 117, pp. 244–256, 2015.
- [117] M. R. Groleau, Y.-B. Shi, A. F. Yee, J. L. Bertram, H. J. Sue, and P. C. Yang, "Mode II Fracture of Composites Interlayered with Nylon Particles," *Compos. Sci. Technol*, vol. 56, pp. 1223–1240, 1996.

- [118] G. Caprino, P. Iaccarino, and A. Lamboglia, “The Effect of Shear on the Rigidity in Three-Point Bending of Unidirectional CFRP Laminates Made of T800H/3900-2,” *Compos. Struct*, vol. 88, pp. 360–366, 2009.
- [119] M. Hojo, S. Matsuda, M. Tanaka, S. Ochiai, and A. Murakami, “Mode I Delamination Fatigue Properties of Interlayer-Toughened CF/Epoxy Laminates,” *Compos. Sci. Technol*, vol. 66, pp. 665–675, 2006.
- [120] T. Beiss, M. Menacher, R. Feulner, G. Heulder, and T. A. Osswald, “Vibration Joining of Fiber-Reinforced Thermosets,” *Polym. Composite*, pp. 1205–1212, 2010.
- [121] M. Hou, “Thermoplastic Adhesive for Thermosetting Composites,” *Materials Science Forum*, vol. 706–709, pp. 2968–2973, 2012.
- [122] A. Naeim abadi, F. Hemmati, and H. Garmabi, “Validation of rheological responses for morphological evaluation of incompatible polyamide 12/thermoplastic elastomer blends filled with nanoclay,” *Polymer Testing*, vol. 65, pp. 78–89, Feb. 2018, doi: 10.1016/J.POLYMERTESTING.2017.11.006.
- [123] M. van Duin, M. Aussems, and R. J. M. Borggreve, “Graft Formation and Chain Scission in Blends of Polyamide-6 and-6.6 with Maleic Anhydride Containing Polymers,” John Wiley & Sons, Inc, 1998.
- [124] D. Tomova and H. J. Radusch, “Morphology and properties of ternary polyamide 6/polyamide 66/elastomer blends,” *Polymers for Advanced Technologies*, 2003, doi: 10.1002/pat.263.
- [125] A. Ebrahimi Jahromi, H. R. Ebrahimi Jahromi, F. Hemmati, M. R. Saeb, V. Goodarzi, and K. Formela, “Morphology and mechanical properties of polyamide/clay nanocomposites toughened with NBR/NBR-g-GMA: A comparative study,” *Composites Part B: Engineering*, vol. 90, pp. 478–484, Apr. 2016, doi: 10.1016/J.COMPOSITESB.2015.12.042.
- [126] J. G. Kim, J. Lee, and Y. Son, “Toughening of nylon 6 with a ethylene-octene copolymer grafted with maleic anhydride and styrene,” *Materials Letters*, 2014, doi: 10.1016/j.matlet.2014.03.186.



- [127] J. J. Huang, H. Keskkula, and D. R. Paul, "Rubber toughening of an amorphous polyamide by functionalized SEBS copolymers: morphology and Izod impact behavior," *Polymer*, vol. 45, no. 12, pp. 4203–4215, May 2004, doi: 10.1016/J.POLYMER.2004.04.002.
- [128] S. C. Tjong, S. al Xu, and Y. W. Mai, "Tensile deformation mechanism of polyamide 6,6/SEBS-g-MA blend and its hybrid composites reinforced with short glass fibers," *Journal of Materials Science* 2003 38:2, vol. 38, no. 2, pp. 207–215, Jan. 2003, doi: 10.1023/A:1021132725370.
- [129] S. C. Tjong, S. A. Xu, and Y. W. Mai, "Impact fracture toughness of short glass fiber-reinforced polyamide 6,6 hybrid composites containing elastomer particles using essential work of fracture concept," *Materials Science and Engineering A*, 2003, doi: 10.1016/S0921-5093(02)00609-3.
- [130] S. C. Tjong, S. A. Xu, R. Kwok-Yiu Li, and Y. W. Mai, "Short glass fiber-reinforced polyamide 6,6 composites toughened with maleated SEBS," *Composites Science and Technology*, 2002, doi: 10.1016/S0266-3538(02)00140-9.
- [131] M. Bräuer, B. Hupfer, J. Nagel, and D. Lehmann, "Chemical modification of polyurethane for two-component injection molding," *Polymer Engineering & Science*, vol. 42, no. 4, pp. 859–869, Apr. 2002, doi: 10.1002/PEN.10997.
- [132] G. Pompe, M. Bräuer, D. Schweikle, J. Nagel, B. Hupfer, and D. Lehmann, "Influence of the temperature profile in the interface on the bond strength of polyamide–polyurethane two-component tensile bars," *Journal of Applied Polymer Science*, vol. 100, no. 6, pp. 4297–4305, Jun. 2006, doi: 10.1002/APP.23842.
- [133] A. M. M. R. Persson, E. L. Hinrichsen, and E. Andreassen, "Adhesion between thermoplastic elastomers and polyamide-12 with different glass fiber fractions in two-component injection molding," *Polymer Engineering & Science*, vol. 60, no. 7, pp. 1642–1661, Jul. 2020, doi: 10.1002/PEN.25408.
- [134] D. ; Weng, J. ; Andries, P. ; Morin, K. ; Saunders, and J. Politis, "Fundamentals and material development for thermoplastic elastomer (TPE) overmolding," 2000.
- [135] L. M. Arzondo *et al.*, "Sequential injection overmolding of an elastomeric ethylene-octene copolymer on a polypropylene homopolymer core," *Polymer Engineering and Science*, 2004, doi: 10.1002/pen.20216.

- [136] M. v. Candal, A. Gordillo, O. O. Santana, and J. J. Sánchez, “Study of the adhesion strength on overmoulded plastic materials using the essential work of interfacial fracture (EWIF) concept,” *Journal of Materials Science*, vol. 43, no. 15, pp. 5052–5060, Aug. 2008, doi: 10.1007/S10853-008-2667-1/FIGURES/10.
- [137] A. Rossa-Sierra, M. Sánchez-Soto, S. Illescas, and M. L. Maspocho, “Study of the interface behaviour between MABS/TPU bi-layer structures obtained through over moulding,” *Materials & Design*, vol. 30, no. 10, pp. 3979–3988, Dec. 2009, doi: 10.1016/J.MATDES.2009.05.037.
- [138] R. Chandran, C. J. G. Plummer, P. E. Bourban, and J. A. E. Månson, “Morphology and interfacial strength of nonisothermally fusion bonded hard and soft thermoplastics,” *Polymer Engineering & Science*, vol. 58, no. S1, pp. E82–E92, May 2018, doi: 10.1002/PEN.24662.
- [139] K. Ramani and J. Tagle, “Process-induced effects in thin-film bonding of PEKEKK in metal-polymer joints,” *Polymer Composites*, vol. 17, no. 6, pp. 879–886, 1996, doi: 10.1002/PC.10681.
- [140] K. Ramani and W. Zhao, “The evolution of residual stresses in thermoplastic bonding to metals,” *International Journal of Adhesion and Adhesives*, vol. 17, no. 4, pp. 353–357, 1997, doi: 10.1016/S0143-7496(97)00030-4.
- [141] K. Ramani and B. Moriarty, “Thermoplastic bonding to metals via injection molding for macro-composite manufacture,” *Polymer Engineering and Science*, vol. 38, no. 5, pp. 870–877, 1998, doi: 10.1002/PEN.10253.
- [142] K. Enami, F. Kimura, K. Yokoyama, T. Murakami, and Y. Kajihara, “Experimental and simulative investigation of the effects of laser-structured metal surface on metal-polymer direct joining,” *Precision Engineering*, vol. 62, pp. 273–281, Mar. 2020, doi: 10.1016/J.PRECISIONENG.2019.12.011.
- [143] K. Taki, S. Nakamura, T. Takayama, A. Nemoto, and H. Ito, “Direct joining of a laser-ablated metal surface and polymers by precise injection molding,” *Microsystem Technologies*, vol. 22, no. 1, pp. 31–38, Jan. 2016, doi: 10.1007/S00542-015-2640-2/FIGURES/13.

- [144] P. A. Fabrin, M. E. Hoikkanen, and J. E. Vuorinen, “Adhesion of thermoplastic elastomer on surface treated aluminum by injection molding,” *Polymer Engineering & Science*, vol. 47, no. 8, pp. 1187–1191, Aug. 2007, doi: 10.1002/PEN.20801.
- [145] S. Yin, Y. Xie, R. Li, J. Zhang, and T. Zhou, “Polymer-Metal Hybrid Material with an Ultra-High Interface Strength Based on Mechanical Interlocking via Nanopores Produced by Electrochemistry,” *Industrial and Engineering Chemistry Research*, vol. 59, no. 27, pp. 12409–12420, Jul. 2020, doi: 10.1021/ACS.IECR.0C01304/SUPPL\_FILE/IE0C01304\_SI\_001.PDF.
- [146] Y. Xie, J. Zhang, and T. Zhou, “Large-area mechanical interlocking via nanopores: Ultra-high-strength direct bonding of polymer and metal materials,” *Applied Surface Science*, vol. 492, pp. 558–570, Oct. 2019, doi: 10.1016/J.APSUSC.2019.06.246.
- [147] F. Yusof, M. Yukio, M. Yoshiharu, and M. H. Abdul Shukor, “Effect of anodizing on pulsed Nd:YAG laser joining of polyethylene terephthalate (PET) and aluminium alloy (A5052),” *Materials & Design*, vol. 37, pp. 410–415, May 2012, doi: 10.1016/J.MATDES.2012.01.006.
- [148] F. C. Liu, P. Dong, W. Lu, and K. Sun, “On formation of Al–O–C bonds at aluminum/polyamide joint interface,” *Applied Surface Science*, vol. 466, pp. 202–209, Feb. 2019, doi: 10.1016/J.APSUSC.2018.10.024.
- [149] F. C. Liu, J. Liao, and K. Nakata, “Joining of metal to plastic using friction lap welding,” 2013, doi: 10.1016/j.matdes.2013.08.056.
- [150] A. Gisario, M. Mehrpouya, and E. Pizzi, “Dissimilar joining of transparent Poly(ethylene terephthalate) to aluminum 7075 sheets using a diode laser,” *Journal of Laser Applications*, vol. 29, no. 2, p. 022418, May 2017, doi: 10.2351/1.4983268.
- [151] S. Katayama and Y. Kawahito, “Laser direct joining of metal and plastic,” *Scripta Materialia*, vol. 59, no. 12, pp. 1247–1250, Dec. 2008, doi: 10.1016/J.SCRIPTAMAT.2008.08.026.
- [152] F. Yusof, Y. Miyashita, N. Seo, Y. Mutoh, and R. Moshwan, “Utilising friction spot joining for dissimilar joint between aluminium alloy (A5052) and polyethylene terephthalate,” <https://doi.org/10.1179/136217112x13408696326530>, vol. 17, no. 7, pp. 544–549, 2013, doi: 10.1179/136217112X13408696326530.

### 3. PROCESSING OF DISSIMILAR MATERIALS

Based on knowledge attained in the previous chapter, this chapter investigates the effect of processing on adhesion between dissimilar materials. It is now clear that combining materials with different mechanical properties can be an effective way to combine the advantageous properties of both materials without sacrificing performance. However, the introduction of a second material invariably necessitates the formation of additional interfaces in a finished part, which energetically unfavorable and in many cases provides a weak point at which failure can initiate.

There are many methods that can be used to improve interfacial adhesion that involve exploiting the theories of adhesion outlined in Chapter 2. For example, increasing the surface roughness of one of the materials can improve mechanical interlocking, while coatings that are compatible with both materials may be introduced to allow chemical bonding across the interface. However, these methods introduce additional and often costly steps to a manufacturing process. Further, there are often environmental consequences to such processes, as they typically require harsh chemicals or energetically expensive equipment. For these reasons, such adhesion promoters are not well-suited to many high-rate manufacturing processes. Therefore, there is great interest in materials that are not only mutually beneficial but are also chemically compatible enough to form spontaneous and robust interfacial bonds.

In a hybrid system, the interfacial bond must be sufficiently strong to transfer energy between the two phases, allowing for each material to perform as designed. For example, in a system consisting of one strong but brittle material and one weaker but more ductile material, the ductile material will be able to dissipate high-rate energy more effectively, but sustained static load will be carried by the stronger material. If the interface is insufficiently strong, the hybrid material will lose this mutually beneficial support as soon as the interface fails. If the interface does fail eventually during the life of the part, a stronger interface will be able to absorb more energy during failure. If the interface is too strong, however, it may limit the ability of the more ductile material to deform and absorb energy. The application and desired part properties will inform the ideal interfacial strength.

Therefore, understanding and characterizing these interfaces is of the utmost importance in designing a system in which multiple materials must interact. The following chapter examines the effect minor changes to the manufacturing process have on the interfacial bond between two

materials. These manufacturing differences are achieved without the introduction of additional processing steps or manufacturing time, making them practical for implementation in existing manufacturing processes. Further, only spontaneous adhesion is considered—no surface treatment or adhesion promoters are used. Though these steps would surely improve adhesion, they would make implementation of these hybrid materials much less practical for high-rate manufacture. Moreover, the goal of this work is not to produce the strongest interfacial bond possible, but merely to characterize. Indeed, a strong bond may prove detrimental for a given application.

### **3.1 Processing of Dissimilar Materials: Epoxy/Polyamide**

Composite materials are increasingly used in a variety of applications due to their low weight and high specific strength and stiffness. However, traditionally epoxy-matrix composites tend to be brittle, limiting their use in applications that need to withstand extensive impact and vibrations. One way to improve these characteristics is to incorporate another, more ductile material, such as a thermoplastic, into the epoxy-based composite. This ductile material can improve energy absorption in a variety of ways depending on the part geometry.

When incorporating a thermoplastic into an epoxy (EP) system, strong adhesion between the two phases is crucial for the system to transfer load across the interface and take full advantage of the mechanical properties of each material. Numerous theories of adhesion have been developed to explain the main factors that contribute to adhesion[1]–[5]. The theories that are most relevant to EP/thermoplastic interfaces are: a) mechanical interlocking, which characterizes the effect of surface roughness on adhesion; b) chemical bonding, which describes the constituent materials' ability to form chemical bonds across the interface; c) inter-diffusion theory, which can be used to describe the diffusion across the interface and subsequent commingling of polymer chains; and d) physical adsorption, which describes van der Waals forces between opposing surfaces and can include wetting of one material with another. Some or all of these may be present in a single interface, and each can contribute to the improvement of an interfacial bond.

Though a variety of materials have been successfully used to toughen EP-based composites, polyamide (PA) is uniquely suited for this purpose. Its polar nature, relatively unique among thermoplastics, makes the EP monomers and PA partially miscible which enables intimate contact and interdiffusion between the two. Further, the amide groups are able to covalently bond with the EP monomers, providing another strong link between the materials. Polyamide has been proven to

be an effective toughening agent for EP-matrix composites in a variety of different sample geometries, where PA has been used as: structural weaves[6]; binding agents for non-crimp carbon fiber fabrics[7]; comingled fibers[8]; thin veil interlayers[9]–[11]; and discrete particle interlayers[12]–[14]. However, these studies emphasize the effect of the material combination and do not directly address the adhesion between EP and PA. This is an important interaction to quantify, as the efficacy of PA as a toughener depends heavily on the adhesion between the EP and PA. If the bond is too weak load cannot be transferred to the PA, but if the bond is too strong the PA may not be able to effectively absorb energy through deformation and delamination from the EP and subsequent plastic deformation. Therefore, understanding the adhesive strength between EP and PA for a given system is an important step in understanding this mechanical behavior.

This paper explores the effect of manufacturing conditions on the mode-I adhesion at the ply level between EP-matrix and PA-matrix composites. Adhesion is quantified using two different test methods—Wedge Testing and DCB testing. SEM imaging is used to examine the failure modes at the fracture surface and qualitatively validate the mode-I test results.

### **3.1.1 Experimental Methods**

#### ***Material Forms***

All samples consisted of two fiber-reinforced composite plates in various combinations as summarized in Table 3.1. Both composites were polymer-matrix pre-impregnated (prepreg) composite materials.

The EP matrix composite is a unidirectional, carbon fiber-reinforced prepreg.  $[0]_{22}$  layups were created but left non-consolidated and uncured until the combined sample plate was manufactured. This enabled full chemical and physical interaction across the layered interfaces.

The polyamide composite used in this study is a unidirectional, glass fiber-reinforced prepreg with a polyamide 6 (PA6) matrix. Plies of the PA6 composite were dried for four hours at 80°C, then compression molded under 690 kPa pressure at 260 °C for 10 minutes in a  $[0]_{14}$  layup. Consolidated PA6 plates were dried again for four hours at 80 °C immediately before being pressed into combined sample plates.

Layup schemes were chosen to provide approximately equal flexural rigidity on either side of the interface in an attempt to ensure even loading of the sample arms.

### ***Sample Preparation***

All samples were formed as 254 mm x 254 mm flat plates and manufactured using compression molding. A 25.4 mm wide strip of polyimide film was placed at the bi-material interface along one edge of the samples to provide an initiation point for crack growth. Two different sets of processing times and temperatures were used for each material combination, illustrated in Table 3.1, and all samples were processed at a molding pressure of 690 kPa.

Table 3.1. Sample nomenclature and processing conditions.

| <b>Material 1</b> | <b>Material 2</b> | <b>177 °C,<br/>180 min</b> | <b>197 °C,<br/>45 min</b> | <b>240 °C,<br/>40 min</b> | <b>260 °C,<br/>10 min</b> |
|-------------------|-------------------|----------------------------|---------------------------|---------------------------|---------------------------|
| <b>PA6/GF</b>     | <b>PA6/GF</b>     |                            |                           | PA/PA240                  | PA/PA260                  |
| <b>EP/CF</b>      | <b>EP/CF</b>      | EP/EP177                   | EP/EP197                  |                           |                           |
| <b>EP/CF</b>      | <b>PA6/GF</b>     | EP/PA177                   | EP/PA197                  |                           |                           |

The PA/PA plates were processed at higher temperatures than the other two material combinations because there was no adhesion between the two PA/PA halves at lower temperatures. Nine 25.4 mm wide samples were cut from each plate, and the 12.7 mm edges of the plate were discarded.

### ***Mechanical Performance***

Two test methods were employed to determine the mode-I fracture toughness of the EP-PA bond. A modified version of the Wedge Test was used to encourage crack growth to remain at the EP-PA interface, rather than deviating into either of the constituent materials. Due to the sensitivity of the Wedge Test to slight differences in the crack length between tests, there is a high degree of variability in the measurements of mode-I fracture toughness obtained from the Wedge Test. Therefore, double cantilever beam (DCB) testing was also conducted on the same samples to provide additional information on the mode-I fracture behavior of these samples.

### *Mechanical Performance: Wedge Testing*

Previous work[15] studied the adhesion between EP and PA using a modified version of ASTM D3762[16] (Wedge Test). A razor blade was inserted into the interface of each sample and the resulting interfacial crack was left to grow under ambient conditions until the crack length equilibrated. The crack tip was determined to be the point along the sample where the bonded sample thickness deviated from its nominal value ( $h_0$ ), and the crack length was measured from the load introduction point on the wedge to the crack tip as shown in Figure 3.1. Once the crack length equilibrated and was measured, the wedge was advanced by 10 mm and the test was repeated, allowing for multiple data points to be collected from each sample.

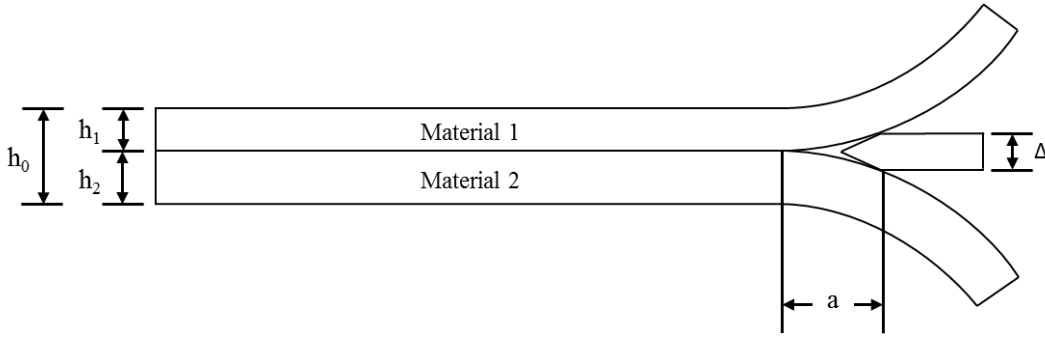


Figure 3.1. Asymmetric Wedge Test geometry.

The mode-I interfacial fracture toughness ( $G_I$ ) was calculated using equation [3.1][17], where  $\Delta$  is the wedge thickness,  $E_i$  and  $h_i$  are the Young's modulus and thickness of material  $i$ , respectively, and  $a$  is the crack length.

$$G_I = \frac{3\Delta^2(E_1h_1^3 + E_2h_2^3)}{32a^4} \quad [3.1]$$

The Wedge Test was repeated until the crack length reached the approximate center of the samples, then stopped to allow subsequent DCB testing on the same samples so that any variation between different samples would be detected.

### *Mechanical Performance: Double Cantilever Beam (DCB) Testing*

The double cantilever test followed ASTM D5528[18]. Aluminum blocks were used to introduce the load to the samples. The blocks offered two distinct advantages over the hinges commonly used in DCB testing: firstly, the blocks extended 50.8 mm along the samples, offering



a large bond area over which to adhere to the sample surfaces; secondly, the strength of the interfacial bond was often sufficiently strong to cause the hinges to plastically deform under the applied load, which was not a concern because of the thickness of the load blocks.

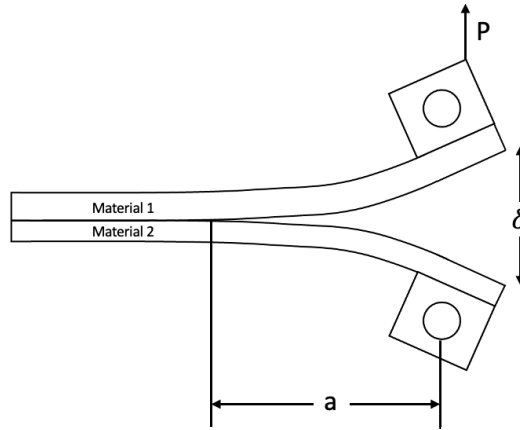


Figure 3.2. Double cantilever beam geometry.

Before testing, the sides of the samples are painted white and marked at 5mm increments. A traveling optical microscope is used to capture pictures of the sample throughout the test to determine the instantaneous crack length.

Because the load blocks introduce artificial stiffness and reduce the ability of the sample arms to bend, correction factors were introduced to the calculation of the interfacial fracture toughness,  $G_I$ [18]. These correction factors,  $F$  and  $N$ , are defined in equations [3.2] and [3.3], where  $\delta$  is the vertical displacement of the load blocks at the load point,  $t$  is the distance from the load introduction point to the centerline of the adjacent beam,  $a$  is the crack length, and  $L'$  is the length of the block from the load introduction point to its edge, as shown in Figure 3.3.

$$F = 1 - \frac{3}{10} \left( \frac{\delta}{a} \right)^2 - \frac{3}{2} \left( \frac{\delta t}{a^2} \right) \quad [3.2]$$

$$N = 1 - \left( \frac{L'}{a} \right)^3 - \frac{9}{8} \left[ 1 - \left( \frac{L'}{a} \right)^2 \right] \left( \frac{\delta t}{a^2} \right) - \frac{9}{35} \left( \frac{\delta}{a} \right)^2 \quad [3.3]$$

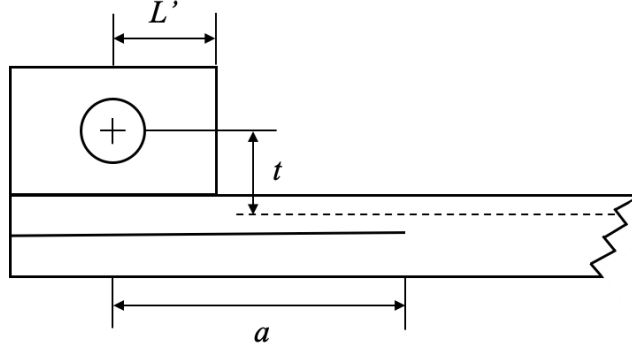


Figure 3.3. DCB geometry with features of interest labeled, adapted from[18].

The mode-I fracture toughness was determined using the modified beam theory (MBT) method, equation [3.4], with the correction factors  $F$  and  $N$  applied. Here,  $P$  is the applied load,  $\delta$  is the vertical displacement at the load point,  $b$  is the sample width, and  $\Delta$  is the correction factor determined graphically as shown in Figure 3.4.

$$G_I = \frac{3P\delta F}{2bN(a + |\Delta|)} \quad [3.4]$$

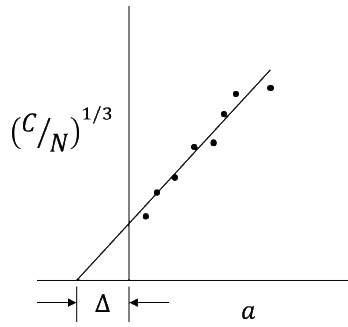


Figure 3.4. Cube root of corrected compliance,  $C/N$ , vs. crack length,  $a$ , used to determine MBT correction factor  $\Delta$  for interfacial fracture toughness calculation[18].

#### *Mechanical Performance: Fractography*

Scanning Electron Microscopy (SEM) was used to examine the fractured surfaces after adhesion testing. The purpose of this was twofold: the resulting images can be used to examine the failure modes in the damaged samples, and they can also be used to qualitatively validate the mode-I results by providing an indication of the relative extents of damage at the interfaces of the

failed samples. SEM samples were taken from the DCB region of test samples, because the wedge sliding through the wedge region of the test samples left tracks that damaged the fracture surfaces and obfuscated the damage due to mode-I failure.

### 3.1.2 Results

#### *Wedge Test*

Processing temperature has a clear influence on interfacial fracture toughness for all material combinations used in this study, as illustrated in Table 3.2. Both PA/PA samples were manufactured above the PA6 melt temperature of 220 °C, and the increase in processing temperature from 240 °C to 260 °C yielded a greater than 200% increase in interfacial fracture toughness.

Table 3.2.  $G_{IC}$  values obtained from Wedge and DCB Testing, given with standard error.

| $G_{IC}$ (J/m <sup>2</sup> ) | PA/PA240 | PA/PA260 | EP/EP177 | EP/EP197 | EP/PA177 | EP/PA197 |
|------------------------------|----------|----------|----------|----------|----------|----------|
| <b>Wedge Test</b>            | 768±70   | 2366±233 | 707±20   | 892±26   | 531±37   | 1140±134 |
| <b>DCB Test</b>              | 1907±92  | 3145±66  | 373±18   | 642±43   | 507±51   | 1606±325 |

Although the improvement due to processing temperature is less pronounced in the EP/EP samples, there is still a 26% increase in interfacial fracture toughness that comes with increasing the processing temperature from the manufacturer-recommended 177°C to 197°C.

Both EP/PA samples are processed below the PA6 melt temperature. However, the improvement in  $G_{IC}$  with increased processing temperature is 115%, which is much greater than the improvement seen in the EP/EP samples processed under the same conditions. Further, the EP/PA197  $G_{IC}$  is 28% higher than the EP/EP197  $G_{IC}$ , representing an improvement over the EP-EP cohesive bond strength with the introduction of PA6.

#### *Double Cantilever Beam Test*

Across all material combinations, there is a clear dependence of bond strength on processing temperature, as illustrated in. Both PA/PA plates were pressed above the PA6 melt

temperature of 220°C, but there is still a 112% increase in interfacial fracture toughness with a further increase in temperature. The EP/EP177 plate was pressed under the manufacturer-recommended conditions but increasing the press temperature from 177°C to 197°C yielded a 62% increase in bond strength in the EP/EP samples.

Even though the EP/PA plates were both manufactured below the PA6 melt temperature, there is a significant difference in bond strength with increased temperature. There is a 215% increase in bond strength that cannot be attributed solely to the differing behavior of the uncured EP at different temperatures.

PA/PA240, PA/PA260, and EP/PA197 samples all exhibited fiber bridging and stick-slip behavior during testing. Stick-slip behavior is common in ductile materials, including some thermoplastic-reinforced composites, owing to matrix plastic deformation around the advancing crack front.[19]

### ***Microscopy Validation***

SEM imaging was conducted on the fracture surfaces of the failed samples to understand the failure mechanisms and to qualitatively validate the mode-I testing results.

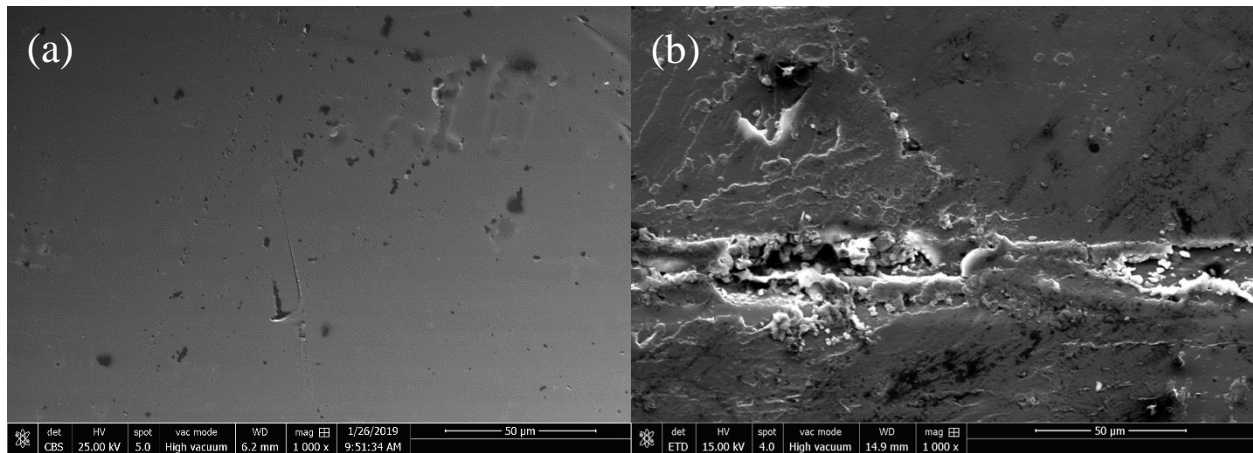


Figure 3.5. SEM images of PA6/GF fracture surfaces from EP/PA177 (a) and EP/PA197 (b) samples at 1000x magnification.

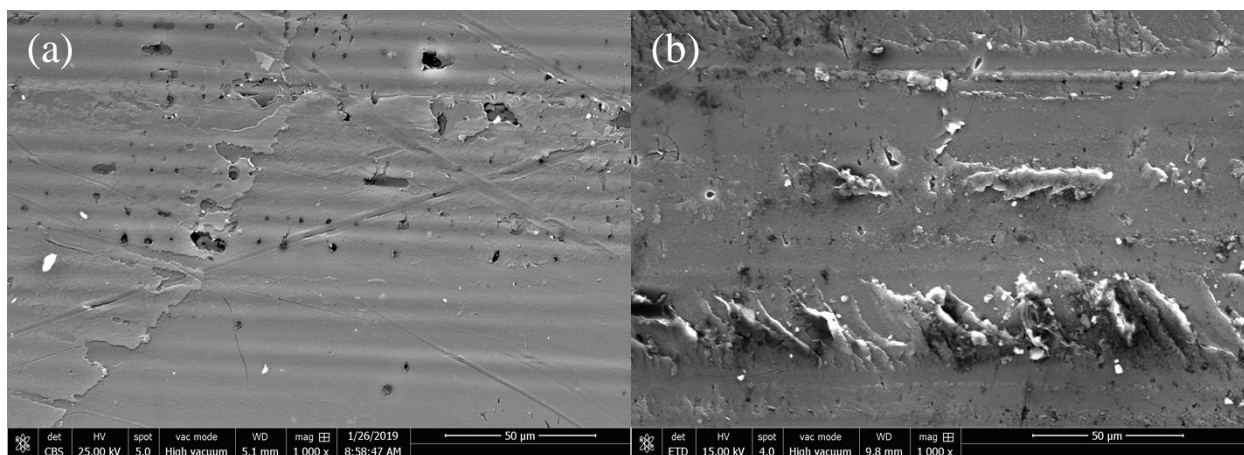


Figure 3.6. SEM images of EP/CF fracture surfaces from EP/PA177 (a) and EP/PA197 (b) samples at 1000x magnification.

Both the PA6/GF and EP/CF fracture surfaces in the EP/PA177 samples are relatively planar, with little evidence of damage in either matrix. There are some faint striations on the EP/CF surface of EP/PA177 (Figure 3.6(a)), reflecting some slight damage to the polymer on that surface. The EP/PA197 sample, on the other hand, has evidence of fracture in both the PA6 and EP matrices, indicating that bonding occurred between the EP and the PA6 across the interface.

### 3.1.3 Discussion

For both Wedge and DCB testing, processing temperature has a clear influence on bond strength. Though the Wedge and DCB tests have quantitative differences, the PA/PA and EP/EP samples all exhibit an increase in  $G_{IC}$  with increasing processing temperature.

A similar trend emerges in the EP/PA samples, where increased processing temperature results in interfacial fracture toughnesses stronger than those in EP/EP samples. This improvement in  $G_{IC}$  in EP/PA197 samples comes despite the fact that these samples are processed below the PA6 melt temperature of 220 °C.

The EP/PA6 crosslinking reactions have been shown[20] to occur at room temperature and at 70°C, well below the manufacturing temperatures used here. However, Zhong and Guo[21] find that in EP/PA blends, the bulk of the reaction occurs above 200°C, possibly due to increased polymer chain mobility and interdiffusion at elevated temperatures. Therefore, the increase in

EP/PA bond strength with the increase in processing temperature may be attributed in part to a higher degree of covalent crosslinking at the interface.

As illustrated in Figure 3.7, the EP/PA197 *adhesive* bond strength obtained during wedge testing is greater than the *cohesive* EP/EP197 bond strength. This improvement points to the benefit of introducing PA as a toughening agent for EP—under the right processing conditions, the more ductile PA phase absorbs more energy than the un-toughened EP. During Wedge Testing, the wedge tended to force the growing crack to stay localized to the bi-material interface, meaning that this improved energy absorption in EP/PA197 samples occurred mainly due to the PA immediately adjacent to the EP phase. This result illustrates the toughening offered by even a relatively small amount of PA.

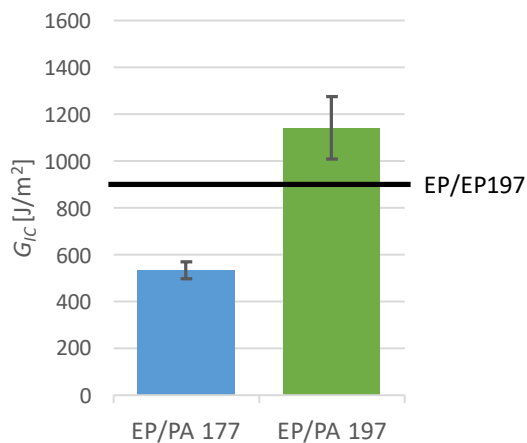


Figure 3.7.  $G_{IC}$  values obtained from Wedge Testing for EP/PA samples, plotted with standard error and  $G_{IC}$  for EP/EP197.[15]

This improvement over EP/EP197 bond strength is even more pronounced in the DCB results, as shown in Figure 3.8. In the DCB results, the cohesive bond strength in the EP/PA197 samples is 150% greater than the adhesive bond strength in the EP/EP197 samples.

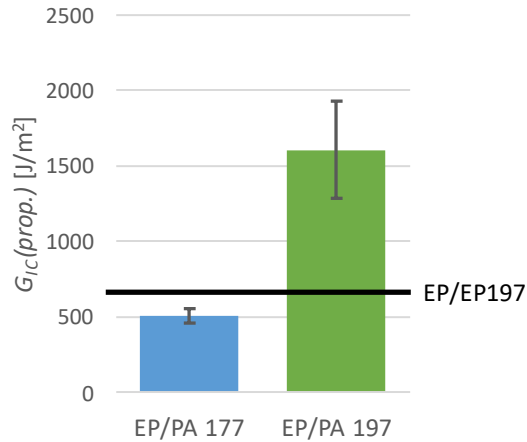


Figure 3.8. Average  $G_{IC}$  (prop.) values for the EP/PA DCB samples, shown with standard error and  $G_{IC}$  (prop.) for EP/EP197.

During the propagation phase of DCB testing, crack growth in EP/PA197 samples tended to travel into adjacent plies of material, away from the immediate interface. These samples had high interfacial fracture toughness and matrix plastic deformation, as seen in the Microscopy Validation section, and the toughness of the interface forced the crack to grow into the bulk PA6/CF composite. This behavior is likely responsible for much of the difference between the quantitative Wedge and DCB results for EP/PA197 samples. Even though this crack growth away from the interface means that the  $G_{IC}$  (prop.) data for these samples will not reflect the true EP-PA bond strength at the interface, they still offer valuable insights into the behavior of PA-toughened EP. In particular, the 150% increase in bond strength points to the improvement in toughening that is possible with a larger PA phase to absorb energy. As the crack travels away from the EP-PA interface and into the PA6/CF composite, energy is absorbed through fiber pullout and bridging and larger-scale plastic deformation, no longer confined to the boundary layer adjacent to the interface with EP.

One notable difference between the Wedge and DCB tests is the difference in fiber bridging behavior. Fiber bridging was observed in the samples with the toughest interfaces—PA/PA260 and EP/PA197—during both Wedge and DCB testing. Bridging behavior in unidirectional composite samples has been well-studied for the DCB geometry[22]–[24]. Typically, fiber bridging tends to artificially increase the mode-I fracture toughness of a sample until an equilibrium bridged length (or “tie zone”) is reached, at which point the fracture toughness reaches a stable value as bridging fibers begin to break. In the Wedge Testing setup used, the crack length

was not sufficiently long to allow for a tie zone of equilibrium length to be reached. Typical Wedge Test crack lengths were between 10 and 20 mm (depending on the adhesive strength), while tie lengths in DCB testing can be several times longer. In the Wedge Test geometry, the bridged fibers are unable to reach an equilibrium tie zone length due to interference with the wedge. Future work might examine the effect of fiber bridging on the Wedge Test by increasing the wedge thickness, thereby increasing the crack length and potentially providing more space for the fiber bridging to occur.

Wedge Testing is known to yield high deviation in  $G_{IC}$  results[25],[26], largely due to the sensitivity to crack length illustrated in equation [3.1]. The combination of high variability, fiber bridging, and stick-slip behavior make the absolute determination of  $G_{IC}$  difficult. This study primarily offers a comparison between the mean  $G_{IC}$  values for each material combination and processing condition; for this reason, standard error is used instead of standard deviation to indicate confidence in the mean values. The large number of measurements taken for each material combination and test method allows high confidence in the means, despite the variability.

### 3.1.4 Section Summary

This work demonstrates that, not only are EP and PA6 compatible, but they can also spontaneously form an adhesive bond up to 150% stronger than the EP-EP cohesive bond, even below the PA6 melt temperature. During DCB testing, the interfacial crack in the EP/PA197 samples often deviated away from the interface and into the PA6 matrix, an indication that further improvement in the bond strength will not be beneficial to the system.

These results illustrate the effectiveness of PA-matrix composites as toughening agents for EP-matrix composites. The spontaneous bond between EP and PA is strong enough to induce plastic deformation in the PA phase prior to EP-PA debonding, introducing a valuable energy absorption mechanism to the system,

The EP-PA6 bond strength is heavily dependent on the manufacturing conditions, with a 20°C increase in processing temperature yielding an increase in bond strength of over 200%. In this study, the only manufacturing differences were an increase in processing temperature and a decrease in time—no processing steps were introduced to improve the bond, and indeed the cycle time was reduced four-fold. Therefore, the study presented here offers an economically viable method to modify the adhesive properties of the EP-PA6 combination.



### 3.2 Processing of Dissimilar Materials: Polyamide/TPE

The combination of a thermoplastic elastomer (TPE) with a thermoplastic-matrix composite allows a part to take advantage of the high stiffness and strength of the composite with the energy absorbing capability of the TPE.

Unlike EP with PA, PA and TPE are not naturally miscible, as TPE molecules are typically non-reactive and non-polar. Therefore, before joining the two materials, a reactive compatibilizer is typically added to the TPE. This involves grafting reactive molecules, such as maleic anhydride (MA), onto the TPE molecule. These reactive molecules improve compatibility both by increasing the TPE polarity and by offering reactive sites that the amide groups in the PA chains can covalently bond to.

Researchers have successfully created blends of reactively compatibilized TPEs with PA, finding that adding even a small amount of TPE to a blend with PA greatly improves the fracture toughness [28]–[32]. Kim et al found that, as the adhesion between the TPE and PA phases improved, the impact strength of samples also increased [32]. Other researchers have overmolded compatibilized TPE onto PA substrates [33]–[35]. Though this work is in its infancy, early results suggest that the interfacial temperature between the TPE overmold and PA substrate has a measurable influence on interfacial bond strength.

In this work, samples of TPE and PA/GF are manufactured via compression molding at two different processing temperatures to determine the effect of processing variations on the bond strength between the TPE and PA.

#### 3.2.1 Experimental Methods

##### *Materials*

A unidirectional glass fiber (GF) prepreg with a polyamide 6 (PA6) matrix was used. Fourteen plies of the prepreg are cut and dried at 80 °C for 4 hours, then laid up in a  $[0]_{14}$  scheme in a 254x254mm square mold. The PA6/GF plates were pressed at 260 °C under 690kPa of pressure for 10 minutes, then allowed to cool under continuously applied pressure.

The thermoplastic elastomer (TPE) is a SEBS-based elastomer (Dryflex A1 600902 from Hexpol TPE AB) that has been specially formulated for compatibility with PA. It arrives in 110x150x2mm sheets, which are cut and laid up to form one 254x254x2mm layer of TPE.

### ***Sample Preparation***

The PA6/GF plates were cleaned with acetone and dried again at 80 °C for 4 hours before being placed on top of the TPE layer in the mold. A 25.4mm-wide strip of polyimide (PI) film was placed at the interface along one edge of the mold, perpendicular to the glass fiber direction. This film served as a crack starter for adhesion testing.

The hybrid PA/TPE plates were compression molded in a hydraulic press under 690kPa of pressure for two different time and temperature cycles—177°C for 3 hours and 197°C for 45 minutes. The plates were allowed to cool in the press under pressure. The plates were cut into 25.4x254mm strips parallel to the glass fiber direction. The edges of the plate were discarded, yielding nine samples per plate.

### ***Mechanical Performance: Floating Roller Peel Testing***

A floating roller peel test (ASTM D3167) was used to assess the bond strength between the TPE and the PA6 under the two sets of processing conditions [36]. The unbonded end of the TPE was gripped in the lower grip of a hydraulic load frame, while the stiff PA/GF side of the sample was allowed to roll through the floating roller fixture, pictured in Figure 3.9.

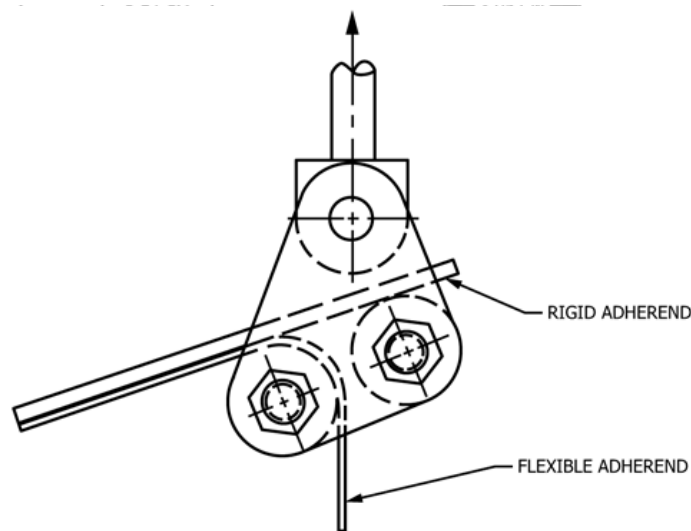


Figure 3.9. Floating roller peel fixture, ASTM D3167.[36]

The lower grip pulled the TPE down at a constant crosshead displacement of 25mm/min while the force and the crosshead displacement were recorded.

In order to limit the effect of TPE deformation on the results of the test, each test was replicated under identical conditions, including ensuring that the initial distance between crossheads was held constant. Therefore, results can only be compared between these samples that were all tested under identical conditions.

### 3.2.2 Results

A sample force-displacement curve is shown in Figure 3.10. There is an initial linear portion of the curve that represents the tensile elastic deformation in the elastomer, followed by a leveling off that indicates debonding between the TPE and the PA composite. In the linear region, it can be assumed that measured displacement can be attributed to the elastomer deformation and that no debonding is occurring. This is consistent with observations of the samples during testing.

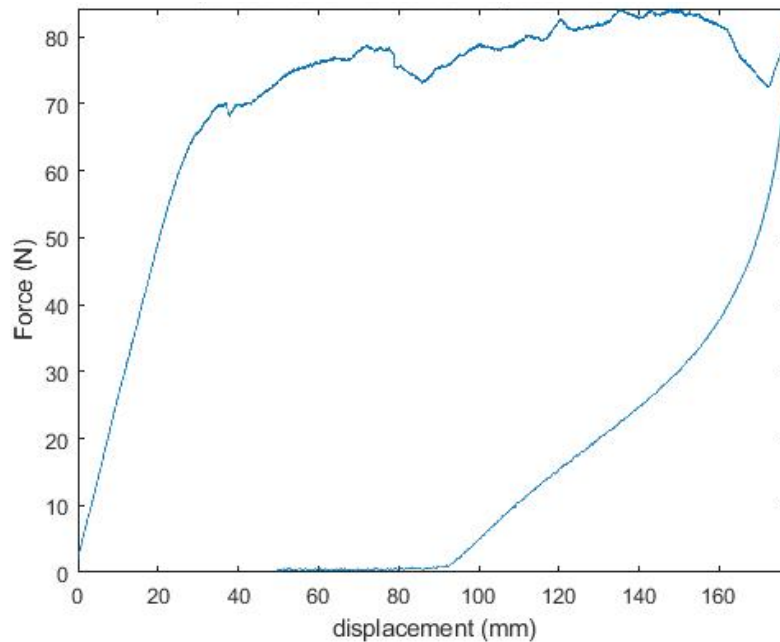


Figure 3.10. Representative force-displacement curve for the TPE and PA peel test.

The measured force was divided by the sample width (25.4mm) to obtain a peel strength. Force values from the initial, linear portion of the force vs. displacement curve were neglected to

avoid including the elastomer tensile deformation in the peel analysis. In addition, the data from the first 25mm of peeling was disregarded, as recommended by ASTM D3167. An average peel strength for each plate was subsequently calculated. It is determined that the average peel strength for the plate processed at 177°C is 2.8 kN/m, while the average peel strength for the plate processed at 197°C is 3.2 kN/m. This represents an 11.9% increase in peel strength with increased processing temperature. These results are illustrated graphically in Figure 3.11.

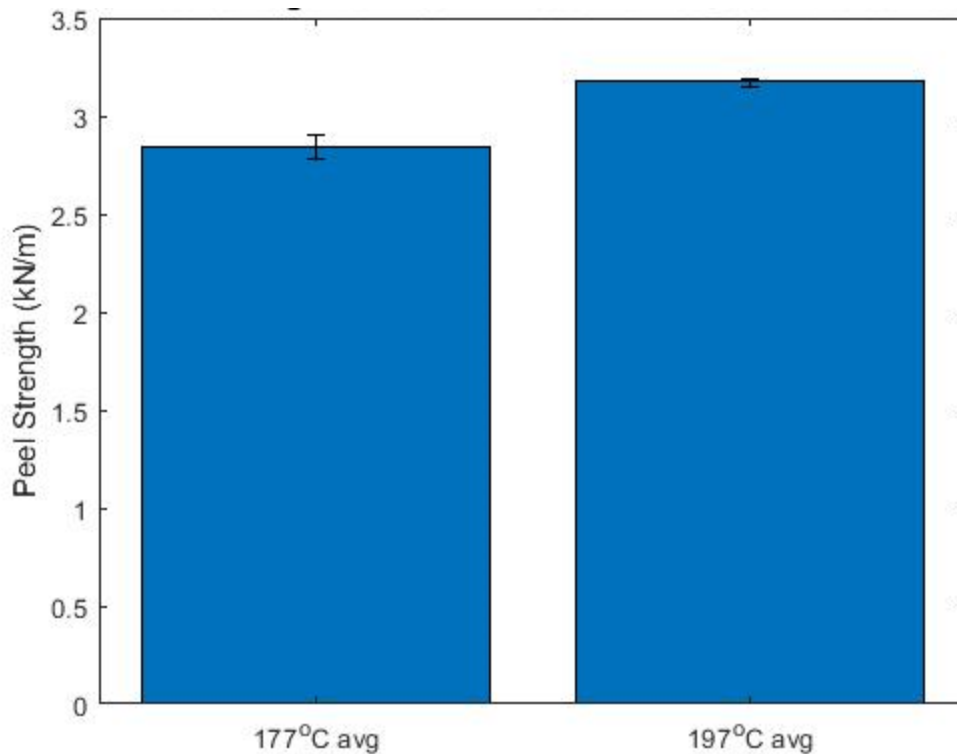


Figure 3.11. Mean peel strengths of PA/TPE plates processed at two different sets of processing conditions, plotted with the 95% confidence interval of the mean.

### 3.2.3 Discussion

Because it is of interest to compare the interfacial fracture toughness of peel-tested samples to samples tested using DCB or wedge testing, it is useful to represent peel results in terms of adhesive toughness. For peel samples, the adhesive toughness,  $G_A$ , can be represented using equation [3.5], where  $G$  is the total energy used to create interfacial area and  $G_P$  is the energy used to plastically bend the peel arm.

$$G_A = G - G_P(R_0) \quad [3.5]$$

Kawashita, et al. [37] find that, if the radius of curvature at the load point,  $R_0$  is less than the radius of curvature of the roller in the test fixture,  $R_1$ , the peel arm will conform to the roller. In this case, the plastic bending energy is dictated by  $R_1$  and the adhesive toughness can be determined using equation [3.6], where  $P$  is the applied peel load and  $b$  is the sample width.  $P_0$  is the load required to test a sample that is not bonded.

$$G_A = \frac{(P - P_0)}{b} \quad [3.6]$$

However, a further simplification can be made. If the assumption is made that the bending arm is perfectly elastic and that none of the applied energy goes to bending the beam, all of the recorded energy is adhesive energy. This is a fairly reasonable assumption for the TPE samples tested here, because the TPE does not need to plastically deform in order to bend and conform to the roller arm. In this case, the adhesive energy can be simply approximated as shown in equation [3.7].

$$G_A = \frac{P}{b} \quad [3.7]$$

In this case, the adhesive energy of the system is simply equal to the peel strength as reported and shown in Figure 3.11.

The fracture surfaces of samples from plates pressed at the two different temperatures were visibly different, as shown in Figure 3.12.

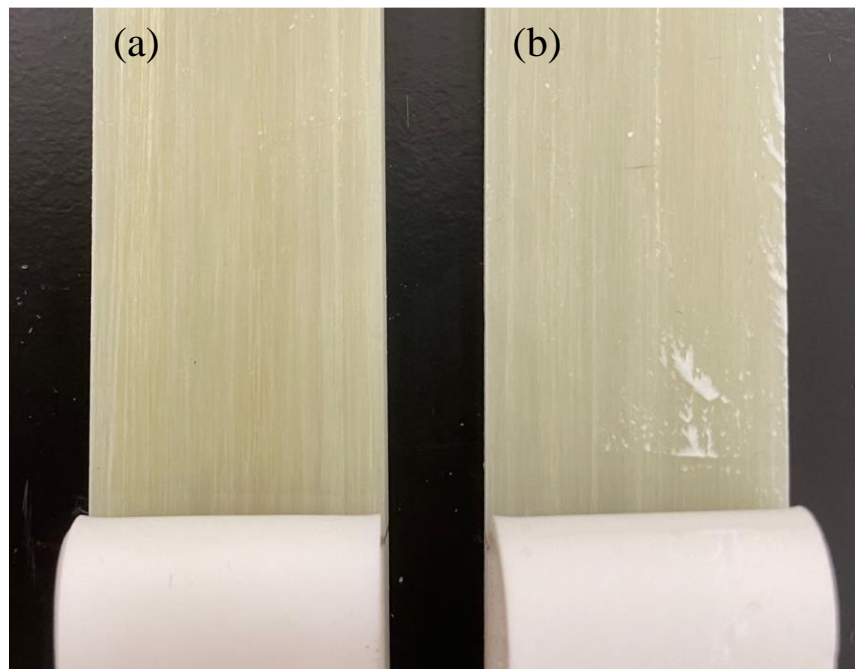


Figure 3.12. Fracture surfaces of peeled PA/TPE samples after testing. Samples processed at (a) 177°C and (b) 197°C.

The surfaces of the lower-temperature plate were very neat, with no tearing in the TPE. The PA side of the lower-temperature interfaces showed no remnants of TPE after debonding. In contrast, the higher-temperature samples often exhibited large regions of torn TPE at the surface, with some regions of TPE remaining on the PA side of the interface. This suggests that, in the higher-temperature samples, the bond between the TPE and the PA was sufficiently strong to deflect the interfacial crack away from the interface and into the bulk of the TPE. This difference in failure mechanisms supports the finding that the peel strength is higher in the higher-temperature samples, as more energy was needed to break the interfacial bond and the tearing of the TPE was an additional energy dissipation mechanism.

One rule of thumb [38] suggests that 90° peel strengths between 1.75 and 2.6 kN/m suggest that the sample has good adhesion, while peel strengths above 2.6 kN/m indicate “superior” adhesion. If this rule of thumb holds true for the floating roller peel geometry, PA/TPE samples processed under both sets of processing conditions used here can be considered to have superior adhesion.

### 3.2.4 Section Summary

Processing temperature has a marked effect on the bond strength between TPE and PA6, even though both processing temperatures examined fall below the PA6 melting temperature and temperature has little to no effect on the melt viscosity for the TPE used here. The increased temperature likely allowed for increased PA6 chain mobility, allowing them to interact more easily across the interface with the polymer chains in the TPE. It is possible that increasing the processing temperature further would yield still better peel strength between PA/TPE samples, although at sufficiently high temperatures the TPE would begin to degrade or burn.

This work shows how easily an 11.7% increase in bond strength can be achieved. This improved adhesion arose through no additional processing steps or additional bonding promoters, making this a practical method to improve bond strengths in existing industrial processes.

## 3.3 Chapter Conclusions

For all material combinations examined in this chapter, interfacial bond strength of EP/PA and PA/TPE could be improved simply via an increase in processing temperature for a compression molding process. This effect was more pronounced in thermoplastic materials than in thermoset ones, although it was present in both. The increase in processing temperature increases polymer chain mobility, which improves chemical interaction and interdiffusion across the interface.

Although the difference in constituent material properties necessitated different mode-I test methods—Wedge and DCB Testing for EP/EP, PA/PA, and EP/PA samples and Peel Testing for PA/TPE samples—the calculations outlined in section 3.2.3 allow for a rough comparison between the different test methods. The *weaker* PA/TPE bond strength,  $2800\text{J/m}^2$ , is higher than the stronger PA/PA bond strength of  $2366\text{J/m}^2$ , as determined by wedge testing. This is an indication that the PA/TPE bond represents a strong interface, and that further improvements to the bond strength beyond those seen here would simply lead to debonding in the bulk PA. A similar phenomenon is seen in the EP/PA samples processed at the higher temperature, where the EP-PA interface becomes stronger than the constituent materials, causing crack growth to deviate away from the interfaces.

Future work will determine whether changes to high-rate manufacturing processes result in similar dramatic improvements in interfacial bond strength. The following chapter will determine the effect that these changes to processing conditions, and in turn bond strength, have on mechanical properties for a simplified part geometry.

### 3.4 References

- [1] K. W. Allen, "Some reflections on contemporary views of theories of adhesion," *International Journal of Adhesion and Adhesives*, vol. 13, no. 2, Apr. 1993, doi: 10.1016/0143-7496(93)90015-2.
- [2] K. W. Allen, "A Review of Contemporary Views of Theories of Adhesion†," *The Journal of Adhesion*, 1987, doi: 10.1080/00218468708074974.
- [3] W. C. Wake, "Theories of adhesion and uses of adhesives: a review," *Polymer*. 1978. doi: 10.1016/0032-3861(78)90223-9.
- [4] A. J. Kinloch, *Adhesion and Adhesives: Science and Technology*. London: Chapman & Hall, 1987.
- [5] J. Comyn, *Adhesion Science*. RSC Publishing, 1997.
- [6] B. Z. Jang, L. C. Chen, C. Z. Wang, H. T. Lin, and R. H. Zee, "Impact resistance and energy absorption mechanisms in hybrid composites," *Composites Science and Technology*, 1989, doi: 10.1016/0266-3538(89)90002-X.
- [7] U. Beier *et al.*, "Mechanical performance of carbon fibre-reinforced composites based on preforms stitched with innovative low-melting temperature and matrix soluble thermoplastic yarns," *Composites Part A: Applied Science and Manufacturing*, 2008, doi: 10.1016/j.compositesa.2008.06.003.
- [8] P. J. Hogg, "Toughening of thermosetting composites with thermoplastic fibres," *Materials Science and Engineering A*, 2005, doi: 10.1016/j.msea.2005.08.028.
- [9] J. P. Favre, "Improving the fracture energy of carbon fibre-reinforced plastics by delamination promoters," *Journal of Materials Science*, 1977, doi: 10.1007/BF00738470.
- [10] J. E. Masters, "Improved Impact and Delamination Resistance through Interleafing," *Key Engineering Materials*, 1989, doi: 10.4028/www.scientific.net/KEM.37.317.
- [11] T. K. Tsotsis, "Interlayer toughening of composite materials," *Polymer Composites*, 2009, doi: 10.1002/pc.20535.



- [12] M. R. Groleau, Y. B. Shi, A. F. Yee, J. L. Bertram, H. J. Sue, and P. C. Yang, "Mode II fracture of composites interlayered with nylon particles," *Composites Science and Technology*, 1996, doi: 10.1016/S0266-3538(96)00080-2.
- [13] G. Caprino, P. Iaccarino, and A. Lamboglia, "The effect of shear on the rigidity in three-point bending of unidirectional CFRP laminates made of T800H/3900-2," *Composite Structures*, 2009, doi: 10.1016/j.compstruct.2008.04.014.
- [14] M. Hojo, S. Matsuda, M. Tanaka, S. Ochiai, and A. Murakami, "Mode I delamination fatigue properties of interlayer-toughened CF/epoxy laminates," *Composites Science and Technology*, 2006, doi: 10.1016/j.compscitech.2005.07.038.
- [15] D. Heflin, J. Dustin, and J.-A. Mansson, "Characterization of Adhesion Between Dissimilar Polymer-Matrix Composites," Apr. 2019. doi: 10.33599/nasampe/s.19.1504.
- [16] "Standard Test Method for Adhesive-Bonded Surface Durability of Aluminum (Wedge Test)".
- [17] J. Cognard, "The mechanics of the wedge test," *The Journal of Adhesion*, 1986, doi: 10.1080/00218468608073236.
- [18] "Standard Test Method for Mode I Interlaminar Fracture Toughness of Unidirectional Fiber-Reinforced Polymer Matrix Composites 1", doi: 10.1520/D5528-13.
- [19] J. W. Gillespie, L. A. Carlsson, and A. J. Smiley, "Rate-dependent mode I interlaminar crack growth mechanisms in graphite/epoxy and graphite/PEEK," *Composites Science and Technology*, vol. 28, no. 1, Jan. 1987, doi: 10.1016/0266-3538(87)90058-3.
- [20] R. B. Prime and E. Sacher, "Kinetics of epoxy cure: 2. The system bisphenol-A diglycidyl ether/polyamide," *Polymer*, vol. 13, no. 9, Sep. 1972, doi: 10.1016/0032-3861(72)90113-9.
- [21] Z. Zhong and Q. Guo, "Miscibility and cure kinetics of nylon/epoxy resin reactive blends," *Polymer*, vol. 39, no. 15, Jul. 1998, doi: 10.1016/S0032-3861(97)10237-3.
- [22] B. J. Briscoe, R. S. Court, and D. R. Williams, "The effects of fabric weave and surface texture on the interlaminar fracture toughness of aramid/epoxy laminates," *Composites Science and Technology*, vol. 47, no. 3, Jan. 1993, doi: 10.1016/0266-3538(93)90035-F.

- [23] W. Bradley and R. Cohen, "Matrix Deformation and Fracture in Graphite-Reinforced Epoxies," in *Delamination and Debonding of Materials*, 100 Barr Harbor Drive, PO Box C700, West Conshohocken, PA 19428-2959: ASTM International. doi: 10.1520/STP36316S.
- [24] Z. Suo, G. Bao, and B. Fan, "Delamination R-curve phenomena due to damage," *Journal of the Mechanics and Physics of Solids*, vol. 40, no. 1, Jan. 1992, doi: 10.1016/0022-5096(92)90198-B.
- [25] J. E. Zanetto, C. J. G. Plummer, P. E. Bourban, and J. A. E. Manson, "Fusion bonding of polyamide 12," *Polymer Engineering and Science*, vol. 41, no. 5, 2001, doi: 10.1002/pen.10787.
- [26] C. J. G. Plummer, P. E. Bourban, J. E. Zanetto, G. D. Smith, and J. A. E. Manson, "Nonisothermal fusion bonding in semicrystalline thermoplastics," *Journal of Applied Polymer Science*, vol. 87, no. 8, 2002, doi: 10.1002/app.11528.

## 4. CRASH PERFORMANCE OF DISSIMILAR MATERIALS

The previous chapter showed that, not only is spontaneous adhesion possible between several sets of dissimilar materials, but it is also adjustable via minor changes to processing conditions. With this knowledge in hand, we turn now to the importance of these differences in adhesion to the mechanical performance of a hybrid part.

Impact performance was chosen as the metric by which to characterize mechanical performance. A primary reason to incorporate a weaker, more ductile material into a relatively strong but brittle composite is to improve the energy absorption of such hybrid structures through deformation and delamination of the more ductile material. Quasi-static indentation is performed to study the crash performance of hybrid structures under sustained load and drop-weight impact testing is conducted to identify rate effects in this crash performance.

Two different material combinations are studied for their impact performance. The first is a combination of an epoxy/CF composite and a PA6/recycled CF mat. The previous chapter showed the PA6/epoxy combination to have the ability to form adhesive EP-PA bonds even stronger than the EP-EP cohesive bond, with a strong dependence on processing condition. In this combination, the relatively ductile PA can elastically and plastically deform to absorb energy, protecting the brittle epoxy from shattering via mechanisms described in detail in Chapter 2. The carbon fiber reinforcement in the PA provides strength to the structure so that part stiffness and strength are not sacrificed in the name of impact toughness.

A second material combination of aluminum with PA6/recycled CF was chosen. Aluminum is desirable for a variety of applications due to its light weight, processability, and ability to deform to absorb energy. However, its high ductility makes it susceptible to denting from minor impacts. This is problematic when aluminum is used as a body panel for automotive applications where minor impacts, such as from hail or small road debris, may leave unsightly surface dents. Composite laminates, on the other hand, are very resistant to visible surface damage. Therefore, there is great potential in the use of a thin panel of an impact tolerant composite, such as PA/CF, to maintain a neat planar surface finish in response to small impacts. As discussed in Chapter 2, PA can chemically bond with the alumina layer on the aluminum surface, and no additional surface treatment is employed to further improve the bond between the PA and aluminum.

All of the PA/CF used in this chapter is a nonwoven mat of comingled PA and recycled carbon fibers. These carbon fibers are sufficiently long and randomly oriented that the laminates behave as quasi-isotropic continuous fiber reinforcement.

#### **4.1 Crash Performance of Dissimilar Materials: Epoxy/Polyamide**

Epoxy-matrix composites are increasingly used in high-performance applications due to their high specific strength and low weight relative to traditional structural materials, such as steel. However, epoxy-based composites tend to be brittle and thus not well-suited to impact applications. One widely used method to improve the impact toughness of such composites is to incorporate a thermoplastic phase into the composite.

Polyamide (PA) is one such thermoplastic toughening agent. Due to its polarity and ability to covalently bond with epoxide groups, it has an innate compatibility with epoxy that is relatively unique among thermoplastics[1], [2]. This compatibility has led to its use as an epoxy toughening agent in a wide variety of geometries, including dispersed particles in the epoxy resin[3], [4], comingled or woven fibers[5], [6], and either discrete particle[7]–[9] or thin veil[10]–[12] interlayers in composite structures. Regardless of the system geometry, PA toughens the epoxy via two main energy absorption mechanisms—debonding at the PA/epoxy interface and deformation of the PA phase. These methods point to the importance of the PA/epoxy bond for energy absorption. If the bond is weak, debonding will absorb less energy, and may occur prematurely so that applied load cannot be transferred to the PA phase. This in turn will prevent energy absorption through PA deformation. If the interfacial bond is too strong, however, failure may occur in the bulk composite before the interface, weakening the structure[3]. Further, in some applications, a strong interfacial bond may limit the ability of the PA to absorb energy via deformation[4], [5].

Many researchers have also found that incorporating thermoplastic toughening agents reduces the performance of the overall structure. Typically, this arises from a reduction in fiber volume fraction as the toughening thermoplastic adds part volume without adding significant strength[6], and in some cases replaces reinforcing fibers that would have otherwise been present[5]. This tradeoff is often accepted and incorporated into design considerations. To ameliorate these concerns, this study uses carbon fiber-reinforced PA as a toughening agent that does not sacrifice composite strength.

Studies have shown that placing tougher materials on the top surface of composite laminates can improve impact performance, enabling laminates to achieve higher peak loads during impact and exhibit greater resistance to penetration for a given impact energy[13]–[16]. The tougher, or more ductile, material is able to dissipate contact stresses from the impact event. Additionally, a stronger material on the bottom surface is better able to withstand the tensile stress imposed by impact-induced bending. This study tests hybrid plates in two orientations, one with the more ductile material on the top and one with the stronger material on the top, to determine if this previous work holds true for this material system and geometry.

#### **4.1.1 Experimental Methods**

##### ***Materials***

The epoxy/carbon fiber (CF) material used in this study was Cytec 977-2/IM7, an epoxy (EP) prepreg with unidirectional carbon fiber reinforcement.

The PA/CF material was a nonwoven mat of commingled PA6 and recycled carbon fibers, supplied by ELG composites. The PA/CF material was pre-consolidated under 10 tons of force at 270°C for 10 minutes to ensure sufficient PA fiber melting and prepreg consolidation. This step was necessary because the epoxy processing temperature of 177°C was well below the PA6 melt temperature of 220°C, so the two composites cannot be adequately processed in a single step.

##### ***Sample Preparation***

Sample plates consisted of 8 plies of pre-consolidated PA/CF composite stacked atop 17 plies of uncured epoxy/CF arranged in a cross-ply layup, as illustrated in Figure 4.1. Layups were compression molded in a heated press, where the epoxy can co-cure with the pre-consolidated PA/CF laminate. All sample plates were pressed at 690kPa.

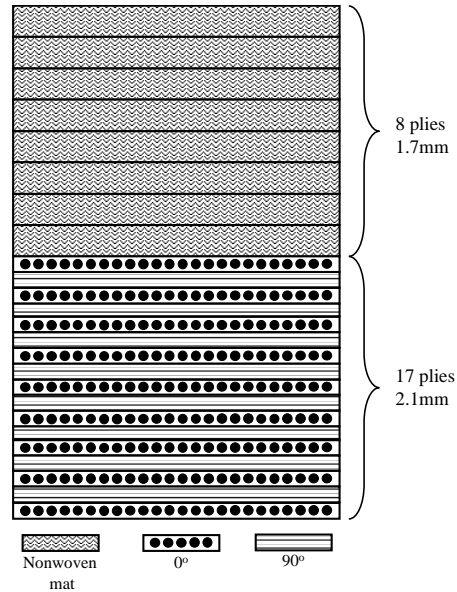


Figure 4.1. Laminate stacking sequence. Wavy lines represent PA/CF plies, while circles and horizontal lines indicate 0° and 90° epoxy/CF plies, respectively.

Two different sets of processing temperature and time were chosen—the manufacturer-recommended 177°C for 3 hours, and 197°C for 45 minutes. Previous work using these same processing conditions [17] showed that the increase in processing temperature from 177°C to 197°C resulted in up to a 215% increase in mode-I fracture toughness at the epoxy/PA interface. Sample nomenclature is shown in Table 4.1.

Table 4.1. Sample orientation, processing temperatures, and nomenclature

| Top Material | Bottom Material | T <sub>proc</sub> (°C) | Sample Label    |
|--------------|-----------------|------------------------|-----------------|
| EP/CF        | PA6/CF          | 177                    | EP/PA177, EP up |
| EP/CF        | PA6/CF          | 197                    | EP/PA197, EP up |
| PA6/CF       | EP/CF           | 177                    | EP/PA177, PA up |
| PA6/CF       | EP/CF           | 197                    | EP/PA197, PA up |

#### ***Mechanical Performance: Quasi-Static Indentation (QSI)***

Quasi-static indentation (QSI) testing was performed based on ASTM D6264[18]. 63.5x63.5mm square samples were fixed between steel blocks with 50.8x50.8mm square openings, as shown in Figure 4.2.

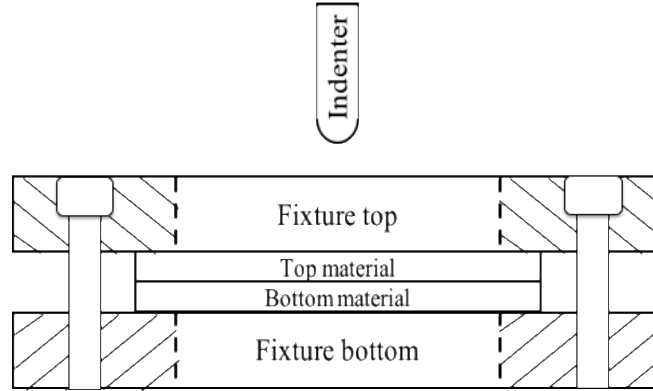


Figure 4.2. Sample holding fixture for QSI and Drop-Weight Impact Testing.

A steel rod with a 6.35mm diameter hemispherical tip was attached to the upper crosshead of a hydraulic load frame and the sample was loaded in compression at a constant crosshead displacement rate of 1mm/min until the impactor fully penetrated the samples. Force and crosshead displacement were measured throughout the test.

Energy absorbed throughout the loading cycle was calculated according to equation [4.1] [18].

$$E_{abs} = \int_{\delta_0}^{\delta_f} F(\delta) d\delta \quad [4.1]$$

#### ***Mechanical Performance: Drop-Weight Impact***

Drop-weight impact testing was undertaken based on ASTM D7136[19]. A 2.5kg steel rod with a 6.35mm diameter hemispherical tip was released in an enclosed column from varying heights to achieve a range of impact energies from 10-22J, with corresponding velocities ranging from 7-10.5m/s. Impact energy was normalized by sample thickness and was calculated using equation [4.2], where  $h$  is the sample thickness (mm) and  $C_E$  is a specified ratio of impact energy to sample thickness (J/mm).

$$E = C_E h \quad [4.2]$$

$C_E$  values were selected to yield sub-critical impact energy (i.e., energy that did not result in sample penetration) and varied from 2.7-5.7J/mm, corresponding to impact energy values ranging from 10-22J and impact velocities from 7-10.5m/s.

Samples were placed in the fixture shown in Figure 4.2. An opening in the drop tower was marked at 1mm intervals, and a camera was placed in front of the opening to capture the rebound height after the impactor made contact with the sample. The impactor was prevented from impacting the sample a second time, and the depth of the dent left on the sample surface by the impactor was measured immediately after impact.

Absorbed energy was calculated using equation [4.3], where  $m$  is the impactor mass,  $g$  is acceleration due to gravity,  $h_0$  is the impactor starting height, and  $h_f$  is the impactor rebound height. This calculation assumed that all the impact energy was either absorbed by the sample or converted to rebound energy, and thus neglected losses due to factors such as friction within the drop tower and air resistance. This was nevertheless believed to be a reasonable approximation.

$$E_{abs} = mg(h_0 - h_f) \quad [4.3]$$

This work also considered percent energy absorbed, to better compare across different impact energies. Percent energy absorbed was calculated simply as the percentage of the input energy that becomes absorbed energy for a given sample.

### ***Mechanical Performance: Non-Destructive Imaging***

A Zeiss Xradia 510 Versa 3D X-ray microscope was used to non-destructively examine the extent of internal damage as a result of the impact event. The X-ray microscope captured images using an 80V power source and exposure time of 0.5 seconds. Each slice was represented by 1012 images and had a resulting pixel size of 55.59 $\mu$ m. The scans were reconstructed and analyzed in VGSTUDIO MAX to find the size of the damage area due to delamination.

Initially, delamination areas were determined through use of the crack segmentation tool in VGSTUDIO MAX, which considered the grayscale gradient to determine an initial region that likely contains damage. An example is shown in Figure 4.3, where the blue outline shows the region of interest (ROI) boundary. This region was extracted as a defect mask ROI to be used in a porosity analysis to identify the delamination volumes. The projected area normal to the impact plane of the damage volume was used to determine the delamination area of each sample.

However, the crack segmentation method was ineffective for samples with less extensive damage. Therefore, for this analysis, crack segmentation was replaced with a grayscale threshold, followed by manual removal of local porosity inherent in the material. The resulting ROIs looked



the same as the representative image in Figure 4.3, but this method was less sensitive to local variations in material density that were inherent to the material and not indicative of damage.

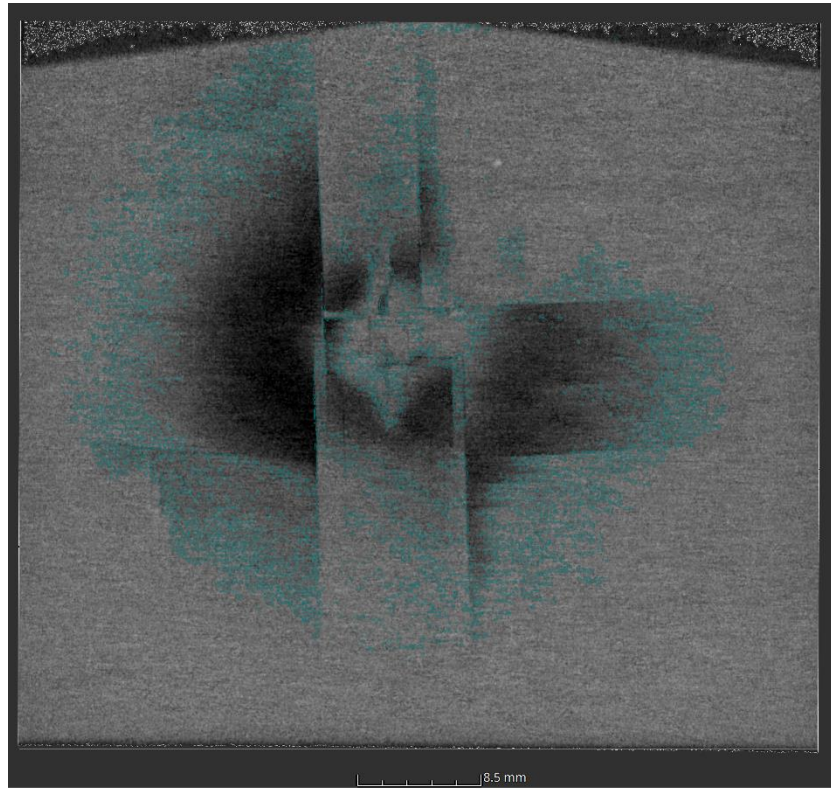


Figure 4.3. Representative defect ROI from the crack segmentation tool shown. The defect ROI represented a region with high probability for damage.

#### 4.1.2 Results and Discussion

##### *Quasi-Static Indentation (QSI)*

Representative force-displacement curves are shown in Figure 4.4 for each category of samples.

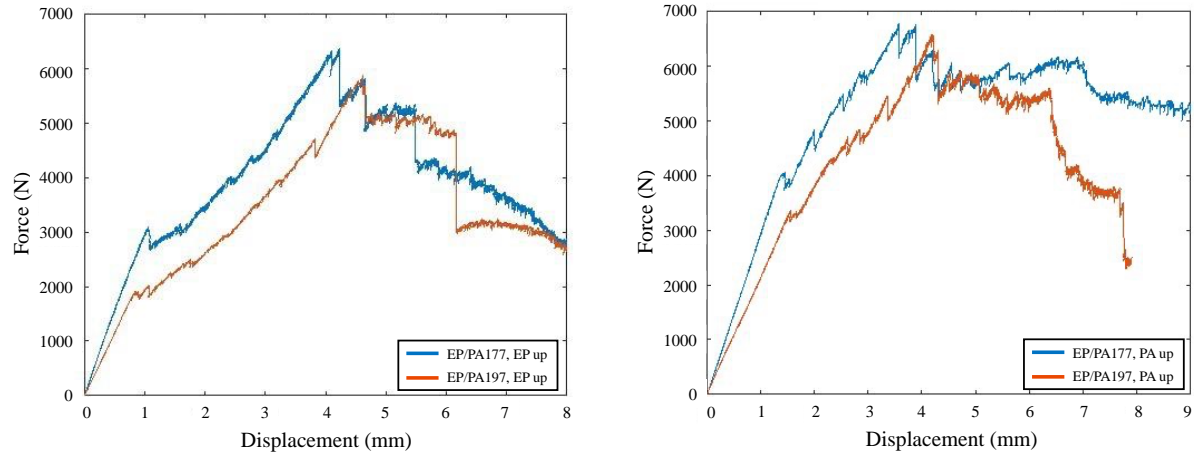


Figure 4.4. Representative force-displacement curves for EP-up samples (left) and PA-up samples (right).

Initial failure, indicated by a deviation from linearity in the initial load curve, appeared to be independent of processing temperature. However, the PA-up samples were able to reach higher loads before initial failure, meaning that if this material combination was used in an application where first failure was the crucial design consideration, a PA-up orientation would be beneficial. This was likely due to the ability of the more ductile PA/CF material to better dissipate lower-energy contact stresses.

The most important metric for determining crash performance is a part's ability to continue to support an applied load after initial failure. The EP/PA197, PA up samples excelled at this, likely due to a combination of factors. Not only was the ductile top surface able to dissipate contact stresses, but the stronger bottom material resisted tensile stresses due to out of plane bending during the test. The strong EP-PA interface was also helpful, as the resistance to delamination ensured that load transfer across the interface can continue even at high out of plane displacement.

The peak load reached for each type of sample, averaged across all samples tested, is shown in Figure 4.5. There was a slight increase in peak load with increased processing temperature, with a 10.3% increase in EP-up samples and an 18.5% increase in PA-up samples.

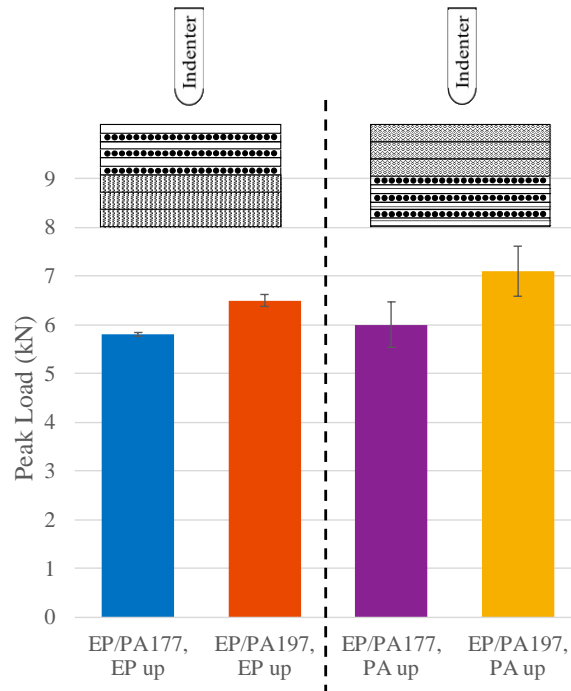


Figure 4.5. Peak load experienced during QSI testing.

The energy absorbed during testing is shown in Figure 4.6, averaged for each type of sample. For both part orientations, there was an increase in absorbed energy—32.6% and 83.0% for EP-up and PA-up samples, respectively—with increased processing temperature. This showed the importance of bond strength on crash performance. In the samples with stronger interlaminar bonding between the EP and PA layer, energy transfer across the interface can continue after greater applied energy, and breaking the interface absorbs more energy when the bond was strong.

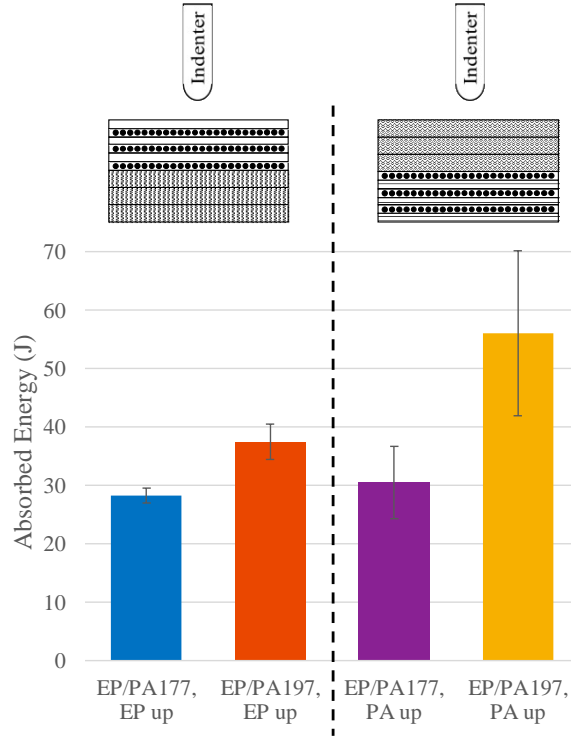


Figure 4.6. Energy absorbed by samples during QSI testing.

As with the drop-weight impact samples, the variability was higher among PA-up samples than among EP-up samples, likely due to the combination of small plate size and relatively large anisotropy in the PA6/CF nonwoven mat.

Despite this high variability, it was clear that the EP/PA197, PA up samples outperformed all others in QSI testing. The stronger EP-PA interface allowed effective load transfer between the two phases even as damage growth continues, the more ductile PA/CF on the top surface can more effectively dissipate contact stresses, and the stronger EP/CF on the bottom surface offered increased resistance to damage from impact-imposed bending. This combination of factors allowed for superior crash performance in EP/PA197, PA up samples, with a 98% increase in absorbed energy attainable through only an increase in processing temperature and an inversion of part orientation.

### ***Drop-Weight Impact***

Dent depth after impact is shown in Figure 4.7, as recommended in ASTM D7136. Regardless of processing temperature or part orientation, the dent depth was sufficiently low to

fall near or below the micrometer sensitivity of 0.25mm. Therefore, visible surface damage will not be a concern in parts made from this combination of materials exposed to low-energy impact, regardless of part orientation relative to the damage.

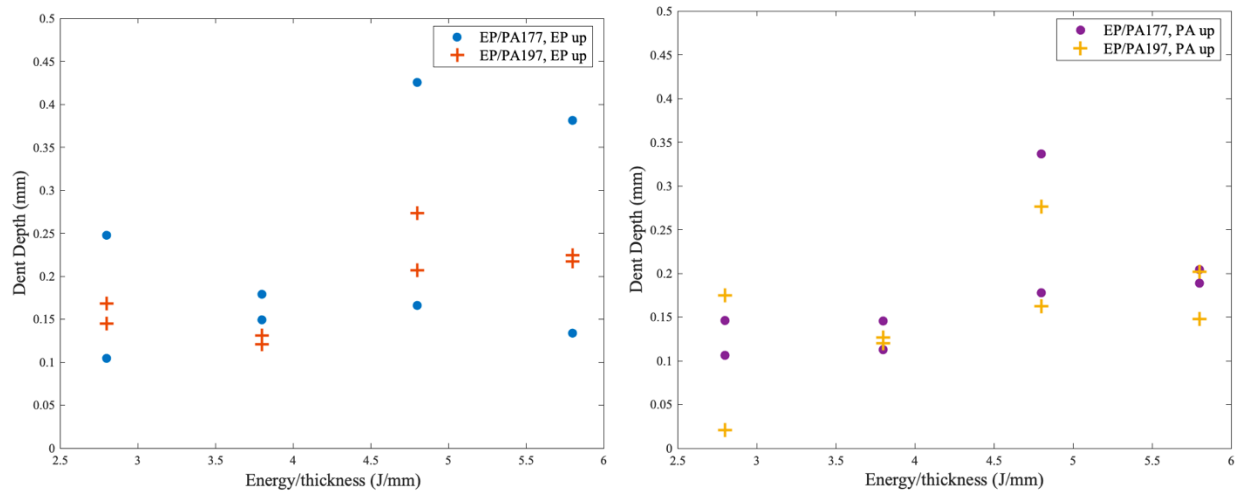


Figure 4.7. Dent depth measured immediately after impact for the case where the epoxy surface was impacted (left) and the case where the PA surface was impacted (right).

The percent of applied impact energy that was absorbed by the samples is shown in Figure 4.8. For the case where the epoxy surface was impacted, the percent energy absorbed by the EP/PA197 samples appeared to be relatively consistent with increasing impact energy. By contrast, the percent energy absorbed by the EP/PA177 samples underwent a sharp increase between  $E/h$  3.8 and 4.8. This step may indicate that a delamination threshold had been reached between the two energy levels, as suggested by Nixon et al [20].

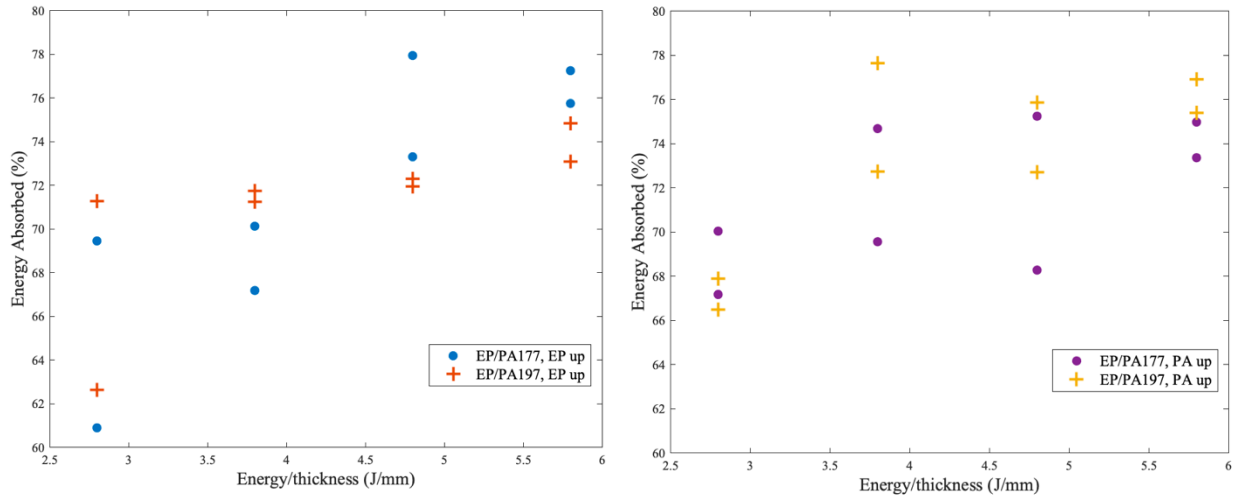


Figure 4.8. Percent of impact energy absorbed during drop-weight impact testing for the case where the epoxy surface was impacted (left) and the case where the PA surface was impacted (right).

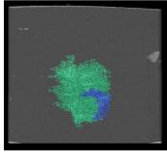
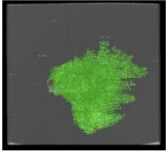
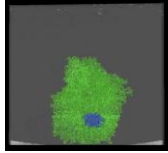
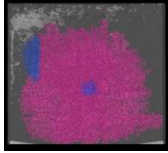

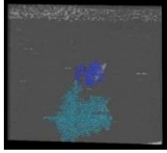
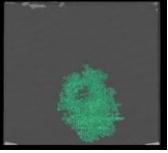
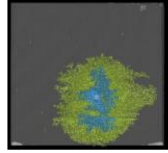
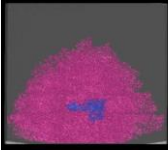
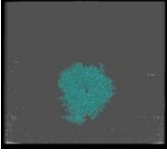
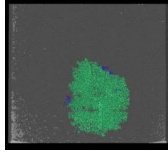
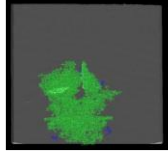
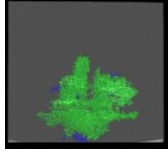
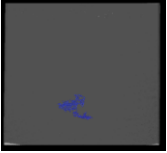
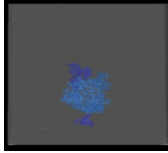
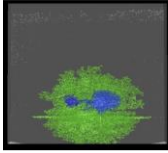
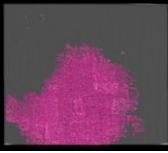
The behavior of the PA-up samples was less predictable, with little statistically significant difference between the two processing temperatures. This may be partially attributed to a combination of the randomness of the carbon fibers on the impacted surface and the relatively small plate size, making the plates more sensitive to local inconsistencies in the material.

### ***Computed Tomography (CT) Analysis***

CT scans were analyzed to find the projected damage area, shown in Table 4.2 with values summarized in Figure 4.9. This damage area represented delamination between the EP plies and at the EP-PA interface. The PA/CF nonwoven mats did not have distinct lamina after compression molding, likely due to the ability of the nonwoven carbon fibers to interact across ply interfaces. Therefore, delamination damage was confined to the EP/CF material.

Delamination tended to grow along the carbon fibers, in the  $0^\circ$  and  $90^\circ$  directions, which resulted in generally diamond-shaped damage regions. In some cases, delamination extended to the edges of the sample, which resulted in more irregularly-shaped damage regions.

Table 4.2. Representative projected damage area determined via CT scanning of impacted samples.

|                  | Impact Energy (J/mm)   |  |   |  | Projected x-y damage area (mm <sup>2</sup> )   |
|------------------|--|--|---|--|--|
|                  | 2.8  | 3.8  | 4.8   | 5.8  |  |
| EP/PA 177, EP up |   |   |   |   |  |
| EP/PA 177, PA up |   |   |   |   |  |
| EP/PA 197, EP up |   |   |   |   |  |
| EP/PA 197, PA up |  |  |  |  |  |

PA/CF damage was not visible in many of the samples at the scanning resolutions used. If present, damage typically appeared as roughly linear matrix cracks that extended in-plane in the 0° and 90° directions.

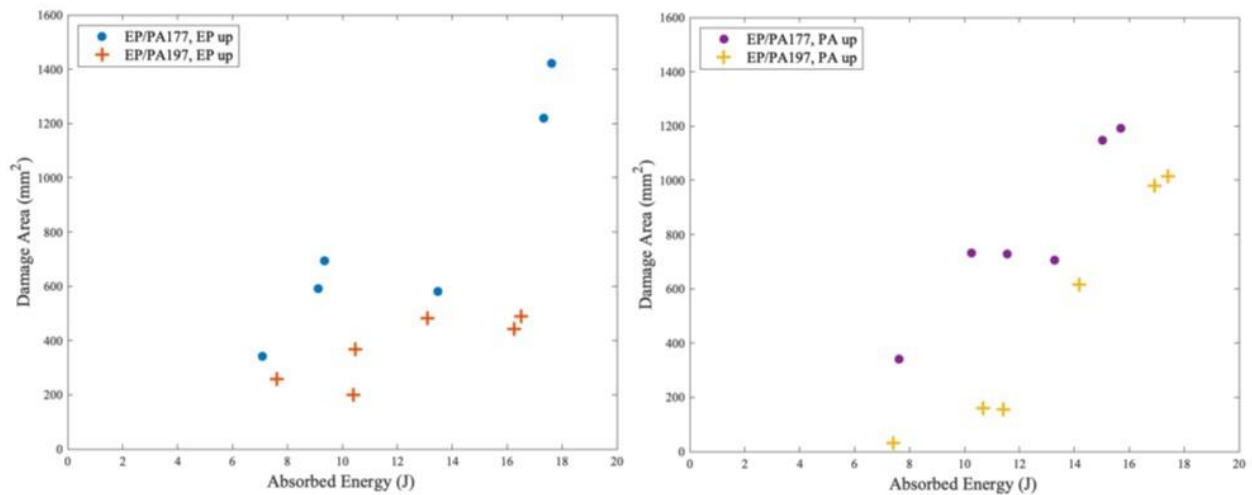


Figure 4.9. Projected damage area in samples damaged via drop-weight impact for EP-up samples (left) and PA-up samples (right). Damage area is plotted here with energy absorbed during impact.

For both part orientations, damage area was consistently larger in samples with weaker EP-PA interfaces. Most of the samples—all but the EP/PA197 PA up samples—exhibited a significant increase in damage area when the impact energy was increased above a threshold that corresponded to the increase in  $E/h$  from 4.8 to 5.8 J/mm. This indicated that in these cases a threshold for damage initiation or growth had been reached with the increased impact energy. Damage area in the EP/PA197, PA up samples remained relatively constant with the increase from 4.8 to 5.8 J/m, suggesting that these samples are more resistant to delamination growth for the impact energy ranges tested.

#### 4.1.3 Section Summary

Hybrid composites were successfully created via spontaneous bonding of epoxy and polyamide matrix composites during compression molding. The changes in EP-PA bond strength introduced by minor processing changes have a marked effect on impact performance of such hybrid composites. Some conclusions are summarized below:

- EP-PA bond strength, dictated by difference in processing temperature, may have more of an influence on drop-weight and QSI performance than part orientation
- When the EP-PA bond strength was low, part orientation does not have a significant effect on either the drop-weight or QSI part performance
- Samples seemed to have a threshold value over which extensive delamination occurred. This threshold may be increased with improved interfacial bond strength, and the EP/PA197, EP up samples did not reach this threshold in the range of energies tested here.
- Though all samples with higher bond strength performed better than their counterparts with weaker bonds, the desired application for hybrid EP-PA parts will dictate the ideal orientation.
  - The PA-up orientation had superior crash performance, as characterized by its ability to continue to sustain applied load after initial failure during QSI testing.
  - The EP-up orientation had better resistance to delamination damage in the mid- to low-energy drop-weight impact range tested here.

Future work could examine the effect of increased sample size, which should reduce limitations imposed by the test fixture, and an increased range of drop-weight impact energies to determine the penetration energy of hybrid EP-PA samples.



## **4.2 Crash Performance of Dissimilar Materials: Aluminum/Recycled Thermoplastic**

Aluminum is commonly used in applications where its light weight is desirable, and its relatively low strength can be accepted. Aluminum is also weldable, making aluminum parts easy to integrate into existing manufacturing lines and allowing for high-rate manufacturing. These qualities make aluminum a popular choice for automotive components. However, due to aluminum's plastic ductility, it is relatively susceptible to dents from minor impacts that a car might experience during a normal service life, including from pebbles and hail.

Composites are well-known for their tolerance to surface damage. In a case where the composite material does not need to withstand significant impact events but merely needs to resist minor cosmetic damage, the dangers of invisible damage within the composite are inconsequential. Further, composites with thermoplastic matrices, including polyamide (PA) tend to be better able to dissipate impact energy than their thermoset counterparts due to the ability of the thermoplastic to elastically deform in response to an applied load.

This study examines the effect of combining aluminum and a PA-matrix composite with recycled carbon fibers on the low-velocity impact performance of hybrid plates. Performance is also compared to homogeneous aluminum and composite plates to determine the effect of hybridization. Combining the two materials, rather than simply replacing the aluminum with composite, allows for ease of integration into existing processes as exposed aluminum edges could still be welded into place. Further, the use of a recycled carbon fiber composite serves as a proof of concept for the use of recycled fibers in impact applications. A recycled composite can be combined with recycled aluminum for a hybrid part with a favorable carbon footprint.

This work relies solely on spontaneous bonding between the polyamide and aluminum. While there are many documented ways to improve the adhesion between aluminum and composite materials, these methods tend to introduce expensive equipment [23]–[27] or harmful chemicals [28]–[31] and additional processing steps and time, making them less suitable for high-rate applications. It is worth noting, however, that a stronger interfacial bond between the composite and the aluminum might improve the impact energy absorption of hybrid plates by allowing for improved load transfer across the interface and requiring additional energy for debonding. For the case where a composite element is being used to improve the surface of an aluminum application which is subjected to low-energy impact the bond strength between the composite and the aluminum is not a concern. For applications where improved crash performance

is desired from an aluminum/composite hybrid plate these methods to improve adhesion are promising.

#### 4.2.1 Experimental Methods

##### *Materials*

The sample plates consisted of either an aluminum plate, a composite laminate, or both, as shown in Figure 4.10. Two thicknesses of 3003 Aluminum were used for the aluminum plates—0.4mm and 2mm.

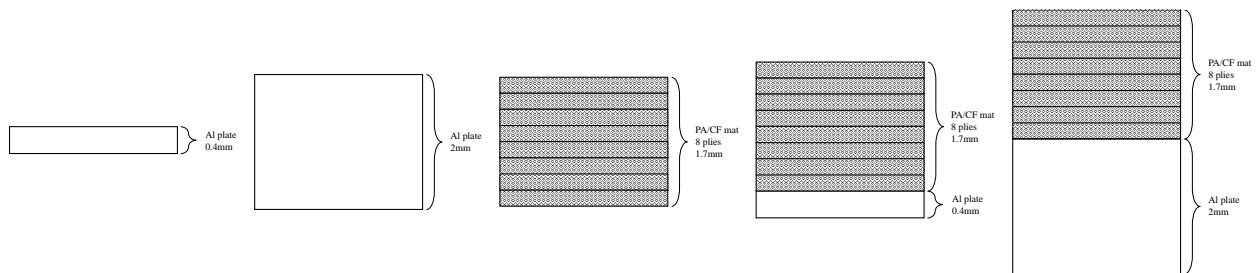


Figure 4.10. Material combinations used in this study. Samples consisted of an aluminum plate, a composite laminate, or a combination of both.

The composite used was a PA6/CF nonwoven mat consisting of commingled PA6 fibers with recycled carbon fibers. Eight plies were used to achieve a thickness of approximately 2mm for ease of comparison between the composite and aluminum. Before sample manufacture, the nonwoven mat plies were dried at 80°C for 4 hours, then immediately compression molded under 690kPa at 270°C for 10 minutes. This initial compression step ensured that the PA6 fibers fully melted to ensure full impregnation and that the nonwoven mat was fully consolidated.

##### *Sample Preparation*

One side of each aluminum plate was sanded, cleaned, and coated with a mild etchant that acted as a cleaning solution. This prevented any foreign material on the aluminum surface from contaminating the interfacial bond.

The aluminum was then placed in a 254mmx254mm mold with the cleaned surface facing up, and a pre-consolidated PA6/CF laminate was placed onto the aluminum. The assembly was

then pressed under 690kPa at 270 °C for 10 minutes and allowed to cool to room temperature under continued applied pressure. A summary of the samples tested is shown in Table 4.3. Results often refer to samples grouped as indicated in the table to facilitate comparison among similar samples.

Table 4.3. Summary of aluminum and PA6/CF hybrid samples used in quasi-static indentation and drop-weight impact testing.

| <b>Impacted Material</b> | <b>Bottom Material</b> | <b>Label</b>           | <b>Sample Group</b> |
|--------------------------|------------------------|------------------------|---------------------|
| PA6/CF mat, 8 plies      | N/A                    | PA                     |                     |
| 0.4mm-thick aluminum     | N/A                    | 0.4mm Al               | Thin Aluminum       |
| 0.4mm-thick aluminum     | PA6/CF mat, 8 plies    | Thin hybrid,<br>Al up  | Thin Aluminum       |
| PA6/CF mat, 8 plies      | 0.4mm-thick aluminum   | Thin hybrid,<br>PA up  | Thin Aluminum       |
| 2mm-thick aluminum       | N/A                    | 2mm Al                 | Thick Aluminum      |
| 2mm-thick aluminum       | PA6/CF mat, 8 plies    | Thick hybrid,<br>Al up | Thick Aluminum      |
| PA6/CF mat, 8 plies      | 2mm-thick aluminum     | Thick hybrid,<br>PA up | Thick Aluminum      |

For testing, each plate was cut into sixteen 63.5mmx63.5mm squares using waterjet cutting to prevent local melting or damage at the edges of the samples.

### ***Mechanical Performance: Drop-Weight Impact Testing***

Drop-weight impact testing was carried out based on ASTM D7136 to examine the effect of low-energy impact damage on the samples. A 0.55kg steel impactor with a 6.35mm diameter hemispherical tip was dropped from varying heights to achieve a range of energies. Due to the large variation in sample thickness, from 0.4 to 4mm, the ratio of impact energy to sample thickness was specified and ranged from 0.8 to 4.8 J/mm. Dent depth was measured on the impacted side (top surface) of the samples immediately after impact.

### ***Mechanical Performance: Quasi-Static Indentation (QSI) Testing***

A steel impactor with a 6.35mm diameter hemispherical tip was driven into the hybrid plate surface at a constant 1mm/min. The force and crosshead displacement were measured, and the force-displacement curve was integrated to determine the total energy absorbed during quasi-static testing. The test fixture is shown in Figure 4.2.

#### **4.2.2 Results**

##### ***Drop-Weight Impact Testing***

Both the PA and the PA-up hybrid samples were fully penetrated at impact energies higher than 1.8 J/mm, so no dent depth data exists for higher impact energies. From the comparison of the impact performance of the thin Aluminum sample group, shown in Figure 4.11, the following observations can be made:

- The dent depth was consistently larger in the PA-up hybrid samples than in the PA samples. This is due to the tendency of the 0.4mm-thick aluminum on the bottom of the PA-up hybrid samples to experience permanent deformation after impact. The adhesion between the aluminum and the PA6 was sufficiently strong in these samples that the PA6/CF on the top of the hybrid samples conformed to the contour of this permanent aluminum deformation.
- Dent depth alone is not an accurate predictor of material failure, especially for composite materials. The PA samples and the PA-up hybrid samples both had smaller dent depths than the 0.4mm Al and Al-up hybrid samples, but both the PA and PA-up hybrid samples experienced penetration at lower energy to thickness ratios.

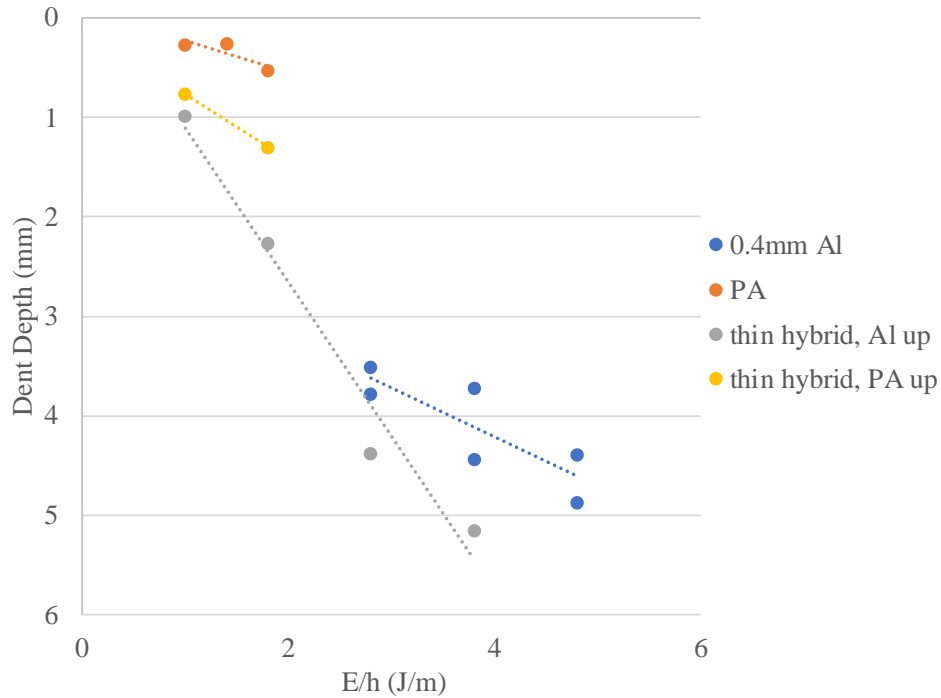


Figure 4.11. Dent depth results for low-velocity impact of thin Al/composite hybrid samples.

Dent dept results for the Thick Aluminum sample group, as defined in Table 4.3, are shown in Figure 4.12. For this group of samples, the following observations can be made:

- At the lowest impact energies, the PA and PA-up hybrid samples performed very similarly, with negligible differences in dent depth.
  - However, while the PA samples were fully penetrated above an energy to thickness ratio of 1.8 J/mm, the PA-up hybrid samples were able to continue to support an approximately 50% increase in relative load beyond that point. This illustrates the synergistic effect that aluminum can have on the hybrid plates.
- Because the bottom aluminum surfaces of these thick PA-up hybrid samples showed greater deformation than the top PA surfaces, there is likely some local debonding at the center of these samples between the aluminum and PA6/CF below the indenter. This debonding remained localized to the center of the samples.
- The large increase in dent depth in the Al-up hybrid samples between 1.4 and 1.8 J/mm reflects almost complete delamination between the aluminum and the PA6/CF composite

in the 1.8 J/mm sample. This meant that the aluminum on the surface was free to deform to absorb the remaining impact energy, resulting in a significant increase in dent depth.

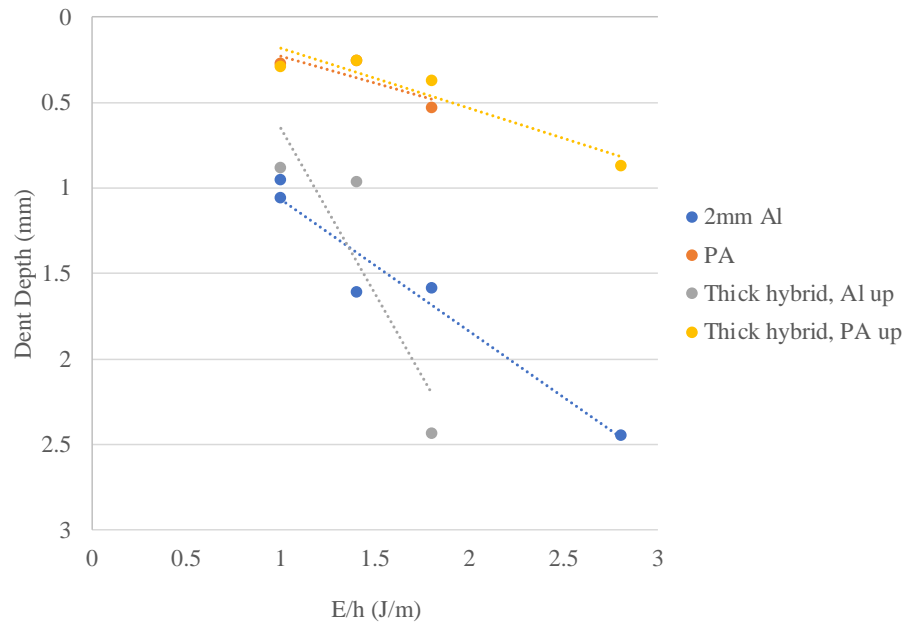


Figure 4.12. Dent depth results for low-velocity impact of thick Al/composite hybrid samples.

### ***Quasi-Static Indentation (QSI)***

Representative force-displacement curves are shown in Figure 4.13 for QSI testing on the thin aluminum group of samples.

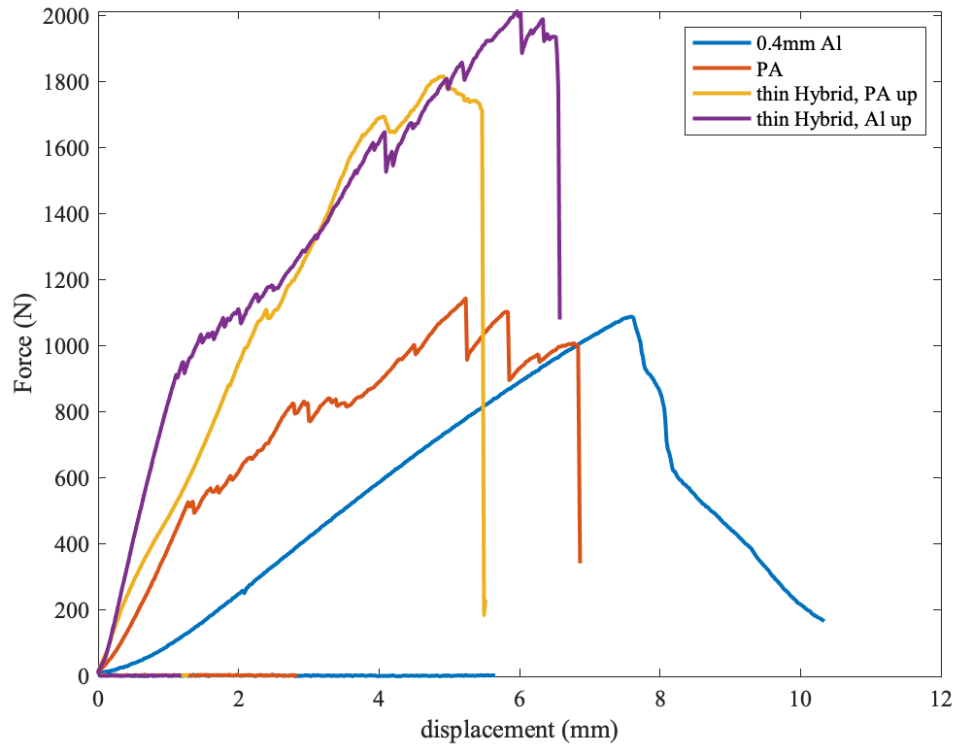


Figure 4.13. Representative force vs. displacement curves from QSI tests for PA6/CF composite, 0.4mm Al, and 0.4mm Al/composite hybrid laminates.

The PA6/CF composite without added aluminum exhibited a short initial linear region, where the first deviation from linearity represents the first matrix fracture within the composite. The subsequent dips in the force vs. displacement curve for the PA6/CF composite represent further failure within the composite in the form of matrix fracture, matrix-fiber deformation, or fiber fracture.

The hybrid aluminum/composite samples showed a strong dependence on which of the two faces was contacted by the indenter. When the aluminum side was contacted (top side), the initial load curve was steeper, indicating a stiffer load response than when the PA6/CF side was impacted. When the aluminum side was impacted, the peak load was also significantly higher, as was the maximum displacement before penetration. The initial fracture in the PA6/CF-up samples, however, indicated by the first deviation from linearity in the load-displacement curve, occurs at almost twice the initial displacement of the Al-up samples.

Table 4.4. Peak load and absorbed energy measured during the QSI load cycle for the thin aluminum group of samples.

|                             | PA/CF | 0.4mm Al | Thin PA-up hybrid | Thin Al-up hybrid |
|-----------------------------|-------|----------|-------------------|-------------------|
| <b>Peak Load (kN)</b>       | 1.14  | 1.09     | 1.82              | 2.01              |
| <b>Absorbed Energy (kJ)</b> | 4.89  | 4.54     | 5.98              | 8.50              |

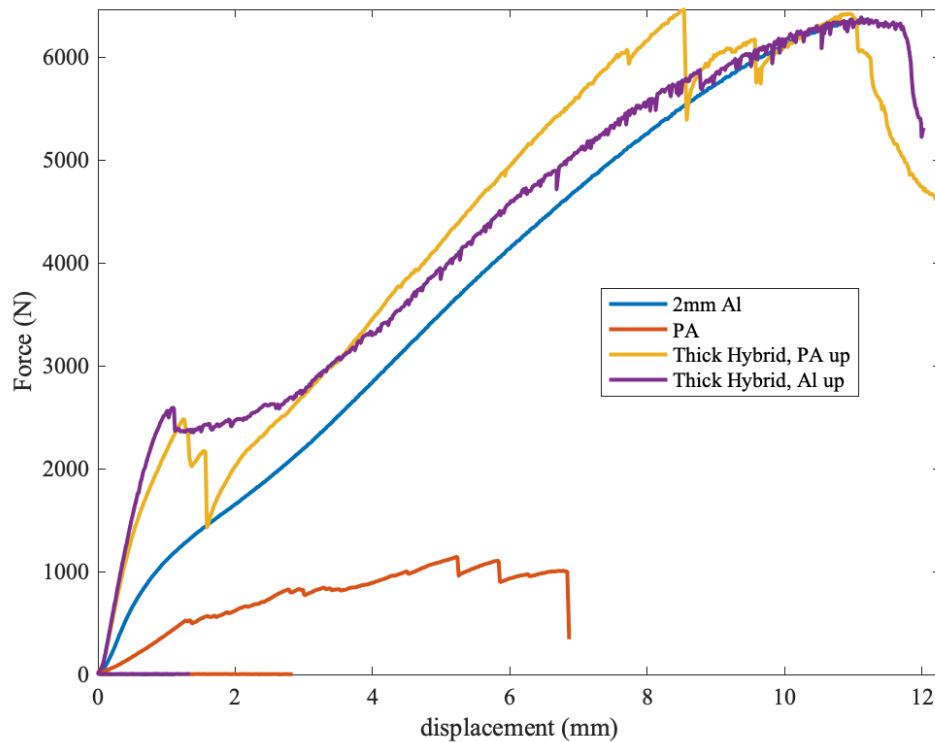


Figure 4.14. Representative force vs. displacement curves from QSI tests for PA6/CF composite, 2mm thick Al, and 2mm Al/composite hybrid laminates.

The neat aluminum samples exhibited a deviation from linearity, indicating the onset of plastic deformation, at a fairly low displacement. Therefore, the majority of the applied load to the aluminum is absorbed through plastic deformation in these samples.

The hybrid samples behaved similarly regardless of whether the aluminum or the PA6/CF surface was contacted by the indenter. However, in the Al-up samples, the curve was generally smooth, with only slight dips along the load cycle. The PA-up samples, on the other hand, had large drops in load along the curve, indicative of larger-scale failures within the composite.



Table 4.5. Peak load and absorbed energy during the QSI load cycle for the thick aluminum group of samples.

|                             | <b>PA/CF</b> | <b>2mm Al</b> | <b>Thick PA-up hybrid</b> | <b>Thick Al-up hybrid</b> |
|-----------------------------|--------------|---------------|---------------------------|---------------------------|
| <b>Peak Load (kN)</b>       | 1.14         | 6.36          | 6.47                      | 6.39                      |
| <b>Absorbed Energy (kJ)</b> | 4.89         | 41.1          | 46.7                      | 49.6                      |

### 4.2.3 Discussion

From the drop-weight impact and quasi-static indentation testing presented here for aluminum/composite hybrid samples, several observations can be made.

- PA6/CF offers a clear reduction in visible damage on the surface of a sample subjected to low-energy impact, while the presence of a thicker aluminum plate on the bottom surface appears to offer a reciprocal resistance to penetration for the composite samples, as illustrated in Figure 4.12.
- As expected, the neat aluminum force vs. displacement QSI curves are all fairly smooth, reflecting the homogeneous nature of the aluminum. By contrast, all of the samples containing the PA6/CF composite exhibited an initial linear load region, followed by a jagged load curve after the initial internal failure in the composite.
- Even the addition of a thin layer of aluminum on either the top or bottom surface of the PA6/CF composite yields a significant improvement in both the peak load and in the absorbed energy over both the aluminum alone and the PA6/CF composite alone.
- The addition of aluminum drastically improved the maximum load sustained by the PA6/CF composite during QSI. This is likely because the plastic deformation of the aluminum, which is significant at the deformations reached here, absorbs a great deal of the applied energy.

It can also be worthwhile to compare the scaled results. Several researchers have attempted to determine the most accurate method of scaling impact and QSI results by thickness, with mixed results. Metals can scale predictably by sample thickness, but reliable scaling for composite materials becomes more difficult. Simply scaling by inverse sample thickness has been shown to be fairly accurate, although not entirely reliable [22], [32], [33]. For the sake of discussion, results scaled by inverse sample thickness are shown in Figure 4.15.

One of the challenges researchers cite in scaling the impact behavior of composite materials is the difference in behavior with different numbers of ply interfaces. Because delamination between adjacent composite plies is such a crucial energy absorption mechanism in composite impact studies, scaling by thickness becomes challenging. For example, doubling the thickness of an 8-ply laminate introduces eight new inter-ply interfaces, which cannot be accounted for by simply scaling the samples. However, in this study, the thicker samples have the same number of composite interfaces as the neat PA/CF samples. Though scaling by thickness is still not expected to be without its drawbacks, it is at least free from the complexity introduced by an increased number of ply interfaces. Therefore, scaling by thickness is suitable based on previously published research.

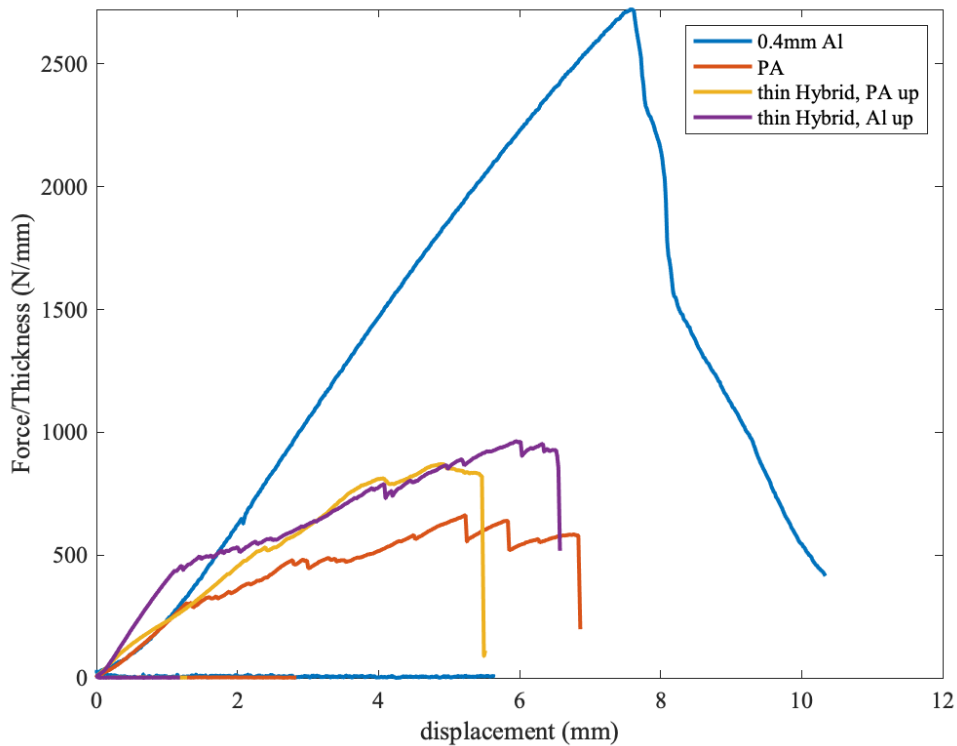


Figure 4.15. Force divided by sample thickness vs. displacement for QSI of thin aluminum and PA6/CF hybrid composites.

Even scaled by thickness, the hybrid samples out-perform the PA6/CF samples, demonstrating the improvement in energy absorption and peak energy available to the composite with the inclusion of even a very thin layer of aluminum.

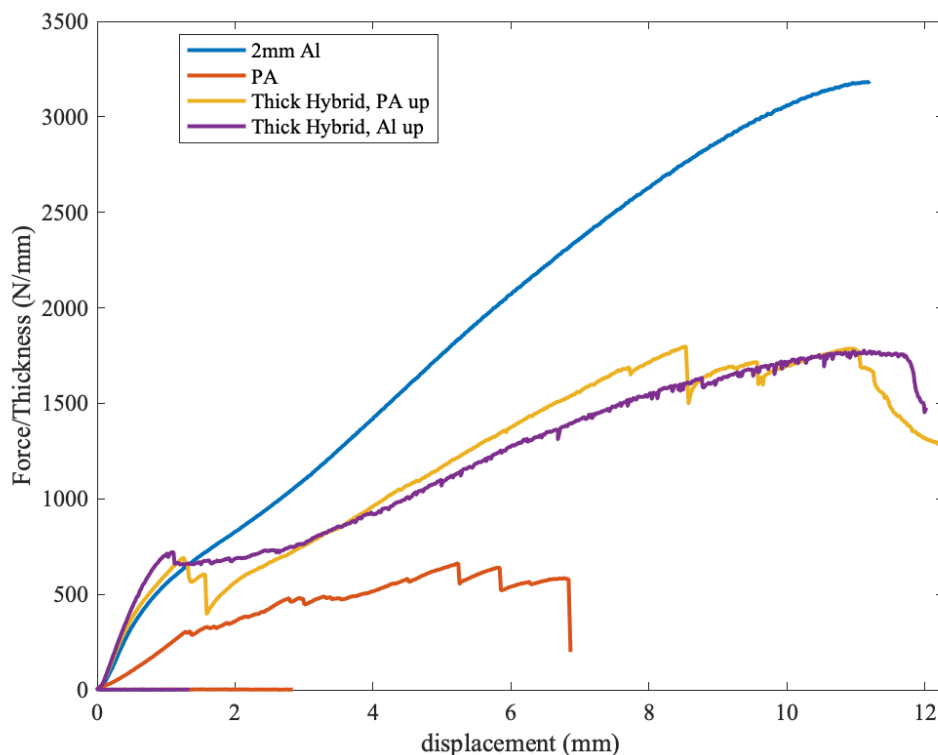


Figure 4.16. Force divided by sample thickness vs. displacement for QSI of thick aluminum and PA6/CF hybrid composites.

Relative to the sample thickness, the pure aluminum samples absorbed the greatest amount of energy and had the highest peak energy for both the thin and thick aluminum groups.

The bond between the aluminum and the PA6/CF is optimal to accommodate both stress transfer and crack propagation. There are a number of ways to improve the bond between a composite and aluminum, including the use of secondary adhesives and using advanced techniques to abrade the aluminum surface, creating more surface area for bonding and mechanical interlocking [23], [24], [29], [34]. However, there is a chance that improving the bond would not be beneficial to the energy absorption. The QSI results from the hybrid composites, particularly those that used 2mm-thick aluminum, suggest that large-scale plastic deformation in the aluminum is a primary energy absorption mechanism. If the hybrid composites had a stronger bond between the aluminum and the PA6/CF, the ability of the aluminum to deform would be diminished. However, it is also possible that failure of the strong interfacial bond could be a similarly valuable energy absorption mechanism. Further testing would be needed to determine how these two effects balance in hybrid composites with stronger interfacial bonds.

#### **4.2.4 Section Summary**

Adding an aluminum sheet to one face of a PA-based composite greatly improves the static and dynamic impact behavior of the PA/CF composite. The presence of the PA/CF laminate does not hinder the aluminum performance in a static test. In a drop test, impacting the PA/CF face results in significantly smaller dent depth than impacting the aluminum face does, as aluminum's high ductility allows it to be easily dented. This combination of factors makes such a hybrid laminate well-suited to applications where the aluminum carries the brunt of the impact load with a thin composite laminate on the surface to protect the aluminum from denting in response to minor impacts, preserving the aesthetics of the part.

The adhesion between aluminum and any polymer-based composite could be greatly enhanced through a number of aluminum pretreatment methods. However, this study has proven that the adhesion between PA and aluminum is sufficiently strong that impact load can be transferred between the materials without causing widespread failure of the interface. If the adhesion were improved, it is possible that the impact energy absorption might actually decrease from that reported here, as the local debonding of the PA/aluminum interface under the impact point is a valuable energy dissipation mechanism. It is possible that if the interface bond were stronger, the loss of debonding as an energy dissipation mechanism could cause earlier failure of one of both of the constituent components.

### **4.3 Chapter Conclusions**

Across QSI and drop-weight impact testing of multiple material combinations, several trends emerge, and are summarized below.

- Dent depth on a composite laminate surface is negligible for the low-energy impacts examined here. Aluminum, on the other hand, is highly susceptible to surface denting even at low impact energy. Therefore, a composite laminate can be effectively used to shield a material that is more prone to surface damage via denting.
- In quasi-static indentation, all material combinations absorb the most energy when the top surface material is more ductile and when the bottom material has a higher yield strength. This is because the ductile surface material helps to dissipate contact stresses from the

impactor, while the stronger bottom surface withstands the tensile forces associated with impact-induced sample bending.

- In drop-weight impact testing, the hybrid plates exhibit mutually beneficial behavior, regardless of which material is contacted by the indenter.
- There is a threshold impact energy above which large-scale delamination occurs between the two material systems. This threshold can be shifted to higher impact energy values if the bond strength between the two material systems is improved.

This chapter has shown the importance of a carefully designed interface for the crash performance of a hybrid material part. Additionally, a hybrid material system must be carefully designed to ensure maximum energy absorption. The material that comes in contact with an impactor should be able to effectively dissipate contact stresses, while the structure should be designed such that the bottom surface is stiff enough to resist impact-induced bending.

#### **4.4 Chapter Acknowledgements**

We would like to thank ELG Composites for provided the recycled PA/CF mat used in this study. We would like to thank Dr. Joshua Dustin for constructing the drop tower and Thomas Beimrohr for his assistance collecting data. We also acknowledge Chven Mitchell who acquired the images of the impacted samples for this paper on a Zeiss Xradia 510 Versa 3D X-ray Microscope that was supported by the EVPRP Major Multi-User Equipment Program 2017 at Purdue University.

#### **4.5 References**

- [1] R. B. Prime and E. Sacher, “Kinetics of epoxy cure: 2. The system bisphenol-A diglycidyl ether/polyamide,” *Polymer*, vol. 13, no. 9, Sep. 1972, doi: 10.1016/0032-3861(72)90113-9.
- [2] Z. Zhong and Q. Guo, “Miscibility and cure kinetics of nylon/epoxy resin reactive blends,” *Polymer*, vol. 39, no. 15, Jul. 1998, doi: 10.1016/S0032-3861(97)10237-3.

- [3] C. Girodet, E. Espuche, H. Sautereau, B. Chabert, R. Ganga, and E. Valot, "Influence of the addition of thermoplastic preformed particles on the properties of an epoxy/anhydride network," *Journal of Materials Science*, vol. 31, no. 11, pp. 2997–3002, Jun. 1996, doi: 10.1007/BF00356014.
- [4] B. J. Cardwell and A. F. Yee, "Toughening of epoxies through thermoplastic crack bridging," 1998.
- [5] C. Thanomsilp and P. J. Hogg, "Penetration impact resistance of hybrid composites based on commingled yarn fabrics," *Composites Science and Technology*, vol. 63, no. 3–4, pp. 467–482, Feb. 2003, doi: 10.1016/S0266-3538(02)00233-6.
- [6] P. J. Hogg, "Toughening of thermosetting composites with thermoplastic fibres," *Materials Science and Engineering: A*, vol. 412, no. 1–2, pp. 97–103, Dec. 2005, doi: 10.1016/j.msea.2005.08.028.
- [7] M. Hojo, S. Matsuda, M. Tanaka, S. Ochiai, and A. Murakami, "Mode I delamination fatigue properties of interlayer-toughened CF/epoxy laminates," *Composites Science and Technology*, 2006, doi: 10.1016/j.compscitech.2005.07.038.
- [8] M. R. Groleau, Y. B. Shi, A. F. Yee, J. L. Bertram, H. J. Sue, and P. C. Yang, "Mode II fracture of composites interlayered with nylon particles," *Composites Science and Technology*, 1996, doi: 10.1016/S0266-3538(96)00080-2.
- [9] G. Caprino, P. Iaccarino, and A. Lamboglia, "The effect of shear on the rigidity in three-point bending of unidirectional CFRP laminates made of T800H/3900-2," *Composite Structures*, 2009, doi: 10.1016/j.compstruct.2008.04.014.
- [10] T. K. Tsotsis, "Interlayer toughening of composite materials," *Polymer Composites*, 2009, doi: 10.1002/pc.20535.
- [11] J. P. Favre, "Improving the fracture energy of carbon fibre-reinforced plastics by delamination promoters," *Journal of Materials Science*, 1977, doi: 10.1007/BF00738470.
- [12] J. E. Masters, "Improved Impact and Delamination Resistance through Interleafing," *Key Engineering Materials*, 1989, doi: 10.4028/www.scientific.net/KEM.37.317.
- [13] W. J. Cantwell and J. Morton, "Impact perforation of carbon fibre reinforced plastic," *Composites Science and Technology*, vol. 38, no. 2, pp. 119–141, Jan. 1990, doi: 10.1016/0266-3538(90)90002-M.

- [14] W. J. Cantwell and J. Morton, "Detection of impact damage in CFRP laminates," *Composite Structures*, vol. 3, no. 3–4, pp. 241–257, Jan. 1985, doi: 10.1016/0263-8223(85)90056-X.
- [15] E. Sevkat, B. Liaw, F. Delale, and B. B. Raju, "Drop-weight impact of plain-woven hybrid glass-graphite/toughened epoxy composites," *Composites Part A: Applied Science and Manufacturing*, 2009, doi: 10.1016/j.compositesa.2009.04.028.
- [16] J. Gustin, A. Joneson, M. Mahinfalah, and J. Stone, "Low velocity impact of combination Kevlar/carbon fiber sandwich composites," *Composite Structures*, 2005, doi: 10.1016/j.compstruct.2004.07.020.
- [17] D. Heflin, J. Dustin, and J.-A. Mansson, "Characterization of Adhesion Between Dissimilar Polymer-Matrix Composites," Apr. 2019. doi: 10.33599/nasampe/s.19.1504.
- [18] "Standard Test Method for Measuring the Damage Resistance of a Fiber-Reinforced Polymer-Matrix Composite to a Concentrated Quasi-Static Indentation Force 1", doi: 10.1520/D6264\_D6264M-17.
- [19] "Standard Test Method for Measuring the Damage Resistance of a Fiber-Reinforced Polymer Matrix Composite to a Drop-Weight Impact Event 1", doi: 10.1520/D7136\_D7136M-20.
- [20] B. L. Wardle and P. A. Lagace, "On the Use of Dent Depth as an Impact Damage Metric for Thin Composite Structures:," <http://dx.doi.org/10.1177/073168449701601202>, vol. 16, no. 12, pp. 1093–1110, Aug. 2016, doi: 10.1177/073168449701601202.
- [21] J. A. Nixon, M. G. Phillips, D. R. Moore, and R. S. Prediger, "A study of the development of impact damage in cross-ply carbon fibre/PEEK laminates using acoustic emission," *Composites Science and Technology*, vol. 31, no. 1, pp. 1–14, Jan. 1988, doi: 10.1016/0266-3538(88)90073-5.

- [22] A. T. Nettles, M. J. Douglas, and E. E. Estes, “Scaling Effects in Carbon/epoxy Laminates Under Transverse Quasi-static Loading - Alan T. Nettles - Google Books,” Hampton, Virginia, 1999. Accessed: Mar. 20, 2022. [Online]. Available: [https://books.google.com/books?hl=en&lr=&id=rE47AQAAMAAJ&oi=fnd&pg=PA18&dq=Scaling+Effects+in+Carbon/Epoxy+Laminates+under+Transverse+Quasi-Static+Loading&ots=a2QD\\_k3E2I&sig=ZLqyCAfKhSqlA8PtmNg3bAdR9io#v=onepage&q=Scaling%20Effects%20in%20Carbon%20Epoxy%20Laminates%20under%20Transverse%20Quasi-Static%20Loading&f=false](https://books.google.com/books?hl=en&lr=&id=rE47AQAAMAAJ&oi=fnd&pg=PA18&dq=Scaling+Effects+in+Carbon/Epoxy+Laminates+under+Transverse+Quasi-Static+Loading&ots=a2QD_k3E2I&sig=ZLqyCAfKhSqlA8PtmNg3bAdR9io#v=onepage&q=Scaling%20Effects%20in%20Carbon%20Epoxy%20Laminates%20under%20Transverse%20Quasi-Static%20Loading&f=false)
- [23] K. Taki, S. Nakamura, T. Takayama, A. Nemoto, and H. Ito, “Direct joining of a laser-ablated metal surface and polymers by precise injection molding,” *Microsystem Technologies*, vol. 22, no. 1, pp. 31–38, Jan. 2016, doi: 10.1007/S00542-015-2640-2/FIGURES/13.
- [24] K. Ramani and J. Tagle, “Process-induced effects in thin-film bonding of PEKEKK in metal-polymer joints,” *Polymer Composites*, vol. 17, no. 6, pp. 879–886, 1996, doi: 10.1002/PC.10681.
- [25] K. Ramani and W. Zhao, “The evolution of residual stresses in thermoplastic bonding to metals,” *International Journal of Adhesion and Adhesives*, vol. 17, no. 4, pp. 353–357, 1997, doi: 10.1016/S0143-7496(97)00030-4.
- [26] K. Ramani and B. Moriarty, “Thermoplastic bonding to metals via injection molding for macro-composite manufacture,” *Polymer Engineering and Science*, vol. 38, no. 5, pp. 870–877, 1998, doi: 10.1002/PEN.10253.
- [27] K. Enami, F. Kimura, K. Yokoyama, T. Murakami, and Y. Kajihara, “Experimental and simulative investigation of the effects of laser-structured metal surface on metal-polymer direct joining,” *Precision Engineering*, vol. 62, pp. 273–281, Mar. 2020, doi: 10.1016/J.PRECISIONENG.2019.12.011.
- [28] P. A. Fabrin, M. E. Hoikkanen, and J. E. Vuorinen, “Adhesion of thermoplastic elastomer on surface treated aluminum by injection molding,” *Polymer Engineering & Science*, vol. 47, no. 8, pp. 1187–1191, Aug. 2007, doi: 10.1002/PEN.20801.



- [29] S. Yin, Y. Xie, R. Li, J. Zhang, and T. Zhou, “Polymer-Metal Hybrid Material with an Ultra-High Interface Strength Based on Mechanical Interlocking via Nanopores Produced by Electrochemistry,” *Industrial and Engineering Chemistry Research*, vol. 59, no. 27, pp. 12409–12420, Jul. 2020, doi: 10.1021/ACS.IECR.0C01304/SUPPL\_FILE/IE0C01304\_SI\_001.PDF.
- [30] Y. Xie, J. Zhang, and T. Zhou, “Large-area mechanical interlocking via nanopores: Ultra-high-strength direct bonding of polymer and metal materials,” *Applied Surface Science*, vol. 492, pp. 558–570, Oct. 2019, doi: 10.1016/J.APSUSC.2019.06.246.
- [31] F. Yusof, Y. Miyashita, N. Seo, Y. Mutoh, and R. Moshwan, “Utilising friction spot joining for dissimilar joint between aluminium alloy (A5052) and polyethylene terephthalate,” <https://doi.org/10.1179/136217112x13408696326530>, vol. 17, no. 7, pp. 544–549, 2013, doi: 10.1179/136217112X13408696326530.
- [32] J. Morton, “Scaling of impact-loaded carbon-fiber composites,” *AIAA Journal*, vol. 26, no. 8, pp. 989–994, 1988, doi: 10.2514/3.10001.
- [33] A. T. Nettles and S. Hromisin, “Normalization of Impact Energy by Laminate Thickness for Compression After Impact Testing - NASA Technical Reports Server (NTRS),” Huntsville, Alabama, 2013. Accessed: Mar. 20, 2022. [Online]. Available: <https://ntrs.nasa.gov/citations/20130013421>
- [34] F. Yusof, M. Yukio, M. Yoshiharu, and M. H. Abdul Shukor, “Effect of anodizing on pulsed Nd:YAG laser joining of polyethylene terephthalate (PET) and aluminium alloy (A5052),” *Materials & Design*, vol. 37, pp. 410–415, May 2012, doi: 10.1016/J.MATDES.2012.01.006.

## **5. MANUFACTURING AND PERFORMANCE ANALYSIS OF AN INJECTION OVERMOLDED POLYAMIDE/TPE HYBRID COMPOSITE**

The final section of this work is a case study in scaling up the understanding gained from the previous chapters to a realistic manufacturing use case. The case study involves high-rate, fully automatable manufacture of a complex, 3D part consisting of a PA6/CF continuous fiber structural preform and a thermoplastic elastomer overmolded structure.

The use of thermoplastic materials allows for ease of manufacture, as they can be melted and formed without the need to ensure adequate cure. Further, the ability of the preform to melt at the PA/TPE interface due to the molten TPE overmold may allow for enhanced intermingling of the polymer chains, improving adhesion.

The TPE surround serves to limit water uptake in the hygroscopic PA, limiting changes in part properties caused by water uptake. TPE also provides a tactile surface that may be desirable for some consumer applications, such as prosthetics or sports equipment handles. Finally, the previous chapter illustrated the benefit of a more ductile surface material for impact applications since the ductile material can dissipate contact energy without damaging the more brittle material. In this capacity, the TPE overmold can prove beneficial for impact and crash performance. The PA/CF preform, on the other hand, provides material stiffness and strength to the part. PA is a relatively ductile polymer, which somewhat reduces the property mismatch at the interface and improves compatibility.

This case study examines the effect of two different changes to part production. The first is to change the temperature of the PA/CF preform just before overmolding, which will in turn effect the interfacial temperature between the PA and the TPE during overmolding. A higher interfacial temperature can improve the polymer chain mobility in the PA, allowing for improved trans-interface interaction and adhesion. The second change to the process is a change to the PA6/CF preform volume, introduced via an increase in PA6/CF tow thickness, to examine the effect of the tow reinforcement on overall performance. The increased tow volume does not increase processing time, which makes it a practical way to alter part properties.

Preform temperature was found to have a negligible influence on bond strength for the manufacturing setup presented. Overmolded beams were also tested in 3-point bending, where the

primary failure mechanisms were preform buckling and tensile failure. Finally, a technical cost model was developed for the process to examine the effect of changes to the manufacturing process on part cost. Increasing the preform volume improved bending performance by over 30% with an accompanying increase in cost of only 3.8% per part, making tow volume increase an efficient and effective method to improve part performance.

## **5.1 Introduction**

Composite materials are widely used in applications that require high strength and stiffness at low weight. However, conventional carbon fiber-reinforced epoxy has shown limited impact performance and tends to fail in a more brittle manner. Traditional continuous fiber composites are time-intensive to produce, meaning that their use is limited to applications with low yearly production volume. Therefore, there is great interest in improving both the impact behavior and the processability of such composites without sacrificing their desirable mechanical properties.

For applications that require significant deformation before failure or soft-touch surfaces, the combination of a thermoplastic with an elastomer can offer substantial benefits. The thermoplastic, which may be part of a fiber-reinforced composite, provides stiffness and strength to the structure, while the elastomer acts as a toughening agent by absorbing energy through elastic deformation. Thermoplastic elastomers (TPEs) are a subset of elastomers that can be melted, which allows for ease of processing and achievable routes for recycling.

Hybrid injection overmolding is an efficient method of combining TPEs with conventional thermoplastics, as it allows for the production of complex parts with short manufacturing cycle times. The process involves forming the thermoplastic to the desired shape, either through injection molding or a separate process, followed by injection molding of the TPE onto the solid thermoplastic substrate. The three stages of the hybrid overmolding process, outlined by Weng et al [1], and further explored by Smith et al [2] are as follows:

- Wetting of the substrate with the melt
- Interaction between substrate and melt polymer chains, which may include chain diffusion or chemical bonding
- Solidification, which may also include crystallization of one of both components

Strong interfaces, which are important for load transfer between phases, can be formed during hybrid overmolding by exploiting phenomena involved in the overmolding stages listed above. For example, the selection of a high surface energy substrate with a low surface energy melt can improve the wetting of the melt onto the substrate[1]. Interaction between the polymer chains can be improved in a variety of ways, including: improving chain interdiffusion by selecting miscible polymers[2]–[6]; increasing chain mobility by increasing the interfacial temperature during overmolding, thereby improving chain interdiffusion[7]–[9]; and using materials that can form covalent bonds across the interface[10], [11]. Finally, crystallization can be exploited such that, under the right processing conditions, crystallization can occur across the interface, strengthening the bond[12], [13].

Polyamide (PA) is a widely-used thermoplastic due to favorable cost and processability. As a polar molecule, it is not compatible with most unmodified TPEs. Therefore, TPEs typically need to be modified with a reactive compatibilizer, commonly maleic anhydride (MAH) or glycidyl methacrylate (GMA), to be compatible with PA. Such compatibilizers are grafted onto the TPE chains, where their functional groups can interact with and bond to the amide groups in the PA. PA has been successfully blended with reactive TPE to create toughened blends[14]–[19]. Even a small amount of reactive compatibilizer is sufficient to create super-toughened blends[16]. Compatibilized TPE can effectively toughen both fiber-reinforced and neat PA, primarily via the typical hybrid polymer failure modes of TPE particle cavitation and PA shear yielding[17]–[20]. In applications where compatibilized TPEs were overmolded onto PA, adhesion was shown to depend strongly on the interfacial temperature during the overmolding process[21], [22]. Pompe et al found that, as long as the interfacial temperature was sufficient to allow polymer chain interaction, a greater temperature gradient across the interface yielded stronger adhesion between the PA and TPE phases.

The strength of overmolded parts can be increased via hybrid injection molding, wherein the TPE is molded onto a continuous fiber reinforced PA. This continuous fiber preform allows for selective reinforcement only where it is required for favorable load introduction and load distribution, with the overmolded TPE providing design stiffness and enhanced energy dissipation. Early research on hybrid injection molded structures has shown that a continuous fiber preform can greatly improve a part's failure loads[23]–[27]. Further, the overmolding material can facilitate energy transfer and prevent premature part failure due to matrix failure in the preform[28].

Early work on PA/TPE overmolding has focused on methods to improve adhesion between the two phases in a simple planar geometry. This work examines the effect of overmolding processing conditions on the bond strength between TPE and a continuous fiber 3D preform geometry, as well as the crash performance of parts made from this hybrid material. This study also includes a technical cost model to assess the manufacturing viability of the process and determine the effect of changes to the manufacturing process on part cost.

## **5.1 Experimental Methods**

### **5.1.1 Materials**

This study uses an L-bracket sample geometry consisting of a continuous fiber PA6/CF structural preform overmolded with a TPE and designed with an additional rib structure. The continuous fiber PA6/CF preform is produced from a 25.4mm-wide prepreg tape provided by DSM, with a matrix melt temperature of 220°C. The TPE is a SEBS-based preform (Dryflex A1 600902, provided by Hexpol TPE AB) that has been modified for improved adhesion to PA. The TPE thermal transition temperature was measured to be approximately 155°C, with a recommended processing range of 180-250°C.

### **5.1.2 Sample Preparation**

Preforms were manufactured using an EELCEE QEE-TECH<sup>®</sup> cell (QTC). In this process, the PA6/CF tape passes through an infrared (IR) oven, then through a heated head that has three axes of motion in addition to the 3-axes provided by the lay-up table. The molten tow is then wrapped around a custom jig on the lay-up table. Aluminum bushings hold the tow in place during this process and serve as load introduction points in the finished parts. Finished preforms are then transferred to an injection molding machine (Krauss-Maffei, CX 300-2000), either manually or using a transfer robot. The process is illustrated in Figure 5.1.

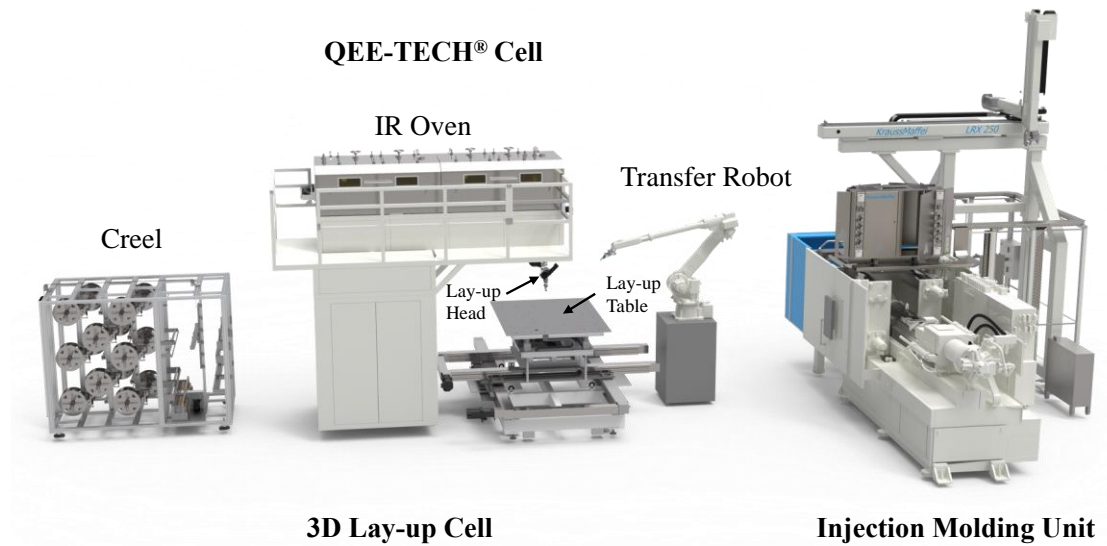


Figure 5.1. Schematic of hybrid overmolding process.

Preform tow thickness can be easily varied by adjusting the number of prepreg tapes that are fed through the IR oven and automated head. For this work, preforms were made using either one or three prepreg tapes at a time, which led to different preform tow diameters. The tow geometry used in this work is shown in Figure 5.2.

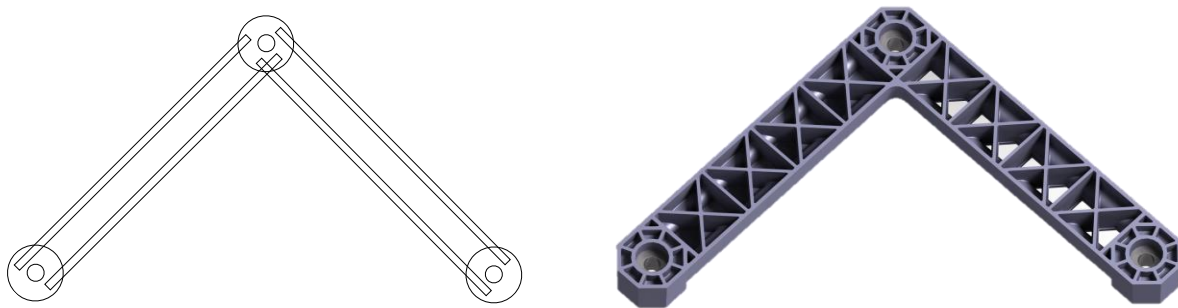


Figure 5.2. Tow (left) and overmolded part (right) geometry used in this study.

Before injection overmolding, preforms are either allowed to cool to 22°C or heated to either 80°C or 180°C to determine what effect preform temperature has on interfacial adhesion and part performance for this geometry and manufacturing process. A summary of samples and the nomenclature used in this paper are shown in Table 5.1. All other molding parameters were kept constant, as summarized in Table 5.2, and were selected to ensure complete mold fill without flash.

Table 5.1. Summary of samples.

|                | <b>Cross Sectional<br/>Area (mm<sup>2</sup>)</b> | <b>Preform Temperature</b> |              |               |
|----------------|--|----------------------------|--------------|---------------|
|                |  | <b>22 °C</b>               | <b>80 °C</b> | <b>180 °C</b> |
| 1-tape preform | 36   | 1T/22                      | 1T/80        | 1T/180        |
| 3-tape preform | 122  | 3T/22                      | 3T/80        | 3T/180        |

Table 5.2. Summary of injection molding parameters.

| <b>Parameter</b>           | <b>Value</b> | <b>Unit</b> |
|----------------------------|--------------|-------------|
| Injection Melt Temperature | 240          | °C          |
| Mold Temperature           | 60           | °C          |
| Injection Pressure         | 50           | MPa         |
| Hold Pressure              | 30           | MPa         |
| Cooling Time               | 85           | s           |

### 5.1.3 Mechanical Performance: Pull-Out Testing

A modified version of ASTM D7913[23] was used for the pull-out testing. Pull-out samples were made from 1-tape tow parts only, to ensure that the tow was fully encased with TPE. Four pull-out samples were made from each part, one from each straight tow section of the two L-bracket arms. The pull-out sample geometry is shown in Figure 5.3(a). Samples were potted in an epoxy resin to minimize vertical compression of the TPE overmold.

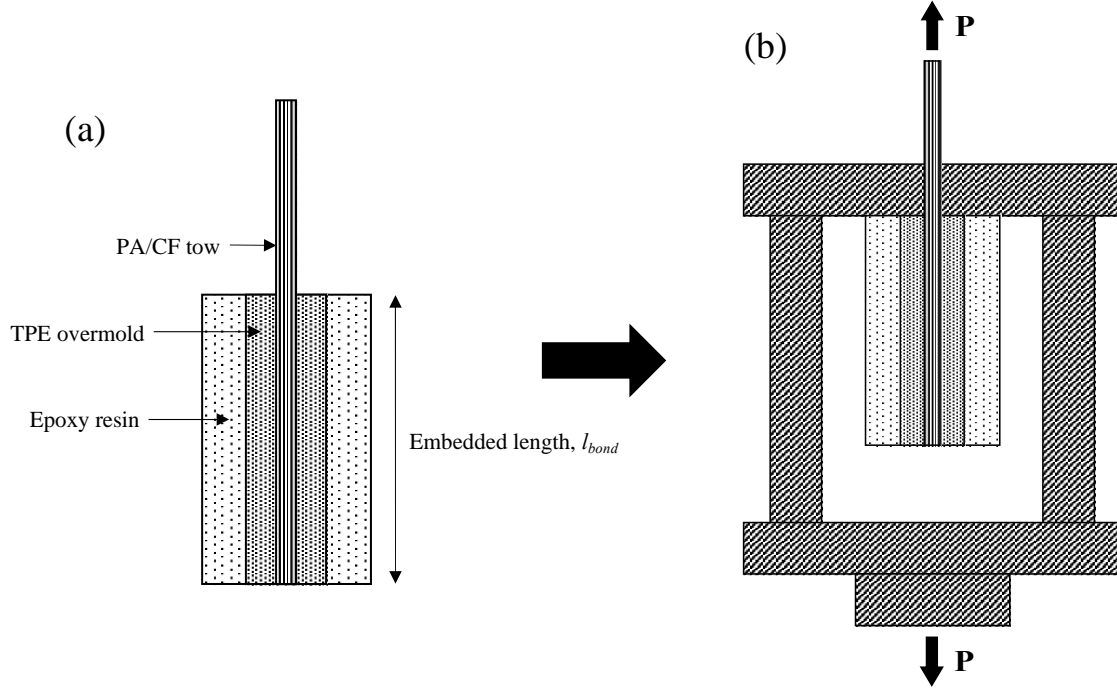


Figure 5.3. Pull-out testing sample (a) and fixture (b).

The exposed tow was passed through a hole in the top of the fixture shown in Figure 5.3(b) and held in the upper hydraulic grips of a load frame. The epoxy-covered region of the pull-out samples rested against the underside of the top plate of the fixture during testing.

A constant tensile displacement rate of 1mm/min was applied, and the force and tow displacement were measured by the load frame. The interfacial shear strength (IFSS) was calculated using equation [5.1], where  $F_{debond}$  is the debonding force, which in this study corresponded to the peak force on the load-displacement curve, and  $A$  is the interfacial area between the tow and the overmold.

$$IFSS = \frac{F_{debond}}{A} \quad [5.1]$$

The 1-tape tow cross section was approximated as an ellipse using Ramanujan's formula, equations [5.2] and [5.3], where  $a$  and  $b$  are the major and minor axes, respectively[24]. The interfacial area between the tow and the overmold is calculated by multiplying the estimated ellipse perimeter by the embedded length of the tow,  $l_{bond}$ .  $l_{bond}$  was nominally 55mm but was measured for each sample to ensure accurate area calculation. Major and minor tow axes were also measured in multiple locations for each sample.



$$h = \frac{(a - b)^2}{(a + b)^2} \quad [5.2]$$

$$p \approx \pi(a + b) \left( 1 + \frac{3h}{10 + \sqrt{4 - 3h}} \right) \quad [5.3]$$

$$A \approx pl_{bond} \quad [5.4]$$

This calculation does not account for surface roughness of the tow, which will likely serve to further increase the interfacial bond by increasing the surface area available for interaction with the TPE overmold.

#### 5.1.4 Mechanical Performance: 3-Point Bending

One L-bracket arm was cut off to create a simplified beam for 3-point bending testing [25], as shown in Figure 5.4. The beam was simply supported by a pin placed through the aluminum bushing on either end, while a steel bar was used to apply force at the center of the beam. The two fixation points had a free lay-up allowing horizontal movement during the bending. Vertical pins extending from the center steel bar along the front and back of the sample prevented beam rotation out of plane.

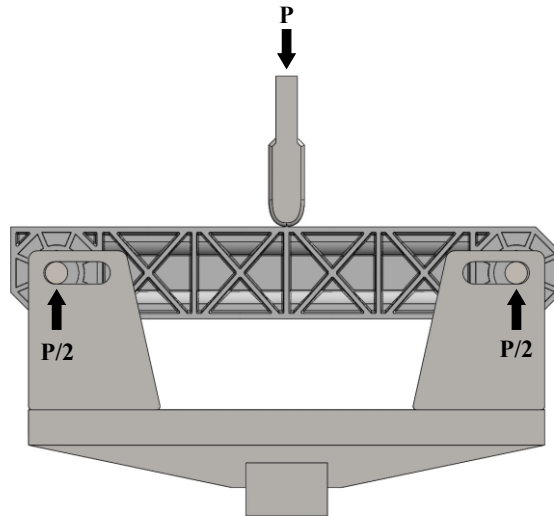


Figure 5.4. 3-point bend fixture with single L-bracket arm.

Beams were loaded at a constant displacement rate of 2mm/min, while the applied load and displacement were measured by the hydraulic load frame. The TPE overmold protected the samples from ultimate failure, so testing was stopped when the center of the sample reached the bottom of the fixture, representing a vertical displacement of around 60mm.

Peak force and total energy absorbed are considered as metrics to compare the quasi-static bending performance of the parts.

### **5.1.5 TPE Characterization**

Because the TPE was expected to have unusual characteristics relative to more traditional thermoplastics, initial characterization was used to define some initial processing parameters, in order to establish a suitable processing window for a hybrid molding process of the PA/CF and the TPE. Differential scanning calorimetry (DSC) was used to determine the melt range, thermogravimetric analysis (TGA) was used to determine the thermal degradation rate, and parallel plate rheometry was used to characterize the viscoelastic response to both temperature and shear rate.

#### ***Differential Scanning Calorimetry (DSC)***

A small sample of the TPE was heated from -40 °C to 230 °C at a constant ramp rate of 5 °C/min, and the melt onset and peak temperatures were determined from the resulting heat flow curve. The test was repeated at a range of ramp rates and the melting ranges remained consistent.

The glass transition temperature ( $T_g$ ) for the TPE is well below room temperature, giving TPE its rubbery qualities under most operating conditions. Therefore,  $T_g$  is not expected to factor in to manufacturing considerations, since all manufacturing will take place at or above room temperature.

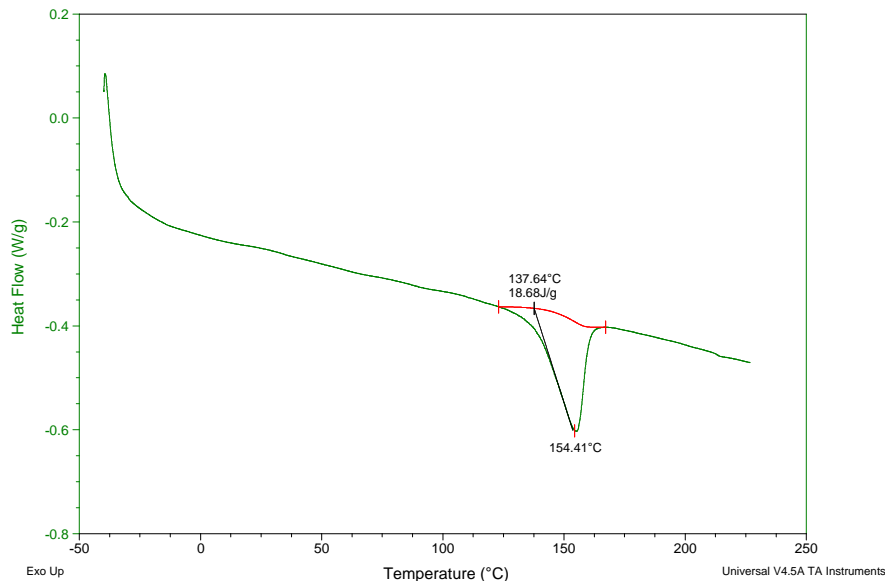


Figure 5.5. DSC heating curve for a TPE sample heated at a constant rate, with the melt onset and peak temperatures indicated.

As shown in Figure 5.5, the TPE begins to melt around 130 °C, with peak melting occurring around 155 °C. The material is fully melted above 165 °C. These results indicate that the minimum processing temperature should be around 185 °C to ensure that all of the TPE is sufficiently melted, which agrees well with the manufacturer-minimum processing temperature of 180 °C.

### ***Thermogravimetric Analysis (TGA)***

An isothermal TGA test was used to determine the rate and extent of any potential degradation the TPE could experience during a typical manufacturing cycle. This TPE will be used processed using injection molding, which is, by design, not an isothermal process. In order to keep the polymer from degrading, the barrel temperature is kept coolest farther away from the injection point, only reaching the target molding temperature shortly before the mold entry. Therefore, 220°C was chosen as the hold temperature for TGA because it is near the middle of the manufacturer-recommended processing range and represents an average temperature that the TPE will be subjected to during the molding cycle.

The TPE used here is not hygroscopic, so it is expected that none of the mass loss can be attributed to evaporation of water from the material and that the mass loss is due entirely to material degradation.

Initially, two different TPE grades were investigated, denoted “TPE A” (“TPE\_SEBS\_902\_220C”) and “TPE B” (“TPE\_220C”). Following the TGA analysis and considering the process used in this study, TPE A was selected for use due to its higher thermal stability.

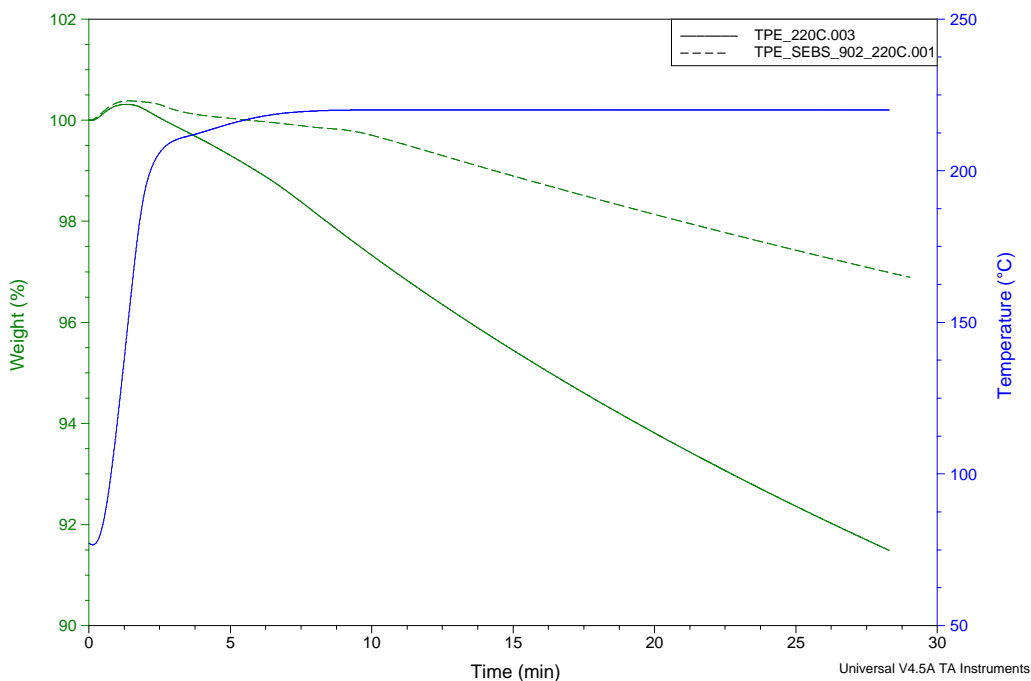


Figure 5.6. TGA curves for two different TPE formulations, TPE A (dashed green line, used in overmolding trials) and TPE B (solid green line).

TPE A loses approximately 2.5% of its mass in 25 minutes, while TPE B loses 8% of its mass in the same duration.

For the time scale used in injection molding, the mass loss at 220 °C is negligible, which suggests that TPE A is well-suited to be used for our Hybrid Injection Molded applications. At higher temperatures, such as those used at the end of the barrel during injection molding, degradation will be faster, but the TPE’s residence time is only one minute or less at our selected processing conditions.

### ***Parallel Plate Rheometry***

Parallel plate rheometry was conducted at a range of temperatures and angular frequencies to determine the effect of temperature and shear rate on the TPE melt viscosity. First, the material was tested at a constant frequency of 1Hz with a 1% strain during a temperature ramp where the temperature was increased from 50 °C to 260 °C at a constant rate of 5 °C/min.

As seen in Figure 5.7, the viscosity steadily decreased as temperature increased, with a sudden drop in viscosity between 210°C and 220°C. Above 220°C, the viscosity no longer decreases with increasing temperature, and instead remains constant. Notably, there is no sudden decrease in viscosity at or near the melting temperature of 150 °C, as found using DSC. Therefore, despite the relatively low melting temperature, the processability of the TPE improves only slightly at the melting temperature.

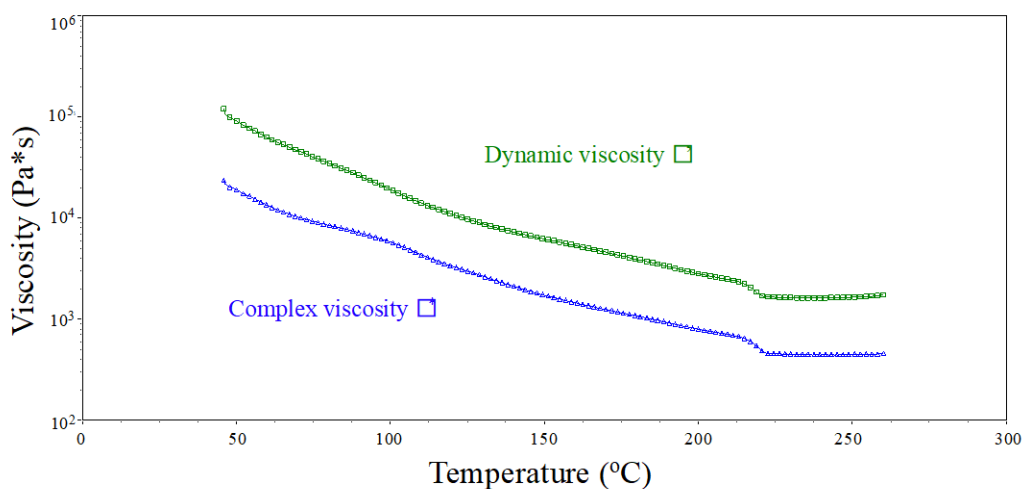


Figure 5.7. Dynamic and complex viscosity of a TPE measured at a constant frequency of 1Hz and a strain of 1% under a temperature ramp from 50 °C to 260 °C at a ramp rate of 5 °C /min.

This material will flow most easily above 220°C, with little to no further viscosity decrease with increased temperature. improvement from increasing the temperature further. In fact, increasing the temperature above 220 °C may increase the rate of degradation.

Rheological characterization of the TPE was also conducted at a range of angular velocities to determine the effect of shear rate on the viscosity. Each of these tests was performed

isothermally, at 10°C increments between 120°C and 260°C. Figure 5.8 shows the complex and dynamic viscosities for tests performed from 120°C to 210°C.

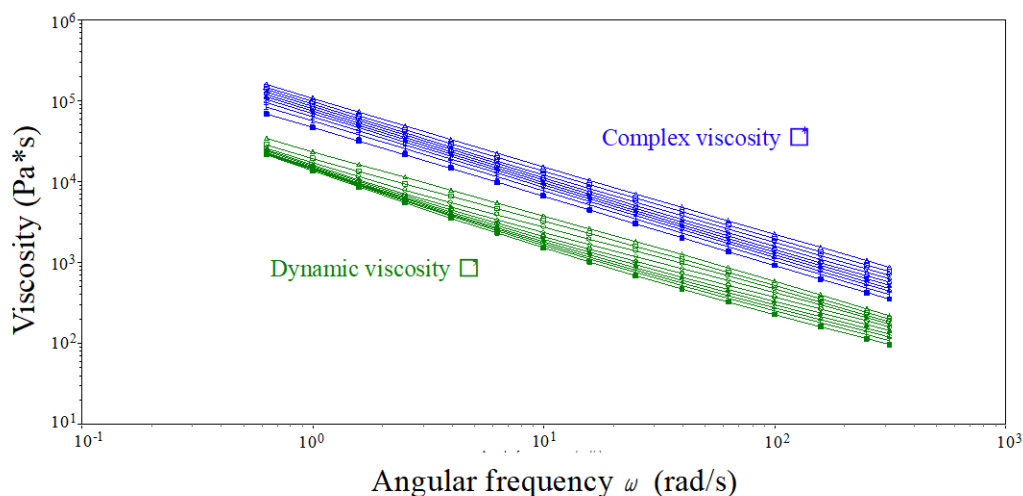


Figure 5.8. Dynamic and complex viscosity of a TPE measured at a range of angular frequencies. Each test was conducted isothermally at 10°C increments, with temperatures ranging from 120°C (top line) to 210°C (bottom line).

As demonstrated by Figure 5.7, increasing the temperature decreases the viscosity across all angular velocities, with the greatest effect of temperature arising at higher angular velocities. Comparatively, though, the angular velocity has a much higher effect on the viscosity than the temperature does. This effect is even greater at temperatures above 220°C, as illustrated in Figure 5.9.

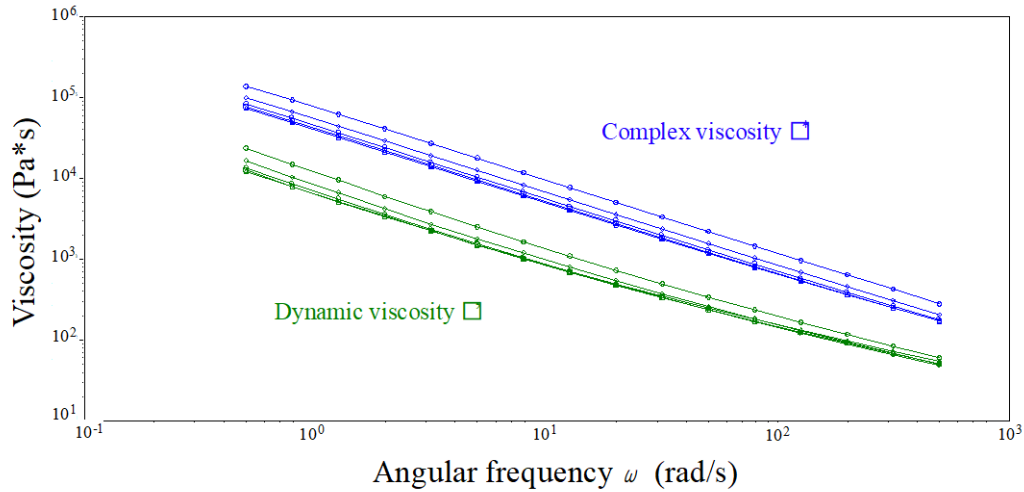


Figure 5.9. Dynamic and complex viscosity of a TPE measured at a range of angular frequencies. Each test was conducted isothermally at 10°C increments, with temperatures ranging from 220°C (top line) to 260°C (bottom line).

As shown in Figure 5.7, there is a steep drop in viscosity between 210°C and 220°C, after which there appears to be little effect of temperature on the viscosity. This trend appears to hold across all angular velocities tested, with the dynamic viscosity curves for the 230°C to 260°C collapsing to a single line at higher angular velocities.

Here, the effect of shear rate is even more apparent than at lower temperatures.

### 5.1.6 Characterization Summary

Based on the results of these material characterizations, a processing temperature suited for our Hybrid Injection Molding process, mold geometry, and overmolding consolidation was selected. Therefore, a melt temperature of 220°C was selected, which also could accommodate the residence time during the melt plasticization. Furthermore, a high shear rate would provide ease of mold filling.

## 5.2 Results

### 5.2.1 Tow Pull-Out Testing

A representative force-displacement curve for the tow pull-out testing is shown in Figure 5.10. The nonlinearity in the loading portion of the curve can be attributed to shear strain in the

TPE surrounding the tow. The initial decrease in load after the peak corresponds to debonding along the length of the tow, and the subsequent drop in load indicates total debonding. The residual force after this drop is due to sliding friction between the tow and the overmolded TPE.

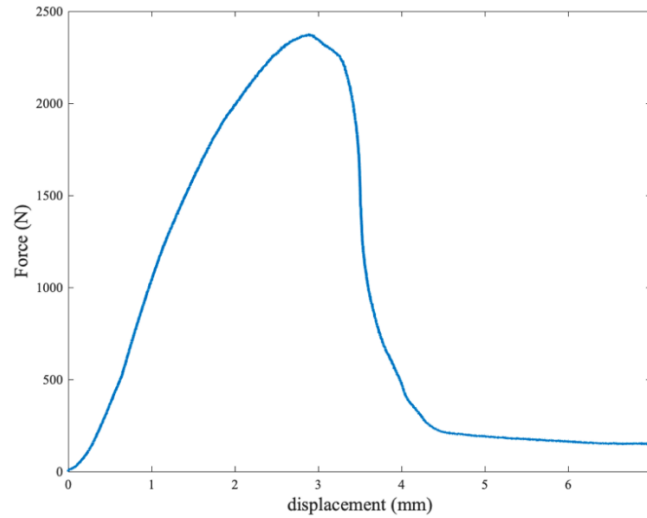


Figure 5.10. Representative force-displacement curve obtained during tow pull-out testing.

Interfacial shear strength (IFSS), as calculated using equation [5.1], is shown in Figure 5.11 for each of the three preform temperatures. There is no statistically significant difference in IFSS with varied preform temperature.

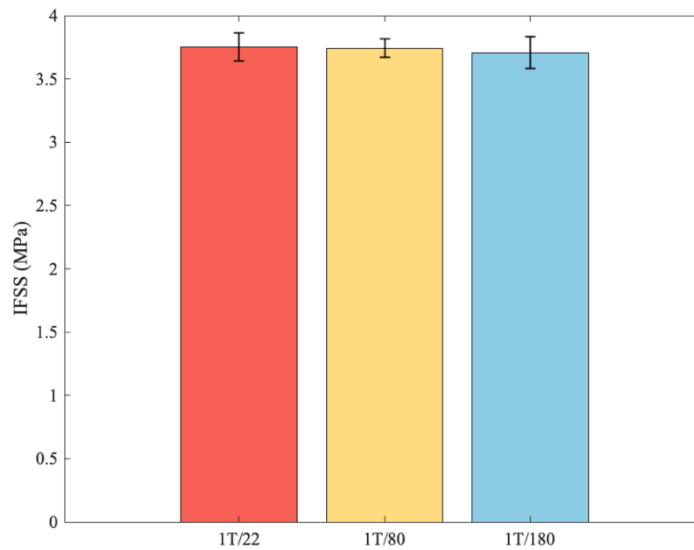


Figure 5.11. Interfacial shear strength of PA/CF tows overmolded with TPE. Tows heated to either 22°C, 80°C, or 180°C before overmolding.



The embedded lengths of PA6/CF tows were sufficiently short so that the pull-out samples failed in shear between the tow and the overmolded TPE, rather than by tow fracture or failure.

In this system, the large surface area and the comparatively small volume both contribute to the rapid cooling of the tow, especially in the 1-tape tow samples. During the manual transfer from the preheating oven to the injection molding machine, the tow surface cools significantly, and the preheat temperature is therefore not indicative of the preform temperature at the time the overmolding material contacts the preform. The cooling of the tow during transfer from the oven to the injection molded machine can be estimated by a heat transfer simulation as shown in equation [5.5].  $T$  is the temperature of the preform as it is placed in the injection molding machine,  $T_\infty$  is the ambient temperature,  $T_i$  is the oven temperature,  $h$  is the convection heat transfer coefficient, which is approximately 10W/m<sup>2</sup>K for air,  $A_s$  is the tow surface area,  $\rho$  is the tow surface area,  $V$  is the tow volume,  $c$  is the tow specific heat, and  $t$  is the transfer time, approximately 20s.

$$\frac{T - T_\infty}{T_i - T_\infty} = \exp\left(-\left(\frac{hA_s}{\rho V c}\right) t\right) \quad [5.5]$$

The heat capacity of the PA/CF tow can be approximated from PA6 and CF properties using a simple rule of mixtures, shown in equation [5.6], where the heat capacities of the two materials are multiplied by their mass fractions and added together.

$$c_p^{mix} = \left(\frac{m_{PA}}{m_{mixture}}\right) c_p^{PA} + \left(\frac{m_{CF}}{m_{mixture}}\right) c_p^{CF} \quad [5.6]$$

If the tow surface is approximated as a smooth ellipse, the linear region of a 1-tape tow should only cool from 180°C to 161°C during the 20s transfer from the oven to the injection molding machine. However, measurements showed the surface temperature to cool to approximately 130°C during that time, which would suggest that the true surface area is approximately 3 times greater than the elliptical approximation. This could be explained by the actual topography of the tow. If this is the case, the IFSS should decrease 3-fold, resulting in a mean IFSS of 1.2MPa. This compares favorably with a similar study [26] in which the IFSS obtained via Pull-Out testing of a smooth tow from an injection overmolded part was found to be between 1.04 and 1.31MPa.

It should be mentioned that the preform surface temperature could be increased via the introduction of additional equipment such as an in-line heater to reduce the time between preheating and overmolding, but was not performed in this study.

Previous work done in our laboratory shows a 12% increase in bond strength between TPE and PA6 when the processing temperature is increased from 177°C to 197°C in a compression molding process, even though both temperatures are well below the PA6 melt temperature of 220°C. Therefore, it stands to reason that, if the manufacturing process could be modified to eliminate transfer time from the oven to the injection molding machine, the bond strength could be increased further.

### **5.2.2 3-Point Bending**

All samples had several common characteristics during 3-point bending, with load-displacement curves shown in Figure 5.12. All beams had a nonlinear initial load curve due to small-scale deformation of the TPE overmold. The first deviation from the smooth load curve was a sharp drop in load corresponding to the buckling of the upper tow under its compressive load [27]. The samples then continued to support the applied load in the overmolding material and the intact lower tow, with a final increase in load above 40mm displacement reflecting an increase in beam stiffness due to the compaction of the TPE ribs.

Several of the 3T/22 and 3T/80 samples exhibited a second, larger load drop above 40mm displacement that can be attributed to the tensile failure of the lower tow. None of the 3T/180 samples experienced this failure mode. The 1-tow samples also did not experience this failure mode, apparently because the smaller tows were less stiff and could therefore withstand the large deformations experienced toward the end of the bending test.

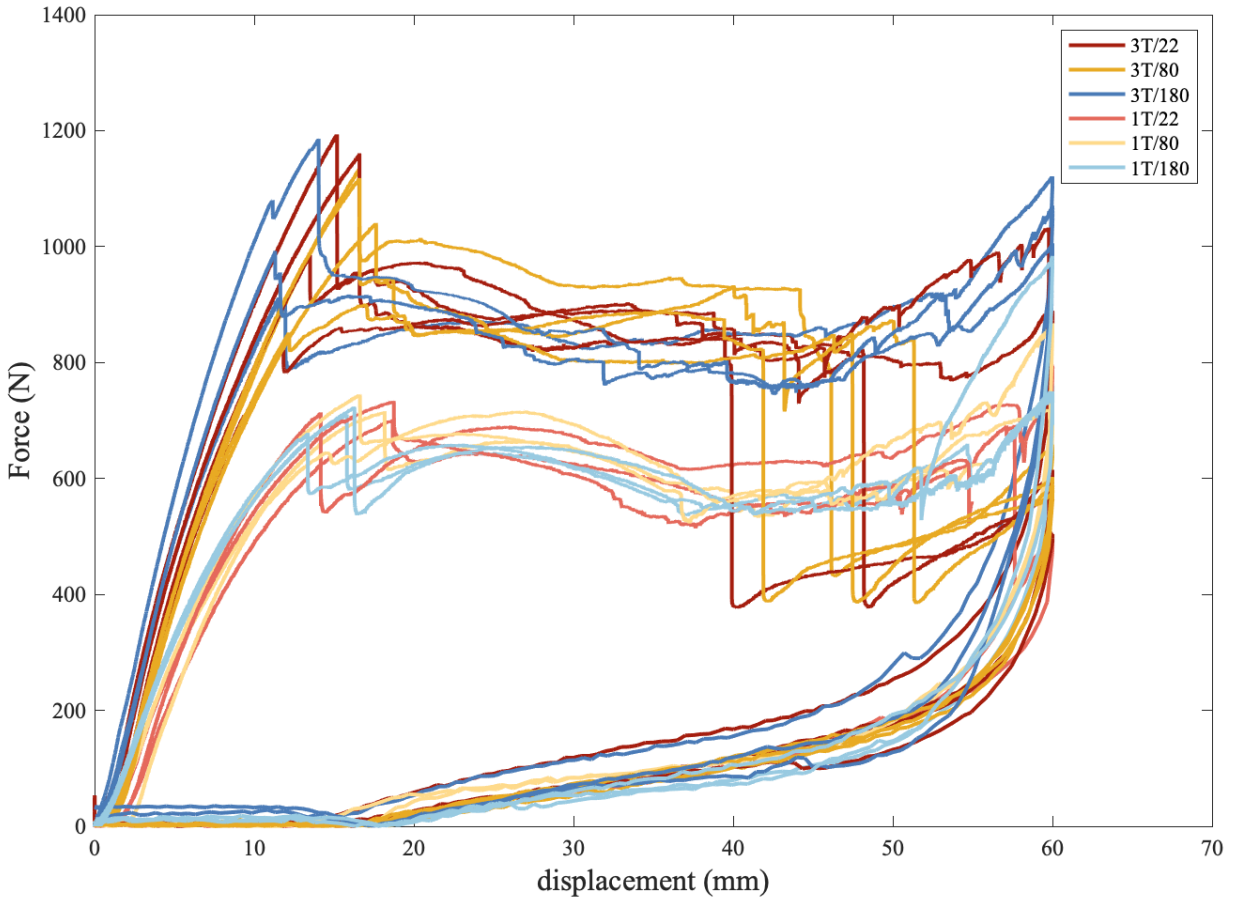


Figure 5.12. Force vs. displacement curves for beams tested in 3-point bending.

The average initial force reached during loading, corresponding to the load reached immediately before initial tow failure, is shown in Figure 5.13 for each tow volume and preform temperature. There is an average 42% increase in peak load with the increase in tow volume from one to three tape tows (1T to 3T).

There is no statistically significant difference in bending performance between the three different tow temperatures for either tow volume. This aligns with the pull-out results that found no difference in bond strength at the three preform temperatures. It further suggests that there is no noticeable difference in tow tensile or compressive behavior due to differences in the preform heating stage, for example due to different morphologies at the interfacial region.

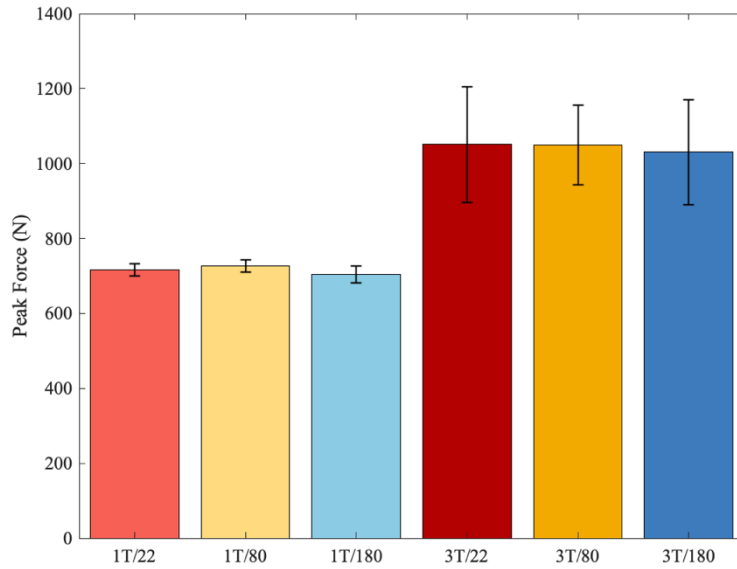


Figure 5.13. Peak force during bending testing for 1-tape and 3-tape preforms at 22°C, 80°C, and 180°C before overmolding. Shown with standard deviation.

Energy absorbed during bending was also used to evaluate the beams' performance and is shown in Figure 5.14. As with peak force, there is no statistically significant difference between samples with the same tow volume and different preform temperatures. There is an average 32% increase in absorbed energy with increased tow volume. The slightly higher absorbed energy for the 3T/180 samples can be attributed to the fact that these samples did not experience the second load drop corresponding to the tensile failure of the lower tow as observed for the 3T/22 and 3T/80 samples. It is possible that if the bend test was able to continue, the difference in absorbed energy between the 3T/180 samples and the other 3-tape samples would be more pronounced.

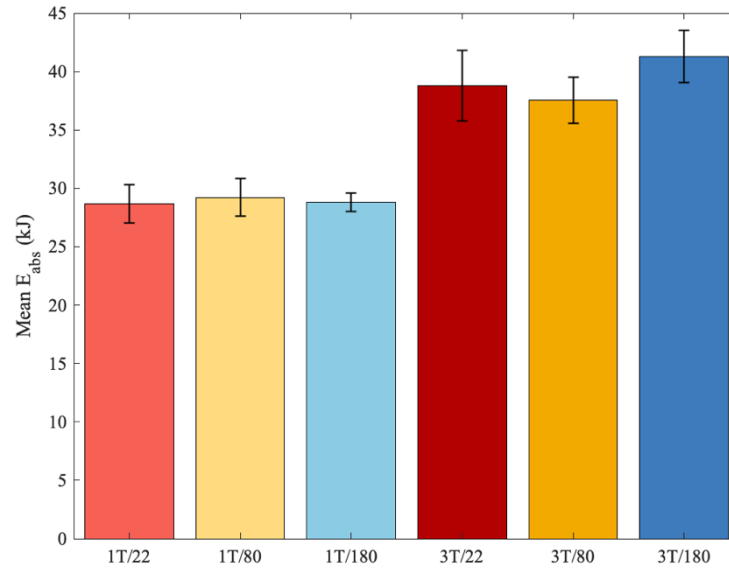


Figure 5.14. Energy absorbed during bending testing for 1-tape and 3-tape preforms at 22°C, 80°C, and 180°C before overmolding. Shown with standard deviation.

With the increase from 1-tape to 3-tape tows, the tow volume triples, but the bending performance only increases by 32-42%. This suggests that the overmolded TPE is responsible for a significant portion of the energy dissipation during bending, confirming that both materials play an important role in part performance.

### 5.3 Predictive Technical Cost Model

Finally, a predictive technical cost model was applied to the part production process to determine its feasibility and the effect of changes to the process on part cost. The cost model was applied to production of the full L-bracket shown in Figure 5.2, and a schematic of the process is shown in Figure 5.15. For the case modeled here, part transfers to the injection molding, trimming, and quality control steps are all performed by a single robot, while an operator controls the preform and injection molding machines. Some of the relevant parameters used in the cost model are outlined in Table 5.3.

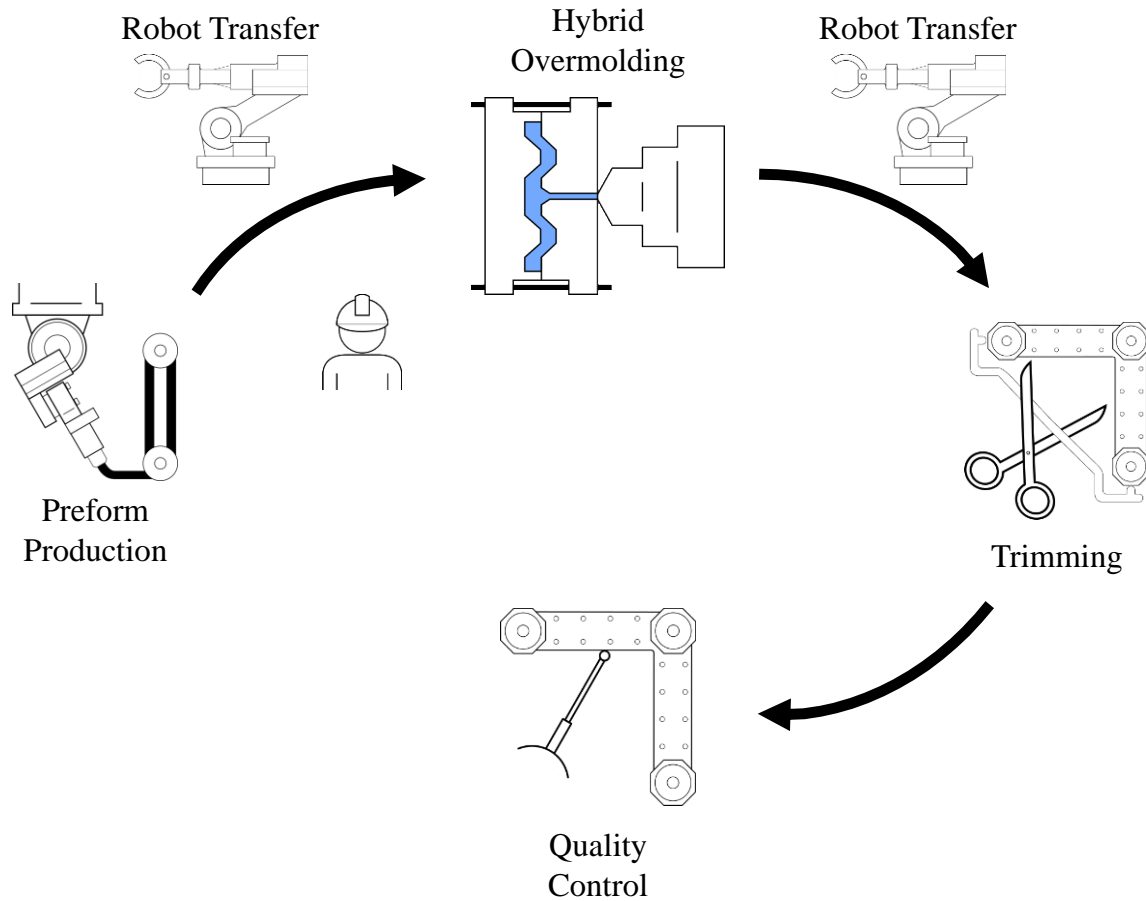


Figure 5.15. Schematic of processing line used to develop cost model.

Table 5.3. Selected cost modeling parameters.

| Parameter                   | Value     | Unit                     |
|-----------------------------|-----------|--------------------------|
| Target production volume    | 120,000   | Parts/year               |
| Equipment cost              | 1,100,000 | \$                       |
| Tooling cost                | 100,000   | \$                       |
| QC cost                     | 215,000   | \$                       |
| Equipment depreciation time | 10        | years                    |
| Project duration            | 5         | years                    |
| Direct labor cost           | 30        | \$/hour                  |
| Working hours               | 5700      | hours/year               |
| PA6/CF tow cost             | 11.50     | \$/kg                    |
| Aluminum bushing cost       | 10.30     | \$/kg                    |
| TPE overmold cost           | 4.40      | \$/kg                    |
| Plant operating cost        | 22.00     | \$/ft <sup>2</sup> /year |
| Energy cost                 | 0.070     | \$/kW                    |
| Water cost                  | 23.00     | \$/ft <sup>3</sup>       |
| Sewage cost                 | 25.00     | \$/ft <sup>3</sup>       |

The effect of annual production volume on part cost is shown in Figure 5.16 for both 1-tape tow and 3-tape tow preforms. Part cost initially falls rapidly as production volume increases due to increase equipment utilization allowing capital costs to be further distributed. Jumps in part cost indicate required capital investments to reach the increased production volume, as one machine becomes insufficient. The injection molding step is the process bottleneck as it has the longest cycle time, making it the first machine that needs to be supplemented to continue to reach production volumes.

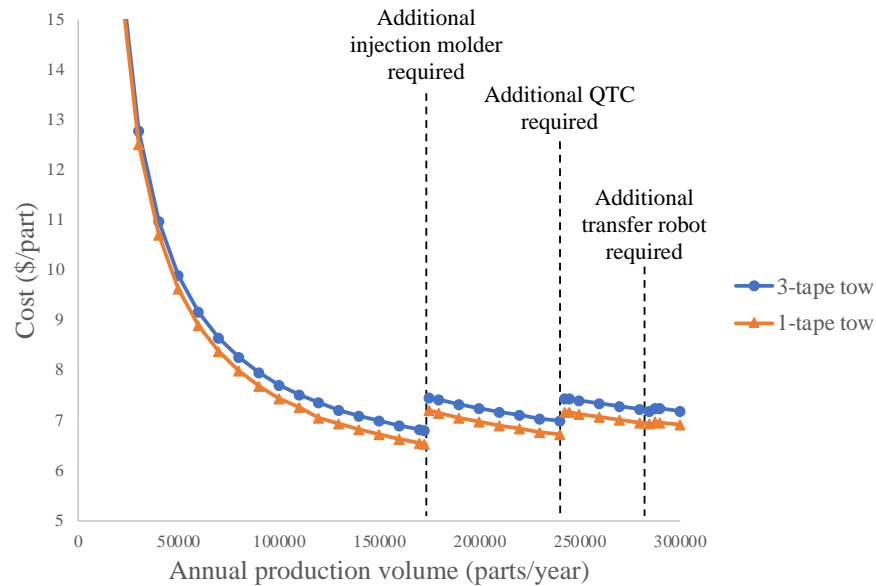


Figure 5.16. Effect of annual production volume on part cost for 3-tape and 1-tape tows. Jumps in cost indicate required capital investment to reach target volumes.

The cost per part is broken down in Figure 5.17 for a 120,000 parts/year target production volume. The material costs, shown in blue, and capital expenses represent the majority of the costs. The TPE overmolding material in turn accounts for the bulk of material costs, largely due to the large volume of TPE required to form the rib structure of the overmolded part. The most significant cost difference between 1-tape and 3-tape parts is, predictably, the increase in preform cost required to produce the 3-tape tows, although there is also a slight decrease in the cost of the overmolding material required in 3-tape parts due to the increased tow volume.

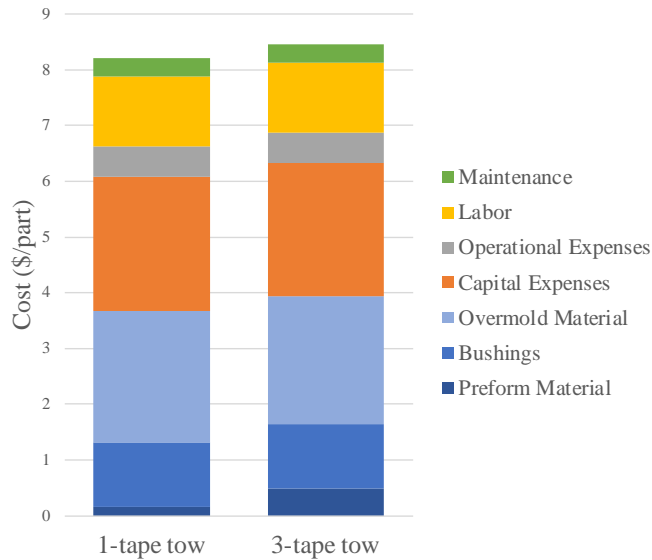


Figure 5.17. Cost breakdown per part for 1-tape and 3-tape tow parts, 120,000 parts/year production volume.

This model was used to determine the effect of increasing the tow volume threefold on the overall cost of the part. Because a larger tow can be produced using the same cycle time as the thinner tow, the only changes between the two cases are increased material cost for the tow and decreased material cost for the overmolding material. This change results in a net 3.8% increase in part cost with the change to the larger tow. This slight increase in cost provides a greater than 30% improvement in high-deformation performance (e.g. crash), as measured by a part's ability to continue to absorb applied bending force after initial fracture.

The addition of a preform heating or cooling step to the process has a negligible effect on the cost per part. Though heating or cooling the preform before overmolding will increase the cycle time, the preheating stage has a shorter cycle time than the injection molding stage, which is the current process bottleneck, so the addition of a preheating step does not affect the maximum production volume for the process. Further, the cost of the part is dominated by the material costs and the capital expenses of the preforming and injection molding equipment.

## 5.4 Chapter Conclusions

The benefit of the TPE overmold on crash performance is illustrated in Figure 5.18, where a representative force-displacement curve for a 3-tape tow overmolded with TPE is compared to a



3-tape tow overmolded with neat PA resin and a part made from only TPE, with no tow. Though the PA-overmolded sample is much stiffer and able to reach higher load before failure, failure is sudden and caused by overmold delamination from the tow and subsequent overmold fracture. In contrast, the TPE-overmolded sample is able to continue to support applied load long after the initial tow failure. Because the TPE did not fracture under the loads applied in this study, energy could be transferred through the part for the duration of the test. The two 3-tape tow samples shown in Figure 5.18 have similar absorbed energies during the bending test, and the TPE-overmolded sample would have been able to absorb even more energy if deformation had not been limited by the test fixture.

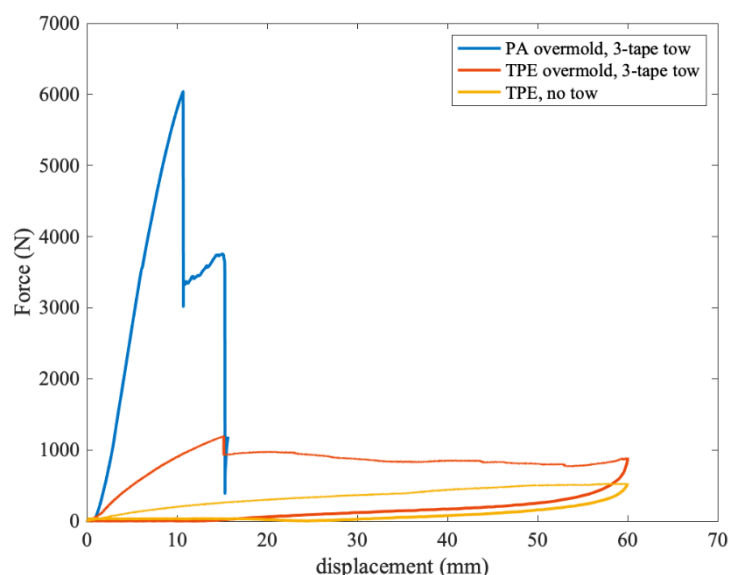


Figure 5.18. Load-displacement curves for 3-tape tow overmolded with PA6, 3-tape tow overmolded with TPE, and TPE with no tow reinforcement.

The interfacial bond between the modified TPE and the PA-reinforced tow is sufficiently strong that bending samples failed via fiber fracture, not debonding between the TPE and the PA. This was true across all manufacturing conditions tested here. Further, bond strength appeared to be insensitive to manufacturing conditions in the realistic test case presented in this study, meaning that additional processing steps such as preheating a preform are not necessary and will not improve performance.

There is no difference in performance for the preform temperatures tested here. While other studies have proven that a higher interfacial temperature can improve adhesion between the

preform and the overmolding material, for the real-world manufacturing process and part geometry used here, the preform temperature could not be heated sufficiently to meaningfully increase the interfacial temperature. Though interfacial molecular entanglements may be limited due to the low interfacial temperature during molding, strong bonding between the tow and the TPE is still achieved, as the tow surface roughness offers a large surface area and opportunities for mechanical interlocking with the TPE overmold.

The increase from 1 tape to 3 tapes in the tow used for the preform results in a 30% increase in absorbed energy during the bending process and comes with only a 3.8% increase in part cost. This makes an increase in tow volume an efficient and cost-effective way to improve the mechanical performance of an overmolded part. Because the tow volume is increased by simply feeding more prepreg tapes through the line and not by increasing the number of passes around the jig, cycle time is preserved with the increase in tow volume.

## 5.5 Chapter Acknowledgements

We would like to thank Hexpol AB and DSM for supplying the material used in this study (TPE and PA/CF prepreg, respectively). We would also like to thank Dr. Robin Glebes for his previous work developing the predictive technical cost model and Jung-Soo Rhim for his help adapting the cost model to this study.

## 5.6 References

- [1] D. Weng, J. Andries, P. Morin, K. Saunders, and J. Politis, “Fundamentals and material development for thermoplastic elastomer (TPE) overmolding - ProQuest,” *Journal of Injection Molding Technology*, vol. 4, no. 1, pp. 22–28, Mar. 2000, Accessed: Feb. 14, 2022. [Online]. Available: <https://www.proquest.com/docview/217276625/fulltextPDF/6E0DD333EB5D4F9DPQ/1?accountid=13360>
- [2] G. D. Smith, C. J. G. Plummer, P.-E. Bourban, and J.-A. E. Månson, “Non-isothermal fusion bonding of polypropylene,” *Polymer (Guildf)*, vol. 42, pp. 6247–6257, 2001, [Online]. Available: [www.elsevier.nl/locate/polymer](http://www.elsevier.nl/locate/polymer)

- [3] L. M. Arzondo *et al.*, “Sequential injection overmolding of an elastomeric ethylene-octene copolymer on a polypropylene homopolymer core,” *Polymer Engineering and Science*, 2004, doi: 10.1002/pen.20216.
- [4] M. v. Candal, A. Gordillo, O. O. Santana, and J. J. Sánchez, “Study of the adhesion strength on overmoulded plastic materials using the essential work of interfacial fracture (EWIF) concept,” *Journal of Materials Science*, vol. 43, no. 15, pp. 5052–5060, Aug. 2008, doi: 10.1007/S10853-008-2667-1/FIGURES/10.
- [5] A. M. Harte and J. F. Mc Namara, “Overinjection of thermoplastic composites: I. Processing and testing of components,” *Journal of Materials Processing Technology*, vol. 182, no. 1–3, pp. 12–20, Feb. 2007, doi: 10.1016/J.JMATPROTEC.2006.06.016.
- [6] J. Qiu, A. Tsuboi, K. Izumi, H. Wu, S. Guo, and Y. Huang, “Effects of interfacial morphology on the welding strength of injection-molded polyamide,” *Polymer Engineering and Science*, vol. 47, no. 12, pp. 2164–2171, Dec. 2007, doi: 10.1002/PEN.20950.
- [7] C. J. G. Plummer, P. E. Bourban, J. E. Zanetto, G. D. Smith, and J. A. E. Månson, “Nonisothermal fusion bonding in semicrystalline thermoplastics,” *Journal of Applied Polymer Science*, vol. 87, no. 8, pp. 1267–1276, Feb. 2003, doi: 10.1002/APP.11528.
- [8] R. Akkerman, M. Bouwman, and S. Wijskamp, “Analysis of the Thermoplastic Composite Overmolding Process: Interface Strength,” *Frontiers in Materials*, vol. 7, p. 27, Feb. 2020, doi: 10.3389/FMATS.2020.00027/BIBTEX.
- [9] R. Giusti and G. Lucchetta, “Modeling the adhesion bonding mechanism in overmolding hybrid structural parts for lightweight applications,” in *Key Engineering Materials*, 2014, vol. 611–612, pp. 915–921. doi: 10.4028/www.scientific.net/KEM.611-612.915.
- [10] G. Jiang, W. U. Hong, Y. A. N. Bowen, G. U. O. Shaoyun, and J. Huang, “Reinforcement of solid-melt interfaces for semicrystalline polymers in a sequential two-staged injection molding process,” *Journal of Polymer Science, Part B: Polymer Physics*, vol. 47, no. 11, pp. 1112–1124, Jun. 2009, doi: 10.1002/POLB.21719.
- [11] J. E. Bidaux, G. D. Smith, N. Bernet, J. A. E. Månson, and J. Hilborn, “Fusion bonding of maleic anhydride grafted polypropylene to polyamide 6 via in situ block copolymer formation at the interface,” *Polymer (Guildf)*, vol. 37, no. 7, pp. 1129–1136, 1996, doi: 10.1016/0032-3861(96)80839-1.

- [12] R. Chandran, C. J. G. Plummer, P. E. Bourban, and J. A. E. Månson, "Morphology and interfacial strength of nonisothermally fusion bonded hard and soft thermoplastics," *Polymer Engineering & Science*, vol. 58, no. S1, pp. E82–E92, May 2018, doi: 10.1002/PEN.24662.
- [13] S. Yamaguchi, Y. W. Leong, T. Tsujii, M. Mizoguchi, U. S. Ishiaku, and H. Hamada, "Effect of crystallization and interface formation mechanism on mechanical properties of film-insert injection-molded poly(propylene) (PP) film/PP substrate," *Journal of Applied Polymer Science*, vol. 98, no. 1, pp. 294–301, Oct. 2005, doi: 10.1002/APP.21590.
- [14] A. Naeim abadi, F. Hemmati, and H. Garmabi, "Validation of rheological responses for morphological evaluation of incompatible polyamide 12/thermoplastic elastomer blends filled with nanoclay," *Polymer Testing*, vol. 65, pp. 78–89, Feb. 2018, doi: 10.1016/J.POLYMERTESTING.2017.11.006.
- [15] J. G. Kim, J. Lee, and Y. Son, "Toughening of nylon 6 with a ethylene-octene copolymer grafted with maleic anhydride and styrene," *Materials Letters*, 2014, doi: 10.1016/j.matlet.2014.03.186.
- [16] J. J. Huang, H. Keskkula, and D. R. Paul, "Rubber toughening of an amorphous polyamide by functionalized SEBS copolymers: morphology and Izod impact behavior," *Polymer (Guildf)*, vol. 45, no. 12, pp. 4203–4215, May 2004, doi: 10.1016/J.POLYMER.2004.04.002.
- [17] S. C. Tjong, S. al Xu, and Y. W. Mai, "Tensile deformation mechanism of polyamide 6,6/SEBS-g-MA blend and its hybrid composites reinforced with short glass fibers," *Journal of Materials Science 2003 38:2*, vol. 38, no. 2, pp. 207–215, Jan. 2003, doi: 10.1023/A:1021132725370.
- [18] S. C. Tjong, S. A. Xu, and Y. W. Mai, "Impact fracture toughness of short glass fiber-reinforced polyamide 6,6 hybrid composites containing elastomer particles using essential work of fracture concept," *Materials Science and Engineering A*, 2003, doi: 10.1016/S0921-5093(02)00609-3.
- [19] S. C. Tjong, S. A. Xu, R. Kwok-Yiu Li, and Y. W. Mai, "Short glass fiber-reinforced polyamide 6,6 composites toughened with maleated SEBS," *Composites Science and Technology*, 2002, doi: 10.1016/S0266-3538(02)00140-9.

- [20] D. Heflin and J.-A. E. Mansson, “Mechanisms for Combining Polyamide and Epoxy and their Effects on Mechanical Performance—A Review,” *Submitted*, 2022.
- [21] G. Pompe, M. Bräuer, D. Schweikle, J. Nagel, B. Hupfer, and D. Lehmann, “Influence of the temperature profile in the interface on the bond strength of polyamide–polyurethane two-component tensile bars,” *Journal of Applied Polymer Science*, vol. 100, no. 6, pp. 4297–4305, Jun. 2006, doi: 10.1002/APP.23842.
- [22] A. M. M. R. Persson, E. L. Hinrichsen, and E. Andreassen, “Adhesion between thermoplastic elastomers and polyamide-12 with different glass fiber fractions in two-component injection molding,” *Polymer Engineering & Science*, vol. 60, no. 7, pp. 1642–1661, Jul. 2020, doi: 10.1002/PEN.25408.
- [23] N. Jansson, W. D. Wakeman, and J. A. E. Månson, “Optimization of hybrid thermoplastic composite structures using surrogate models and genetic algorithms,” *Composite Structures*, vol. 80, no. 1, pp. 21–31, Sep. 2007, doi: 10.1016/J.COMPSTRUCT.2006.02.036.
- [24] M. D. Wakeman, E. Eble, P. Beyeler, T. Herrmann, and J.-A. E. Månson, “Hybrid thermoplastic composite beam structures integrating UD tow, stamped fabric, and over-injection/compression moulding”.
- [25] N. Jansson, P. O. Hagstrand, M. D. Wakeman, and J. A. E. Månson, “Finite element modelling and testing of an injection moulded generic tow reinforced structure,” *Composites Part B: Engineering*, vol. 36, no. 6–7, pp. 487–495, Jan. 2005, doi: 10.1016/J.COMPOSITESB.2005.04.002.
- [26] J. Haas, O. N. Hassan, B. Beck, L. Kärger, and F. Henning, “Systematic approach for finite element analysis of thermoplastic impregnated 3D filament winding structures – General concept and first validation results,” *Composite Structures*, vol. 268, p. 113964, Jul. 2021, doi: 10.1016/J.COMPSTRUCT.2021.113964.
- [27] C. Oztan *et al.*, “Microstructure and mechanical properties of three dimensional-printed continuous fiber composites:,” <https://doi.org/10.1177/0021998318781938>, vol. 53, no. 2, pp. 271–280, Jul. 2018, doi: 10.1177/0021998318781938.
- [28] R. Matsuzaki *et al.*, “Three-dimensional printing of continuous-fiber composites by in-nozzle impregnation,” *Scientific Reports 2016 6:1*, vol. 6, no. 1, pp. 1–7, Mar. 2016, doi: 10.1038/srep23058.

- [29] “Standard Test Method for Bond Strength of Fiber-Reinforced Polymer Matrix Composite Bars to Concrete by Pullout Testing 1”, doi: 10.1520/D7913\_D7913M-14R20.
- [30] Srinivasa Ramanujan, *Ramanujan’s Collected Works*. New York: Chelsea, 1962.
- [31] “Standard Test Method for Flexural Properties of Polymer Matrix Composite Materials 1”, doi: 10.1520/D7264\_D7264M-15.
- [32] S. J. Joo, M. H. Yu, W. Seock Kim, J. W. Lee, and H. S. Kim, “Design and manufacture of automotive composite front bumper assemble component considering interfacial bond characteristics between over-molded chopped glass fiber polypropylene and continuous glass fiber polypropylene composite,” *Composite Structures*, vol. 236, p. 111849, Mar. 2020, doi: 10.1016/J.COMPSTRUCT.2019.111849.

## 6. THESIS CONCLUSIONS

The objective of this thesis has been to provide opportunities and conditions for extending conventional molding processes into high-performance processes for hybrid molding of multi-material systems. This thesis has shown that this can be performed for different material combinations—EP/PA, PA/TPE, and Al/PA. We have also managed to prove that these are commercially viable techniques, as processing temperature and cycle times follow conventional conditions and no exceptional equipment setups or reconfiguration of processing lines is needed. My work is exemplified in three different material systems, as explained below.

The combination of EP and PA composites is beneficial for a variety of applications, including high-performance aerospace applications, and can be rapidly manufactured using RTM to overmold EP onto a PA-reinforced preform. In this work, manufacturing conditions were altered to increase the spontaneous EP-PA interfacial bond by over 200%, resulting in a cohesive bond that is up to 150% stronger than the EP-EP adhesive bond. This stronger interfacial bond improved the crash performance of the multi-material composites, resulting in up to 83% greater energy absorption and 18% greater peak energy in QSI and as much as 64% reduction in damage area in drop-weight impact. Further, impact testing illustrated the importance of part orientation on performance. Where possible, EP/PA multi-material parts should be designed so that an impactor will hit the PA surface, as this allows the PA to dissipate contact stresses.

For applications where greater toughness is required without sacrificing strength, such as sports equipment, a TPE can be hybrid injection molded onto a continuous fiber reinforced PA preform. This work showed that the PA-TPE bond strength can be increased by 11% in a conventional manufacturing process by altering the processing conditions, while bond strength was shown to be insensitive to processing conditions for a hybrid injection molding process. Further, tripling the PA/CF preform volume resulted in a 30% improvement in energy absorbed during bending for a less than 4% increase in part cost, showing that increasing tow volume is an economically viable method to improve part performance.

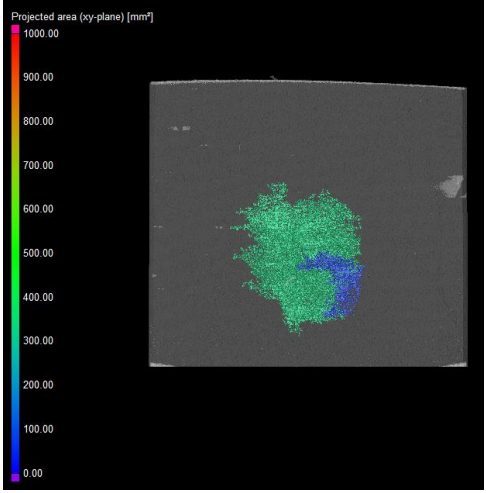
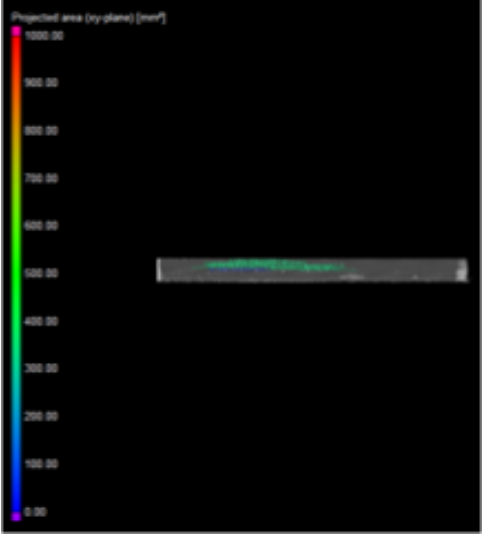
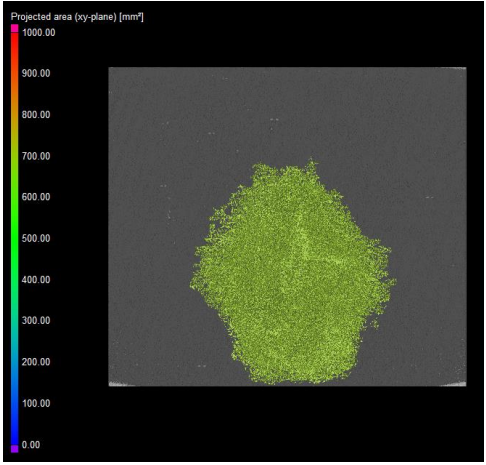
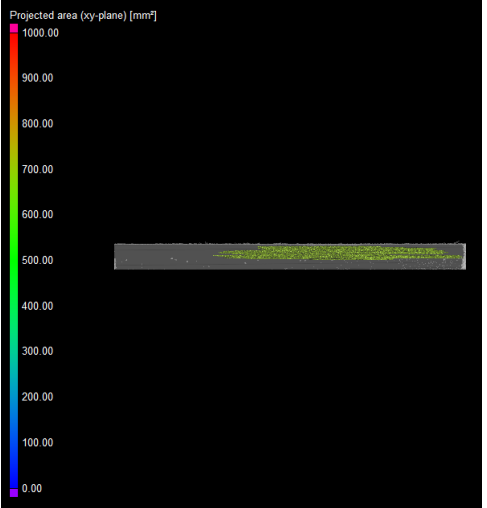
Finally, the combination of aluminum with recycled fiber-reinforced PA can be desirable for automotive applications that require low weight, ease of processability, and improved resistance to low energy impact that might be expected from pebbles or other road debris. Both the PA/CF and the aluminum may be recycled, which results in a favorable environmental impact.

As tested here, the spontaneous adhesion between the two materials is optimal for energy transfer and absorption. The combination of materials has a synergistic relationship whereby the PA/CF impacted surface reduces the dent depth caused by low energy impact by up to 80%, while the aluminum on the reverse side increases the sample's perforation energy.

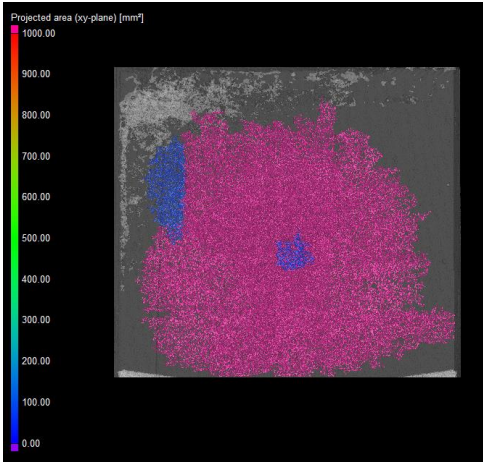
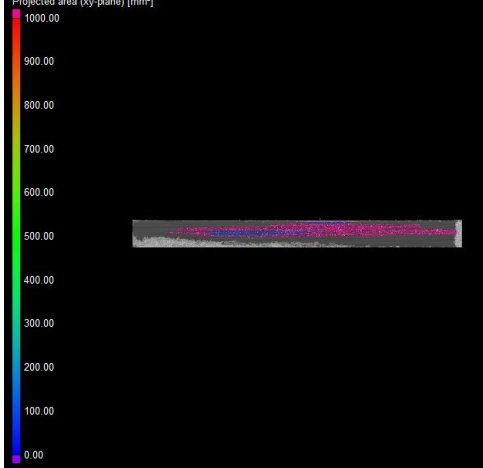
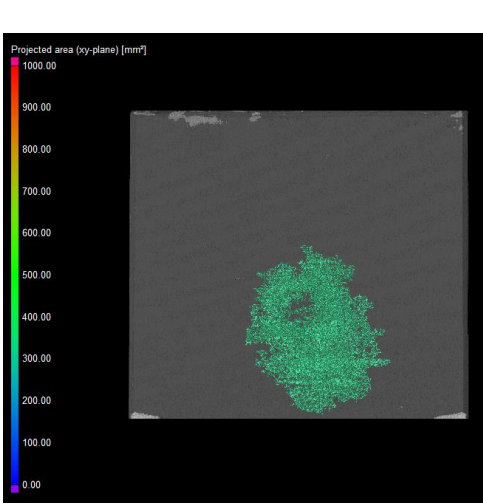
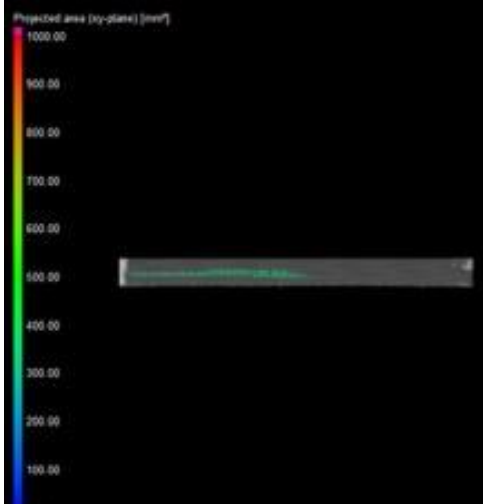
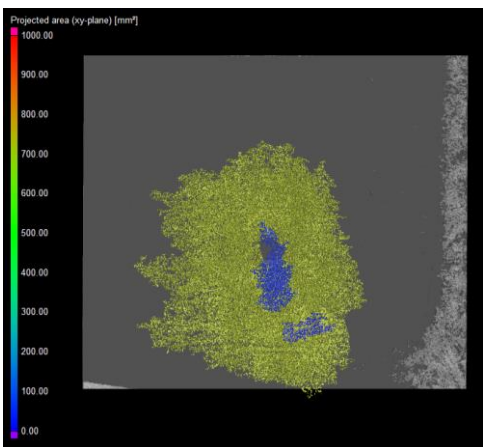
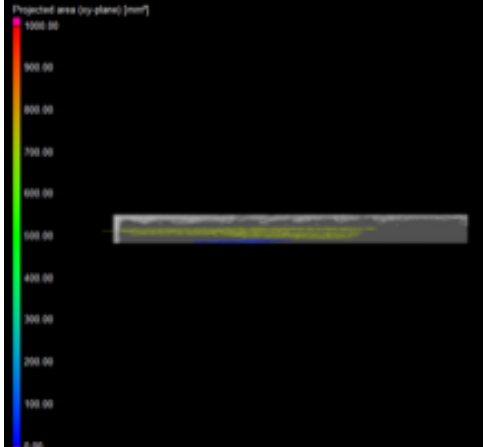


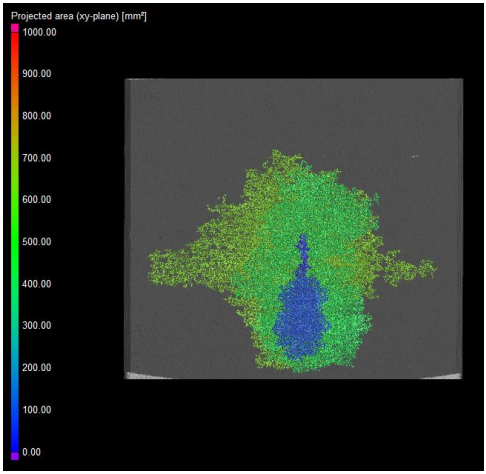
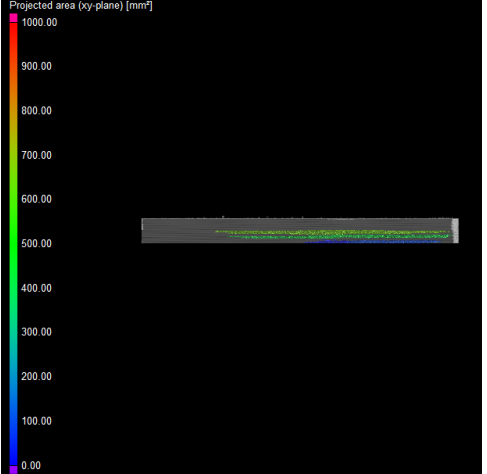
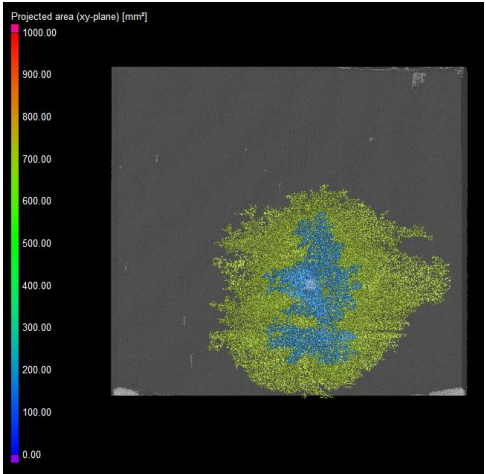
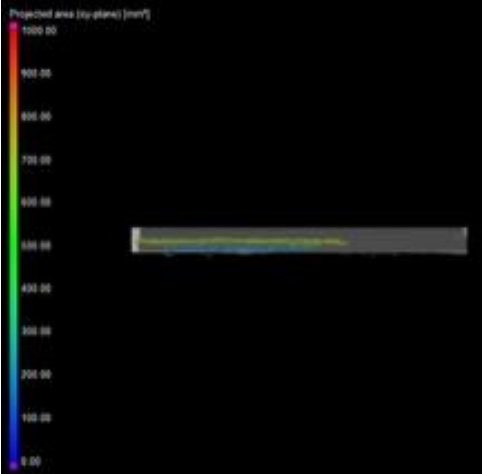
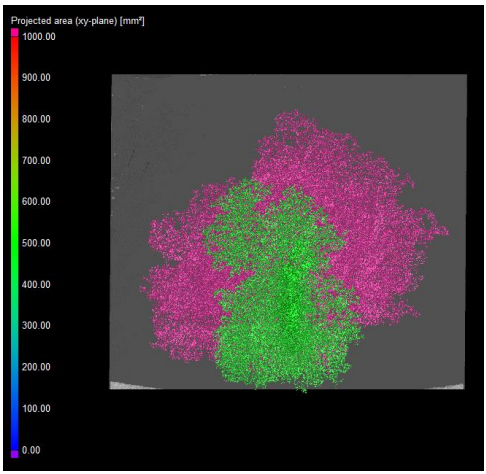
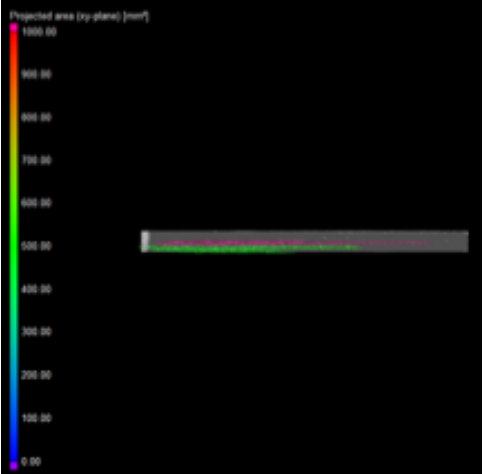
## APPENDIX A: CHAPTER 4 – DAMAGE AREA CT IMAGES

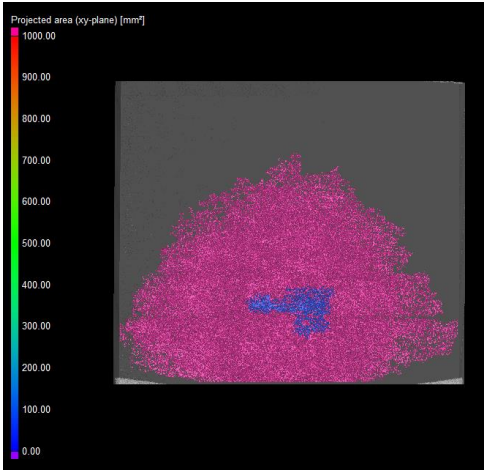
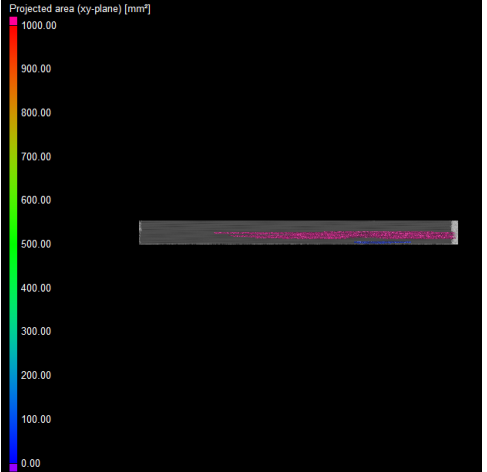
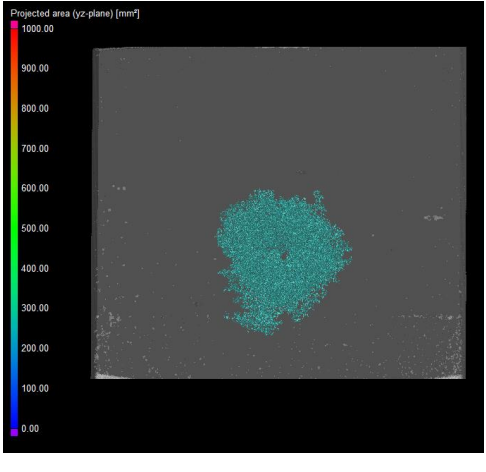
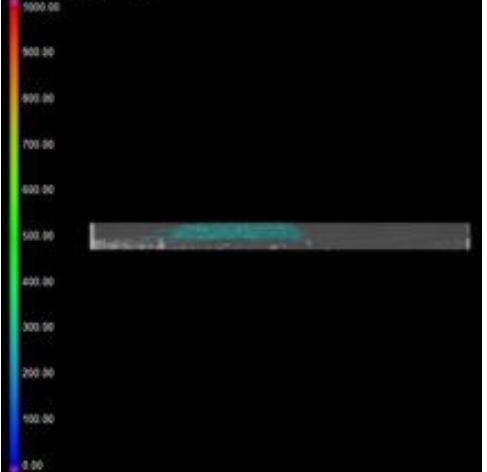
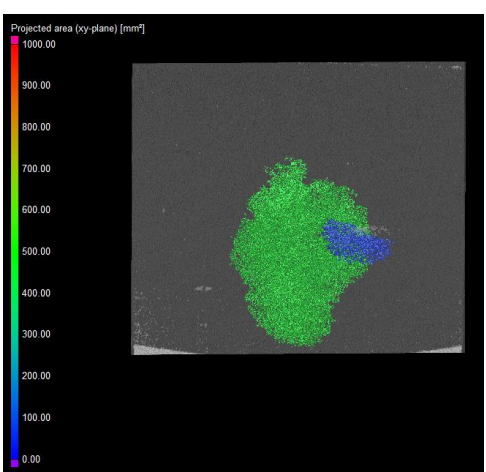
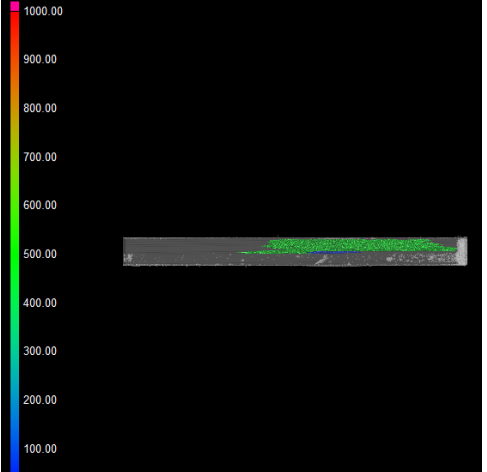
This appendix contains damage area, determined by CT imaging, for all of the CT scanned samples. Samples are shown from the top and the side to illustrate both the breadth and depth of damage in samples, and damage area is color-coded by projected area in the x-y plane. The x-y plane is in line with the page. The description includes the processing temperature, which is an indicator of bond strength, the part orientation, and the impact energy to sample thickness ratio with which the samples were impacted.

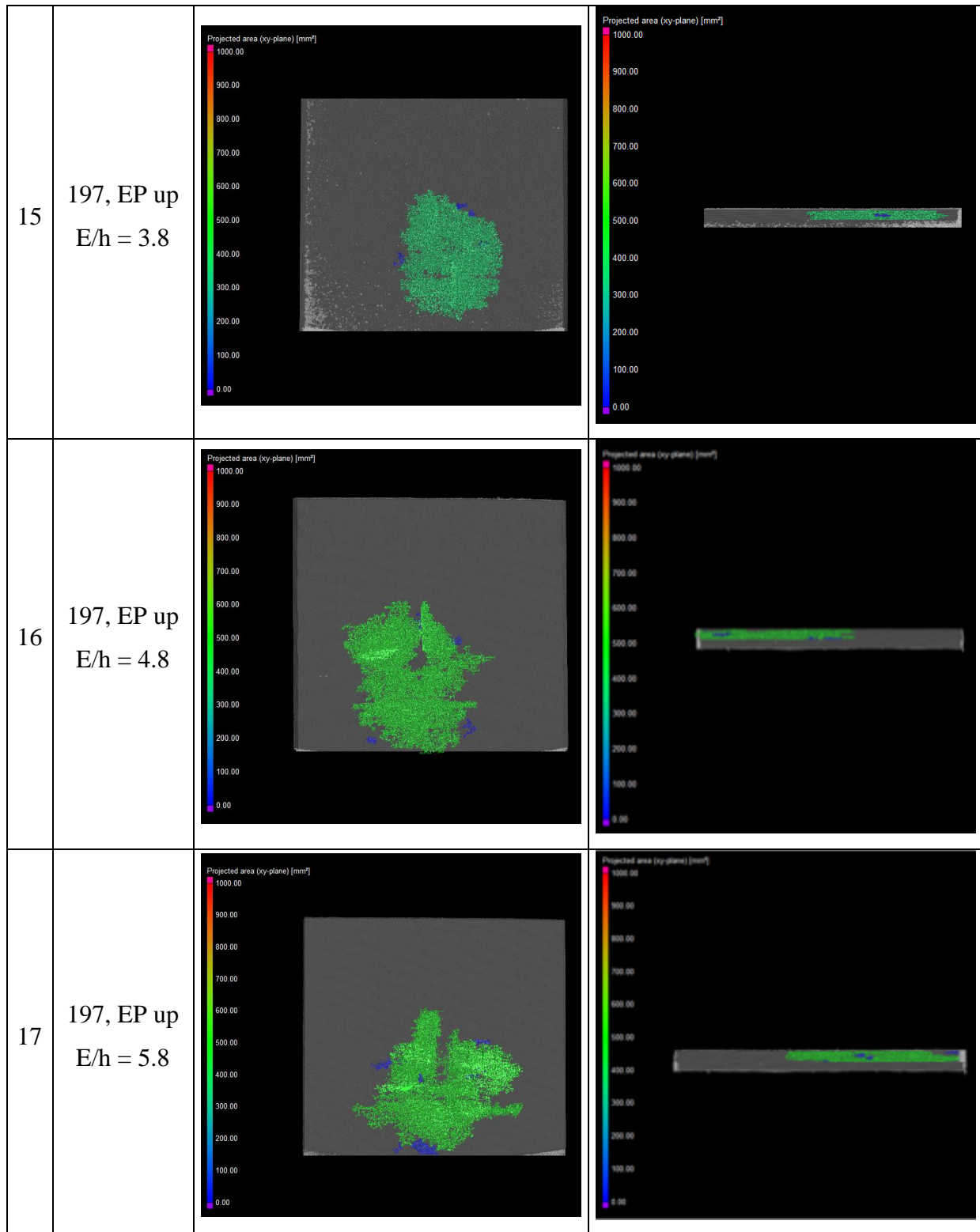
| # | Description               | Top View  | Side View  |
|---|---------------------------|---|--|
| 1 | 177, EP up<br>$E/h = 2.8$ |   |   |
| 2 | 177, EP up<br>$E/h = 3.8$ |  |  |

|   |                           |  |  |
|---|---------------------------|--|--|
| 3 | 177, EP up<br>$E/h = 3.8$ |  |  |
| 4 | 177, EP up<br>$E/h = 4.8$ |  |  |
| 5 | 177, EP up<br>$E/h = 5.8$ |  |  |

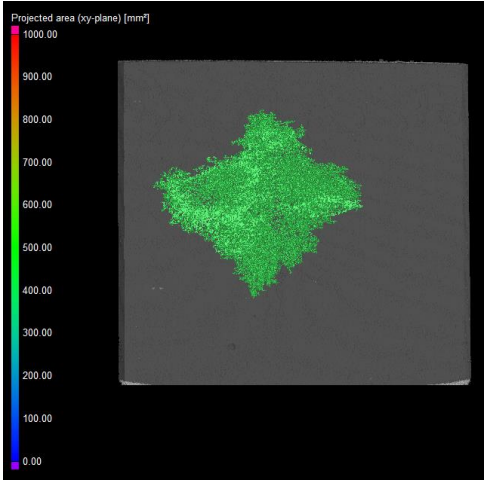
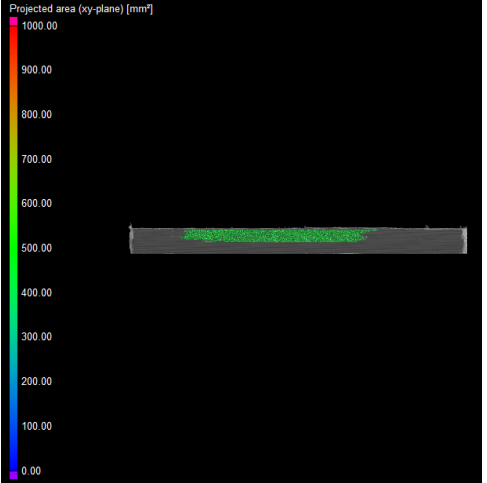
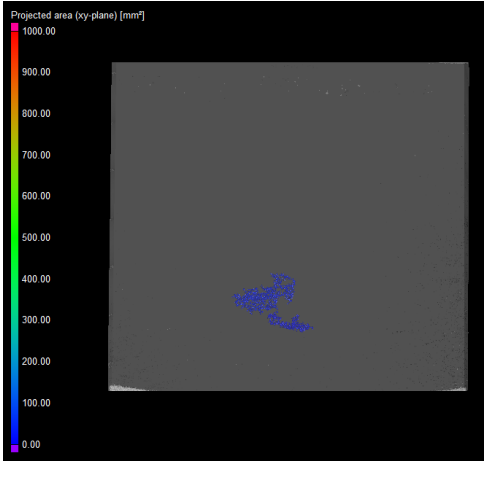
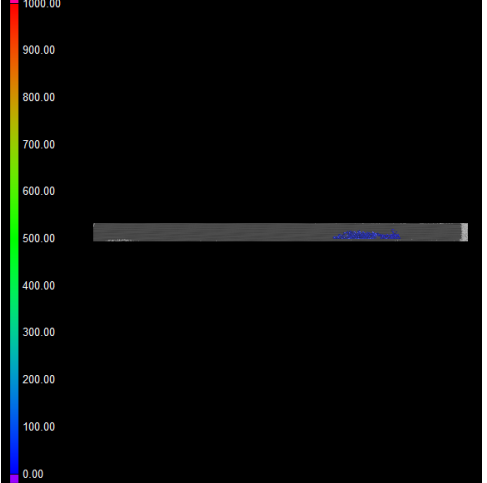
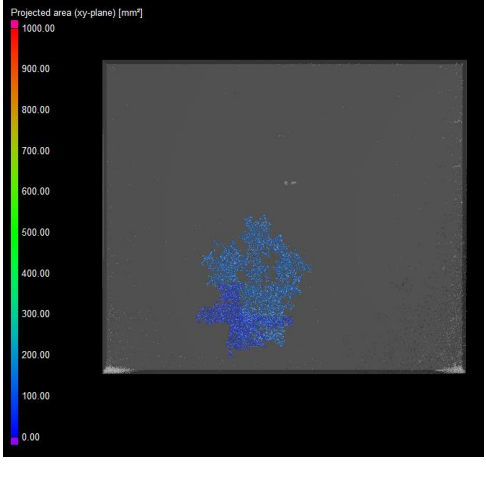
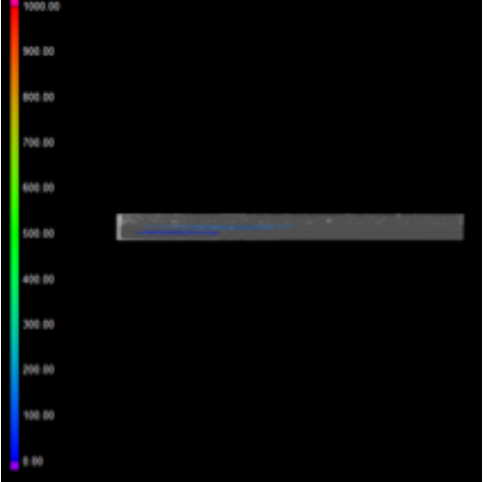
|   |                           |   |  |
|---|---------------------------|---|--|
| 6 | 177, EP up<br>$E/h = 5.8$ |    |    |
| 7 | 177, PA up<br>$E/h = 2.8$ |   |   |
| 8 | 177, PA up<br>$E/h = 3.8$ |  |  |

|    |                           |   |  |
|----|---------------------------|---|--|
| 9  | 177, PA up<br>$E/h = 3.8$ |    |    |
| 10 | 177, PA up<br>$E/h = 4.8$ |   |   |
| 11 | 177, PA up<br>$E/h = 5.8$ |  |  |

|    |                           |   |  |
|----|---------------------------|---|--|
| 12 | 177, PA up<br>$E/h = 5.8$ |    |    |
| 13 | 197, EP up<br>$E/h = 2.8$ |   |   |
| 14 | 197, EP up<br>$E/h = 3.8$ |  |  |





|    |                           |   |  |
|----|---------------------------|---|--|
| 18 | 197, EP up<br>$E/h = 5.8$ |    |    |
| 19 | 197, PA up<br>$E/h = 2.8$ |   |   |
| 20 | 197, PA up<br>$E/h = 3.8$ |  |  |

